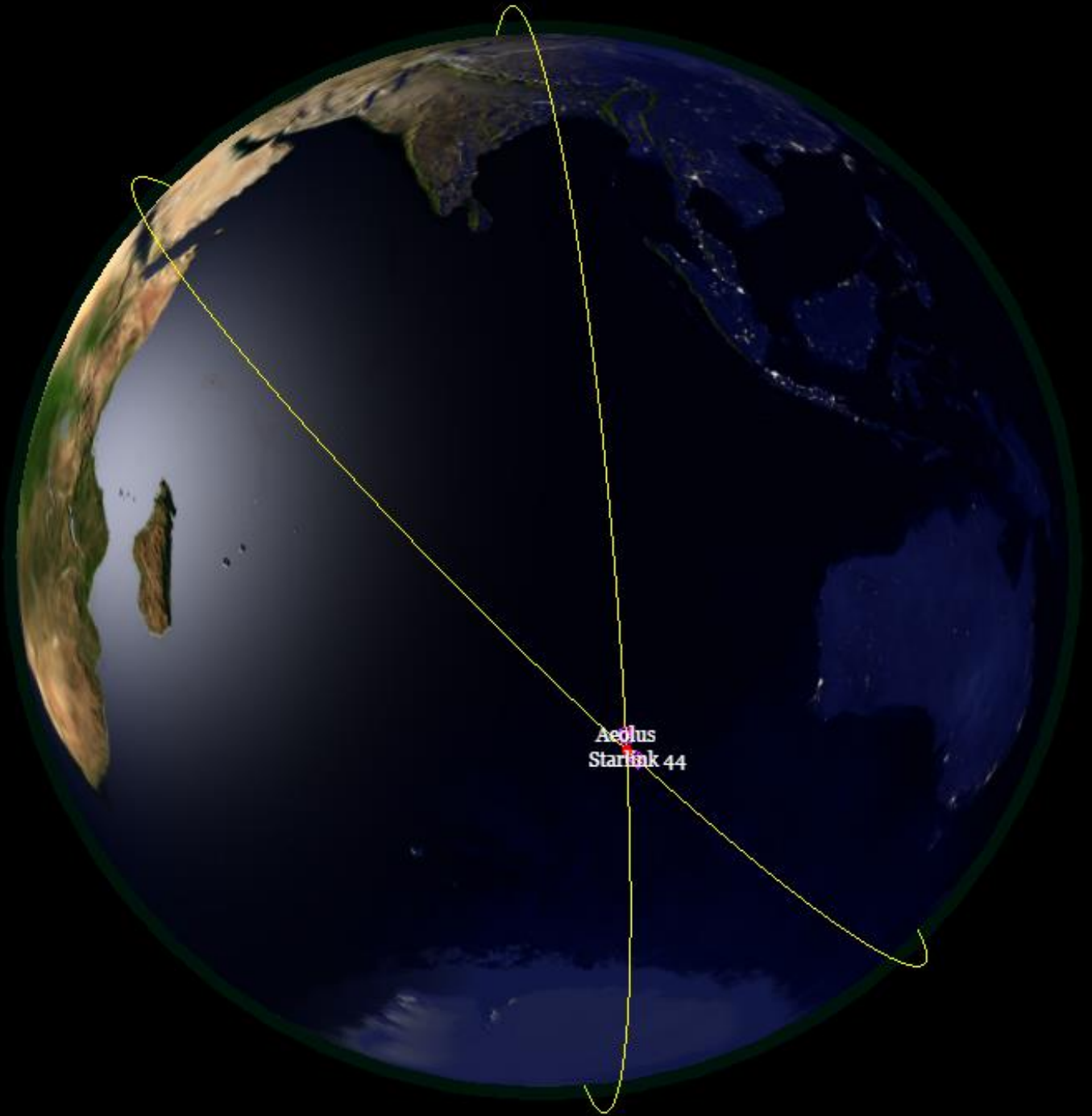


# Collision Avoidance with Collaboration between Operators

Master thesis

Luana Capus

Technische Universiteit Delft



*Page left blank intentionally.*

# Collision Avoidance with Collaboration between Operators

## Master thesis

by

L. Capus

to obtain the degree of Master of Science  
at Delft University of Technology,  
to be defended publicly on Friday 21 July, 2023 at 14:00.

Student number: 4653580

Project duration: October 4, 2021 – July 7, 2023

Thesis committee:	Ir. R. Noomen	TU Delft, supervisor
	Dr. ir. E. Mooij	TU Delft, chair
	Dr. ir. C.J.M. Verhoeven	TU Delft, external examiner

An electronic version of this thesis is available at <http://repository.tudelft.nl/>.

Cover image taken from: 'Predicted near miss between Aeolus and Starlink 44' ESA [1].



*Page left blank intentionally.*



# Preface

All throughout my studies in Aerospace Engineering at Delft University of Technology, I have been attracted to topics surrounding space debris. I am pleased that my interests in finding solutions to this problem have continued growing. This thesis "Collision Avoidance with Collaboration between Operators" to obtain my master's degree is the outcome of my enthusiasm. First, it delves into an analysis of the current space debris environment in LEO and the single action to collision avoidance. The proposal of this thesis is to implement a combined action to collision avoidance where operators collaborate to find the best solutions. However, the proposal also works for the more common collision scenarios between one maneuverable spacecraft and space debris. Through an investigation on Space Traffic Management, the special considerations, and the real-world constraints, a framework for the decision making on the combined approach to collision avoidance is proposed in this work. It allows for proper collaboration between the operators.

This work is achieved with the support of many actors, the main one being my supervisor Ron Noomen. We had several passionate discussions about flight dynamics, space debris and many other non-research topics. I will truly miss our talks and the guidance and support provided. Then, I would like to thank for the support provided by the TU Delft Astrodynamics Toolbox and Delftblue community. Many students and professors helped me solve problems and advance in my research. Without them, this thesis would not have been possible. I would also like to thank Stefano Speretta from the Department of Space Engineering, who provided me with the CDM files necessary to conduct this work.

This process has been challenging but certainly rewarding, with many opportunities to expand my knowledge. This thesis topic helped me accomplish a 6 month internship at SES in the flight dynamics team (from April to September 2022), working on automating collision avoidance processes within the team with machine learning. After my internship I was thrilled to stay within the team as a full-time-hire. The consequence, was that after a six month break from the thesis work, I started working only part-time on it afterwards. Nevertheless, a lot of insight was gained by working for an operator and I would like to thank the Flight dynamics team for all the support and opportunities provided. Notably, I was part of the launch mission team working closely with Boeing in April 2023!

Lastly, I would like to thank my close friends in Delft and in Luxembourg that supported me during this thesis work. I would also like to thank everyone that contributed to my student experience in the Netherlands, I will remember these years and my time with you very fondly. My special thanks goes out to my partner Nils that has completely supported me during this master study and my brother Leo that has always been there for me. Last but certainly not least, my mother Maria. Thank you for the example you have set for me and for pushing me forward while always believing in me.

*Luana Capus  
Luxembourg,  
July 2023*





# Abstract

Space debris has become a rising problem in the aerospace community, leading to the need for effective spacecraft collision avoidance processes. Currently, these processes can be called unilateral as only one object in conjunction is considered maneuverable. This thesis focuses on the implementation of a combined action approach to collision avoidance and proposes a cooperation process between operators. The research objective is to optimize the dual maneuver solutions and explore negotiation proposals within a Space Traffic Management system.

The study utilizes an optimization algorithm based on multiple objectives, including propellant mass consumption, collision probability, and mission disturbance. The decision variables used in the optimization are related to the three-direction maneuvering within both objects in conjunction. The optimization is first carried out to minimize the three objectives listed above. These optimization results are considered preliminary as they do not allow for a proper trade-off for the operators. Hence, a review of the objectives used in the optimization algorithm yields the two new criteria used for the final results: the Collision parameter and the Cost parameter. The latter combines propellant mass consumption and mission disturbance.

The results, displayed as Pareto fronts, demonstrate that these objectives allow for the identification of optimal maneuver solutions. Adding on, a sensitivity analysis highlights the importance of precise maneuver timing and lower  $\Delta V$  contributions within the solutions. The operator is recommended to re-analyze the CAM if the maneuver timing varies by more than 5 minutes. Through the exploration of various study cases and scenarios, insights are provided into the interaction between different systems in space. In general, the chaser showed higher values of  $\Delta V$  magnitude than the target but the optimization results showed that both interacted together to reach the collision avoidance solution. The  $I_{sp}$  factor proved to not affect the optimization results significantly, and the single maneuvering spacecraft scenarios were successfully solved with the optimization method. This scenario led to higher Cost parameters and higher Collision parameter, the  $P_c$  could only be lowered slightly further than  $10^{-10}$ . As this is below the defined threshold, the results were accepted.

In addition, a proposal is drafted for a communication flow and cooperation framework. The Middle Man, acting as a central authority between the two parties, facilitates the cooperation process, ensuring fair and efficient collaboration between operators. The proposed framework for decision-making is called "rule and resource following shared approach". While specific rules and procedures are not defined in this thesis, the framework allows for them to be included once agreed upon by operators. This thesis concludes that the proposed combined action and cooperation process offers potential solutions to the challenges posed by space debris and contributes to the safety and sustainability of space activities.



# Nomenclature

## Abbreviations

BFE	Batch Fitness Evaluation
CAM	Collision Avoidance Maneuver
CAMOS	Collision Avoidance Maneuver Optimization Software
CDM	Conjunction Data Message
COPUOS	Committee on the Peaceful Uses of Outer Space
CORAM	Collision Risk Assessment and Avoidance Maneuver
CORCOS	Collision Risk COmputation Software
CRASS	Collision Risk ASessment Software
CSM	Conjunction Summary Message
CSpOC	Combined Space Operations Center
DE	Differential Evolution
DO	Degree and Order
DISCOS	Database Information System Characterizing Objects in Space
DRAMA	Debris Risk Assessment and Mitigation Analysis
ECI	Earth Centered Inertial
ECEF	Earth Centered Earth Fixed
ESA	European Space Agency
ESOC	European Space Operations Center
FCC	Federal Communications Commission
GA	Genetic Algorithms
GEO	Geostationary Earth Orbit
HIE	High Interest Event
IADC	Inter-Agency Space Debris Coordination Committee
ISS	International Space Station
ITRF	International Terrestrial Reference Frame
ITU	International Telecommunications Union
LEO	Low Earth Orbit
LTSS	Long-term Sustainability of Outer Space Activities
MASTER	Meteoroid and Space Debris Terrestrial Environment Reference model
MEO	Medium Earth Orbit
MOEA/D	Multi-objective Evolutionary Algorithm based on Decomposition
NSPSO	Non-dominated Sorting Particle Swarm Optimization
ODIN	Orbit Determination by Improved Normal Equations
PM	Point Mass
PMD	Post-Mission Disposal
PSO	Particle Swarm Optimization
PSOGSA	Particle Swarm Optimization - Gravitational Search Algorithm

Pygmo	Python Global Multi-Objective Optimiser
RK	Runge-Kutta
RAAN	Right ascension of the ascending node
SCARF	Spacecraft Conjunction Assessment and Risk Frontend
SA	Simulated Annealing
SH	Spherical Harmonics
SOC	Satellite Operations Center
SSA	Space Situational Awareness
STM	Space Traffic Management
TCA	Time of Closest Approach
TLE	Two-line Elements
TudatPy	TU Delft Astrodynamics Toolbox Python

## Symbols

Roman Symbols		
$a$	Semi-major axis	[m]
$a$	Acceleration	[m/s <sup>2</sup> ]
$A$	Cross-sectional area	[m <sup>2</sup> ]
$c$	Speed of light	[m/s]
$C$	Covariance matrix	[-]
$C_D$	Drag coefficient	[-]
$C_R$	Solar radiation pressure coefficient	[-]
$D$	Distance	[m]
$e$	Eccentricity	[-]
$E$	Eccentric anomaly	[rad]
$g_0$	Gravitational acceleration at sea level	[m/s <sup>2</sup> ]
$G$	Universal gravitational constant	[m <sup>3</sup> /(kgs <sup>2</sup> )]
$i$	Inclination	[rad]
$I_{sp}$	Specific impulse	[s]
$m$	Mass	[kg]
$m_0$	Initial mass	[kg]
$m_p$	Propellant mass	[kg]
$M$	Mean anomaly	[rad]
$n$	Mean motion	[rad/s]
$P_c$	Probability of collision	[-]
$P_{n,m}$	Legendre polynomial of degree n and order m	[-]
$r$	Distance	[m]
$t$	Time	[s]
$u$	Argument of latitude	[rad]
$v_x$	Velocity in x-direction	[m/s]
$v_y$	Velocity in y-direction	[m/s]
$v_z$	Velocity in z-direction	[m/s]
$W$	Intensity of solar radiation	[W/m <sup>2</sup> ]

---

$x$	Position in x-direction	[m]
$y$	Position in y-direction	[m]
$z$	Position in z-direction	[m]

---

**Greek symbols**

---

$\alpha$	Flight-path angle	[rad]
$\Delta V$	Velocity change	[m/s]
$\epsilon$	Error	[-]
$\theta$	True anomaly	[rad]
$\mu$	Gravitational parameter of Earth	[m <sup>3</sup> /s <sup>2</sup> ]
$\rho$	Atmospheric density	[kg/m <sup>3</sup> ]
$\rho$	Correlation factor	[-]
$\sigma$	In-plane rotation angle	[rad]
$\sigma$	Standard deviation	[case specific]
$\gamma$	Out-of-plane angle	[rad]
$\omega$	Argument of pericenter	[rad]
$\Omega$	Right ascension of the ascending node	[rad]



# Contents

<b>Preface</b>	<b>v</b>
<b>Abstract</b>	<b>vii</b>
<b>Nomenclature</b>	<b>ix</b>
<b>1 Introduction</b>	<b>1</b>
1.1 Research question . . . . .	1
1.2 Layout . . . . .	2
<b>I Problem introduction</b>	<b>3</b>
<b>2 Background Information</b>	<b>5</b>
2.1 Research gap . . . . .	5
2.2 Space debris environment in LEO . . . . .	6
2.3 Single action to collision avoidance . . . . .	8
2.4 STM tendencies . . . . .	9
<b>3 Theory</b>	<b>11</b>
3.1 Coordinates and reference frames . . . . .	11
3.1.1 Coordinates . . . . .	11
3.1.2 Reference frames . . . . .	11
3.1.3 Transformations . . . . .	12
3.2 Probability calculation . . . . .	14
3.3 Perturbations . . . . .	16
3.3.1 Earth's gravitational perturbation . . . . .	16
3.3.2 Atmospheric drag . . . . .	17
3.3.3 Third-body gravitational perturbation . . . . .	17
3.3.4 Solar radiation pressure perturbation . . . . .	17
3.4 Optimization algorithm selection . . . . .	18
3.4.1 General optimization aspects . . . . .	18
3.4.2 Algorithm choice . . . . .	18
<b>II Approach to solving the problem</b>	<b>21</b>
<b>4 Methodology</b>	<b>23</b>
4.1 Tools and inputs . . . . .	23
4.2 Definition of dynamics model - propagation . . . . .	23
4.3 Collision probability calculation . . . . .	28
4.3.1 Data description . . . . .	28
4.3.2 Verification and validation . . . . .	28
4.4 Collision avoidance maneuver implementation . . . . .	30
4.4.1 Modeling . . . . .	30
4.4.2 Implementation . . . . .	31
4.4.3 Results . . . . .	31
4.5 Application of the optimization algorithm . . . . .	38
4.5.1 Decision variables and constraints . . . . .	38
4.5.2 Objectives and fitness function . . . . .	40
4.5.3 Algorithm tuning . . . . .	43

<b>5</b>	<b>Code set-up</b>	<b>45</b>
5.1	Pre-processing . . . . .	45
5.2	Propagation . . . . .	45
5.3	Optimization and parallel computing . . . . .	46
5.4	Verifying Delftblue calculations . . . . .	48
<b>6</b>	<b>Preliminary results</b>	<b>51</b>
6.1	Visualization options . . . . .	51
6.1.1	Third objective as color map . . . . .	51
6.1.2	Three-dimensional graphs . . . . .	53
6.1.3	Projection in two dimensions. . . . .	54
6.2	Review of optimization methodology . . . . .	55
6.3	New approach results . . . . .	57
6.4	Tuning the new optimization algorithm . . . . .	58
<b>7</b>	<b>Simulation scenarios</b>	<b>69</b>
7.1	Study cases . . . . .	69
7.2	Input for selected cases . . . . .	70
<b>III</b>	<b>Cooperation process and implemented combined action</b>	<b>73</b>
<b>8</b>	<b>Cooperation process</b>	<b>75</b>
8.1	STM definition . . . . .	75
8.2	Current practices . . . . .	76
8.2.1	DLR . . . . .	76
8.2.2	Politecnico di Milano . . . . .	77
8.2.3	SpaceX . . . . .	77
8.2.4	ESA . . . . .	77
8.2.5	CNES/NASA . . . . .	78
8.2.6	Comparison. . . . .	79
8.3	Special considerations . . . . .	81
8.3.1	Derelict spacecraft and space debris . . . . .	81
8.3.2	Small spacecraft . . . . .	81
8.3.3	Mega-constellations . . . . .	82
8.3.4	Manned spacecraft . . . . .	82
8.4	Developing an approach: aspects and ideas . . . . .	82
8.4.1	Aspects/criteria . . . . .	83
8.4.2	Approaches . . . . .	83
8.4.3	Evaluation. . . . .	85
8.5	Real-world constraints . . . . .	86
8.6	Framework for decision making . . . . .	88
<b>9</b>	<b>Results</b>	<b>91</b>
9.1	Sensitivity analysis . . . . .	91
9.1.1	Changes of $\pm 5\%$ . . . . .	92
9.1.2	Changes of $\pm 10\%$ . . . . .	94
9.2	Cases . . . . .	98
9.2.1	First cases batch . . . . .	98
9.2.2	Second cases batch . . . . .	101
9.2.3	Third cases batch. . . . .	104
9.3	Discussion . . . . .	107
9.3.1	Link to cooperation process . . . . .	108
<b>10</b>	<b>Conclusions</b>	<b>111</b>
<b>11</b>	<b>Recommendations</b>	<b>113</b>
	<b>Bibliography</b>	<b>115</b>



---

<b>A</b>	<b>Appendix: CDM example</b>	<b>119</b>
<b>B</b>	<b>Methodology extra information</b>	<b>125</b>
B.1	Collision probability verification and validation . . . . .	125
B.2	Maneuver implementation . . . . .	128



# Introduction

The rising problem of space debris is well-known in the aerospace community. In 2019, the Committee on the Peaceful Uses of Outer Space (COPUOS) agreed on the Guidelines for the Long-term Sustainability of Outer Space Activities (LTSS) [2]. These guidelines recommend that the post-mission lifetime of a spacecraft in orbit should not exceed 25 years, with a 90% probability of successful disposal. To solve the "space debris problem" many investigations are done into passive and active debris removal. However, one of the alternatives is to limit the growing number of debris by reducing collisions. Increasing the capability to avoid these is crucial.

For instance, the collision between Iridium 33 and Cosmos 2251 in 2009 resulted in the creation of nearly 2000 fragments, making it one of the largest individual contributors to the space debris issue [3]. Current collision avoidance processes aim to prevent such accidents, but they are outdated as they rely on manual actions and are single-operator based.

Such processes are initiated when operators receive a conjunction data message (CDM), which provides information such as the miss distance, collision probability, time of closest approach, as well as the relative position and velocity. Operators monitor the evolution of the CDMs and decide to take action when a certain threshold of collision probability is reached. This is considered a single action to collision avoidance because only one of the objects is considered maneuverable. Subsequently, they engage in planning to determine when and by how much the spacecraft should be maneuvered, ensuring that the new orbit is free from any potential conjunction. This is carried out by an engineering group and requires a large effort done under time pressure. Typically, maneuvers are performed to avoid space debris, including fragments of spacecraft, non-functioning satellites, and even launcher components.

However, due to the rising number of spacecraft in orbit, conjunctions between active spacecraft are bound to become more frequent. In GEO the interaction of spacecraft in neighboring station-keeping boxes often lead to CDMs, though, if active, they will conduct station-keeping maneuvers to remain within their box and thus eliminate the conjunction warning. The CDMs are generated because the ephemeris files do not always contain maneuvers in the future. In other orbital regimes, the situation is not as clear and the approach operators should take when faced with a conjunction between two active spacecraft has not been defined. This lack of clarity leads to cases such as the infamous AEOLUS/Starlink conjunction in September 2019 [4]. ESA and SpaceX did not have a clear communication stream and a combined action could not be decided upon. Finally, ESA decided to maneuver its spacecraft to avoid the collision.

The growing number of cataloged space objects due to improved space surveillance services and the increasing prevalence of CubeSats and mega-constellations necessitates a shift in current processes. It is crucial for operators to collaborate in order to identify the most optimal maneuver(s) when encountering conjunctions between two active spacecraft. The possibility of maneuvering both spacecraft should be considered in a fair way, open, and transparent system. It calls for an optimization of this combined action, along with the establishment of negotiation guidelines or procedures within a Space Traffic Management (STM) system. This leads to the research objective of this thesis.

## 1.1. Research question

The research objective is to develop a combined action to spacecraft collision avoidance where the operators work together to solve the conjunction warning. This includes taking into account the manner in which operators could work together. From this, several questions can be generated:

1. Does the inclusion of three objectives relating to propellant consumption, collision probability, and mission disturbance allow for an optimization algorithm to find the best dual maneuver solution?

2. What is the best dual maneuver solution, and what is the sensitivity of the objectives to changes in the control parameters?
3. Can different study cases help understand how systems should interact in space?
4. How do the best dual maneuver solutions translate into negotiation procedures between operators?
5. What are the limitations and challenges for an implementation of such negotiation procedures?

To answer these questions, considered as sub-research questions, the thesis will focus on optimizing different study cases with collision avoidance maneuvers, several objectives, and different characterizations. The results will lead to technical optimum solutions which can be converted to a negotiation proposal between operators accounting for fairness in their usage of the space environment. From this, an overall research question is derived:

*How should a combined action to optimal collision avoidance be implemented and what negotiation proposals can it lead to?*

To solve the questions raised a simulation model is set up along with an optimization algorithm. CDM data is used to compute collision probabilities and the resulting orbits are checked for new conjunctions. The study cases are defined to illustrate several cases of particular interest in the future space environment. The results from the optimization aim at finding maneuvers that minimize overall propellant consumption, mission disturbance, and collision probability. These resulting maneuvers are looked into closely to identify recommendations for future negotiation rules between operators. By investigating these study cases, proposals for rules that will help protect and preserve the space environment are formulated.

## 1.2. Layout

To answer the research question(s), this thesis is divided into three parts. Part I introduces the thesis problem. The background information necessary to understand the research objective and explain the research gap is presented Chapter 2. Then, the theory necessary to solve the problem is given in Chapter 3.

Next, Part II outlines the approach taken to solve the optimization problem. For this, the methodology is defined in Chapter 4. This links directly into the next topic which is the code set-up, shown in Chapter 5. With this, preliminary results are generated and discussed in Chapter 6. Finally, Chapter 7 presents study cases to answer the research question.

Finally, Part III concludes this thesis report. It introduces and explains the combined action to collision avoidance and cooperation process in Chapter 8. The final results are displayed and discussed in Chapter 9. To wrap up the report, the conclusion and recommendations for future research are provided in Chapters 10 and 11. Afterward, an input file example is given in Appendix A. Appendix B presents more in-depth information on the verification conducted.



# Problem introduction

This part contains the background information that sets the scene and underlines the necessity for answering the research question in Chapter 2. This includes details on the space debris environment in LEO and the method currently employed by operators to conduct collision avoidance maneuvers. Additionally, the theory necessary to answer the research question is introduced in Chapter 3.



## Background Information

To answer the research questions, further investigation is necessary to understand the problem fully. This chapter delves into the research gap in Section 2.1, where choices will be made on what to explore. Following that, the space debris environment is investigated in Section 2.2. As the thesis searches for an answer to collision avoidance using a combined action, the current action is described in Section 2.3. This is called from here onwards a single action to collision avoidance as only one operator is meant to take action. Finally, linking to the negotiation part of the research question, Section 2.4 explains the current STM tendencies.

### 2.1. Research gap

In September 2019, the European Space Agency (ESA) implemented measures to prevent a possible collision between its Earth observation satellite AEOLUS and a Starlink constellation spacecraft. Both operators receive conjunction data messages (CDMs), which contain different pieces of information on the conjunction. An example of a CDM is shown in Appendix A and more information is given in Section 4.3. Operators monitor these messages and decide on a course of action when the collision probability surpasses a predefined threshold. This process involves planning the timing and extent of spacecraft maneuvers to avoid potential collisions, ensuring the new orbit remains free from new conjunctions, and informing relevant parties of the maneuver plans. Typically, such maneuvers are carried out to evade space debris.

The AEOLUS/Starlink incident was exceptional as it involved two functioning spacecraft capable of maneuvering in LEO. Initially, both operators were in contact although the discussions were inconclusive as the collision probability was below the widely accepted threshold ( $10^{-6}$ ). As more CDMs were received, indicating a rising collision probability, ESA did not receive any response from SpaceX. Eventually, ESA decided to maneuver its spacecraft to avoid a collision. While ESA was confident that the Starlink spacecraft would not move and could maneuver on its own, the incident highlights the need for modern and efficient communication and negotiation protocols between operators. In this case, SpaceX had a system bug that resulted in fewer CDMs being received and missed emails [4].

With the growing number of objects monitored by space surveillance services and the increasing prevalence of CubeSats and mega-constellations, the collision avoidance process must evolve. Operators should collaborate to determine the optimal strategy when conjunction involves two active spacecraft, with the option to move both objects in the conjunction geometry. Achieving this requires an optimized combined approach, as well as the establishment of negotiation guidelines or procedures through an STM system. Additionally, as the number of CDMs operators receive is anticipated to rise significantly, the system will require additional automation. It will become impractical for study groups to manually track and manage the volume of warnings and maneuvers.

The aerospace industry is acutely aware of the escalating issue of space debris. The Space Debris Environment Report 2023 from ESA's Space Debris Office indicates that there are approximately 33700 traceable objects in orbit<sup>a</sup> [5]. In 2019, the Committee on the Peaceful Uses of Outer Space (COPUOS) reached a consensus on the Guidelines for the Long-term Sustainability of Outer Space Activities (LTSS) [2]. These guidelines stipulate that spacecraft in orbit should have a post-mission lifetime of no more than 25 years and a 90% probability of successful disposal. Although the guidelines are not legally binding they oftentimes are translated into rules by national entities. In 2022, the Federal Communications Commission (FCC) adopted a new five year Post-Mission Disposal rule (PMD) [6], where the term "space station" is used interchangeably with satellite and

<sup>a</sup>Consulted on: 30/06/2023

spacecraft, and the term "end of mission" is defined when the spacecraft is no longer capable of conducting collision avoidance maneuvers<sup>b</sup>:

Accordingly, we adopt a rule requiring space stations ending their mission in, or passing through, the LEO region below 2000 km altitude and planning disposal through uncontrolled atmospheric re-entry to complete disposal as soon as practicable following end of mission, and no later than five years after the end of the mission.

The FCC will apply this rule to new licensees and existing applicants with authorized satellites to be launched after September 2024, though individual waivers will be considered. The rule will be applicable to all U.S.-licensed satellites, but also, to entities seeking access to the U.S. market with non-U.S.-licensed satellite. Additionally, the FCC will continue to assess whether a shorter PMD requirement, such as one year, would be appropriate for large constellations in light of the potential risks to the orbital environment posed by those systems.

The increasing number of satellites in space are mostly focused in the Low Earth Orbit (LEO) environment which brings advantages for latency and resolution. Other orbit regimes are not as popular with few operated spacecraft in Medium Earth Orbit (MEO) and classic telecommunication spacecraft in Geostationary orbits (GEO). GEO spacecraft are operated differently than LEO spacecraft as they focus on staying within their station-keeping boxes which are clearly defined and delimited. Nevertheless, GEO operators are used to conjunction scenarios such as the AEOLUS/Starlink and have systems in place to deal with it.

Figures 2.1 and 2.2 allow to compare the evolution of payload launches into both main regions over the year. In recent years, the number of objects launched into LEO is significantly larger than the number of objects launched into GEO. There is a clear tendency towards a populated LEO with small spacecraft. GEO has the characteristic of having spacecraft that appear static for an observer on Earth, leading to an environment where spacecraft are not supposed to cross paths. LEO has a more dynamic environment with spacecraft orbits evolving and changing constantly. This dynamic environment coupled with the larger number of objects leads to a more volatile environment with a larger number of conjunctions that need action. For this reason, it is decided to focus the efforts of this thesis on the LEO environment.

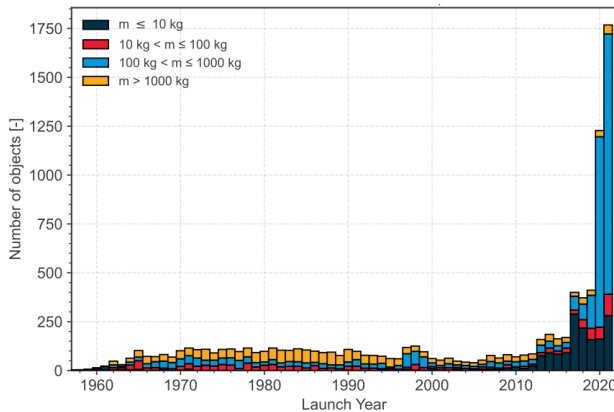


Figure 2.1: Payload launches in LEO [5].

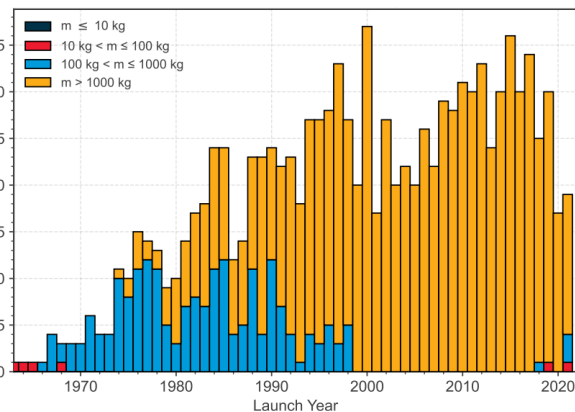


Figure 2.2: Payload launches in GEO [5].

## 2.2. Space debris environment in LEO

The Kessler syndrome, named after NASA scientist D.J. Kessler, stipulates that if the number of objects in Earth's orbit reaches a critical point, collisions between these objects trigger a snowball effect of further and self-sustained collisions [7]. The number of objects in LEO has grown significantly, with less noticeable increases in MEO and GEO. Figure 2.3 shows the expected evolution of object number in LEO compared to the evolution in case of no future launches. While the current situation has not yet reached the catastrophic scenario of the Kessler syndrome, the rising number of space objects is expected to bring with it an increasing cumulative number of catastrophic collisions. Sturza and Carretero [8] modeled the time until the Kessler syndrome by accounting for the changing debris environment through the lifetime of a constellation. Key elements to increase the time to Kessler syndrome are: reducing the number of initial passive objects and reducing the number of active satellites that fail each year.

<sup>b</sup>For spacecraft without collision avoidance capabilities it is defined as when it has completed its primary mission.



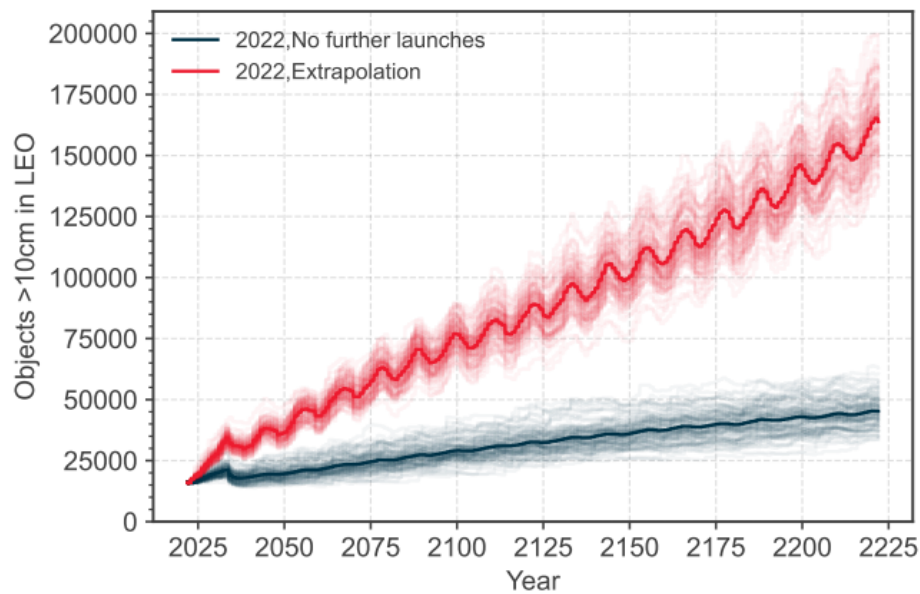


Figure 2.3: Long-term evolution of LEO objects [9, p. 19].

Additionally, LEO has seen a significant increase in the number of CubeSats and SmallSat mega-constellations. Many operators choose to deorbit their spacecraft in LEO using the Earth's atmosphere. The current LTSS guidelines require the de-orbiting of LEO spacecraft within 25 years, and many countries have incorporated these guidelines into laws. Although, from 2024 onward U.S.-licensed spacecraft will be required to deorbit within five years.

The growing number of constellations is evident in Table 2.1, which lists several proposed and ongoing projects. While there are many more projects in the works, it is worth noting that operators have filed applications for more than 100,000 new spacecraft until 2030. While not all of these plans are expected to come to fruition, even 10% of them would result in the addition of 10,000 new spacecraft to the LEO environment. This would be a significant increase, with the number of active spacecraft in orbit expected to be multiplied by a factor of 10 compared to 2014 [10].

Table 2.1: Planned satellite constellations [11] and adapted from [9] and [12].

Operator	Number of satellites	Altitude [km]	Project status
Swarm	150	300-550	Demonstration
Hongyan	320	1100	Demonstration
Astrocast	80	500-600	Demonstration
IRIS <sup>2</sup>	170	Multi-orbit (MEO and LEO)	Demonstration
Boeing V-band	2956	1200	Development
Kepler	140	550	Development
Amazon Kuiper	3236	590-630	Development
Telesat LEO	72	1000	Development
SpaceX Starlink	1584 and 7500	550 and 1110-1325	Deployment and In operation
OneWeb	720	1200	Deployment
Planet	150	370-430	In operation
Spire	100	651	In operation
Iridium	72	780	In operation
Globalstar	40 (24)	1412	In operation
LeoSat	108	1400	Suspended operations

A recent notable new constellation plan is the IRIS<sup>2</sup> from the European Commission. The multi-orbit constellation plans to provide secure communication services to the EU and its Member States as well as broadband

connectivity, with an estimated 170 LEO satellites [12].

Broadly the issues the current space debris environment brings are the following:

- The guidelines for debris mitigation set out in the 2000s are outdated, and international relations make it hard for new guidelines to be accepted quickly and uniformly.
- The current collision avoidance process of manually sorting through CDM warnings and designing maneuvers is too slow to be able to manage the increasing number of warnings.
- De-orbiting mega-constellations have high impact probabilities due to the long descent phase passing by dense altitude regimes [11].
- CubeSats or small satellites having no maneuvering capability relying on differential drag to avoid collisions brings an extra challenge.

Some of the proposals are the use of artificial intelligence to improve the collision avoidance approach, along with the use of active removal of carefully selected objects in certain regions, and the increase in reliability of maneuverability and PMD strategies especially in mega-constellations [10]. Additionally, it is recommended that future CubeSats do have maneuver capabilities for their disposal phase. Developing PMD capabilities for CubeSats is crucial to limit their impact on the LEO environment.

As space exploration progresses, the perception of an infinite frontier has been replaced by that of a crowded environment. This underscores the importance of establishing effective guidelines and regulations for space operations and emphasizes the crucial need for operators to collaborate.

## 2.3. Single action to collision avoidance

Currently, collision avoidance actions can be called unilateral. That means that whenever a conjunction is predicted (if the probability is above a certain threshold) the operators receive a warning and can decide to take action. In their modeling, their spacecraft is maneuverable while the other object is assumed to not be maneuverable; it is generally called the "target". This approach is taken because there are no guidelines on how operators should work together in case both objects in the possible conjunction are maneuverable. Until recently, this was not a problem as most conjunctions were with objects that were not maneuverable. The space industry considers a failed spacecraft a greater threat than all the operational satellites [11].

However, as illustrated by the past section the space environment is changing and warnings such as the AEOLUS/Starlink conjunction are bound to become more frequent. Regarding the emerging constellations' impact on the space environment, the Inter-Agency Space Debris Coordination Committee (IADC) and others [13] suggest that the number of conjunction alerts will rise and, as such, other operators will be impacted as well. This underlines the necessity of having efficient processes in place. Collision avoidance between maneuverable spacecraft will need to be performed more often and it is of utmost importance for maneuver plans to be communicated quickly to those affected.

The systems in place used for collision avoidance purposes include detection and tracking systems, orbit propagation, and maneuver modeling systems. The systems currently in place to warn operators are shown in the following list [14].

- U.S. Strategic Command: catalog of traceable space objects around Earth available to the public.
- Combined Space Operations Center (CSpOC) space surveillance network and orbit determination and propagation algorithms: construct the algorithm.
- Simplified general perturbation model: orbit determination and propagation algorithms.
- Two-line elements (TLE's): data format of the catalog, accuracy is limited, and information about uncertainties is omitted.
- CDMs and conjunction summary messages (CSMs): improved accuracy with respect to TLE's, more useful for time of closest approach (TCA) prediction. These messages contain detailed orbit information and full covariances of uncertainties. Only available for spacecraft operators after collision avoidance prediction. This is the preferred method of data sharing for conjunctions.

After receiving the message, operators can choose whether to take action or not. This choice is done according to the probability of collision and varies from case to case. It is recommended that operators maneuver for probabilities over  $10^{-4}$ . More information about the collision probability is given in Section 4.3, while more information on CDMs is given in Subsection 4.3.1.

## 2.4. STM tendencies

To deal with the growing space environment, STM has become a buzzword where the goal is to foster cooperation between the different actors and have better guidelines. The industry has different ideas of how an STM system should look like, and current coordination between operators is tricky [9]. STM should be defined properly so that possible solutions can be thought of.

The definitions have common and diverging points. Regarding the objectives, the common idea is that STM should provide a safer space environment by reducing collisions and radio/frequency interference. This would also require a long-term sustainable set of activities to mitigate impacts on the space environment. STM should also be built with the evolution of space activities in mind; there is a trend towards a globalization of space activities which will lead to more objects in space as outlined in Section 2.2. Space actors also agree that STM should be applied to all phases of the system's life cycle, although there is a focus on the operational and disposal phases. Additionally, STM should set rules, norms, and verification methods, as well as have operational and organizational entities such that services for all aspects mentioned can be ensured.

The disagreements lie in its implementation. One of the main debates is how much STM should regulate space activities while still allowing for self-regulation by nations. Some regulations are crucial for ensuring safety and sustainability in space, yet it is challenging to reach an international agreement on them. COPUOS established by the UN General Assembly to facilitate international cooperation in outer space, operates on a consensus basis, making it challenging to reach a global agreement on STM regulations. The Outer Space Treaty was signed in 1967 under international law, but guidelines such as the LTSS took eight years to negotiate and are not legally binding. Despite this, they are usually incorporated into national laws.

Other disagreements center on how STM regulations should be enforced and verified. While it is agreed that international cooperation is essential for an effective STM system, the division of responsibilities, the inclusion of civil and military actions, and sharing of sensitive information present challenges that must be resolved.

STM itself is not a new term and is already widely employed; the issue is making it an international cooperation system. Currently, space actors operate in a shared space with no protocols relating to collision avoidance or what procedures to follow when alerts are issued. When constellations are set up in the vicinity of an existing system many more conjunction alerts are expected which need to be manually sorted through with no real international protocol. For constellations there is also the possibility of self-conjunctions, while the operator might have procedures for this (Starlink spacecraft have automated maneuvers to avoid self-conjunction [15]), for an STM agency this could pose a problem [11].

### STM implementation proposals

Different proposals were investigated to understand what points are important for a well-functioning STM system. The common points are the need for more data sharing, the duality between transparency and security, and the preservation of autonomy.

Lal et al. [16] identifies that data sharing and coordination should be the focus of STM. This is triggered by the improvements in tracking space objects through the use of better sensors as well as including machine learning in data processing for more efficient and accurate results. Additionally, it was identified that companies and governments want to be part of the solution and are making active efforts towards it; meaning that this complex interaction will require transparency in a sector where security is important.

Furthermore, it is suggested to support the best practices and standards outlined by several entities. Regulation of collision avoidance practices needs to consider special cases such as non-propulsive CubeSats and mega-constellations. The end goal would be to have an active space traffic control similar to air traffic control, albeit this is not considered in the near future.

The French space agency CNES [17] conducted interviews and has as its aim an STM system for 2030. As before the proposal is directly linked to Space Situational Awareness (SSA) and is based on air and maritime traffic management. The system's objectives are to add coordination and rules for a shared space, to guarantee safety both in space and on ground, to support sustainable practices, and to set protocols in case of any interference. This idea is also consistent with the European Space Policy Institute as a constraint for the STM

proposal in that it does not interfere with self-regulation at a national level. The STM system translates SSA data into services for operators. This requires real-time messages, the use of artificial intelligence and data mining, traffic prediction, and reliable systems.

Lastly, a study by Nag et al. [18] identifies that an STM implementation should allow for self-regulation and work even with non-participating operators and private data. The collision avoidance applications proposed are: registration of spacecraft, conjunction screening, and proposal of avoidance maneuvers. As many factors impact possible maneuvers the decisions should be made by combining policies and the technologically optimal option. The STM system includes a Spaceflight Information Management System which serves as a connector between national authorities, themselves linked to international authorities, and the STM system.

The need for autonomy to help track patterns, add additional observations and sensors, and perform trade-offs is clear. Trade-offs are required for weighting between having more data and increased cost, increased certainty of maneuver necessity, and increased  $\Delta V$  cost.

Nag et al. [18, p. 5-6] presents several systems for avoiding collisions between active spacecraft: the "rules-based-system", "dual-maneuver implicit cost split", "auction-based system", "resource-based system", and "space-chicken". In the rules-based system, operators must follow a predefined set of rules for all scenarios. The dual-maneuver system requires the quantification of costs for halting activities and financial compensation from one operator to another. The auction system involves one operator proposing financial compensation to the other, and a bargaining process ensues to ensure the maneuvering operator is compensated. The resource-based system suggests that the operator with the lowest cost for maneuvering should act. Lastly, the "space-chicken" system provides no guidance, and operators must either wait for the other to act or take action themselves, or both operators may choose to do nothing.

These systems do not seem ideal, the cost of different mission aspects is hard to quantify and there is no direct way to ensure that all operators will follow the protocol set out. However, they are a step in the right direction. In the following chapters, the focus will be put on building up a combined action for collision avoidance and proposing a framework for negotiation between operators.

This chapter introduces the concepts necessary to construct the combined action model to collision avoidance. First, the coordinates and reference frames used in this thesis are presented in Section 3.1. Then, the concepts used in the calculation of collision probability are explained in Section 3.2. The focus is changed onto orbit perturbations in Section 3.3. Finally, the optimization algorithm selection is given in Section 3.4.

### 3.1. Coordinates and reference frames

Coordinates and reference frames are the basis of any problem related to orbital dynamics, it is crucial to know which are used to understand the problem fully. A quick explanation on useful coordinates is given in Subsection 3.1.1, followed by the definition of reference frames used in this thesis in Subsection 3.1.2. The methods to change between these frames are presented in Subsection 3.1.3.

#### 3.1.1. Coordinates

Coordinates are used to describe the spacecraft's state vector in the reference frame. With this, their current behavior can be explained allowing for dynamical equations in time [19]. Two main coordinate systems will be used and interchanged in this thesis: the Cartesian coordinates and the orbital elements also known as Keplerian elements.

Keplerian elements describe a unique orbit of a celestial object, in terms of its size, shape, and orientation. A Cartesian state vector, on the other hand, describes the position and velocity of the object in three-dimensional space. Converting from Keplerian elements to Cartesian state vector and vice-versa is a standard operation.

As mentioned, Cartesian coordinates are used in three dimensions, allowing to describe the position, velocity and acceleration of the spacecraft. The following vector will be used:  $[x, y, z, v_x, v_y, v_z]^T$ . Here  $x, y, z$  are the position components on the three axes of the reference frames and  $v$  describes the velocity components on these axes.

The Keplerian elements are described with the following vector:  $[a, e, i, \Omega, \omega, \theta]^T$  [19].  $a$  stands for the orbit's semi-major axis,  $e$  the eccentricity and  $i$  the inclination.  $\Omega$  is known as the right ascension of the ascending node,  $\omega$  as the argument of periapsis and  $\theta$  as the true anomaly. Additionally,  $E$  and  $M$  can be used as well, representing the eccentric and mean anomaly respectively.

#### 3.1.2. Reference frames

The inertial frame is defined based on Newton's first law: "An inertial reference frame is a reference frame with respect to which a particle remains at rest or in uniform rectilinear motion if no resultant force acts upon that particle." [19, p. 3]. This means that when an inertial reference frame is used no apparent forces need to be accounted for in the spacecraft dynamics, which is why it is so useful in this problem formulation.

As the problem at hand deals with spacecraft around Earth, the Earth Centered Inertial (ECI) frame will be used as a baseline. The ECI frame has its origin at the center of the Earth but is not fixed to the Earth, hence it does not rotate with the Earth. The positive X-axis points to the vernal equinox while the Z-axis points in the direction of the geographical North Pole with the Y-axis completing the right-hand coordinate set.

There are different definitions of the ECI frame; a common one is the J2000. It is defined with the Earth's mean equator and mean equinox as defined at 12:00 on the 1<sup>st</sup> of January 2000. In this frame the Z-axis is pointed towards the North Pole as it was at that time and the Y-axis is rotated by 90° East around the celestial

equator. The propagation done in this thesis will use the J2000 frame as orientation.

Additionally, it is important to define local object frames when the spacecraft itself is included in the problem. This will be necessary when the position relative to the orbit becomes important, for example when the spacecraft maneuvers need to be defined.

A local SNW frame can be defined where S is the radial direction component, N is the component in the orbital plane perpendicular to the radius vector pointing in the direction of motion and W is the component perpendicular to the orbital plane in the direction of the orbital angular momentum vector.

This frame has several alternative names, such as RIC with R denoting the radial direction, I the in-track direction and C the cross-track direction.

Specifically for collision probability calculation, the conjunction encounter plane also called the B-frame is important. To describe the probability of collision three-dimensional position error covariance matrices are used to quantify the position uncertainty of objects. These can be formulated into different density functions. The three-dimensional position error covariance matrix can be projected onto this special frame. The B-frame is defined as perpendicular to the relative velocity vector ( $v_r$ ) of the conjunction objects (debris denoted as  $d$  and satellite denoted as  $s$ ) as shown in Figure 3.1.

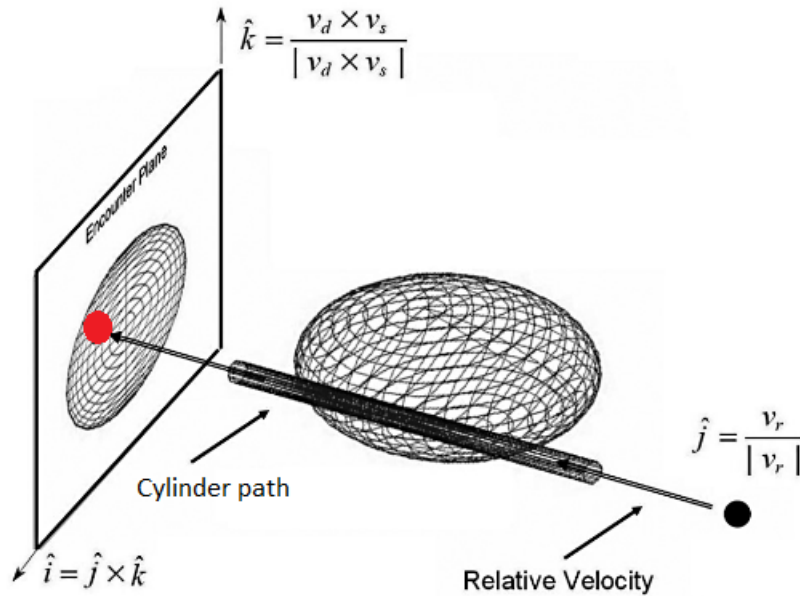


Figure 3.1: Projection of conjunction onto the B-frame as a circle (marked in red) [20, p. 486].

The secondary object travels along the relative velocity vector passing through the ellipsoid. This creates a cylinder path, which when perpendicularly projected onto the B-frame becomes an ellipse. Conjunction is defined to occur when the cylinder collides with the primary object. At this point, the distance between the centers of the two objects involved  $s$  is less than the sum of their radii in the B-frame [20].

### 3.1.3. Transformations

The above mentioned coordinates and reference frames are used interchangeably during the thesis so it is important to understand how the information can be converted from one convention to the other. The transformation between Keplerian and Cartesian coordinates (or vice versa) is straightforward and often applied in this thesis using standard functions from TudatPy. The reader can find more information about this in Chapter 11 of Wakker [19]. The frame transformations are explained in more detail in the coming paragraphs.

#### ECEF to ECI

The main frame used in this thesis is the ECI frame. However, the data necessary includes the object states given by CDMs which are represented in an Earth Centered Earth Fixed reference frame (ECEF). This means they need to be transformed into the ECI frame. The difference between both frames can be seen in Figures 3.2 and 3.3. ECEF coordinates have the same origin (Earth center) and third (polar) axis as ECI coordinates but co-rotate with the Earth. As a consequence, ECI and ECEF longitudes differ only by a linear function of time.

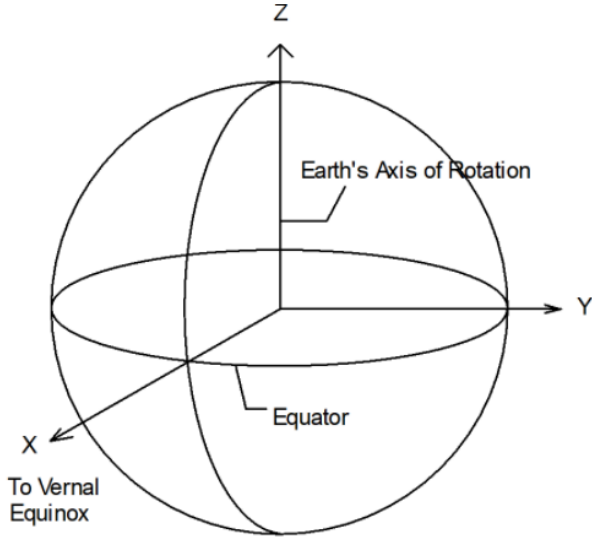


Figure 3.2: Earth-Centered Inertial (ECI) coordinate system. [21]

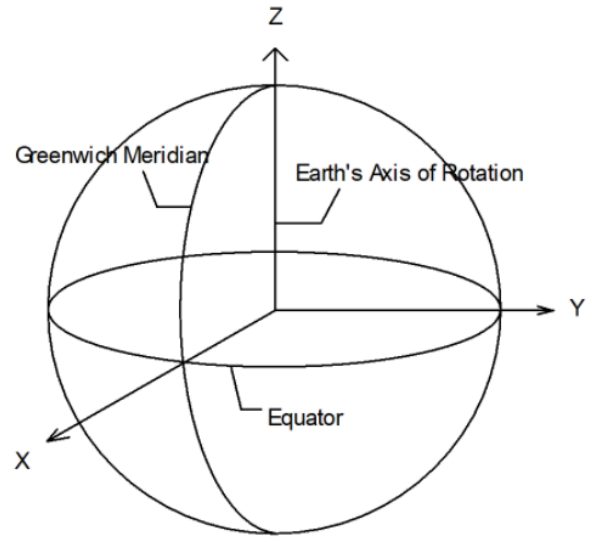


Figure 3.3: Earth-Centered Earth-Fixed (ECEF) coordinate system [21].

The transformation from ECI to ECEF coordinates is a time-varying rotation due primarily to the Earth's rotation, containing also slower varying terms for precession, nutation and polar wander. The ECI-to-ECEF rotation matrix is expressed as a composite of these transformations:  $T = ABCD$  (A=polar motion, B=sidereal time, C=nutation, D=precession), with each term a 3x3 matrix.

#### ECI to RTN

Later it will be shown that the covariance matrix delivered by the CDMs are necessary in the ECI frame for the collision probability calculation. However, they are provided in the local spacecraft frames. Hence, determining the rotation between the ECI and local frames is necessary. To do so, the position and velocity vectors  $\mathbf{r}$  and  $\mathbf{v}$  of the objects are necessary. They are used to build the rotation matrix as shown below:

$$\begin{aligned} \mathbf{n} &= \mathbf{r} \times \mathbf{v} \\ \bar{R} &= \|\mathbf{r}\| \\ \bar{N} &= \|\mathbf{n}\| \\ \bar{T} &= \bar{N} \times \bar{R} \end{aligned} \quad (3.1)$$

$$R_{ECItoRTN} = \begin{bmatrix} \bar{R}_x & \bar{T}_x & \bar{N}_x \\ \bar{R}_y & \bar{T}_y & \bar{N}_y \\ \bar{R}_z & \bar{T}_z & \bar{N}_z \end{bmatrix} \quad (3.2)$$

#### ECI to B-frame

For the collision probability calculation two steps require the transformation from the ECI frame to the B-frame so understanding this transformation is important.

The 2D B-frame origins at the target object (Figure 3.1). Equation 3.3 defines the relative position and velocity vector as the state of the risk object relative to the target object. The vectors  $\bar{X}_B$  and  $\bar{Y}_B$  are dependent upon the inertial position and velocity difference at the Time of Closest Approach (TCA) as shown in Equation 3.4.

$$\Delta \mathbf{r}(t) = \mathbf{r}_{chaser}(t) - \mathbf{r}_{target}(t) \quad \Delta \mathbf{v}(t) = \mathbf{v}_{chaser}(t) - \mathbf{v}_{target}(t) \quad (3.3)$$

$$\begin{aligned} \bar{X}_B &= \frac{\Delta \mathbf{r}_{TCA}}{\|\Delta \mathbf{r}_{TCA}\|} \\ \bar{Y}_B &= \frac{(\Delta \mathbf{r}_{TCA}) \times (\Delta \mathbf{v}_{TCA})}{\|(\Delta \mathbf{r}_{TCA}) \times (\Delta \mathbf{v}_{TCA})\|} \end{aligned} \quad (3.4)$$

The transformation vector  $R_{X_B, Y_B}$  in Equation 3.5 is used to create the covariance matrix  $C_B$  in Equation 3.6 in the B-frame; mapping the 3D covariance matrix  $C = C_{X,Y,Z}$  (shown in Equation 3.7) onto the 2D plane. The  $C_B$  covariance is used in the probability calculation.

$$R_{X_B, Y_B} = \begin{pmatrix} X_{B,X} & X_{B,Y} & X_{B,Z} \\ Y_{B,X} & Y_{B,Y} & Y_{B,Z} \end{pmatrix} \quad (3.5)$$

$$C_B = C_{X_B, Y_B} = R_{X_B, Y_B} C R_{X_B, Y_B}^T \quad (3.6)$$

### 3.2. Probability calculation

For the probability calculation inputs from the CDMs are necessary. The data needed is explained in the following list and a CDM example is given in Appendix A.

1. Size of the objects:

- The size of the primary and secondary objects is given in square meters and is referred to as AREA\_PC in the CDM.
- In the probability of collision calculation, as done by the CSpOC, the size is specified in meters using the Radius of Exclusion Volume.
- Default values for the Radius of Exclusion Volume are provided: 5 m for payloads and platforms, 3 m for rocket bodies and unknown objects, and 1 m for debris.

2. Position and velocity vectors:

- The CDM contains the position and velocity vectors of both the primary and secondary objects at time of closest approach (TCA).
- The position vectors (X, Y, Z) in kilometers, and the velocity vectors (X\_DOT, Y\_DOT, Z\_DOT) in kilometers per second.
- These vectors are typically referenced to the International Terrestrial Reference Frame (ITRF). Other coordinate frames may also be specified according to the relevant standards given in *Conjunction Data Message* [22].

3. Relative position and velocity:

- The CDM provides the relative position and velocity of the secondary object with respect to the primary object at TCA.
- The relative position and velocity are given in the RTN frame of the primary object.
- Additionally, the overall MISS\_DISTANCE and RELATIVE\_SPEED are included to provide information about the separation distance and relative speed between the objects at TCA.

4. Covariance matrix:

- The CDM includes separate covariance matrices for the primary and secondary objects.
- The covariance matrices are typically provided in a 6x6 form as seen in Equation 3.7. For the probability of collision calculation only the position portion is needed.

$$C = \begin{bmatrix} \sigma_R^2 & \sigma_{R,T} & \sigma_{R,N} & \sigma_{R,\dot{R}} & \sigma_{R,\dot{T}} & \sigma_{R,\dot{N}} \\ \sigma_{T,R} & \sigma_T^2 & \sigma_{T,N} & \sigma_{T,\dot{R}} & \sigma_{T,\dot{T}} & \sigma_{T,\dot{N}} \\ \sigma_{N,R} & \sigma_{N,T} & \sigma_N^2 & \sigma_{N,\dot{R}} & \sigma_{N,\dot{T}} & \sigma_{N,\dot{N}} \\ \sigma_{\dot{R},R} & \sigma_{\dot{R},T} & \sigma_{\dot{R},N} & \sigma_{\dot{R}}^2 & \sigma_{\dot{R},\dot{T}} & \sigma_{\dot{R},\dot{N}} \\ \sigma_{\dot{T},R} & \sigma_{\dot{T},T} & \sigma_{\dot{T},N} & \sigma_{\dot{T},\dot{R}} & \sigma_{\dot{T}}^2 & \sigma_{\dot{T},\dot{N}} \\ \sigma_{\dot{N},R} & \sigma_{\dot{N},T} & \sigma_{\dot{N},N} & \sigma_{\dot{N},\dot{R}} & \sigma_{\dot{N},\dot{T}} & \sigma_{\dot{N}}^2 \end{bmatrix} \quad (3.7)$$

$$\text{Units:} \begin{pmatrix} \text{m}^2 & \text{m}^2 & \text{m}^2 & \text{m}^2/\text{s} & \text{m}^2/\text{s} & \text{m}^2/\text{s} \\ \text{m}^2 & \text{m}^2 & \text{m}^2 & \text{m}^2/\text{s} & \text{m}^2/\text{s} & \text{m}^2/\text{s} \\ \text{m}^2 & \text{m}^2 & \text{m}^2 & \text{m}^2/\text{s} & \text{m}^2/\text{s} & \text{m}^2/\text{s} \\ \text{m}^2/\text{s} & \text{m}^2/\text{s} & \text{m}^2/\text{s} & \text{m}^2/\text{s}^2 & \text{m}^2/\text{s}^2 & \text{m}^2/\text{s}^2 \\ \text{m}^2/\text{s} & \text{m}^2/\text{s} & \text{m}^2/\text{s} & \text{m}^2/\text{s}^2 & \text{m}^2/\text{s}^2 & \text{m}^2/\text{s}^2 \\ \text{m}^2/\text{s} & \text{m}^2/\text{s} & \text{m}^2/\text{s} & \text{m}^2/\text{s}^2 & \text{m}^2/\text{s}^2 & \text{m}^2/\text{s}^2 \end{pmatrix}$$



- A covariance matrix represents the uncertainty in a satellite's state vector. The diagonal elements represent the variance in each component (R, T, and N), and the off-diagonal terms represent the covariances between the components.
- The covariance matrix for each object is referenced to its own RTN coordinate frame.
- By generating a diagonal matrix from the 3x3 covariance matrix, the size, shape, and orientation of the one-standard-deviation three-dimensional error ellipsoid is obtained, which visualizes the position uncertainty at TCA. The matrix's eigenvalues give the sizes of the ellipsoid axes, and the eigenvectors that make up the new set of axes of the diagonal matrix provide the orientation of the axes relative to the object's RTN coordinate frame.

The following assumptions are implemented into the calculation [23]:

- Object sizes are known or can otherwise be assigned an upper bound.
- The conjunction is "hyperkinetic", meaning that the conjunction duration is short; this allows the additional simplifying assumption that the relative motion between objects is rectilinear throughout the encounter.
- Gaussian theory and statistics apply.
- Covariance for both objects is known and constant throughout the hyperkinetic encounter.
- Primary and secondary errors are independent allowing "combined" covariance to be the simple sum of the individual covariances (in a common frame), resulting in the "joint" covariance.
- The covariance is not "too large" nor is it "too small". A correct calculation of  $P_c$  is confined by the quality of the covariance [24]. A too large covariance matrix can trigger false alarm while a too small one can fail to trigger an alarm.

If the conjunction is long-term (small relative velocity), both the magnitude and direction of the relative velocity will change during the conjunction [24]. The linear relative motion region might be smaller than the encounter region, meaning an incorrect  $P_c$  could be obtained. This would be the case for example for formation flying spacecraft, rendezvous or conjunctions in GEO. None of these cases will be handled in this thesis, so the  $P_c$  calculation for long-term encounter will not be discussed.

The density function of the probability of encountering an object within  $\Delta \mathbf{r}$  of another object's position is calculated from Equation 3.8 [25]. It needs to be integrated over the volume generated by combining the spheres around the primary and secondary objects  $V_c$  as shown in Equation 3.9.  $C$  is the combined covariance matrix:  $C = C_1 + C_2$ .

$$p(\Delta \mathbf{r}) = \frac{1}{\sqrt{(2\pi)^3 \det(C)}} \exp \left[ -\frac{1}{2} \Delta \mathbf{r}^T C^{-1} \Delta \mathbf{r} \right] \quad (3.8)$$

$$P_c = \frac{1}{\sqrt{(2\pi)^3 \det(C)}} \int_{V_c} \exp \left[ -\frac{1}{2} \Delta \mathbf{r}^T C^{-1} \Delta \mathbf{r} \right] dV \quad (3.9)$$

The volume integral can be reduced to a surface integral. This is done by mapping the position error ellipsoid on a constant B-frame, which consists of the elliptical contours with constant probability (as seen in Figure 3.1). The range vector at time of closest approach  $\Delta \tilde{\mathbf{r}}_{tca}$  then lies within the B-frame.

The last step before continuing with the full collision probability equation is the determination of the orientation of the elliptic contour, which is determined with the eigenvalues and the eigenvectors of the B-frame covariance matrix  $C_B$ . The semi-major axis of the ellipse is defined by the highest value of the two eigenvalues and the semi-minor axis of the ellipse is defined by the lowest of the two values. Using this orientation, the eigenvectors can then be used to translate the conjunction position to coordinates in the B-frame. The eigenvectors are depicted by  $\mathbf{x}_B$  and  $\mathbf{y}_B$  and the eigenvalues by  $\sigma_1$  and  $\sigma_2$ .

To simplify further, the elliptical collision area is assumed to be square. Now, the collision probability does not have to be integrated over a sphere, but instead can be done by integrating over a rectangle. The last step that will be added is to rewrite the entire equation in error function terms, defined in Equation 3.10. This simplifies the implementation in code. This simplification is also mentioned by 18SPCS, which provides the CDMs to the operators [14].

$$\left(\frac{c}{\pi}\right)^{\frac{1}{2}} \int_a^b e^{-cx^2} dx = \frac{1}{2} (\text{erf}(b\sqrt{c}) - \text{erf}(a\sqrt{c})) \quad (3.10)$$

$$P_c = \frac{1}{2} \left[ \text{erf}\left((x_B + R_c) \sqrt{\frac{1}{2\sigma_1^2}}\right) - \text{erf}\left((x_B - R_c) \sqrt{\frac{1}{2\sigma_1^2}}\right) \right] \cdot \frac{1}{2} \left[ \text{erf}\left((y_B + R_c) \sqrt{\frac{1}{2\sigma_2^2}}\right) - \text{erf}\left((y_B - R_c) \sqrt{\frac{1}{2\sigma_2^2}}\right) \right] \quad (3.11)$$

This formulation of the collision probability is used in this thesis.

Besides the collision probability, the miss distance and the relative speed are also important as they provide important insight on the geometry of the problem. This means getting the position and velocity of the target satellite relative of the chaser satellite in the RTN frame. To do the following equations can be used.

$$\begin{aligned} \delta &= \mathbf{x}_{ECI,target} - \mathbf{x}_{ECI,chaser} \\ \mathbf{r}_{RTN} &= R_{ECItoRTN} \cdot \delta \end{aligned} \quad (3.12)$$

$$\begin{aligned} \dot{\mathbf{f}} &= \frac{||(\mathbf{r}_{chaser} \times \mathbf{v}_{chaser})||}{||\mathbf{r}_{chaser}||^2} \\ \omega &= [0, 0, \dot{\mathbf{f}}]' \\ \dot{\delta} &= \mathbf{v}_{ECI,target} - \mathbf{v}_{ECI,chaser} \\ \mathbf{v}_{RTN} &= R_{ECItoRTN} \cdot \dot{\delta} - (\omega \times \mathbf{r}_{RTN}) \end{aligned} \quad (3.13)$$

From this the miss distance between the satellites and the relative speed can be found by:

$$\begin{aligned} D_{miss} &= ||\mathbf{r}_{RTN}|| \\ V_{rel} &= ||\mathbf{v}_{RTN}|| \end{aligned} \quad (3.14)$$

The verification for the probability of collision calculation is carried out in Section 4.3 for a number of CDMs received. In the verification, also the CDM present in Appendix A is examined, file number 86.

### 3.3. Perturbations

To model avoiding collisions, the object states need to be propagated. This section focuses on introducing the perturbations that will be used for the dynamical model generation. These perturbations are chosen to match the model used to generate CDMs as closely as possible. The model parameters to generate CDMs vary in the following way [22]:

- Gravity model: different geo-potential gravity models that use spherical harmonic coefficients can be used with varying degree and order.
- Atmospheric model: different Earth atmospheric models are available to model the drag on the object.
- Third-body perturbations: how many (if any) other celestial bodies perturbations should be included
- Solar radiation pressure: these perturbations are included or not
- Earth tides: perturbations due to solid Earth and ocean tides are included or not.

The specifics of these perturbations will be described in the following subsections. Unless stated otherwise this information was obtained from Wakker [19]. The Earth tides are not modeled in this thesis because no model was available.

#### 3.3.1. Earth's gravitational perturbation

The Earth's shape and mass distribution are not uniform, which affects spacecraft orbits. The gravitational attraction of the Earth can be described by Equation 3.15 using spherical coordinates  $(r, \phi, \Lambda)$  and Legendre functions and coefficients  $(P_{n,m}, C_{n,m}, S_{n,m})$ , where  $n$  and  $m$  indicate the degree and order. Another formulation, Equation 3.16, replaces the model coefficients with  $J_n$  and  $J_{n,m}$  terms, assuming a static external potential and neglecting the effects of solid-Earth and ocean tides. The perturbing acceleration is given by Equation 3.17.

$$U = -\frac{\mu}{r} \left[ 1 + \sum_{n=2}^{\infty} \sum_{m=0}^n \left(\frac{R}{r}\right)^n P_{n,m}(\sin \phi) \{C_{n,m} \cos m\Lambda + S_{n,m} \sin m\Lambda\} \right] \quad (3.15)$$

$$U = -\frac{\mu}{r} \left[ 1 - \sum_{n=2}^{\infty} J_n \left( \frac{R}{r} \right)^n P_n(\sin \phi) + \sum_{n=2}^{\infty} \sum_{m=1}^n J_{n,m} \left( \frac{R}{r} \right)^n P_{n,m}(\sin \phi) \{ \cos m (\Lambda - \Lambda_{n,m}) \} \right] \quad (3.16)$$

$$\mathbf{f}_{gravity,pert} = -\nabla \left( U + \frac{\mu}{r} \right) \quad (3.17)$$

State-of-the-art gravity models can include coefficients up to high degrees and orders, but computational time can be reduced by truncating the model at a certain degree and order. For most problems, the effects of  $J_{n,m}$  terms are negligible due to their averaging out over periods longer than a day. The degree and order two ( $J_{2,2}$ ) effect can cause orbital resonance over long periods, and the  $J_2$  effect, being much larger than other  $J$  coefficients, is often the only coefficient included initially. Nonetheless, other coefficients can also have a significant influence, especially in LEO, and should be considered.

### 3.3.2. Atmospheric drag

The Earth's atmosphere exerts drag on spacecraft in LEO, causing them to lose energy and move to a lower orbit. To counteract this effect, thrusters must be used, while if it is desired, drag can be used for collision avoidance and de-orbiting. The perturbing acceleration acting on the spacecraft due to atmospheric drag is given by Equation 3.18.

$$\mathbf{f}_{drag,pert} = -C_D \frac{1}{2} \rho \frac{A}{m} \|\mathbf{v}\| \mathbf{v} \quad (3.18)$$

The acceleration experienced by the spacecraft due to drag depends not only on its geometry and mass but also on the density of the atmosphere, which varies diurnally due to the Earth's rotation, semi-annually due to the Earth-Sun distance, monthly due to the Sun's rotation, and over the 11-year solar activity cycle which causes the solar minimum and maximum. Hence, the atmospheric density is a function of altitude, latitude, time, solar activity, and season.

### 3.3.3. Third-body gravitational perturbation

The motion of a spacecraft orbiting Earth can be affected by the gravitational pull of other celestial bodies. Depending on the problem, the Moon and/or the Sun may be included as point-mass perturbations, or more precise gravity models may be necessary. The gravitational influence of third bodies can be described using the perturbing potential in Equation 3.19, where  $j$  represents the perturbing celestial body and  $i$  the spacecraft. The rectangular components of the perturbation acceleration (in an inertial, Earth-centered frame) are shown in Equation 3.20.

$$R = -G \sum_{j \neq k, i} m_j \left( \frac{1}{r_{ij}} - \frac{\mathbf{r}_i \cdot \mathbf{r}_j}{r_j^3} \right) \quad (3.19)$$

$$\begin{aligned} f_{body,x,pert} &= \mu_j \left( \frac{x_j - x_i}{r_{ij}^3} - \frac{x_j}{r_j^3} \right) \\ f_{body,y,pert} &= \mu_j \left( \frac{y_j - y_i}{r_{ij}^3} - \frac{y_j}{r_j^3} \right) \\ f_{body,z,pert} &= \mu_j \left( \frac{z_j - z_i}{r_{ij}^3} - \frac{z_j}{r_j^3} \right) \end{aligned} \quad (3.20)$$

### 3.3.4. Solar radiation pressure perturbation

To account for solar radiation pressure perturbation, different types of radiation forces may be considered, such as direct sunlight, albedo, or thermal infrared radiation. Typically, only direct sunlight is considered. This effect is described in Equation 3.21, where  $C_R$  represents the spacecraft's reflectivity,  $A$  is the cross-sectional area,  $c$  is the speed of light,  $W$  is the intensity of radiation, and  $\hat{\mathbf{u}}_s$  is the relevant unit vector. As the Sun's activity varies over time, this perturbation can also experience changes.

$$\mathbf{f}_{srp,pert} = -C_R \frac{WA}{mc} \hat{\mathbf{u}}_s \quad (3.21)$$

### 3.4. Optimization algorithm selection

Once the collision probability is calculated and the states are propagated, the need for collision avoidance maneuvers needs to be identified and then the optimal ones need to be designed. To do so an optimization algorithm is used. This section deals first with general choices regarding optimization methods in Subsection 3.4.1 and then with the selection of the algorithm in Subsection 3.4.2.

#### 3.4.1. General optimization aspects

Heuristic algorithms are less limited by problem characteristics compared to classical optimization methods. However, they can have exponentially increased computation time due to the number of searches per generation or population [26].

Optimization algorithms, such as genetic algorithms and particle swarm optimization, can be used to solve spacecraft collision avoidance problems by finding the optimal trajectory for a spacecraft to avoid colliding with other objects in space.

The optimization problem aims to find a trajectory that minimizes a cost function considering various factors, such as spacecraft-object positions and velocities, velocity and acceleration constraints, and mission requirements. The algorithm generates candidate trajectories, evaluates their cost, and iteratively adjusts them until an optimal solution is obtained.

Overall, optimization algorithms are a powerful tool for solving spacecraft collision avoidance problems as they can take into account a large number of constraints and factors, and generate solutions that are robust and reliable.

Two different types of algorithms can be used to reach the best solution: single-objective and multi-objective optimization algorithms. As the names hint at, the main difference between the two lies in the number of objectives that the algorithm seeks to optimize.

Single-objective optimization algorithms find the solution that maximizes or minimizes a single objective. In contrast, multi-objective optimization algorithms aim to find a set of trade-off solutions for problems with multiple (typically conflicting) objectives. These algorithms balance multiple objectives instead of focusing on a single best solution. For instance, in an engineering design problem, objectives may include minimizing mass, maximizing propellant efficiency, and reducing cost.

In multi-objective optimization, the challenge is that there is typically no single optimal solution for all objectives. The objective is to find a set of solutions that represent a trade-off between the objectives, known as Pareto optimal solutions, which are preferred by the decision-maker.

As the problem in this thesis will introduce the combined action for collision avoidance, it is expected that operators will want to account for different factors in their discussion. With that in mind, a multi-objective formulation is required for the optimization.

To represent graphically multiple, often conflicting objectives, Pareto fronts are used. The Pareto front represents the set of optimal solutions that are not dominated by any other solution in the collection of potential solutions [27]. A solution is said to dominate another solution if it is better in all objectives and no worse in at least one objective. A solution is Pareto optimal if there is no other solution that dominates it. In a multi-objective optimization problem, the Pareto front can help the decision-maker to understand the trade-off relationships between the objectives and make informed decisions.

#### 3.4.2. Algorithm choice

To select the optimization algorithm, different attempts at optimizing the Collision Avoidance Maneuver (CAM) are looked into. However, in literature most attempts found reformulated the multiple objectives into a single-objective equation. As they deal with different cases and explore different optimizers, important insight can be gained from them as to which algorithm would be suitable for the problem at hand.

The first article investigated compares four algorithms for CAM optimization in the scenario where multiple objectives create conjunctions with the spacecraft [28]. The main objective is to minimize  $\Delta V$ . The algorithms used are: Genetic Algorithm (GA), Particle Swarm Optimization (PSO), Differential Evolution (DE) and Simulated Annealing (SA).

Then, a study on CAM optimization with multiple space debris using GA is reviewed. This article is interesting

as it considers 3D maneuvering. In [29], the objective is to minimize  $P_c$  and penalties are introduced to minimize propellant usage.

Next, the study related to CAM optimization for cluster spacecraft avoiding a space debris cloud is delved into. Here, it was important to also maintain the configuration within the cluster. Seong and Kim [26] explores several algorithms: GA, PSO, DE and a combination of PSO and Gravitational Search Algorithm, the PSOGSA algorithm. The objective is to minimize propellant usage.

The last article with a single-objective formulation that is looked into is [30]. It considers both LEO and GEO cases, where the algorithm used is GA. The fitness function is made from a combination of propellant,  $P_c$  and orbit disturbance related to the station-keeping area.

Wolfhagen [31] proposes an optimization of 3D maneuver in a spacecraft to avoid the conjunction and account for the constellation performance loss, this formulation is further explained in Subsection 4.5.2. The thesis uses a Multi-objective Evolutionary Algorithm based on Decomposition (MOEA/D) with different function evaluations to solve the problem. MOEA/D is based on DE.

These studies are used to compare the outcome from different optimization algorithms for problems similar to the problem this thesis deals with. A summary of the conclusions drawn is presented in Table 3.1.

**Table 3.1: Summary of different algorithm investigations from literature.**

	Algo.	Description	Inputs	Findings
[26]	GA, PSO, DE, PSOGSA	Maintain satellite cluster while avoiding debris cloud	Pop. size: 50; Gen. # 50 Pop. size 25; Gen. # 100	PSOGSA achieved the best results in optimizing the avoidance maneuver plan for cluster satellites. Larger population sizes (50) generally led to better solutions for all algorithms except DE. PSOGSA had the fastest convergence speed, while GA had the lowest efficiency and longest convergence time.
[28]	GA, PSO, DE, SA	Benchmark tests  Single object avoidance using 1D CAM  Multiple object avoidance using 3D CAM	Pop. size: 20 (GA, PSO, DE); Gen. # 1000 (20000 SA)  Pop. size: 20 (GA, PSO, DE); Gen. # 50 (1000 SA)  Pop. size: 20 (GA, PSO, DE); Gen. # 50 (1000 SA)	PSO was the most effective algorithm, followed by DE, while GA and SA had lower performance.  All heuristic algorithms met the minimum range requirement for collision risk mitigation. DE and PSO performed well with minimal $\Delta V$ , while GA and SA had poorer $\Delta V$ minimization performance.  DE had the lowest fitness value, followed by PSO, SA, and GA. All algorithms met the minimum range requirement by reducing the satellite's altitude. The maneuver start times were mostly near the lower boundary, except for SA.
[29]	GA	Simple case  Complex case - 3D maneuver	Pop. size: 20; Gen. # 300  Pop. size: 200; Gen. # 200	Only considering the in-track direction velocity increment does not satisfy the allowable $P_c$ for Space Debris 3. However, when considering the velocity increments in all three RIC directions, the $P_c$ requirement is met. This emphasizes the need to consider maneuvers in directions other than just the in-track direction, depending on the specific case and purpose.
[30]	GA	GEO station keeping  LEO ground track maintenance	Pop. size: 5; Gen. # 200  Pop. size: 5; Gen. # 200	GA showed good performance for avoidance maneuvers regarding GEO satellites.  GA showed good performance for avoidance maneuvers regarding LEO satellites.

Table 3.1: Summary of different algorithm investigations from literature.

	Algo.	Description	Inputs	Findings
[31]	MOEA/D	Minimize: $P_c$ , constellation performance loss and $\Delta V$ impulse with 3D maneuver	Pop. size: 100; Gen. # 30, Neighborhood # 10	Results were reached for minimizing $P_c$ and propellant consumption in 3000 function evaluations. Including constellation performance loss increase the function evaluations to 7875. The solutions require almost the maximum amount of available propellant per maneuver (0.1 m/s).

The SA algorithm presented bad results in comparison to the others while also requiring high generation numbers, so it is not considered further. GA is the most used algorithm, yet it does not present the best results in all cases. Additionally, it comes with the restraint that a large number of generations are necessary.

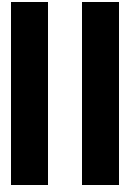
DE is also a commonly used algorithm and it presented good results in this problem. However, DE algorithms are known for having larger convergence speeds especially in high-dimensional problems, as well as requiring larger population sizes [32]. As pointed out in [31] (using MOEA/D), a larger number of generations (more than double) is necessary when three objectives are considered in the fitness function. PSOGSA demonstrated faster convergence when finding specific local solutions [26]. For the problem dealt with in the article, it provided good results. However, its behavior could lead to finding only local solutions and not global ones.

Although, in [28], DE showed the best performance, the results from PSO were similar in all cases. It showed a very stable behavior. In the other case, where PSO was also considered, it came in second in terms of convergence speed [26]. This algorithm is known for its good search capabilities and its sensitivity to parameters. This algorithm performs better for large search spaces than other algorithms [26].

As the problem at hand will require optimization with multiple objectives and different propagations, the PSO algorithm is preferred over the other algorithms presented here. Its implementation in multi-dimensions can be done with the Non-dominated Sorting Particle Swarm Optimization (NSPSO) algorithm. The algorithm works as follows [33]:

- Initialization: The population is initialized with a set of particles, each with a randomly generated position in the solution space and a velocity.
- Non-dominated sorting: The particles are sorted into non-dominated fronts, where the solutions in the first front are considered the most desirable (hence the Pareto front). The solutions in each subsequent front are considered less desirable, as they are dominated by at least one solution in the previous front.
- Update personal best positions: The personal best position of each particle is updated to its current position if it is on a non-dominated front and better than its previous personal best position.
- Update global best position: The global best position is updated to the position of the particle in the first non-dominated front that has the best fitness value.
- Update velocities: The velocities of the particles are updated using a combination of their personal best position, the global best position, and a random factor, guided by the inertia weight, and social acceleration coefficient.
- Update positions: The positions of the particles are updated based on their velocities.
- Repeat: The algorithm continues to repeat the above steps until a stopping criterion is met, such as a maximum number of iterations.

The final output of the NSPSO algorithm is the set of non-dominated solutions stored in the archive, representing the "best" trade-off solutions for the multi-objective optimization problem. These particles are part of the Pareto front. It is important to note that NSPSO is a stochastic algorithm, so the exact behavior of the algorithm may vary depending on the specific optimization problem being solved and the values of the algorithm's parameters. The tuning of this algorithm is important. The tuning methodology is presented in Subsection 4.5.3 and the results in Section 6.4.



## Approach to solving the problem

The second part contains the details of the methodology utilized to solve the problem: the tools necessary, the defined dynamics model, the collision avoidance probability calculation and maneuver implementation, and finally the application of the optimization algorithm. It is presented in Chapter 4. Furthermore, details of the code set-up are given in Chapter 5. The first, preliminary results are presented in Chapter 6, along with a review of the optimization method. Finally, this part defines the simulation scenarios in Chapter 7.





# Methodology

After having identified the theoretical rationale necessary, this chapter deals with the procedure applied to optimize the collision avoidance problem. First in, Section 4.1 the tools and input files necessary to perform the methodology are introduced. In Section 4.2 the dynamics model used in the propagations is defined through a parameter analysis and verified. Next, the data necessary for the collision probability calculations are detailed and the method applied for the calculation itself is verified and validated in Section 4.3. Afterward, details about the maneuvering process are given in Section 4.4. This includes maneuver modeling, the implementation process in the propagation, and the implementation results with verification and validation. Lastly, Section 4.5 describes the decision variables, the constraints, the objectives linked to the fitness function definition, and the optimization algorithm parametrization and tuning method.

## 4.1. Tools and inputs

This section introduces the tools and input files necessary to apply the methodology explained in this chapter. Two main tools are used: TU Delft Astrodynamics Toolbox Python (TudatPy) for the propagation part and Python Global Multi-Objective Optimiser (Pygmo) for the optimization part. The platforms/machines where these tools are applied throughout the thesis are introduced in Section 5.4.

TudatPy is the interface in python of the original C++ libraries<sup>a</sup>. It is selected due to its strong background in the field of space research and its affiliation to the the Delft University of Technology. This allows for direct support of the staff and comprehensive documentation [34]. Functions relating to state conversions, frame transformations, perturbations, integration and propagation are especially important and frequently used in this work. The acceleration models, the integrator and propagator schemes needed for the dynamics model defined in this chapter can all be found in TudatPy.

Another convenient aspect of this tool is the possibility of using it with ESA's Pagmo library for optimization, a C++ library that also has a Python equivalent Pygmo [35]. It is a scientific library for optimization, where a wide range of optimization algorithms are available and constrained, unconstrained, single or multi-objective problems are supported. The optimization algorithm chosen in Subsection 3.4.2 is also available.

As previously introduced, CDMs are necessary inputs to answer the research questions. Due to confidentiality issues, CDM data is not accessible to the public; CDM warnings provided by CSpOC are directly sent to operators. TU Delft has its own satellites from the Delfi Program (Delfi-C<sup>3</sup>, Delfi-n3Xt, and Delfi-PQ) and so receives CDM warnings. With the help of Stefano Speratte CDM messages could be obtained by the AE faculty for Delfi-C<sup>3</sup> and Delfi-n3Xt for a certain period [36]. An example of a CDM originating from this data set can be seen in Appendix A. Due to confidentiality issues, only one CDM is provided as example.

## 4.2. Definition of dynamics model - propagation

The propagation part of this problem requires a little extra attention. The states provided by CDMs are given at the Time of Close Approach (TCA). As the problem at hand is designing a maneuver to avoid said collision, first the states need to be back-propagated to a starting point and re-propagated forward with a maneuver to change the orbit. The CDM states are generated at the time of CDM creation, as that is close to the time the operator would receive the CDM; this time is used as the start time for the back propagation.

CDMs are usually received within the week leading up to the TCA. A margin of around two days is assumed to be enough to allow the operator to plan the collision avoidance maneuver. Additionally, the object should be

<sup>a</sup>An open-source Python library designed for astrodynamics and space mission analysis.

propagated three days past TCA. This will allow for quantifying the orbit disturbance explained at a later stage in Subsection 4.5.2. The total propagation time is of 5 days: TCA - 2 days until TCA + 3 days.

The first step is to set up a baseline dynamics model that will allow the back propagation. The parameters defined in Section 3.3 need to be chosen. The  $C_D$  and  $C_R$  values needed for the atmospheric drag and the solar pressure radiation are taken directly from the CDMs, using a chaser of 3 kg and a cross-sectional area of 0.0995 m<sup>2</sup> for the drag and 0.075 m<sup>2</sup> for the solar radiation pressure. The chosen parameters are:

- Integration step size: 1 second,
- Integrator: Runge-Kutta 4,
- Degree and order (D/O) of Earth's spherical harmonics (SH): 36,
- Atmosphere model: NRLMSISE 00,
- Third-body point masses (PM): Sun and Moon,
- $C_D = 2.197$
- $C_R = 1.014$

To validate the back propagation implementation two CDMs are used that have the same creation date but different TCA's. This happens when objects have several encounters at different moments in their orbits. It could be between the same two objects but also between the chaser and multiple other objects. As they have the same generation date, the same orbit determination is used to generate them but they are propagated to different moments in the orbit. The longer propagation state can be used to obtain the shorter one. If the dynamics model defined in this section is close to the model used in the CDM state generation, little difference should be observed between the states. It is expected that back-propagating from the later TCA to the earlier one will introduce some uncertainties in the model but it should be within an acceptable range such that the collision avoidance process can still be linked to the real scenario.

As the available dataset is limited, only some CDM pairs could be identified that meet the requirements. The promising ones are:

- CDM pair: 222 and 221; time in between TCA is 4.85 h.
- CDM pair: 197 and 198; time in between TCA is 15.9 h.
- CDM pair: 220 and 219; time in between TCA is 22.2 h.

The last pair has the largest time spread so it is selected for the back propagation validation. As for the chaser object, Delfi-C<sup>3</sup> is used as it is present in the selected CDM. This is done by taking the state further in time, propagating it backward, and comparing the propagated state to the state of the earlier CDM. The important frame for conjunctions is the local frame (RIC), hence it is used to express the comparison results. The final differences in local states are shown in Table 4.1.

**Table 4.1: States difference after chaser object back-propagation.**

CDM pair	$\Delta t$ [h]	$\Delta R$ [m]	$\Delta I$ [m]	$\Delta C$ [m]	$  \Delta \mathbf{R}  $ [m]	$\Delta \dot{R}$ [m/s]	$\Delta \dot{I}$ [m/s]	$\Delta \dot{C}$ [m/s]	$  \Delta \dot{\mathbf{R}}  $ [m/s]
220, 219	22.24	39.32	0	0	39.32408	-0.32	-0.01	0	0.32

A position norm difference of around 40 m and a velocity norm difference of around 0.32 m/s after 20 hours of propagation, is considered an acceptable limitation of the propagation. In Subsection 4.5.1 it will be shown that a miss distance of 1000 m is a CDM generation threshold. Note that  $\Delta I$  and  $\Delta C$  do not have 0 meters difference, but their difference is negligible compared to the radial one.

The next step is to do the forward propagation past the TCA. At this stage, a sensitivity analysis is carried out on the baseline model chosen before. This is done to understand if other dynamics model parameters can be used for the propagation. Each parameter is varied individually and the position and velocity of the objects are compared to the baseline model positions and velocity. The result is a position and velocity error. Small errors would justify changing the model parameters. The perturbation accelerations occurred in the baseline model are shown in Figure 4.1. The spacecraft has an apogee and perigee altitude of 561 km and 536 km, respectively and an inclination of around 97.8° inclination. This helps determine which parameters are expected to have big impacts. The larger contribution is the Earth's gravity field (shown as SH Earth in the graph). The variations to this parameter are expected to have larger errors as they contribute significantly to the object's orbit.

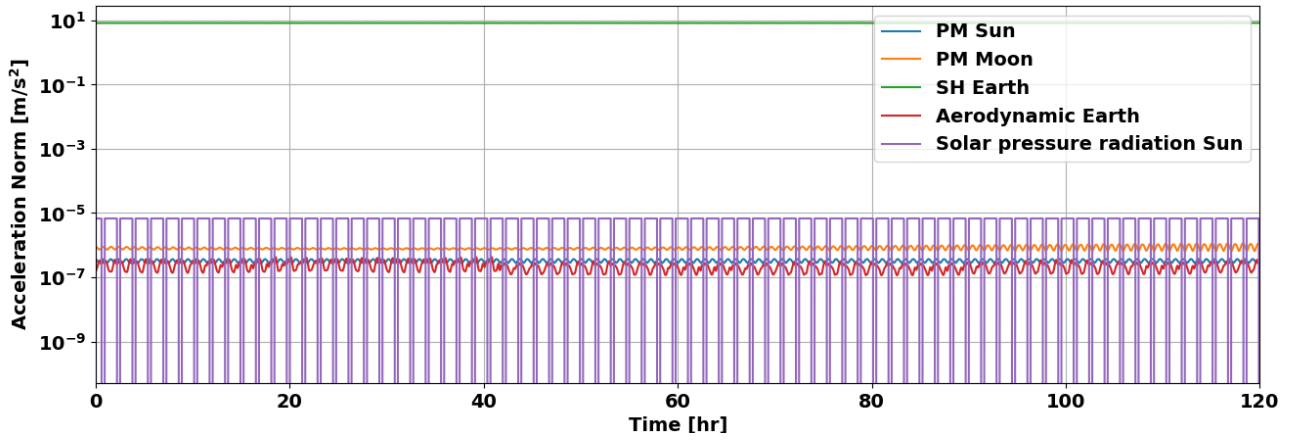


Figure 4.1: Individual perturbation norms in the baseline dynamical model.

The variations applied to the dynamics model and the initial model used as the baseline are listed in Table 4.2. The results are displayed in Figures 4.2 to 4.8 in the order that they are presented in the table (left to right).

Table 4.2: Sensitivity analysis conducted on dynamics model: reference and alternative values/models for each element.

Try	Step size [s]	D/O	$C_D$	$C_R$	Atmosphere	Integrator	PM
Initial	1	36	2.197	1.014	NRLMSISE 00	RK4	Sun, Moon
	2	50	1	1	Default TudatPy	RKF45	Sun
	5	25	1.5	1.25	Exponential atmosphere	RKF456	Moon
	10	15	2	1.5		RKF78	None
	20	10	2.5	1.75		RKDP87	Mars, Jupiter, Moon, Sun
	30	2	3.5	2			Mars, Moon, Sun

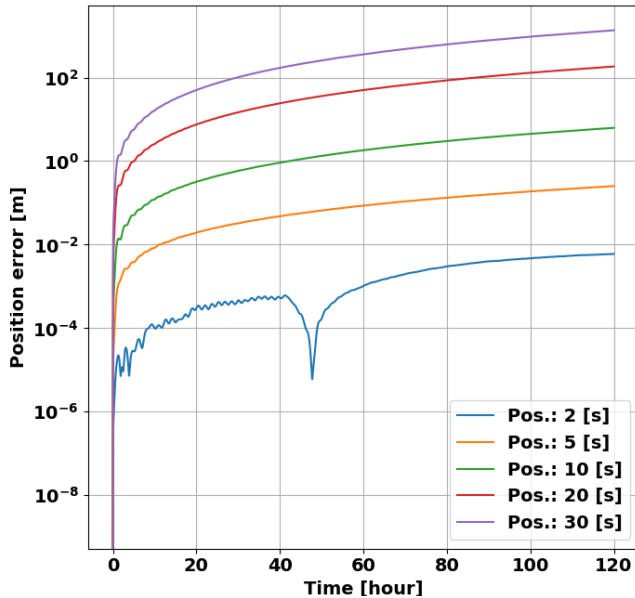


Figure 4.2: Effects of integrator step size variation on orbit propagation.

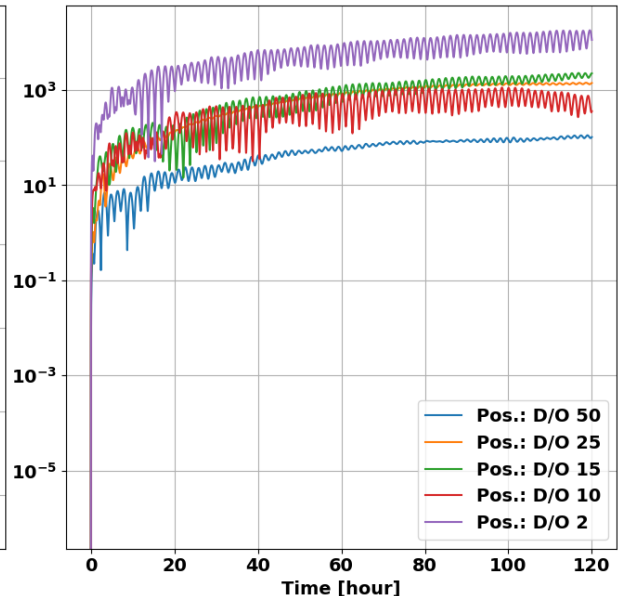


Figure 4.3: Effects of gravity model D/O variation on orbit propagation.

In Figure 4.2, the position errors reach values of  $10^3$  m for step sizes of 30 s. For smaller step sizes, the results are much better. A step size of 10 m has position errors within 10 m. Considering that the back propagation showed an uncertainty of around 40 m, this error is within that uncertainty and considered acceptable. The benefit of increasing the step size is that fewer computation steps are required and so the computation times are lower.

The spherical harmonics terms were identified as an important contribution to the model so changing their number requires special attention. The errors presented in Figure 4.3 are larger than the ones seen before. When conducting this analysis no significant timing benefits were detected. For this reason, no changes will be made to this model parameter: D/O 36 will be used.

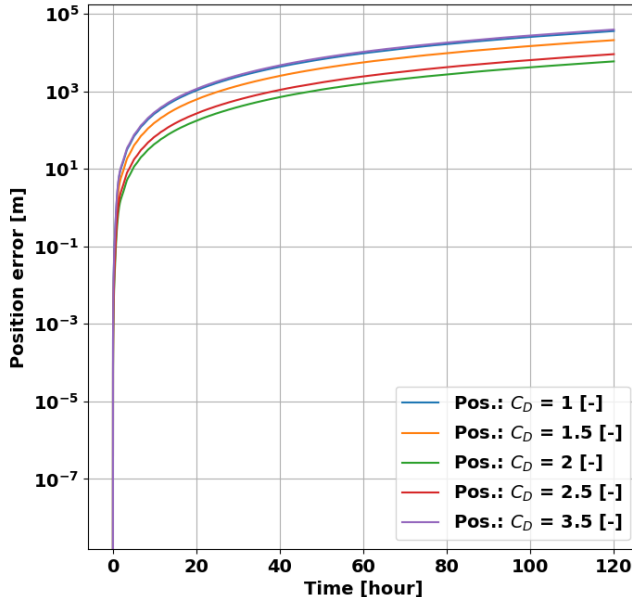


Figure 4.4: Effects of spacecraft  $C_D$  variation on orbit propagation.

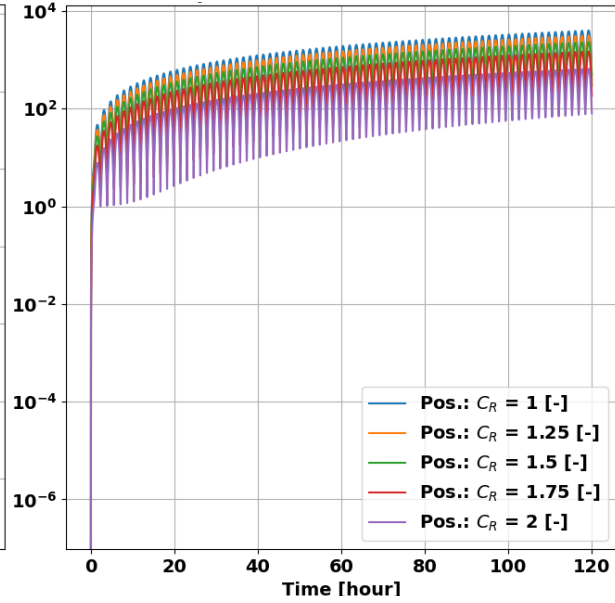


Figure 4.5: Effects of spacecraft  $C_R$  variation on orbit propagation.

The drag perturbation uncertainty is mainly driven by two components: the  $C_D$  of the spacecraft and the environment's density. As shown in Figure 4.1, the drag has a smaller contribution to the object's state than the gravity effects (PM Sun and Moon, and SH Earth). Figure 4.4 shows that varying the drag coefficient does impact the state of the object. The  $C_D$  values further from the baseline (2.19) introduce larger errors, while those that do not differ as much introduce smaller errors.

The  $C_R$  parameter is considered in Figure 4.5. For this coefficient, a value of zero means the spacecraft is translucent to incoming radiation. A value of 1.0 indicates all radiation is absorbed (no reflection) and all the force is transmitted to the spacecraft (no re-emission). A value of 2.0 indicates all radiation is reflected and twice the force is transmitted to the spacecraft. Values 1.0 and 1.25 show similar results, while the others are slightly more spread out. In the figure, the big drops indicate the same behavior seen in Figure 4.1.

As the errors are significant for these two parameters and it is expected that CDM values are accurate, no changes are made to this parameter either; a value of 2.197 will be used for  $C_D$  and 1.014 for  $C_R$ .

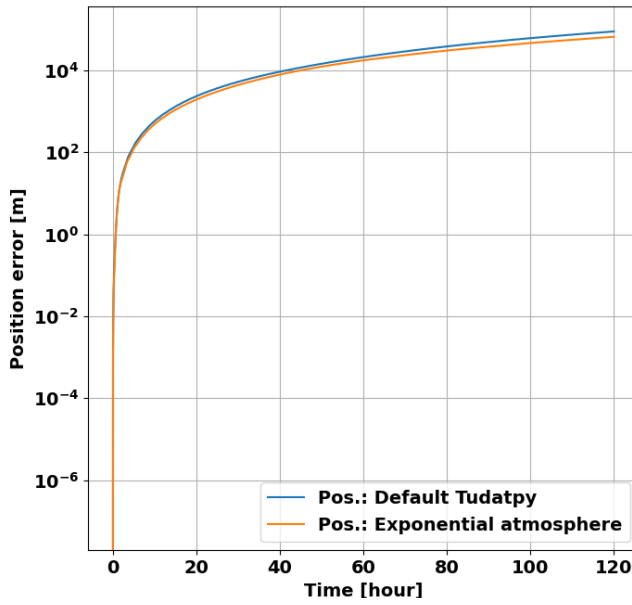


Figure 4.6: Effects of atmosphere model variation on orbit propagation.

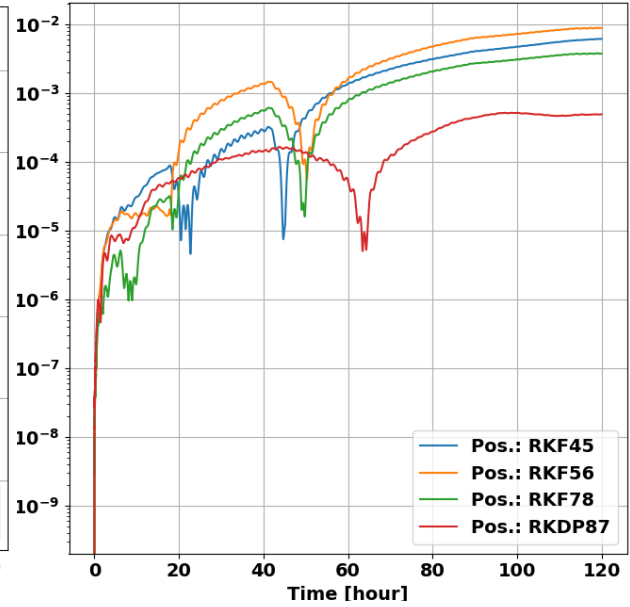


Figure 4.7: Effects of integrator variation on orbit propagation.

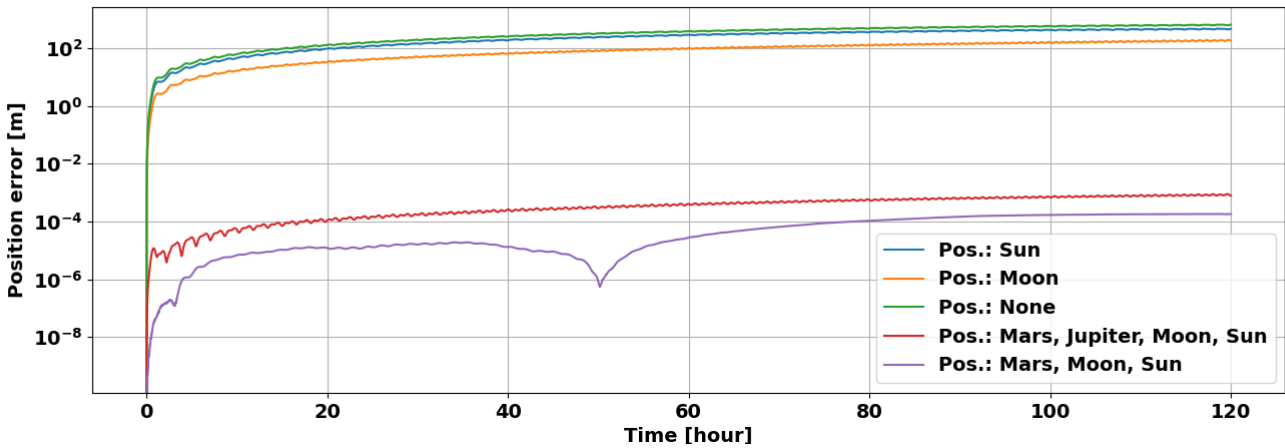


Figure 4.8: Effects of 3<sup>rd</sup> body perturbation variation (all PM) on orbit propagation.

The second component of the drag perturbation is the atmosphere model. The effect of its variation is shown in Figure 4.6. Here, both the default TudatPy and exponential atmosphere models vary significantly from the NRLMSISE 00 model. It is hard to say whether the initial dynamics model used the correct atmosphere model, but NRLMSISE 00 is known for its accurate behavior in low altitudes of LEO. It is then decided to limit this parameter's changes from the default and the NRLMSISE 00 model is chosen.

The second-to-last parameter considered is the integrator used in the propagation. Here, fixed step-size integrators are preferred. During the propagation, a maneuver needs to be implemented and the optimization will determine at which time it should be conducted. It is beneficial to have a fixed step-size integrator because then the states can be extracted directly without further interpolation helping in the computational time necessary. Implementing variable step-size integrators would add another complexity level. In Figure 4.7, low errors are observed between the integrators. The Runge-Kutta 4 integrator performs well (shows Figure 4.7 small errors) and so it is chosen for the final model.

The final comparison done is for the third-body PM perturbations. The CDM chosen included both the Sun and the Moon in the model just as the initial model (Table 4.2). Figure 4.8 shows that varying the contribution of the Sun and the Moon introduces larger position errors (curves green for no PM, blue for only Sun PM and orange for only Moon PM). The other variations show much smaller position errors; including Mars or Jupiter inside the dynamics model, does not influence the object significantly. For this reason and to limit complexity they are not included in the final model. The final model is defined as follows:

Table 4.3: Final dynamics model after sensitivity analysis.

Step size [s]	D/O	$C_D$	$C_R$	Atmosphere	Integrator	PM
10	36	2.197	1.014	NRLMSISE 00	RK4	Sun, Moon

### 4.3. Collision probability calculation

This section shows the methodology applied to calculate the collision probability, as well as the miss distance and the relative speed. This section uses the information previously provided in Section 3.2.

First, the data received to allow for the collision probability calculation is described in Subsection 4.3.1. Then, a step-by-step technique of calculating the collision probability is given in Subsection 4.3.2. Here, also the verification and validation of the method is presented.

#### 4.3.1. Data description

The CDMs received by Stefano Speretta contained warnings for Delfi-C<sup>3</sup> (launched in 2008) and Delfi-n3Xt (2013) both are CubeSats of around 3 kg. They have similar initial orbits with a semi-major axis of around 700 km, inclination of around 98°, and eccentricity of 0.001 and 0.01 respectively. They differ mostly in the argument of periapsis. When going through the CDMs it was noticed that most of the warnings involved debris (from the COSMOS-IRIDIUM collision and Fengyun debris) or several Starlink satellites.

Additionally, two CDM warnings contained no value prediction for the collision probability and did not include a method of calculation "COLLISION\_PROBABILITY\_METHOD", thus they were excluded from the analysis. Several files contained the same warning so they were also filtered out. Furthermore, some CDMs also contained collision probabilities predictions of 0 and values below  $10^{-6}$ . These were also set aside as the focus of the thesis is reducing  $P_c$  that requires action.

*Note: not all CDM files come with the "COMMENT MEETS EMERGENCY CRITERIA" field or the "COMMENT Operator Hard Body Radius" field. The first relates to the value of the probability of collision and indicates to the operators the emergency level of the conjunction. The second field is given by the operator to CSpOC for a more accurate calculation of the exclusion volume radius. From the CDM data, it becomes clear that for the Delfi satellites, this started being applied from October 25<sup>th</sup> 2021 forwards. Besides these CDMs two others present this field but related to the target spacecraft; Starlink-1715 and Spacebee-90 both present values for the "COMMENT Operator Hard Body Radius" field. However, this value is not used for the probability of collision calculation. One of the reasons for this is the inconsistency of the data; clearly, not all operators provide it and the values can be incorrect (for example the values for the Delfi satellites are specified as 0 m).*

#### 4.3.2. Verification and validation

The probability of collision is given by the CDMs but in the context of planning a collision avoidance maneuver, a new  $P_c$  needs to be calculated afterward to determine the effectiveness of the CAM in avoiding the collision. Hence, it is necessary to verify and validate the collision probability calculation implemented. This can be done by taking the CDMs received, reconstructing their  $P_c$ , and comparing them to the values given.

The calculation is implemented in the code as described below. This process follows the collision probability calculation explained in Section 3.2. The reader can refer back to that section for the equations that are applied.

1. The states of the target and risk objects provided in ITRF are transformed into the ECI reference frame in TudatPy. This is possible because the TCA is provided.
2. Both covariance matrices, which are provided in the local RIC frame, are rotated to the ECI frame by rotation matrices derived from both object states in ECI.
3. The covariance matrices are summed.
4. The rotation matrix from ECI to B-frame is derived from the position and velocity difference at TCA.
5. The combined inertial covariance matrix and position difference vector are translated to the B-frame.
6. Values  $x_B$ ,  $y_B$ ,  $\sigma_1^2$ , and  $\sigma_2^2$  of the covariance matrix in the B-frame are determined. These are used to rotate the covariance matrix and position difference vector such that they align with the B-frame to facilitate computation. Note that the covariance matrix now has zeros on the off-diagonals and standard deviations squared on the diagonal.

7. Both exclusion volume radii are summed ( $R_c$ ).
8. To calculate the square that circumscribes the combined radius error functions are applied, where  $x_B$  and  $y_B$  are taken from the position difference vector projected onto the B-frame and  $\sigma_1$  and  $\sigma_2$  are the square root of the diagonals of the covariance matrix in the B-frame.

The comparison between the given collision probability and the reconstructed one is done by calculating the absolute and the relative error, as well as the difference in the order of magnitude as shown in Equations 4.1 and 4.2. Additionally, as the miss distance and the relative speed is interesting to operators, also those parameters are calculated and compared to the ones given in the CDMs. Their comparison is only done with the absolute and relative errors though.

$$\text{Diff} = P_{c, \text{code}} - P_{c, \text{CDM}}, \quad \epsilon_{rel} = \frac{P_{c, \text{code}} - P_{c, \text{CDM}}}{P_{c, \text{CDM}}} \cdot 100\% \quad (4.1)$$

$$O_{diff} = \log(P_{c, \text{code}}) - \log(P_{c, \text{CDM}}) \quad (4.2)$$

A selection of CDMs is used for the verification and validation as there are too many to start with (278 files were received). First, the files are filtered as described before. Then, the files are sorted by  $P_c$  values, and those above  $10^{-6}$  are selected as they are most relevant for action. After the selection, a total of 98 CDM files are considered valid. From these, 50 files are randomly selected to limit computational efforts and the comparison is conducted. Throughout the thesis, eight CDM files are used: six for initial states needed in the dynamics model and two for the optimization model. In the optimization model  $P_c$  is calculated, so those two files are chosen from the 50 files selected. Table 4.4 shows the mean, median and standard deviations of the difference found over the 50 files selected. In Section B.1, an extended version of this table is presented with all the values.

**Table 4.4: Summary of  $P_c$ , miss distance and relative speed comparison.**

	$O_{diff}$	Diff.	$\epsilon_{rel}$ [%]
$P_c$			
<b>Mean</b>	0.005	$-1.05 \cdot 10^{-5}$	-0.52
<b>Median</b>	0.002	$-3.15 \cdot 10^{-8}$	-0.01
<b>Std.</b>	0.007	$6.81 \cdot 10^{-5}$	1.95
$D_{miss}$ [m, %]			
<b>Mean</b>		0.46	0.218
<b>Median</b>		0.41	0.100
<b>Std.</b>		0.28	0.346
$V_{rel}$ [m/s, %]			
<b>Mean</b>		0.41	0.004
<b>Median</b>		0.36	0.003
<b>Std.</b>		0.28	0.346

The miss distance and relative speed comparison serve as verification and validation of the rotations applied to the state vectors and the calculation of the position and velocity differences at TCA. As the table shows, very small differences are found probably introduced by uncertainties in the rotation from ITRF to ECI. At this point, the method is considered validated.

Then, the probability of collision calculation allows to validate the rotations applied to the covariance matrices, the calculation of the position vector projected on the B-frame and the square root of the diagonals of the covariance matrix, the B-frame rotation, and the application of error functions. With more calculations and rotations more uncertainties are introduced and so the results are expected to show higher differences. This is also the case, although the mean and median presented here are small; the standard deviation indicates that there is a bigger fluctuation in the computed values. The biggest  $\epsilon_{rel}$  variation present in Table B.2 is -5.89%; it is accompanied by an order of magnitude difference of 0.026 and an absolute difference of  $-4.23 \cdot 10^{-7}$ .

Although these  $P_c$  differences are higher than those for the miss distance and relative speed, they are still low enough to allow for determining whether the CAM is effective or not. For example, the biggest differences  $P_{c,CDM}$  value is  $7.18 \cdot 10^{-6}$  while the  $P_{c,code}$  is  $6.76 \cdot 10^{-6}$ . The CAM avoidance maneuver should change the collision probability by several orders of magnitude to make sure the collision is avoided and the operator will not receive more warnings. Even with the differences presented here, this change will still be noticeable.

#### 4.4. Collision avoidance maneuver implementation

Typically in this study, the probability predicted by the conjunction requires a collision avoidance maneuver. Often, such maneuvers are combined with already planned station-keeping maneuvers but sometimes a completely new maneuver needs to be planned. The most efficient way to create a separation between two objects is usually in the normal direction with changes to semi-major axis and eccentricity. However for the purpose of this thesis and to completely answer the research question, avoidance maneuvers will be investigated in three directions: in-track, cross-track and in the radial direction in the spacecraft frame. This is also a recommendation from literature presented in Subsection 3.4.2.

The modeling used for the maneuvers is explained in Subsection 4.4.1. After this the maneuver implementation method is provided in Subsection 4.4.2. The modeling is verified and validated in Subsection 4.4.3 along with an analysis of the results.

##### 4.4.1. Modeling

The purpose of the maneuver is to impact the orbit such that the collision can be avoided. This can be modeled by the maneuver's impact on orbital elements. The impact of a maneuver can be described by Equations 4.3 to 4.7; impulsively. From these it becomes clear that the velocity change in each direction (radial = R, in-track = I, and cross-track = C) has a different impact on the orbit [19]. These equations are valid for the cases of  $e \neq 0$  and  $i \neq 0^\circ$ .

$$\Delta a = 2 \sqrt{\frac{a^3}{\mu(1-e^2)}} [\Delta V_R e \sin \theta + \Delta V_I (1 + e \cos \theta)] \quad (4.3)$$

$$\Delta e = \sqrt{\frac{a(1-e^2)}{\mu}} \left[ \Delta V_R \sin \theta + \Delta V_I \frac{2 \cos \theta + e(1 + \cos^2 \theta)}{1 + e \cos \theta} \right] \quad (4.4)$$

$$\Delta i = \sqrt{\frac{a(1-e^2)}{\mu}} \Delta V_C \frac{\cos(\omega + \theta)}{1 + e \cos \theta} \quad (4.5)$$

$$\Delta \omega = \sqrt{\frac{a(1-e^2)}{\mu}} \left[ -\Delta V_R \frac{\cos \theta}{e} + \Delta V_I \frac{\sin \theta (2 + e \cos \theta)}{e(1 + e \cos \theta)} - \Delta V_C \frac{\cot i \sin(\omega + \theta)}{1 + e \cos \theta} \right] \quad (4.6)$$

$$\Delta \Omega = \sqrt{\frac{a(1-e^2)}{\mu}} \Delta V_C \frac{\sin(\omega + \theta)}{\sin i (1 + e \cos \theta)} \quad (4.7)$$

The first term of the equations is purely dependent on the orbital parameters  $\left(\sqrt{\frac{a(1-e^2)}{\mu}}\right)$ . This component is multiplied by the velocity change contributions which vary per orbital element. First, it should be noted that the contribution of the velocity changes depends on the location of the spacecraft in its orbit, characterized by the true anomaly. This indicates that certain locations within the orbit will produce optimal maneuvers. Then, it should be noted that the orbital element changes are achieved with different velocity change directions. An impulsive maneuver in the radial or in-track direction yields a change in semi-major axis and eccentricity, while an impulsive maneuver in the cross-track direction yields a change in the inclination and the right ascension of the ascending node, and the argument of pericenter; whereas other maneuver directions will be futile for the same impact.

As implied the velocity changes will be modeled as instantaneous maneuvers. Collision avoidance maneuvers usually have a small magnitude, from  $\pm 1$  m/s to  $\pm 0.1$  m/s [31, 29].



### 4.4.2. Implementation

The implementation of the maneuver will be done to characterize its influence on the orbital elements by instantaneous thrust. TudatPy has different functions that allow to include thrust as an acceleration. However, the simplest way to include an instantaneous thrust is to directly add the changes to the state vector. This can be done by converting the changes in Keplerian elements into a Cartesian state vector impact. As the impact of the maneuver depends on the position of the spacecraft within the orbit, the process can be divided into three phases: a pre-maneuver phase, a maneuver computation and implementation phase, and a post-maneuver phase. This implementation is described by the following steps:

1. Propagate spacecraft orbit until maneuver time.
2. Extract spacecraft state and convert into Keplerian elements.
3. Compute the change in orbital elements based on maneuver impulse magnitude and direction.
4. Update Keplerian elements and convert to Cartesian state.
5. Continue propagation after the maneuver.

TudatPy allows for a different approach: including within the acceleration model of the propagation, a specific maneuver based on engine thrust. This method does not allow for the flexibility of choosing different maneuver timing. As shown previously, the impact on the orbital elements depends greatly on the spacecraft's location along its orbit. The problem at hand calls for optimization of collision risk, propellant usage, and mission impact. Wisely choosing the maneuver timing allows maximizing the mission impact with the same  $\Delta V$ .

The same analysis can also be conducted about the maneuver timing based on the conjunction problem. Often a trade-off between the maneuver time and uncertainties needs to be conducted: when to perform the maneuver based on conjunction analysis, and link the maneuver timing to its effect on  $P_C$ . The current implementation allows to fully describe the maneuver effect depending on its timing and 3D thrust.

### 4.4.3. Results

A verification exercise is conducted with examples provided in Wakker [19], where the changes in orbital elements are related to a certain thrust direction and magnitude as well as optimum orbital location. The orbit used for the verification is defined by these orbital elements:  $a = 7000$  km,  $e = 0.005$ ,  $i = 80^\circ$ ,  $\omega = 0^\circ$ ,  $\Omega = 0^\circ$ . The inputs and results expected from the exercise are shown in Table 4.5. The aimed change is provided by the verification exercise while the remaining changes are calculated with Equations 4.3 to 4.7. The exercise does not provide an example for a radial direction maneuver because the optimal changes in semi-major axis, eccentricity, and argument of pericenter can be found with in-track maneuvers.

In reality, the definition of the optimal location for the inclination and  $\Omega$  change are with respect to the argument of latitude  $u$ . This element describes the angular position of the spacecraft along its orbit relative to the ascending node and can be computed by:  $u = \omega + \theta$ . As in this example  $\omega = 0^\circ$ :  $u = \theta$ .

**Table 4.5: Verification exercise inputs and results for effect of a maneuver components (R, I, C) on Kepler elements (taken from [19, p. 610]).**

$\Delta V$ [m/s]	Optimal burn location ( $\theta$ )	Aimed change	Remaining changes
[0, 1.07, 0]	0	$\Delta a = 2$ km	$\Delta e = 0.00028$ , $\Delta \omega = 0^\circ$
[0, 3.78, 0]	0 and $\pi$	$\Delta e = 0.001$	$\Delta a = 6.978$ km, $\Delta \omega = 1.4 \cdot 10^{-15}^\circ$
[0, 3.29, 0]	$\frac{\pi}{2}$ and $\frac{3\pi}{2}$	$\Delta \omega = 10^\circ$	$\Delta a = 6.103$ km, $\Delta e = 2 \cdot 10^{-6}$
[0, 0, 13.1]	0 and $\pi$	$\Delta i = 0.1^\circ$	$\Delta \Omega = 0^\circ$
[0, 0, 12.9]	$\frac{\pi}{2}$ and $\frac{3\pi}{2}$	$\Delta \Omega = 0.1^\circ$	$\Delta i = 6 \cdot 10^{-18}^\circ$

The exercise is conducted by inserting the defined maneuvers into the propagation and changing the maneuver time over the complete true anomaly range. This allows to determine the effect of the maneuver along the spacecraft orbit, to identify where the maximal effect is. The impact on the orbital elements are shown in Figure 4.9. All the maneuvers are shown over all the orbital elements to facilitate defining whether or not there is an impact.

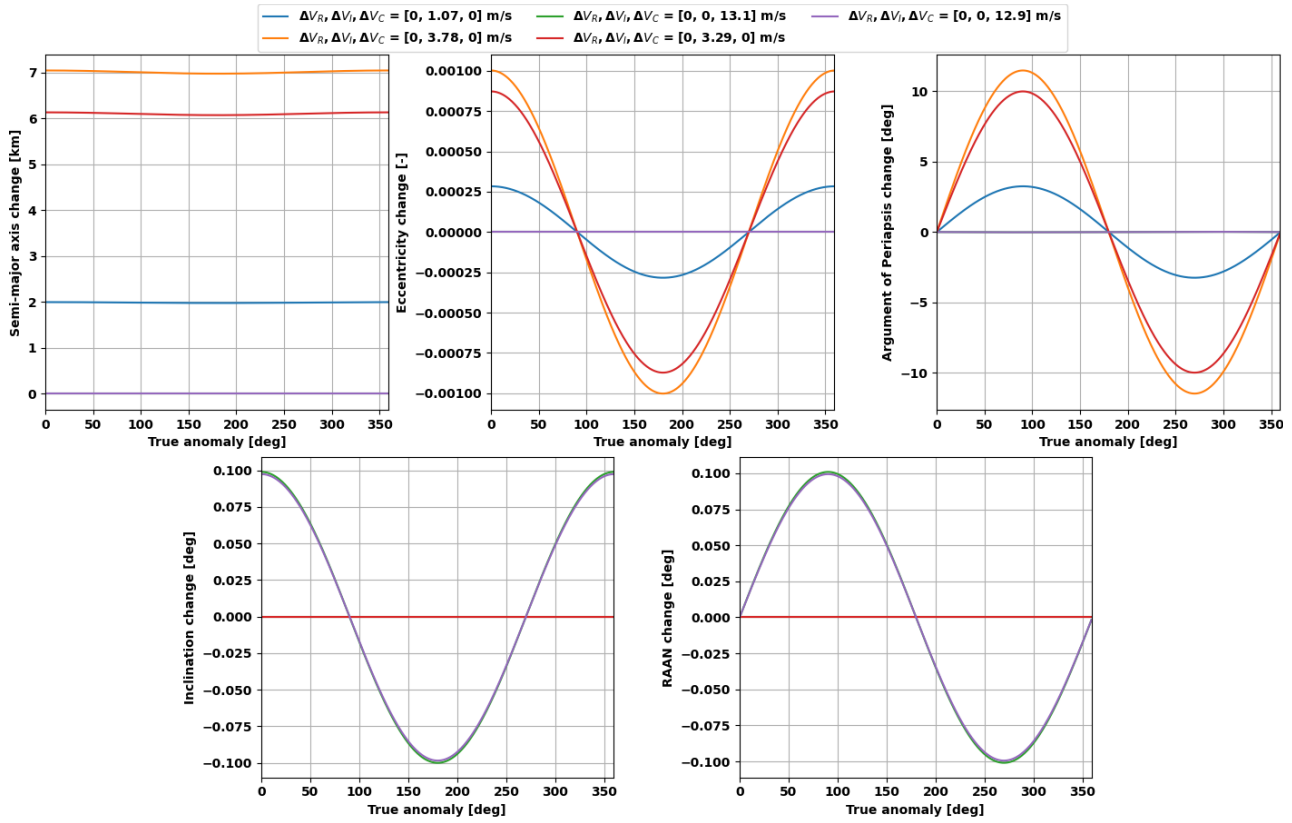


Figure 4.9: Results of verification exercise for the effect of the maneuver on Kepler elements along the orbital location described by the true anomaly.

Comparing the graphs with the table above, it becomes clear that the expected result is matched. The maneuvers in cross-track direction produce no effect on  $a$ ,  $e$  and  $\omega$ , while they do produce effects in  $i$  and  $\Omega$ . The opposite can be said for the maneuvers in in-track direction. It should be noted that for the semi-major axis it is hard to discern the optimum location of the burn due to the small eccentricity used for the orbit. This exercise underlines how the orbital elements are affected simultaneously and that carefully timing the maneuver is necessary to minimize/maximize an effect.

Additionally, the maneuver modeling as an impulsive maneuver should be verified. This is done by splitting a 1 m/s maneuver over 10 seconds; 0.1 m/s every second for the total maneuver. Comparing the difference in orbital elements between a split maneuver and an impulsive maneuver allows to determine if it is a valid simplification of the model. As the impact of the maneuver depends on the spacecraft's position in the orbit, a difference is expected. The ten seconds difference will induce differences in the true anomaly which will impact the final contribution. First the changes in Keplerian elements of a ten second delay in maneuver timing are compared to the discontinuous modeling. Then, graphs showing the discontinuous modeling are provided.

The orbital period is calculated with a semi-major axis of 7500 km to be around 6464 seconds. In the worst-case scenario of a maneuver being postponed by ten seconds, this leads to a true anomaly change of 0.0097 radians or 0.5570°. This true anomaly can be filled into Equations 4.3 to 4.7 along with maneuver magnitudes and an orbit characterized by  $a = 7500$  km,  $e = 0.3$ ,  $i = 45^\circ$ ,  $\omega = 235.7^\circ$ ,  $\Omega = 100.4^\circ$ , to determine the worst-case scenario changes expected. The results are shown in Table 4.6.

Table 4.6: Outcome of Equations 4.3 to 4.7 with true anomaly of 0.5570° for different maneuvers. Semi-major axis in meters and angles in radians.

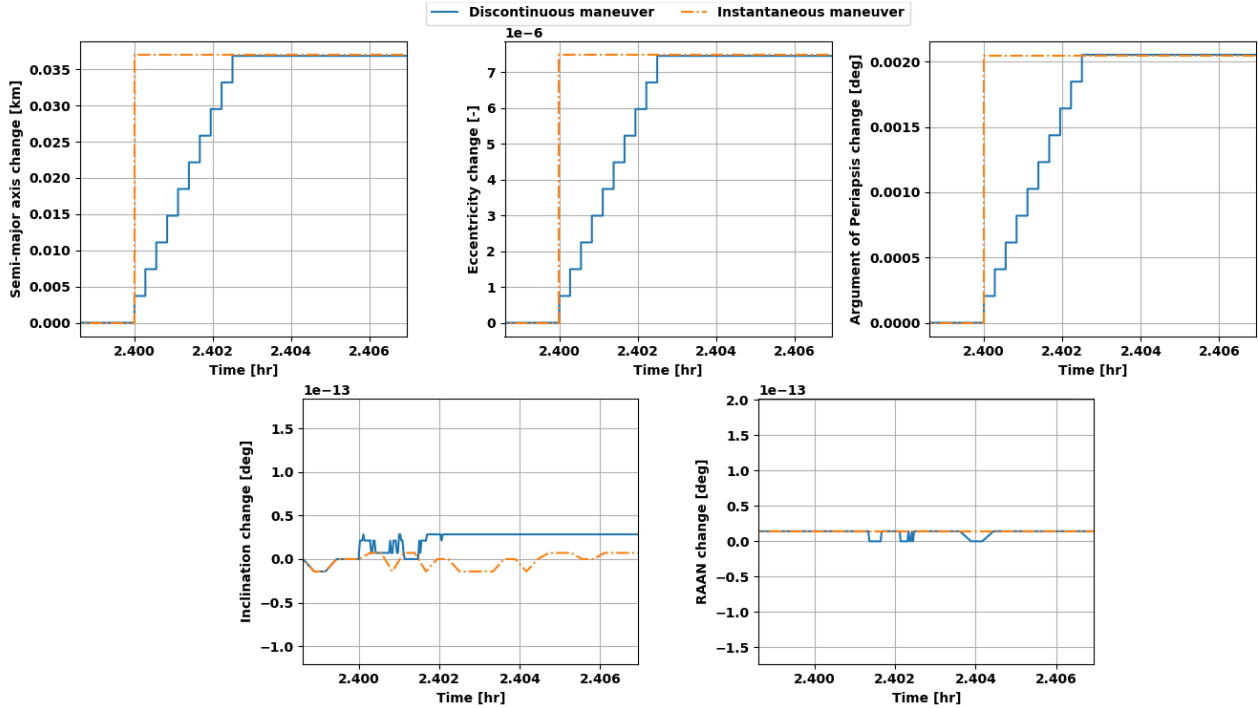
	$\Delta V_R, \Delta V_I, \Delta V_C = [1, 0, 0]$ m/s	$\Delta V_R, \Delta V_I, \Delta V_C = [0, 1, 0]$ m/s	$\Delta V_R, \Delta V_I, \Delta V_C = [0, 0, 1]$ m/s
$\Delta a$	5.67	2528.29	0.0
$\Delta e$	$1.23 \cdot 10^{-6}$	$2.52 \cdot 10^{-4}$	0.0
$\Delta i$	0.0	0.0	$-5.40 \cdot 10^{-5}$
$\Delta \omega$	$-4.21 \cdot 10^{-4}$	$7.25 \cdot 10^{-6}$	$8.09 \cdot 10^{-5}$
$\Delta \Omega$	0.0	0.0	$-1.14 \cdot 10^{-4}$

Table 4.7 shows the difference in Keplerian elements at the end of the maneuver implementation for the two different maneuver models, one instantaneous (inst.) and one split over 10 seconds (disc.). The results are much lower than the worst-case scenario results shown in Table 4.6 and demonstrate that the maneuver has been split correctly. The last row shows that a difference in true anomaly is present which explains the small differences seen in the remaining Keplerian elements. Overall for collision avoidance purposes, warning thresholds are around  $10^{-6}$ , meaning that this difference will not affect the conjunction geometry significantly and the same collision avoidance scenario can be modeled.

**Table 4.7: Orbital elements after maneuver implementation with two different maneuvering models and their differences. Semi-major axis in kilometers and angles in radians.**

	$\Delta V_R, \Delta V_I, \Delta V_C = [1, 0, 0]$ m/s			$\Delta V_R, \Delta V_I, \Delta V_C = [0, 1, 0]$ m/s			$\Delta V_R, \Delta V_I, \Delta V_C = [0, 0, 1]$ m/s		
	$K_f$ , inst.	$K_f$ , disc.	Diff.	$K_f$ , inst.	$K_f$ , disc.	Diff.	$K_f$ , inst.	$K_f$ , disc.	Diff.
$a$	7500.04	7500.04	$1.5 \cdot 10^{-4}$	7500.16	7500.16	$1.0 \cdot 10^{-4}$	7500.00	7500.00	$-9.9 \cdot 10^{-11}$
$e$	0.30	0.30	$3.1 \cdot 10^{-8}$	0.30	0.30	$5.6 \cdot 10^{-8}$	0.30	0.30	$1.7 \cdot 10^{-15}$
$i$	0.79	0.79	$2.2 \cdot 10^{-15}$	0.79	0.79	$-2.0 \cdot 10^{-15}$	0.79	0.79	$7.2 \cdot 10^{-9}$
$\omega$	4.11	4.11	$-7.1 \cdot 10^{-8}$	4.11	4.11	$2.2 \cdot 10^{-7}$	4.11	4.11	$5.0 \cdot 10^{-8}$
$\Omega$	1.75	1.75	$3.6 \cdot 10^{-15}$	1.75	1.75	$4.7 \cdot 10^{-15}$	1.75	1.75	$-7.1 \cdot 10^{-8}$
$\theta$	3.79	3.80	$-5.8 \cdot 10^{-3}$	3.79	3.80	$-5.8 \cdot 10^{-3}$	3.79	3.80	$5.8 \cdot 10^{-3}$

The difference between the two maneuver models can also be seen in Figures 4.10 to 4.12 for the same maneuvers described above. The graphs show the differences only around the maneuver time which allow for the visualization of the ten 0.1 m/s maneuver steps. The changes in Keplerian elements are minimal and again it is made clear that they come only into effect because of the different time moments in the maneuver.



**Figure 4.10: Orbital elements change propagation before and after maneuver in in-track direction.**

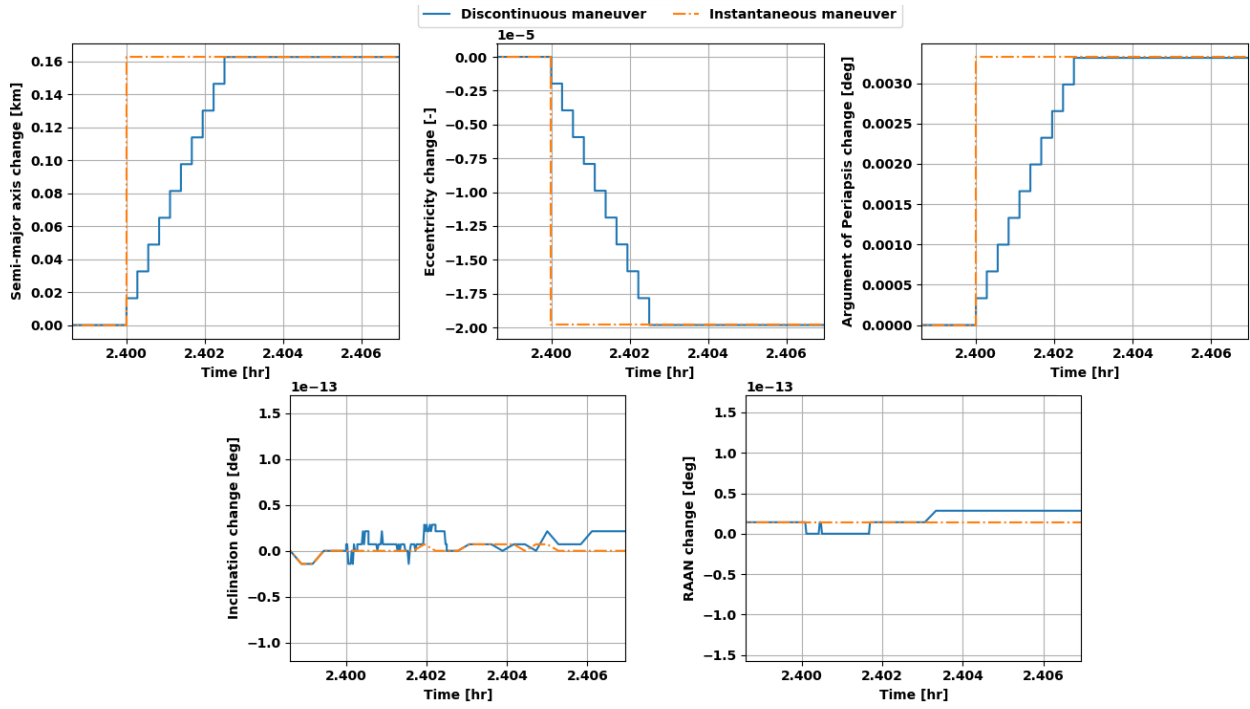


Figure 4.11: Orbital elements change propagation before and after maneuver in radial direction.

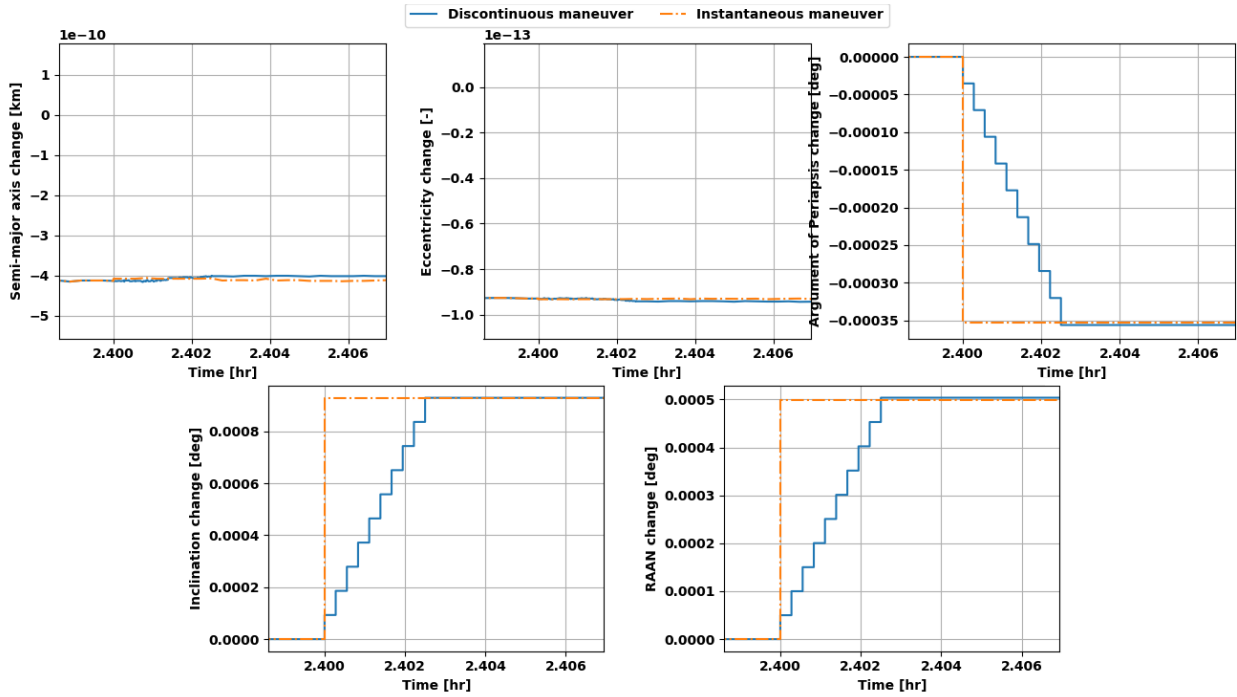


Figure 4.12: Orbital elements change propagation before and after maneuver in cross-track direction.

With the verification conducted, the maneuver model can be implemented into the propagation problem. Here, the perturbations on the orbit are removed and a purely Keplerian orbit is provided. In Figures 4.13 to 4.15, a three-dimensional representation of the orbit can be seen where the impact of the maneuver in each direction is shown. For better visualization the magnitude of the maneuver is exaggerated to 1000 m/s.

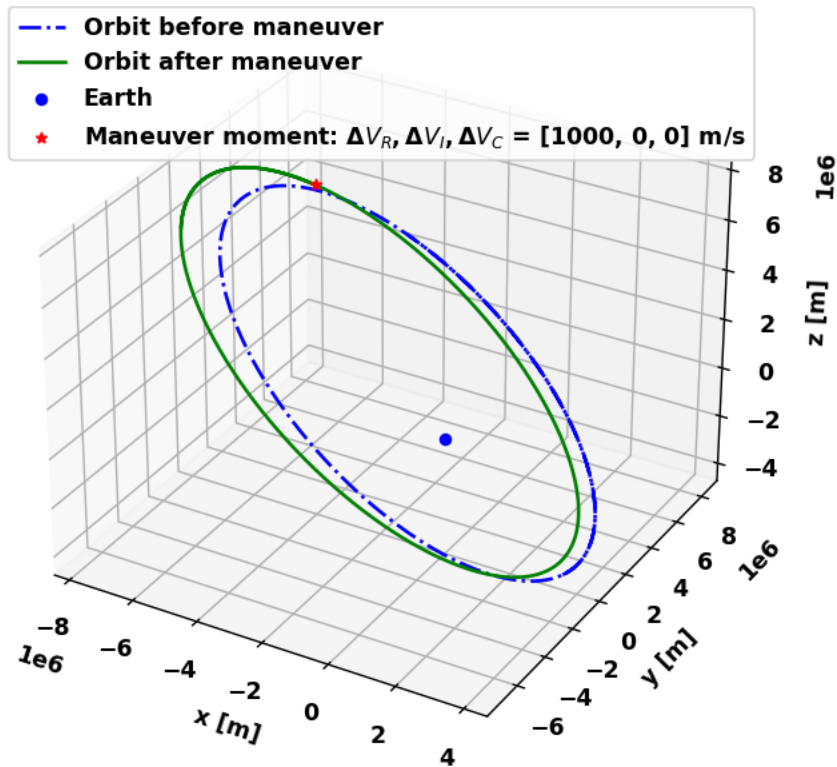


Figure 4.13: Spacecraft orbit before and after an exaggerated maneuver in the radial direction.

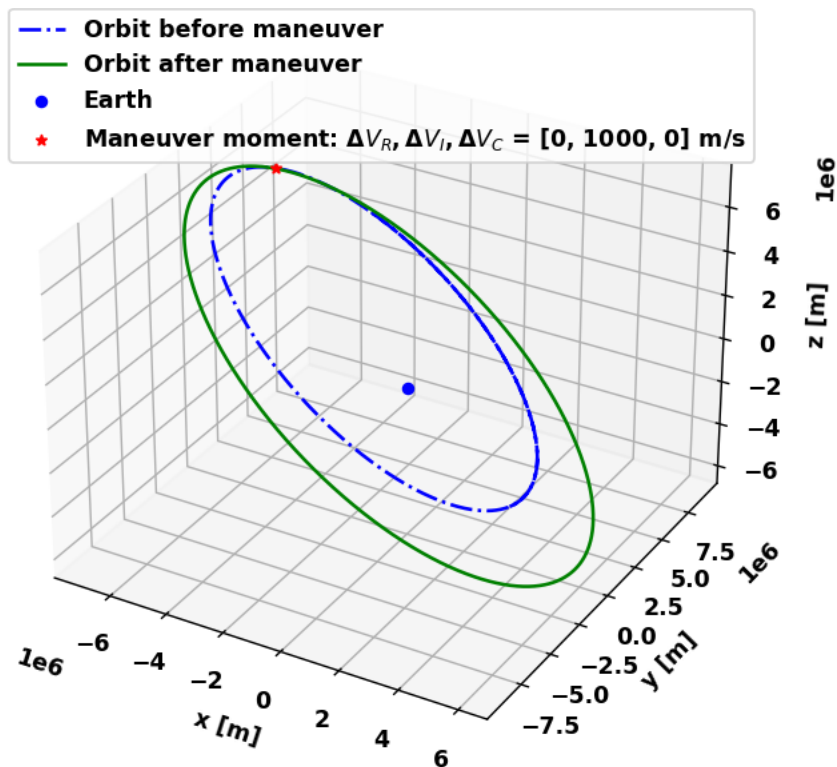


Figure 4.14: Spacecraft orbit before and after an exaggerated maneuver in the in-track direction.

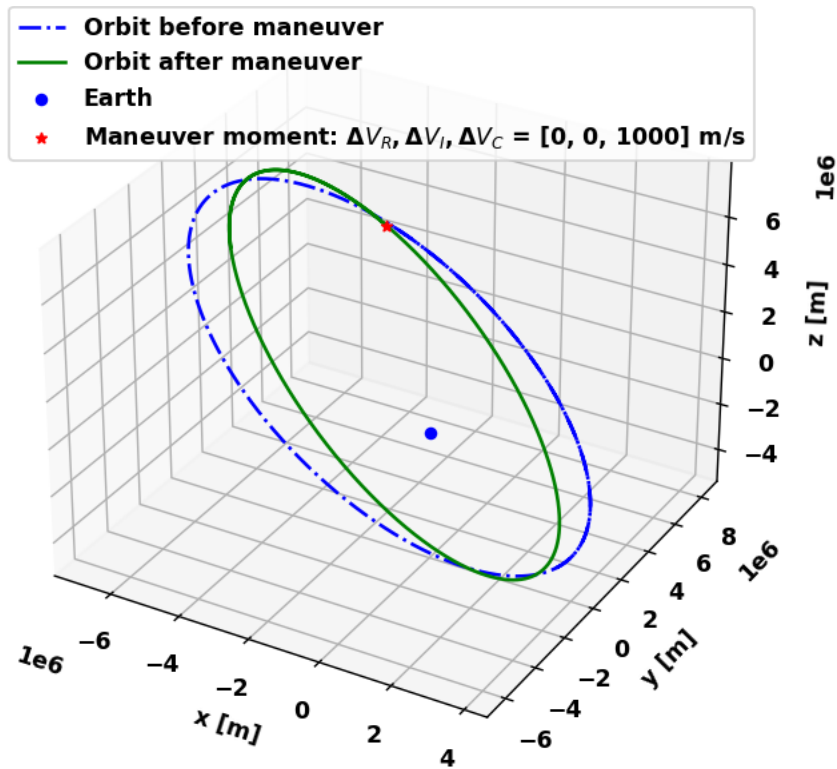


Figure 4.15: Spacecraft orbit before and after an exaggerated maneuver in the cross-track direction.

The maneuver impacts the orbit in the expected way: an increase in eccentricity and semi-major axis for the radial and in-track maneuvers, with the latter having a bigger impact and no semi-major axis or eccentricity change but inclination change in case of a cross-track maneuver. For a more detailed analysis by orbital element, the reader is referred to Section B.2. The above figures and the information provided in the appendix support the correct implementation of the maneuver model. From here onward, the instantaneous maneuver model can be applied to the remainder of the thesis.

In the context of the thesis problem, the moment of the maneuver is an optimization variable. Hence, the maneuver impact based on the spacecraft location in the orbit is shown in Figure 4.16.

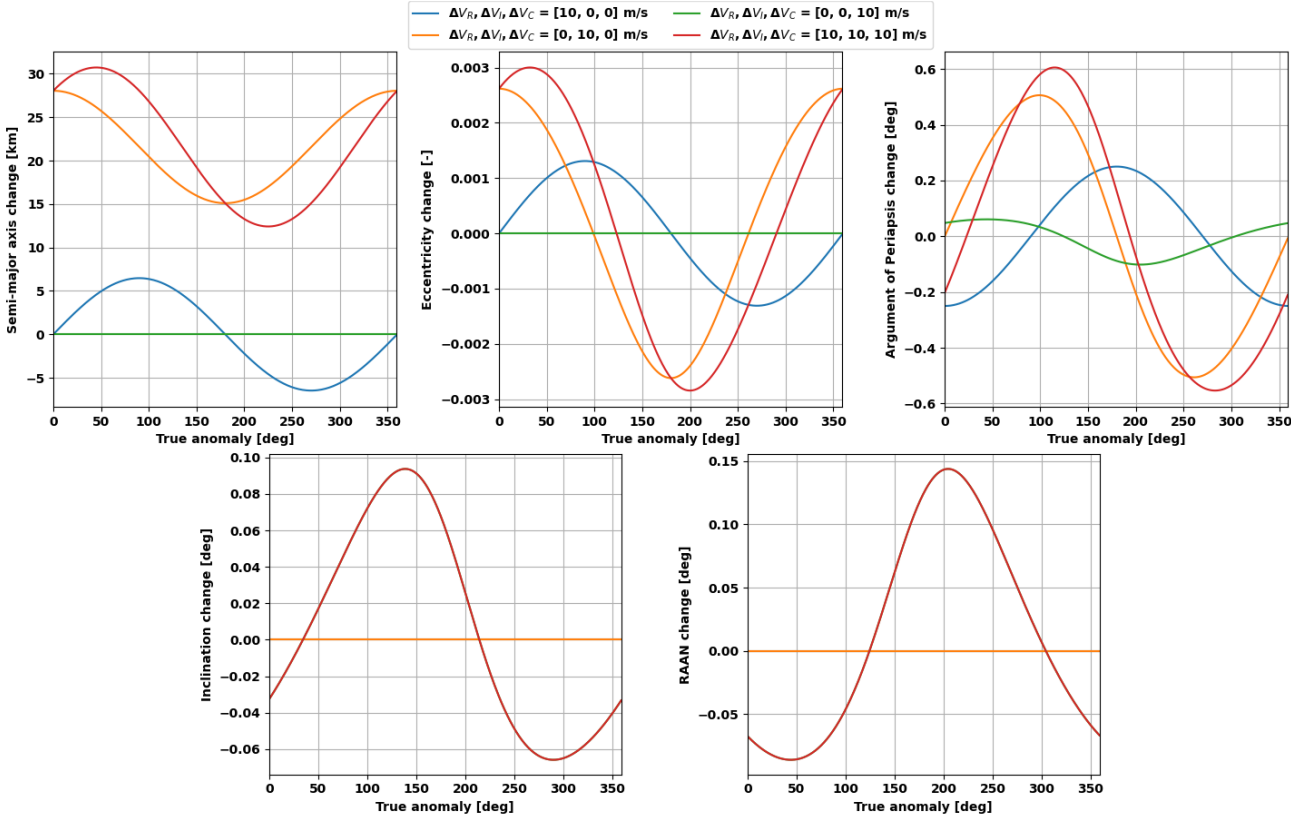


Figure 4.16: Effect of the maneuver on the Kepler elements with respect to when it is applied in the orbit.

In addition to the maneuvers in the three directions, a fourth maneuver is added to the analysis. This maneuver represents a velocity change in the three directions of the same magnitude simultaneously. The purpose of adding it, is to see how the effects can be combined. It generates the biggest changes, but the optimal locations are shifted with respect to the single-direction maneuvers.

The upper-left graph shows the changes to the semi-major axis. It can be seen that a maneuver in the in-track direction will always be more efficient than the maneuver in the radial direction. According to Wakker [19], this is true for any eccentricity value. It can also be seen that the optimal maneuver ( $\Delta V_I$ ) should be executed at perigee which is described by  $\theta = 0^\circ$ , meaning it will be oriented along the spacecraft's local velocity.

The upper-center graph shows the eccentricity changes. The optimal radial maneuver causes about 0.00125 eccentricity change at  $\theta = 90^\circ$  while the optimal in-track maneuver causes a change at  $\theta = 0^\circ$  of about 0.0025. This doubling of the value corresponds to the theory.

The upper-right graph shows the argument of periapsis change. It is shown that a maneuver in any of the three directions affects this orbital element as predicted by Equation 4.6. For the optimal  $\Delta V_R$  change the maneuver should be executed at perigee or apogee. For the optimal  $\Delta V_I$  change the maneuver should be executed at  $90^\circ$  and  $270^\circ$ . It can also be seen that the optimal  $\Delta V_R$  is half as efficient as the optimal  $\Delta V_I$  ( $0.25^\circ$  versus  $0.5^\circ$ ) and that the optimal  $\Delta V_R$  is more efficient than the optimal  $\Delta V_C$  maneuver.

The lower-left graph shows the inclination changes. Here the radial and in-track curves overlap at  $0^\circ$  change while the cross-track and combined maneuver also overlap showing the same inclination changes. This confirms that a change of inclination can only be realized with a velocity change in the cross-track direction. Following Wakker [19], the optimal maneuver needs to be executed close to the nodes (ascending or descending). Here, the argument of periapsis is  $235.7^\circ$ , this indicates that the ascending and descending nodes are around  $\theta = 124.3^\circ$  and  $304^\circ$ . These points do coincide with the surroundings of the optimal maneuver. The higher magnitude of inclination change around the first node indicates that this is closer to the apogee.

Finally, the lower-right graph shows the changes to the right ascension of ascending node. Similar to the inclination,  $\Omega$  can only be changed by a velocity change in the cross-track direction. The optimal locations are at  $u = 90^\circ$  and  $270^\circ$ , with  $\omega = 235.7^\circ$  this translates to the optimum locations being at  $\theta = 34.3^\circ$  and  $214.3^\circ$ . The graph shows values in accordance to the theory.

Overall, it can be said that the resulting effects on the spacecraft orbit depending on the maneuver performed (magnitude, direction, location) are in line with the expected results as discussed in Section 22.7 of Wakker [19]. In general, the in-track maneuver is more efficient than the radial maneuver. The cross-track maneuver is only relevant for changes in inclination and right ascension of ascending node.

## 4.5. Application of the optimization algorithm

The algorithm selected for the optimization was described in Section 3.4. However, this section works on defining the problem for the optimization. The elements necessary for the application are the decision variables, the constraints and the fitness function. The fitness function is based on the objectives of the optimization. Globally, the objective of this thesis is to find solutions that minimize the propellant mass usage, minimize the probability of collision and minimize the impact of the maneuvers on the orbit.

The decision variables and constraints are explained in Subsection 4.5.1, while Subsection 4.5.2 expands on the objectives and relates them to the fitness function. Finally, Subsection 4.5.3 defines the framework and shows results related to the algorithm tuning.

### 4.5.1. Decision variables and constraints

To describe the domain of the optimization problem, decision variables and constraints need to be established. They will guide the solutions and aid in representing the problem in a realistic domain. First an overall list of the decision variables is presented, followed by the constraints and their reasonings. Both definitions are merged to define the decision variable range.

#### Decision variables

The decision variables for this optimization problem are presented below. They are linked to the maneuvering aspect of the problem; timing and maneuver specifics.

1. Time of the first object maneuver
2. Time of the second object maneuver
3.  $\Delta V$  in the first direction of the first object's maneuver
4.  $\Delta V$  in the second direction of the first object's maneuver
5.  $\Delta V$  in the third direction of the first object's maneuver
6.  $\Delta V$  in the first direction of the second object's maneuver
7.  $\Delta V$  in the second direction of the second object's maneuver
8.  $\Delta V$  in the third direction of the second object's maneuver

Equation 4.8 defines the decision variables for the problem. Different conditions might apply to them depending on the simulation case and/or feasibility. These considerations are explained in the following paragraphs.

$$\mathbf{x} = [t_{\Delta V_1}, t_{\Delta V_2}, \Delta V_{1,R}, \Delta V_{1,I}, \Delta V_{1,C}, \Delta V_{2,R}, \Delta V_{2,I}, \Delta V_{2,C}]^T \quad (4.8)$$

#### Constraints

Defining constraints is important to make sure that the solution found by the optimizer is valid and can be used in the problem application. To apply these constraints they can be translated into penalties and added to the fitness function, or they can be used to limit the decision variable range. The list below gives the constraints, and their application and reasoning are presented thereafter.

1. Time of the maneuvers
2. Final collision probability below the threshold value of  $10^{-5}$
3. No new warnings between the two objects in conjunction within three days of the original TCA
4. Mass of the propellant used for each object
5. Orbit within limits of nominal performance

The first constraint is implemented by limiting the range of the first two decision variables. Within the problem, the maneuvers need to respect certain timings which is why it is necessary to set such a constraint. A more thorough explanation is given under the definition of the decision variables range.

The next three constraints are formulated into penalties that are applied to the fitness functions. Constraint number 2 makes sure that after the CAM implementation the conjunction does not trigger a reaction anymore. Constraint number 3 avoids that these objects get in a new conjunction scenario within 3 days of TCA triggered



by the new orbits. Finally, constraint number 4 avoids that more propellant is used than budgeted for. As this is a theoretical approach not linked to a real mission, values are assumed for the CAM  $\Delta V$  budget.

Constraint number 3 is monitored by checking the miss distance of both objects in the conjunction problem over a period of 3 days. If at any point the miss distance of both objects is under 1000 m, then the constraint is violated and it is not a viable solution. A limit of 1000 m was chosen because in the received database of CDM files no CDM was present that had a higher miss distance. Hence, this value is considered the safe margin. In real life, it would be important to check the proposed orbits against other objects in the neighboring regions of the conjunction and in the resulting orbit. However, this data is not widely available and could not be implemented at this moment. The current check allows for sufficient discussion on a dual approach as is the aim of this thesis. The implementation of this check would be necessary for real-world applications and is recommended as advancements to this thesis with the purpose of generating such a collision avoidance tool.

The last constraint (number 5), is implemented at this moment as part of the third objective of minimizing the orbit disturbance of both spacecraft. Checking whether both orbits are within their limits of nominal performance could be added as a next step to ensure that the CAM does not cause an orbit disturbance that is significant to the mission, while now the orbit disturbance is simply minimized. Applying this constraint could lead to the conclusion that a recovery maneuver would be necessary after the conjunction has been avoided. It is recommended that this constraint and backward maneuver be implemented in the future.

### Decision variables range

The first range to be defined is the timing of the maneuver. These variables are given to the optimization algorithm as a factor that is multiplied by the duration of a day. The goal is then to optimize for this factor which represents the moment of maneuvering. This factor needs to be between the time the CDM is generated and the TCA time, however, it is further limited by operational constraints that define the first moment the CAM can happen and the last one. The visualization of the timeline between CDM generation time and TCA time is shown in Figure 4.17.

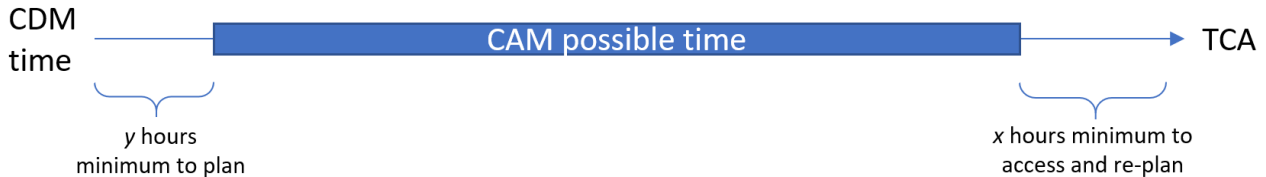


Figure 4.17: Visualization of possible CAM time.

The variables  $x$  and  $y$  can be changed case-by-case, but they will be pre-emptively set with broad operational constraints in mind.  $y$  denotes the minimum time needed to plan a maneuver and upload it to the spacecraft. As this deals with collision avoidance maneuvers, more time is needed to also discuss the necessity of the maneuver and potentially contact other operators. The following estimation is used to determine the value of  $y$ :

- Plan maneuver: 2 hours
- Discuss necessity of maneuver: 1 hour
- Contact other operators: 1 hour
- Upload maneuver to spacecraft and Satellite Operations Center (SOC) preparation time: 2 hours

**Total:**  $y = 6$  hours

A similar approach can be taken to estimate the factor  $x$ , which defines the minimum amount of time necessary between the CAM and the TCA. At this point, it is decided to allow for the possibility of a second maneuver after the CAM in the worst case that it does not fulfill its intended purpose. This means that it is necessary to allow for orbit determination to assess the impact of the maneuver. The following estimation is used to determine the value of  $x$ :

- Assess orbit with orbit determination: 6 hours
- Plan maneuver: 2 hours
- Upload maneuver to spacecraft and SOC preparation time: 2 hours
- Safety margin: 2 hours

**Total:**  $x = 12$  hours

In the optimization algorithm, this rationale translates to the maneuver time having a lower boundary of 0.25 and a higher boundary of 0.667, assuming 1.5 days available for operator maneuver planning.

Then, the decision variable range related to the  $\Delta V$  executed in each direction needs to be established. This depends on the propellant budget allocated to collision avoidance in each mission. As no specific mission is followed in this thesis, literature is used to define this range. A study on CAM optimization uses a range of  $\pm 1$  m/s in each direction [29]. As the problem at hand includes two maneuvering spacecraft as the main focus a lesser range can be applied. Iteratively the range was lowered until a value was found that allowed solutions with limited orbital disturbance; thus decision variables 3 to 8 are within a range of  $\pm 0.01$  m/s.

#### 4.5.2. Objectives and fitness function

The objectives are directly linked to the fitness function. They are used by the optimization algorithm to evolve the individuals and find the optimum solutions. The global objectives of the problem at hand have already been mentioned, but here they will be expanded upon and finally converted to the fitness function.

##### Objective definition

**1 - Minimize propellant usage:** The previously defined mass of the spacecraft and the specific impulse  $I_{sp}$  can be used to calculate how much propellant is consumed with the  $\Delta V$  conducted. Here, it becomes clear that the mass of the propellant used will be directly linked to the conducted  $\Delta V$  by Tsiolkovsky's equation (with the initial propellant mass  $m_0$  and the gravitational acceleration at sea level  $g_0$ ), as the other aspects will not change on the different tries. The objective needs to include the propellant used by both objects in conjunction if both are active and so this objective formulation also includes a weight factor for both of them as shown in Equation 4.9 by the terms  $w_{p_1}$  and  $w_{p_2}$ . This allows to set one object's propellant consumption as more important than that of the other one. At the start, the weight factors are set to be equal.

$$\begin{aligned}
 m_p(x) &= m_p(\Delta V_{1,R}, \Delta V_{1,I}, \Delta V_{1,C}, \Delta V_{2,R}, \Delta V_{2,I}, \Delta V_{2,C}) \\
 &= \frac{w_{p_1} m_{p_1}(\|\Delta \mathbf{V}_1\|) + w_{p_2} m_{p_2}(\|\Delta \mathbf{V}_2\|)}{w_{p_1} + w_{p_2}} \\
 &= \frac{w_{p_1}}{w_{p_1} + w_{p_2}} \left( m_{1,0} - \frac{m_{1,0}}{e^{\frac{\|\Delta \mathbf{V}_1\|}{I_{sp_1} \cdot g_0}}} \right) + \frac{w_{p_2}}{w_{p_1} + w_{p_2}} \left( m_{2,0} - \frac{m_{2,0}}{e^{\frac{\|\Delta \mathbf{V}_2\|}{I_{sp_2} \cdot g_0}}} \right)
 \end{aligned} \tag{4.9}$$

**2 - Minimize collision probability:** The initial collision probability will be taken from the CDMs. The covariances can be assumed to be constant along the conjunction period. A reason for keeping it constant is the small conjunction duration, as explained in Section 3.2. Furthermore, this limits the CPU time necessary while still allowing for a fair  $P_c$  comparison. Scaling the  $P_c$  value with a variable covariance will not affect the results significantly in terms of order-of-magnitude as the covariance will not change significantly (the goal is to minimize  $P_c$  above  $10^{-4}$  to below  $10^{-6}$ ).

The new conjunction geometry is used to calculate a new collision probability after the conducted maneuvers [37]; the changes will be due to a new relative position. This new collision probability is compared to the original to see how it has evolved. Obviously, the goal is to decrease it. Equation 4.10 describes the relationship between the collision probability (cf. Equation 3.9) and the decision variables. The probability as explained in Section 3.2 is dependent on many factors including the state of the objects which is related to the decision variables.

$$\begin{aligned}
 P_c(x) &= P_c(t_{\Delta V_1}, t_{\Delta V_2}, \Delta V_{1,R}, \Delta V_{1,I}, \Delta V_{1,C}, \Delta V_{2,R}, \Delta V_{2,I}, \Delta V_{2,C}) \\
 &= \frac{1}{\sqrt{(2\pi)^3 \det(C)}} \int_{V_c} \exp \left[ -\frac{1}{2} \Delta r(x)^T C^{-1} \Delta r(x) \right] dV
 \end{aligned} \tag{4.10}$$

**3 - Minimize mission impact:** The third objective requires some discussion on the implementation. This objective is dependent on the object's orbit and its purpose. For example, spacecraft in GEO must stay within their station-keeping box to be able to conduct their services; when collision avoidance maneuvers need to be performed this limit must be respected and so there will be no mission impact. The situation in LEO is more dynamic, spacecraft have varying purposes and varying geometric constraints. Additionally, this orbital region is more

prone to have constellations which need to respect the formation flying geometry defined to serve their intended purposes. Different ideas are discussed below before determining how to implement this objective within the optimization.

The first idea defined by Wolfhagen [31], considers the difference of the updated orbit ( $\mathbf{r}_{\text{man}}$ ) with respect to the original orbit. It is shown in Equation 4.11. The scenario discussed is about spacecraft bound to a certain formation where a difference in the orbit could be detrimental for the services. To assess the difference in orbit the author defines an integration period of 30 days (which is the expected station-keeping maneuver interval). Additionally, the second integral is called a corrective term to account for the fact that the nominal orbital position ( $\mathbf{r}_{\text{nom}}$ ) is different to the optimally designed one ( $\mathbf{r}_{\text{org}}$ ) due to perturbations and such.

$$\psi = \int_{t_1}^{t_2} |\mathbf{r}_{\text{nom}}(t) - \mathbf{r}_{\text{man}}(t)| dt - \int_{t_1}^{t_2} |\mathbf{r}_{\text{nom}}(t) - \mathbf{r}_{\text{org}}(t)| dt \quad (4.11)$$

The second idea from Laan [38] would be to define a 'fictitious' station-keeping box around the spacecraft similar to the GEO spacecraft method. The author defines the limits in the in-track and cross-track component and argues that the radial direction will be controlled with the in-track component. A fixed limit is set for the in-track direction of 17.5 km while the aim for the cross-track is to minimize any disturbances.

The third idea is to monitor the ground-track. Some LEO missions need a specific ground-track and so need to be operated within a certain range from the designed case. Seong and Kim [26] analyze a mission with formation flying around a chief spacecraft. The article proposes a 5 km boundary of ground-track distance from the chief spacecraft. Another constraint is to maintain the formation range between 50 m and 5000 m.

The final idea, proposed in a literature review conducted by Kerr and Sanchez [37], is to characterize this objective by the time outside of the nominal orbit. Minimizing this time is important to limit the disruptions of the services, where these could be of lesser quality or even complete interruption. However, this is dependent on the specific mission requirements.

Overall, it can be said that different missions would require different formulations for this objective as it strongly depends on the mission type and requirements. As this thesis will tackle different simulation scenarios (introduced in Chapter 7) with no real mission linked to them, it is hard to define this objective based on mission needs and for the different scenarios individually. As such it is decided to take a general formulation of the mission disruption objective, and not have it as a hard limit but as an objective that is to be minimized, where the weight should be lower than that of the other two. The reason for a lower weight factor is that it is expected that an operator prefers conducting a CAM to avoid a significant collision over stopping or reducing services for a limited time period.

The formulation of this objective is based on the position difference of the spacecraft in an orbit without and with the CAM. This difference is integrated from the time of maneuver until three days later. If the results indicate significant difference that would drastically affect the services of any spacecraft mission, including a come-back maneuver should be considered. In this case the propellant cost of the come-back maneuver would be added into the propellant mass objective as well. However, a back maneuver is not implemented in this thesis and is proposed as recommendation for future work.

Equation 4.12 shows how the objective is defined. It is related to the decision variables because it depends on the states of both objects. At the moment it accounts for mission impact to both objects in conjunction with weights ( $w_{O_1}$  and  $w_{O_2}$ ). They are set to be equal but can be varied to simulate different scenarios. This equation is different from Equation 4.11 in two aspects: it does not consider the corrective term<sup>b</sup> and it sums differences in orbit experienced by both objectives to define the final mission impact.

$$\begin{aligned} O_{\text{dist}}(\mathbf{x}) &= O_{\text{dist}}(t_{\Delta V_1}, t_{\Delta V_2}, \Delta V_{1,R}, \Delta V_{1,I}, \Delta V_{1,C}, \Delta V_{2,R}, \Delta V_{2,I}, \Delta V_{2,C}) \\ &= \frac{w_{O_1} O_{\text{dist}_1}(t_{\Delta V_1}, ||\Delta \mathbf{V}_1||) + w_{O_2} O_{\text{dist}_2}(t_{\Delta V_2}, ||\Delta \mathbf{V}_2||)}{w_{O_1} + w_{O_2}} \\ &= \frac{w_{O_1}}{w_{O_1} + w_{O_2}} \int_{t_{\Delta V_1}}^{t_{\text{TCA}+3}} |\mathbf{r}_{\text{nom}, 1}(t) - \mathbf{r}_{\text{man}, 1}(t, t_{\Delta V_1}, ||\Delta \mathbf{V}_1||)| dt + \\ &\quad \frac{w_{O_2}}{w_{O_1} + w_{O_2}} \int_{t_{\Delta V_2}}^{t_{\text{TCA}+3}} |\mathbf{r}_{\text{nom}, 2}(t) - \mathbf{r}_{\text{man}, 2}(t, t_{\Delta V_2}, ||\Delta \mathbf{V}_2||)| dt \end{aligned} \quad (4.12)$$

<sup>b</sup>This work is not linked to any real scenarios, so quantifying how the nominal orbital position varies from the optimally designed one is impossible.

### Fitness function

These objectives need to be translated to generate a proper fitness function shown in Equation 4.13. For this the following parameters are introduced: Mass parameter defined in Equation 4.14 (representing the first objective), Collision parameter defined in Equation 4.15 (representing the second objective), and Orbit parameter defined in Equation 4.16 (representing the third objective). These parameters will make sure the range of optimization is similar over all the objectives leading to better behavior of the optimization algorithm, moreover, they are selected to allow minimization of all three objectives in the fitness function optimization. Additionally, these parameters are selected to aid in results visualization and interpretation. The parameters are directly linked to the objectives and can be traced back to the real objective value.

The Mass parameter is built up of the combined propellant mass with its weights as shown in Equation 4.9 and a penalty ( $P_{\text{mass}}$ ) in case the propellant mass used for either object is above their respective thresholds for propellant mass usage. The penalty depends on the simulation case as it needs to be significantly higher than the normal objective values. For the first simulation case, low values of propellant mass used are expected so the penalty is set to  $10^6$ .

The Collision parameter needs more attention to be defined. First, all collision probabilities that are calculated to be 0 after the CAM implementations<sup>c</sup> are set to a very low probability:  $10^{-100}$ . Then, a penalty ( $P_{\text{coll.}}$ ) is included for all probabilities of collisions above  $10^{-5}$  as they are all unfeasible solutions according to constraint number 2. This formulation is used for the optimization, but to interpret the results in a more straightforward manner the following transformation is applied:  $-1/\log_{10}(P_c)$ .

The Orbit parameter is formed by taking the common logarithm of the orbit disturbance objective and adding a penalty. The reason for taking the common logarithm is that the values of orbit disturbance (outcome of Equation 4.12) are expected to be high. The penalty ( $P_{\text{orbit}}$ ) is again set to  $10^6$  as it will be significantly higher than the outcome of the common logarithm. A penalty is added to the parameter if constraint number 3 is violated.

$$f(\mathbf{x}) = \begin{bmatrix} f_{\text{mass}}(\mathbf{x}) \\ f_{\text{coll.}}(\mathbf{x}) \\ f_{\text{orbit}}(\mathbf{x}) \end{bmatrix} \quad (4.13)$$

$$f_{\text{mass}}(\mathbf{x}) = m_p(\mathbf{x}) + P_{\text{mass}} \quad (4.14) \quad f_{\text{coll.}}(\mathbf{x}) = P_c(\mathbf{x}) + P_{\text{coll.}} \quad (4.15)$$

$$f_{\text{orbit}}(\mathbf{x}) = \log_{10}(O_{\text{dist}}(\mathbf{x})) + P_{\text{orbit}} \quad (4.16)$$

Table 4.8 shows how the objective space is expected to look after the optimization. This helps understand how the individuals will be rated. An individual with low Orbit and Mass parameters and with the color green would be an optimal individual, minimizing all three objectives. As shown in Subsection 6.1.1 this would correspond to the lower left corner in the objective space. With the introduction of the selected parameters, the values and their ranges are comparable, which is beneficial for multi-objective optimization.

Table 4.8: Linking the fitness values to their objectives.

Propellant mass [g]	Mass parameter	$P_c$ [-]	Collision parameter		Orbit disturbance [m · s]	Orbit parameter
0.0	0.0	0	0.000		$10^8$	8.0
0.1	0.1	$10^{-40}$	0.025		$3.16 \cdot 10^8$	8.5
0.2	0.2	$10^{-20}$	0.050		$10^9$	9.0
0.3	0.3	$4.64 \cdot 10^{-14}$	0.075		$3.16 \cdot 10^9$	9.5
0.4	0.4	$10^{-10}$	0.100		$10^{10}$	10.0
0.5	0.5	$10^{-8}$	0.125			
		$2.15 \cdot 10^{-7}$	0.150			
		$1.93 \cdot 10^{-6}$	0.175			

<sup>c</sup>Values of 0.0 and -0.0.

### 4.5.3. Algorithm tuning

Tuning the parameters of the Non-dominated Sorting Particle Swarm Optimization (NSPSO) algorithm is important for improving its performance and achieving better results for a particular optimization problem. Here, the focus is given to explaining certain parameters that are deemed important for a well-functioning algorithm. The initial model is shown in Table 4.9. The main parameters that can be tuned in NSPSO are:

- **Swarm Size:** The number of particles in the population. A larger swarm size may result in better exploration of the solution space, but it can also increase the computational time.
- **Inertia Weight:** The inertia weight determines the balance between exploration and exploitation in the algorithm. A high inertia weight will result in more exploration, while a low inertia weight will result in more exploitation. A general rule of thumb suggests that it is better to initially set the inertia weight to a larger value, and gradually decrease it [33].
- **Cognitive Acceleration Coefficient:** The cognitive acceleration coefficient determines the influence of the particle's personal best position on its velocity. A high value will result in particles moving more aggressively towards their personal best position, while a low value will result in a more conservative movement.
- **Social Acceleration Coefficient:** The social acceleration coefficient determines the influence of the global best position on the velocity of the particles. A high value will result in particles moving more aggressively towards the global best position, while a low value will result in a more conservative movement.

The optimal values for these parameters can be determined through a process of trial and error, or through more sophisticated methods such as sensitivity analysis or meta-heuristic tuning. It is important to note that the optimal parameter values for NSPSO may depend on the specific optimization problem being solved and may need to be adjusted for each new problem. Additionally, NSPSO is a stochastic algorithm, so even with optimal parameter values, it may not always produce the same results for the same optimization problem.

- Population size equivalent to the swarm size.
- Number of generations.
- Omega which is equivalent to the inertia weight. It takes a value between 0 and 1.
- C1 is the magnitude of the force, applied to the particle's velocity, in the direction of its previous best position. This is equivalent to the cognitive acceleration coefficient and it takes values larger than zero.
- C2 is the magnitude of the force, applied to the particle's velocity, in the direction of its global best position, which is equivalent to the social acceleration coefficient. As C1, it takes on values above zero.
- Chi: the velocity scaling factor, taking values above or equal to 0.
- $V_{\text{coeff}}$ : the velocity coefficient which needs to be between 0 and 1.
- Leader selection range: determines the optimum solutions considered for the leader. It takes values below 100.
- Diversity mechanism: defines the leader selection range. The options are crowding distance, niche count, and max-min.

The different diversity mechanism options determine how the algorithm evolves at each step so it is important to understand the three options. The niche count of a particle is determined by the number of other particles within a specific distance. When comparing two particles in the non-dominated front, the one with a lower niche count is preferred [33]. This approach promotes a more diverse non-dominated front.

The crowding distance is used to sort particles based on their diversity. Particles are ordered in descending order of crowding distance, and a random selection is made from the top of the sorted list [33]. This favors particles located in less crowded areas of the Pareto front.

The max-min approach involves two steps [39]. First, the minimal difference in fitness values across all objectives is determined. Then, by iterating over the population, the maximum of these minima is found. For a decision vector to be considered a non-dominated solution, its max-min fitness value must be less than zero. As with the two other options, the max-min function promotes diversity, penalizes clustering, and identifies non-dominant solutions.

Furthermore, the population size is important to consider during the tuning. A large population is important for good convergence in NSPSO algorithms. A small population can lead to sub-optimal fronts and a limited number of non-dominated solutions, which affects solution spread and coverage. Fewer particles do not adequately explore the search space, causing dominant particles to hinder the generation of potentially good particles with

different non-dominated solutions.

**Table 4.9: Initial NSPSO optimization model with the parameters to be varied and/or tuned.**

Parameter	Value	Reason
Seed	10, 50, 100	Consistency check
Population size	50 (to be tuned)	High initial guess as recommended.
Number of generations	25 (to be tuned)	Convergence must be reached.
Omega	0.5 (to be tuned)	[39]
C1	2.0 (to be tuned)	[39]
C2	2.0 (to be tuned)	[39]
Chi	1	[39]
$V_{\text{coeff.}}$	0.5	[39] and [26]
Leader selection range	50	[39]
Diversity mechanism	Crowding mechanism (to be tuned)	Algorithm evolves differently.

In this thesis, the tuning is done for the following parameters: number of generations, population size, cognitive acceleration coefficient (referred to as C1), Social Acceleration Coefficient (referred to as C2), diversity mechanism, and the inertia weight (referred to as omega). The tuning is conducted through trial and error by varying the individual parameters one by one and finally combining the results into the final model. After the model is defined a quick sensitivity analysis is done to determine the sensitivity of the problem to uncertainties in the decision variables. Every optimization is run three times with different seeds (randomly selected at 10, 50, and 100) to check the consistency (or robustness) of the solutions and to ensure that the best Pareto front is found.

## Code set-up

This chapter deals with the scripts generated to solve the collision avoidance problem. First, the pre-processing part is explained in Section 5.1. Then, the schematic of the propagation part is explained in Section 5.2, including the maneuver computation unit. The next step is related to the optimization. Here, the use of parallel computing is introduced in Section 5.3. This also meant using the Delftblue machine so the implementation is verified in Section 5.4.

### 5.1. Pre-processing

The main source of input files used in this thesis are the CDM files received on the TU Delft CubeSats (Delfi-C<sup>3</sup> and Delfi-n3Xt)[36]. These files all include the same type of information and the relevant parts need to be extracted. For this, a CDM reading script is made. After clearing out formatting issues, the information extracted is the following:

- **Orbital information:** states of both objects retrieved in km and km/s and directly converted to m and m/s, and covariance matrices of both objects as shown in Equation 3.7.
- **Object information:** exclusion volume of both objects in m, and details on drag and solar pressure radiation:  $C_D A/m$  and  $C_R A/m$  in  $m^2/kg$ .
- **Conjunction information:** TCA converted to seconds from the J2000 epoch, CDM generation date converted to seconds from the J2000 epoch, collision probability, miss distance m, and relative speed m/s.

Additionally, information about the objects mass, geometry, and cross section are taken on DiscosWeb<sup>a</sup> with the NORAD ID provided in the CDM file.

### 5.2. Propagation

As explained in Chapter 4, the first step of solving the problem is to implement the propagation and the maneuvering of the objects so that afterward the collision avoidance can be optimized. The results of these first steps have been presented in the previous chapter but it is also important to understand how the code is set up to reach the results.

For orbit propagation, a dynamics model is required. The inputs to the dynamics model are the propagation times, the bodies, the perturbations or accelerations, and the termination conditions. Next, the dynamics model is generated with the help of the selected integrator and propagator. The results are the object's states and the dependent variables defined as important. This flow is shown in Figure 5.1.

---

<sup>a</sup><https://discosweb.esoc.esa.int/>

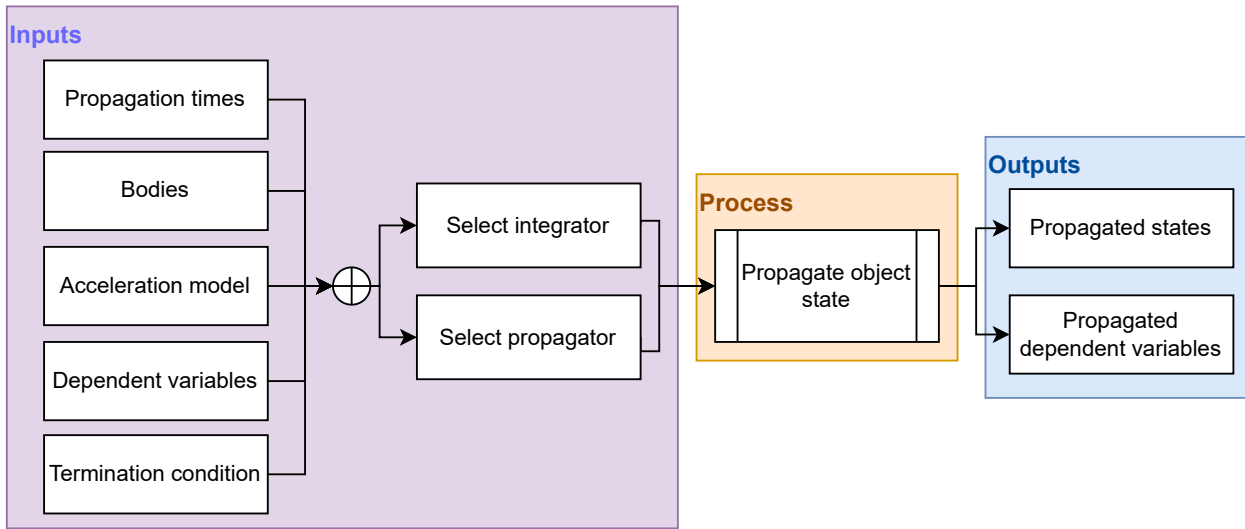


Figure 5.1: Objects propagation diagram.

This is just the basic propagation; for the collision avoidance also maneuvering needs to be included. To do so the propagation is split into three phases: pre-maneuver, perform a maneuver, and post-maneuver. The middle phase consists of implementing the maneuver and no propagation is conducted. Figure 5.2 shows the relationship between the phases, as the pre-maneuver and the post-maneuver consist of the same process they are displayed as 'Propagate object'. This block is essentially the process shown in Figure 5.1.

The first phase leads to the inputs for the second phase: 'Perform maneuver'. The outputs of the maneuvering are new states for the objects. These are fed back into the third phase. If more maneuvers are necessary, the process can then continue by generating more inputs and another set of maneuvers.

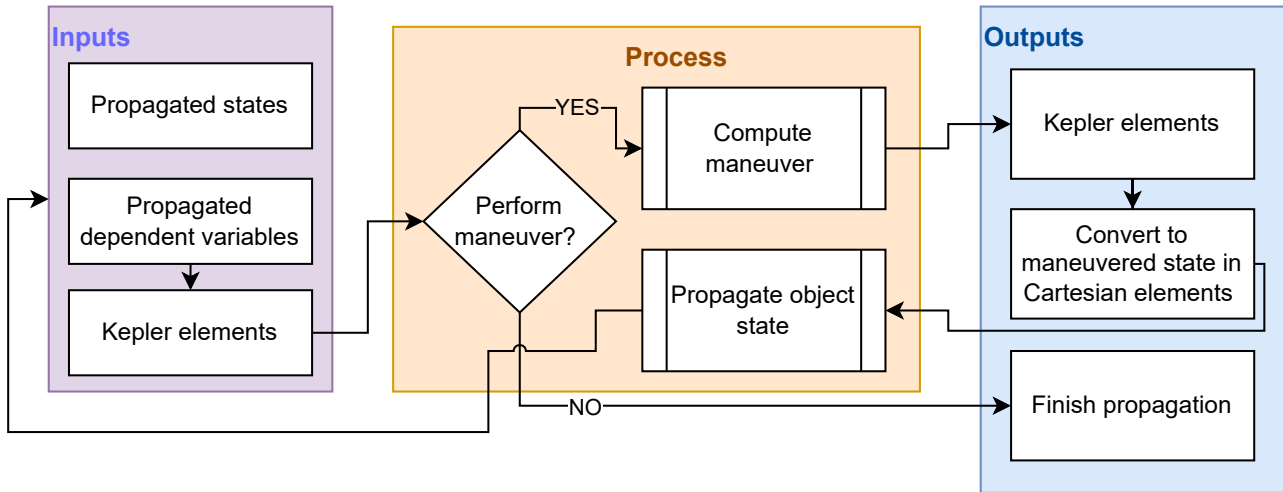


Figure 5.2: Maneuver implementation diagram.

### 5.3. Optimization and parallel computing

After the propagation and maneuver implementation, the optimization of the problem is the next step. Each individual in the optimization will go through the steps shown in the previous section.

Due to the CPU time-intensive nature of the optimization problem tackled in this thesis, parallel computing is used. Parallel computing refers to the use of multiple processors or cores to perform computations simultaneously. Some of the benefits of parallel computing are [40]:

- Increased speed: tasks are divided among cores and so the optimization is completed faster than with a single processor.
- Improved performance: as the data is processed more efficiently, the overall performance of the software is increased.
- Cost-effective: parallel computing allows for the existing hardware to be used to its full extent.
- Scalability: the computing needs might change over the evolution of the thesis. Parallel computing allows for easy scalability.



- High-throughput: multiple tasks can be processed simultaneously allowing for an overall more efficient process.

Initially, implementing parallel computing onto the local machine of the thesis author allowed to use the four CPU's available and generate results faster. The local machine refers to the student's standard laptop with the following specifications:

- Processor: Intel(R) Core(TM) i7-7700HQ CPU @ 2.81 GHz
- OS: Windows 10
- Usable RAM: 7,88 GB

However, the parallel computation can be taken a step further by using TU Delft's supercomputer, called Delftblue<sup>b</sup>. Delftblue is designed for scientific research and engineering simulations and consists of thousands of processors connected by a high-speed network [41]. It is used by researchers at the university and other institutions to perform CPU-intensive calculations and simulations.

The use of Delftblue to solve this thesis' problem allows for improved performance as while the simulations run other work can be done on the local machine; the documentation process did not interfere with the CPU time of the simulations. It also allows to extend the usage of parallel computing as more CPU's can be used: a limit of 45 per student. Although preparing for the usage of Delftblue required some effort to adapt the scripts, it is worth it for the improved performance and higher throughput.

A way to use the higher throughput capabilities is to upload the three independent optimizations (with three different seeds) in one go to Delftblue. Whenever there are enough nodes available, the jobs are run, even simultaneously at times. This is illustrated in Figure 5.3. The case definition and the optimization definition are the same (except for the seed) and the optimization results are generated for each one.

This can be pushed further by uploading different cases and different optimization models at once as well. For example, for the algorithm tuning, several optimization models are uploaded as different jobs at once to Delftblue.

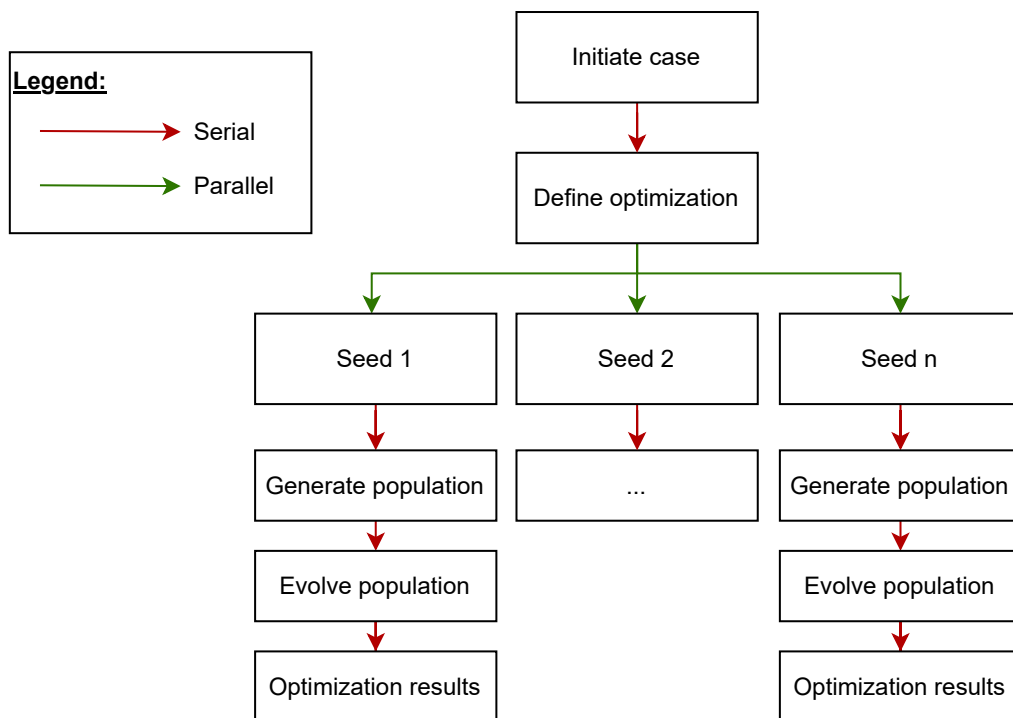


Figure 5.3: Multiple jobs (n) uploaded onto Delftblue at once.

Additionally, parallel computing is used within the optimization under multi-threading with Batch Fitness Evaluation (BFE). This means that the fitness function can be evaluated in batches or groups, leading to better clock-time effectiveness [35]. The fitness batches are then combined before continuing with the generations. A schematic of how this works for the problem is shown in Figure 5.4.

<sup>b</sup>It was named after the famous Delft Blue pottery.

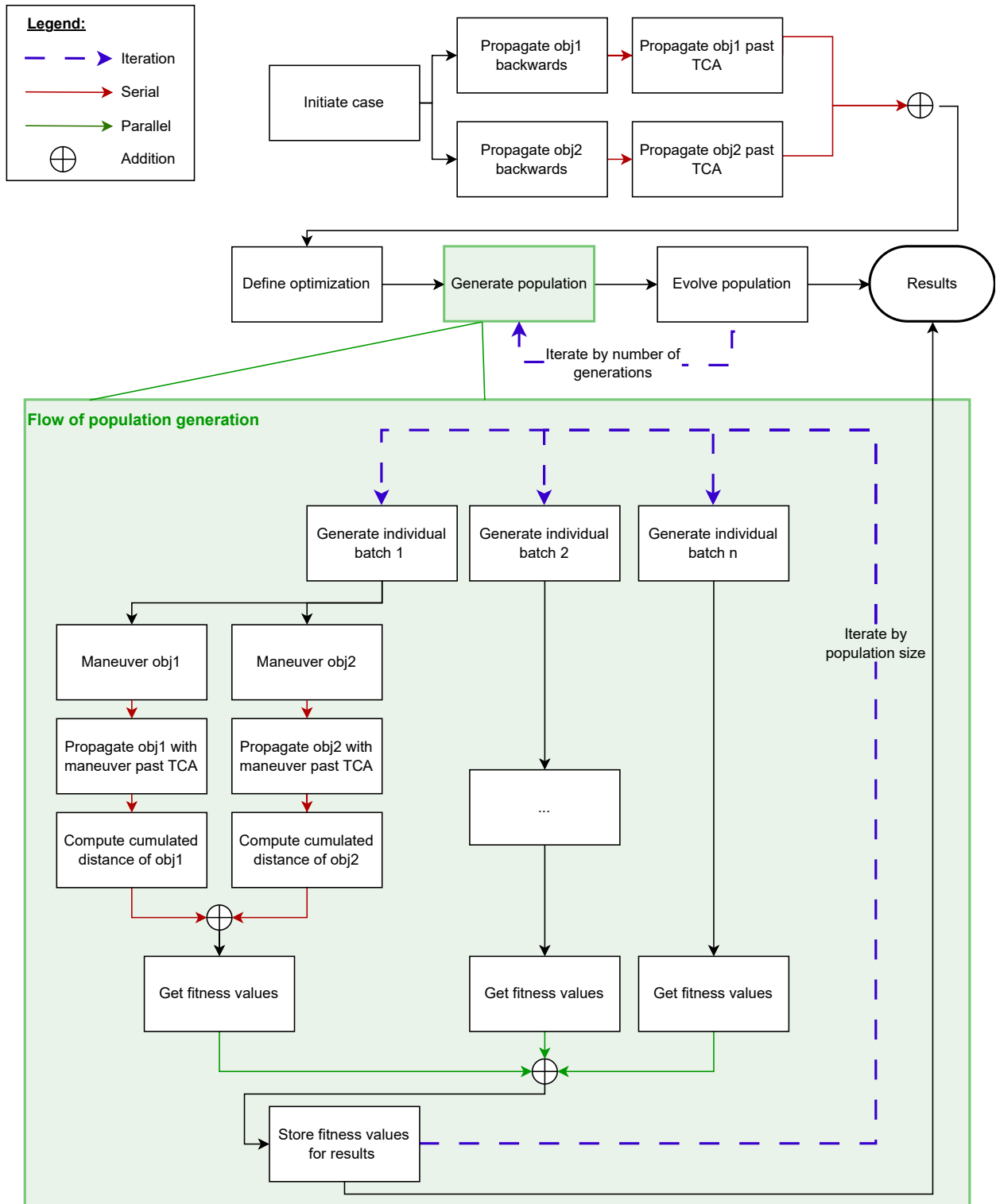


Figure 5.4: Breakdown of optimization algorithm with BFE.

## 5.4. Verifying Delftblue calculations

To verify the implementation within Delftblue, the same runs were uploaded as were conducted previously on the local machine. Quickly, a difference between the fitness values was noticed. Investigating it further, a discrepancy within one of the objectives was noticed, namely the orbit disturbance factor. The fitness values of the individuals of the first generation were compared and a small difference in the order of  $10^{-10}$  was noticed, although the decision variables selected by the algorithm were verified to be the same. After this, the next generations showed differences in all objectives. Due to the slight difference in the first generation, different individuals are chosen for the following generations leading to bigger differences in fitness values. However, the differences stayed within the same range afterward, they did not get exponentially worse.

The orbit disturbance factor relies significantly on the propagation of the two objects. It evaluates the differences between the original orbit and the orbit affected by the CAM over time, integrates them and adds them. Investigating the root of this difference led to the discovery that the accumulated distance over the two orbits (no CAM and with CAM) was different. At this point, comparing a propagation run on Delftblue and on the local machine was the next step, as it is at the root of the accumulated distance.

To do so, the propagation used in this optimization case was extracted and run on both machines. Their orbits were compared and slight differences were observed. Below the distance between the orbit found locally and the one on Delftblue is displayed in Figure 5.5, along with the difference in velocity in Figure 5.6. Over the course of around 6 days of propagation a final difference of 0.00015 m was found.

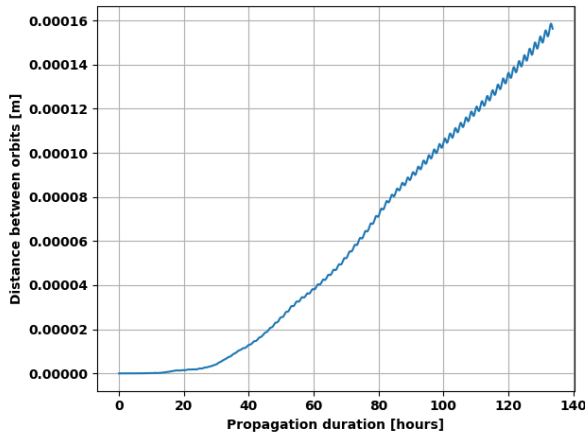


Figure 5.5: Distance between Delftblue and local machine orbit over time.

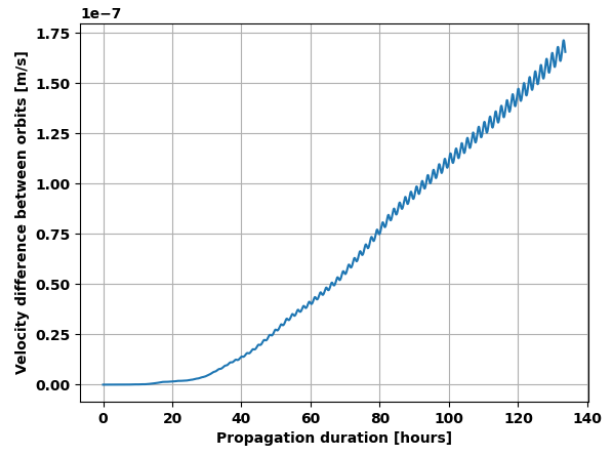


Figure 5.6: Velocity between Delftblue and local machine orbits over time.

To understand where this difference originates from, the perturbations used in the propagations were looked into. Figure 5.7 shows the divergence in total acceleration norm found in both machines. The divergence per perturbation type is shown in Figure 5.8.

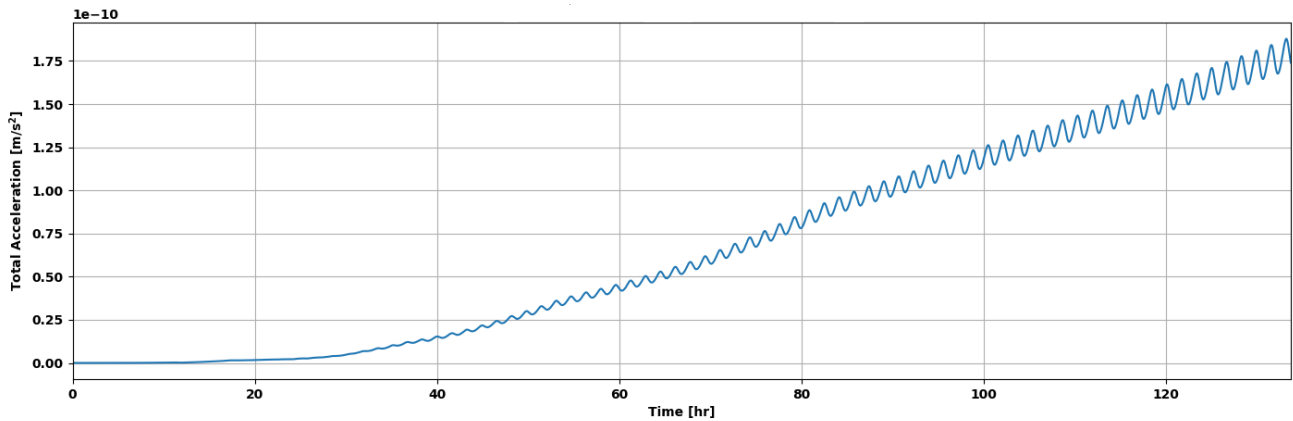


Figure 5.7: Total acceleration norm difference between Delftblue and local machine over time.

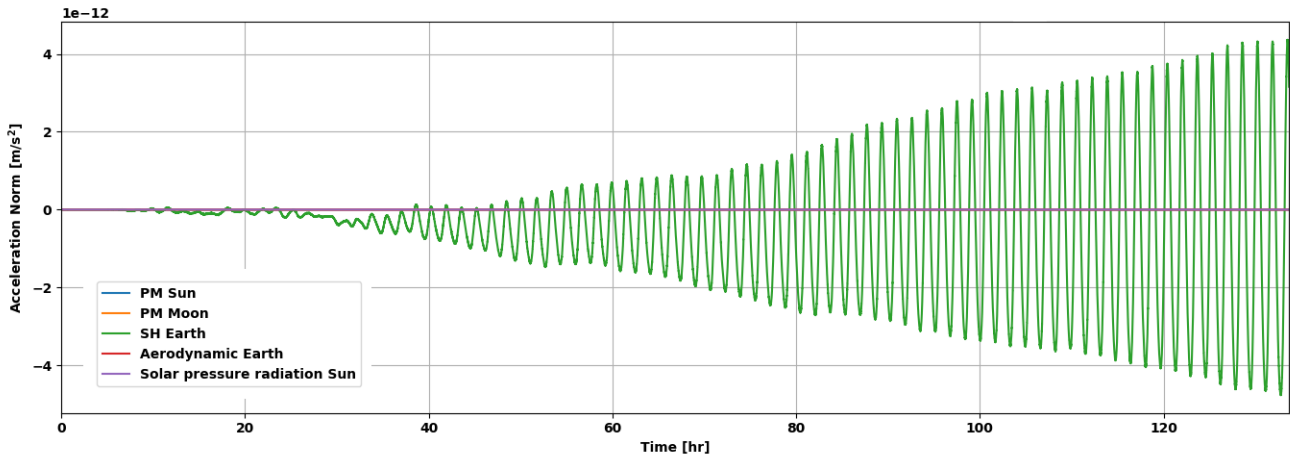


Figure 5.8: Perturbation differences between Delftblue and local machine over time by perturbation type.

The largest influence in the perturbations comes from the spherical harmonics caused by the Earth. Over the course of the propagation, the difference increases to a value in the order of  $10^{-12}$  m/s<sup>2</sup>. The increasing and sinusoidal shape in the perturbation discrepancies can be explained by the orbit position changing slightly at each instant, and thus new perturbations are induced resulting in bigger orbit position differences. Zooming into the start of Figure 5.8, the first errors are seen to be in the order of  $10^{-16}$  which corresponds to rounding error values. These results are displayed in Figure 5.9.

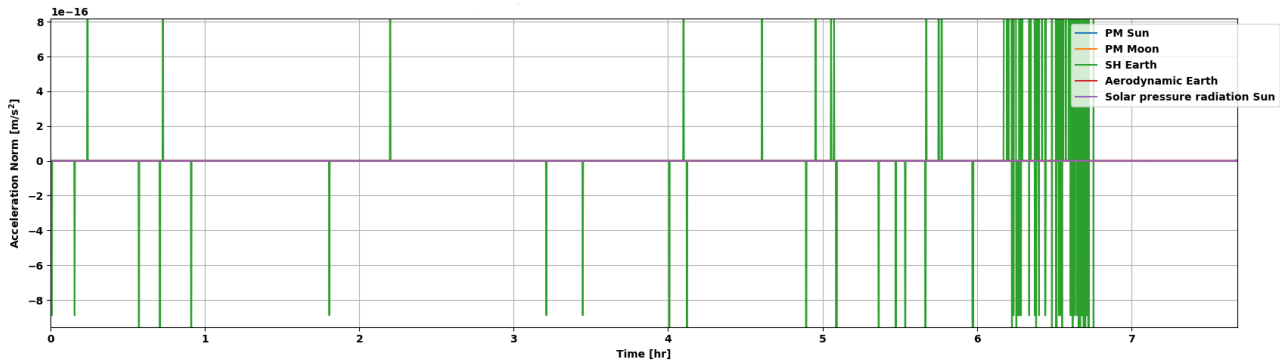


Figure 5.9: Zoomed into first 8 hours of Figure 5.8.

It was concluded that due to using different machines and different systems (the local machine runs on Windows 10 and Delftblue runs on Linux), rounding errors were introduced into the propagation. These rounding errors lead to different orbital positions and thus different perturbation values. This effect is mostly in the spherical harmonics which is also responsible for the biggest perturbation in the dynamics model (see Figure 4.1). The slightly different perturbations lead to different propagated orbits which explain the diverging orbits.

The original issue was detected in the mismatch between the accumulated distances. As there are slightly different orbits, it also led to different accumulated distances in the first generation. Afterwards, new individuals were selected and this effect was carried onto the following optimization generations. Hence, it can be concluded that finding the exact results between Delftblue and the local machine is impossible. This difference is visualized in Section 6.1.

## Preliminary results

After selecting a starting point for the algorithm before moving on to tuning, preliminary results can be generated to understand the characteristics of the problem, including that of the results. At this stage a comparison between runs conducted on Delftblue and on the local machine can be presented. Keeping in mind the findings of Section 5.4, it is not expected that the comparison produces overlaying perfectly results but that they are similar. At this stage they can be interpreted as results obtained with different seeds. For this chapter the results produced by Delftblue are marked with crosses ('x') while the results from the local machine are marked with dots ('.'). The algorithm used for the generation of these results uses the preliminary parameter settings and a population of 50 individuals and 25 generations as shown in Table 4.9.

First different visualization options for the results will be presented in Section 6.1. Interpreting them will lead to the conclusion that a new problem formulation needs to be used in the optimization algorithm, which is described in Section 6.2. Finally, a review of the comparison is presented with the new method in Section 6.3.

### 6.1. Visualization options

Due to the difficulty of displaying results from a three-dimensional optimization problem, different visualization options are explored in this section. The goal is to be able to identify the Pareto fronts within these graphs. This allows to find the optimal results and conduct the necessary interpretation (ideally, by operators). First, the original idea of the objective parameters definition shown in Subsection 4.5.2 is presented, where the third objective is shown as a color map. Then, the use of three-dimensional graphs is explored. Finally, the option of presenting the three-dimensional problem as three projections onto two-dimensional planes is shown. In this section the graphs shown contain only individuals that meet the constraints and all the acceptable individuals in the optimization are shown (over the different generations).

#### 6.1.1. Third objective as color map

Three-dimensional graphs are hard to interpret in two dimensions, so an idea is to represent one dimension with colors. The results are presented in Figures 6.1, 6.2, and 6.3 for three different seeds: 10, 50 and 100. To interpret these graphs first attention is given to the Orbit parameter and the Mass parameter. Then, the analysis of where the optimal solutions lie needs to be combined with the color scheme provided for the Collision parameter. The three graphs show a similar cloud-like behavior where the optimal Collision parameter solutions (lower values displayed in green) tend to correlate with the higher values of Orbit and Mass parameters (cf. Table 4.8).

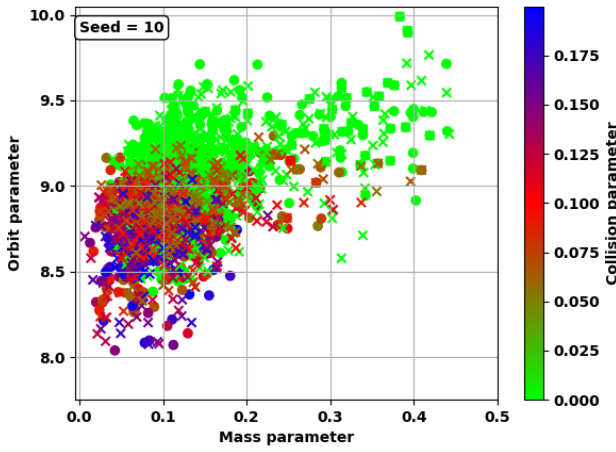


Figure 6.1: Objective space with color map (seed = 10).

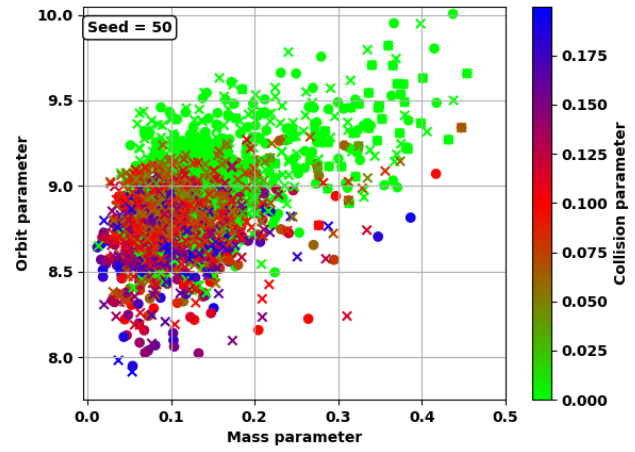


Figure 6.2: Objective space with color map (seed = 50).

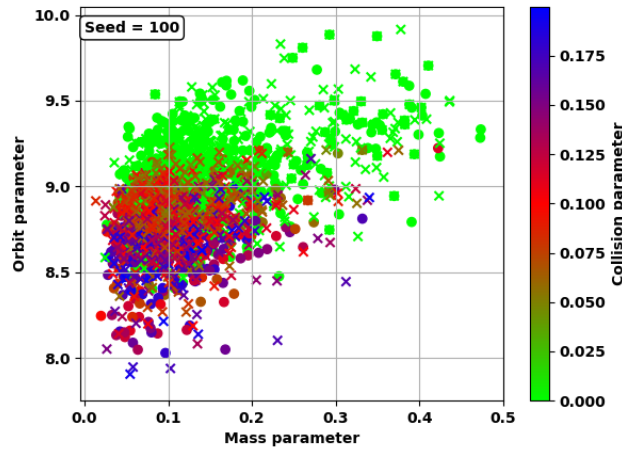


Figure 6.3: Objective space with color map (seed = 100).

The goal is to minimize all three objectives, so individuals that are displayed as green in the bottom-left corner would be the optimal solutions. However, the bottom-left corner does not contain any green individuals. As expected, it is not possible to minimize all three objectives. By definition, lowering the collision probability requires some contribution in propellant mass and causes an orbit disturbance. In that corner individuals that are blue and red can be found. According to the scale the blue individuals are the worst while the red are medium. These values translate to:

- Collision parameter = 0.0  $\rightarrow P_c = 0.0$
- Collision parameter = 0.1  $\rightarrow P_c = 10^{-10}$
- Collision parameter = 0.175  $\rightarrow P_c = 1.93 \cdot 10^{-6}$

More examples of conversion can be found in Table 4.8.

Comparing the visualization over different seeds also does not allow to determine whether similar final results are reached. Although similar behaviors are seen in the results obtained with all three seeds, they are scattered differently. This is expected, but the optima should tend in the same direction and such a trend cannot be observed with this representation. As such this visualization does not permit to identify the consistency of the optimization results.

Additionally, Delftblue produced individuals can be compared to the local machine individuals. They do not always overlap but they respect the same tendencies. Their differences are comparable to the differences between the results obtained with different seeds as hinted at in Section 5.4. Again, it is confirmed that both machines can be used for the analysis.

This representation allows to identify the traits that were expected from the results. However, it does not permit to identify a Pareto front or any variation uncertainty of it when plotting all the individuals. The individuals seem to be within a cloud of results where the identification of a worst and a best part is impossible. This visualization will not allow for a correct discussion. As the end goal is to be able to present such results for a negotiation between operators, with these graphs they would not be able to identify the good options. If the

graphs included only the Pareto front

### 6.1.2. Three-dimensional graphs

As the visualization with color maps has proven to be difficult, the original representation for three-objective optimizations is shown here with three-dimensional graphs. These graphs display the Delftblue results and the local machine results, but here also the Pareto fronts per generation are shown: the individuals marked blue are normal individuals while the green ones were found to be part of the Pareto front for their generation. As all the individuals over the different generations are shown here, there is a cloud of green individuals and a cloud of blue individuals. As before, the results are shown for three different seeds; seed 10 in Figure 6.4, seed 50 in Figure 6.5, and seed 100 in Figure 6.6.

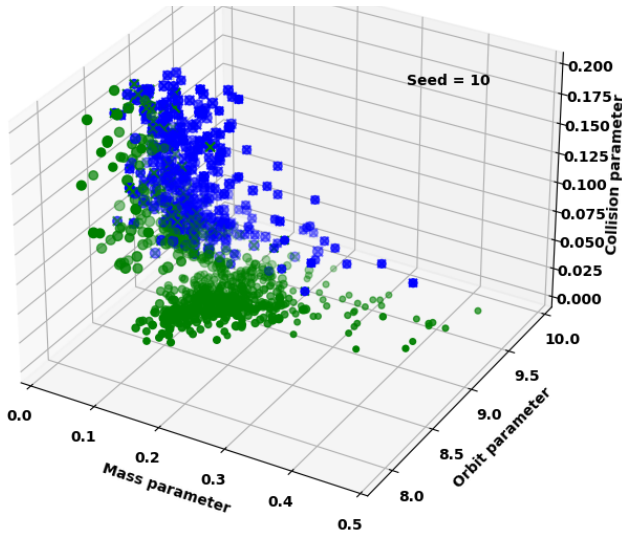


Figure 6.4: Objective space in 3D (seed = 10).

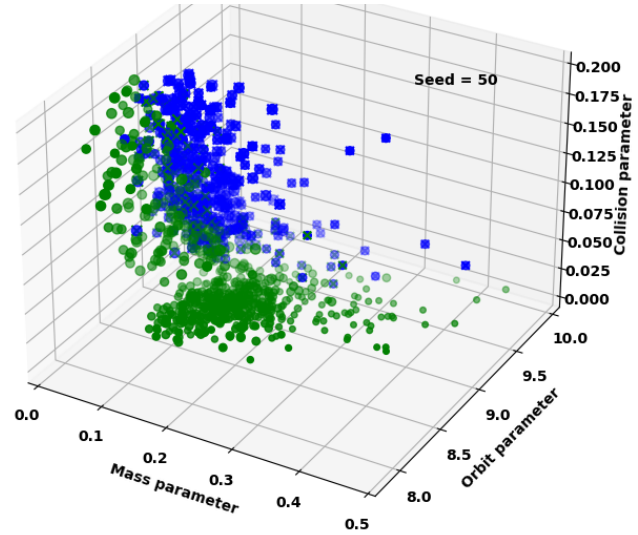


Figure 6.5: Objective space in 3D (seed = 50).

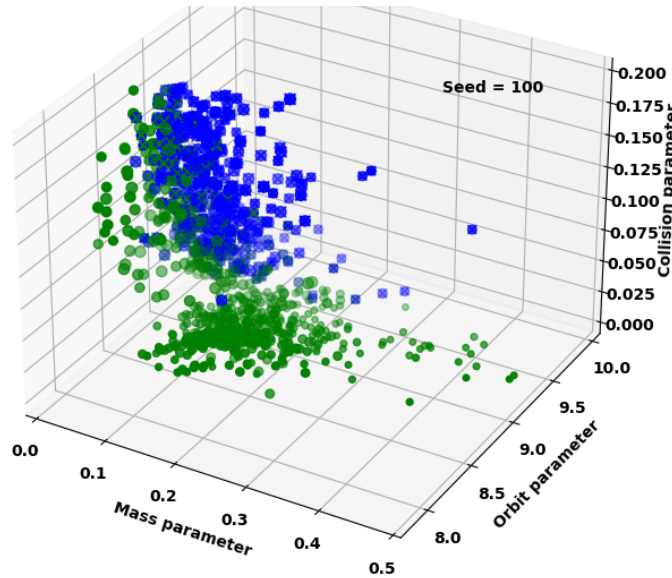


Figure 6.6: Objective space in 3D (seed = 100).

The results shown here in 3D are the same as before with the color maps, and even so the interpretation of the results remains complicated. Previously, it was seen that the lower values of Collision parameter were accompanied by higher values of Mass and Orbit parameters. This cannot be easily identified in these graphs, although higher Collision parameter values tend towards the left-inside part of the graphs. There is an accumulation of green individuals on the left of the Mass parameter axis and towards the middle of the Orbit parameter axis, but identifying their value in terms of Collision parameter is complicated.

This representation does allow for an additional conclusion: a gathering of green individuals with low Colli-



sion parameter values. There appears to be no or little blue points in that region. This indicates the presence of a Pareto front, although pinpointing it is hard.

### 6.1.3. Projection in two dimensions

The last option to show the three-dimensional results is to have projections onto two-dimensional planes. This will lead to three different graphs: Collision parameter versus Mass parameter, Collision parameter versus Orbit parameter, and Orbit parameter and Mass parameter; they need to be read together to understand the overall picture. As before, the Pareto fronts for each generation are included so there is a duality between crosses and dots (comparison between Delftblue and the local machine) and a duality between the individuals marked green (Pareto front) and the individuals marked blue. Figure 6.7 shows the 2D projections for the optimization conducted with seed 10, while Figure 6.8 shows them with seed 50 and then Figure 6.9 with seed 100.

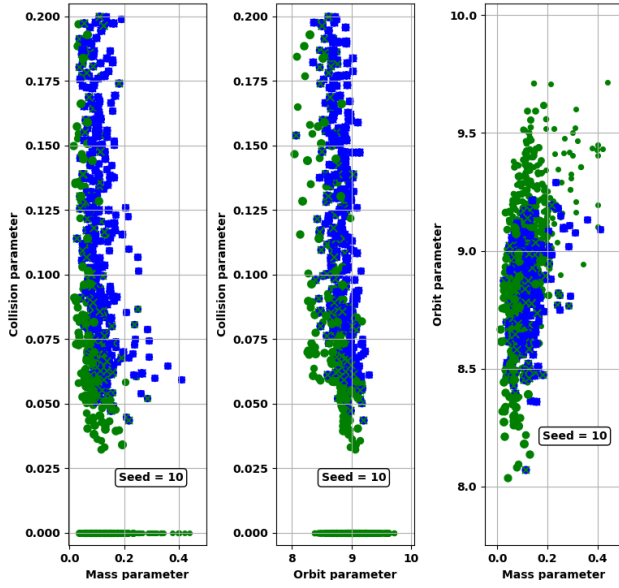


Figure 6.7: Objective space projected onto 2D (seed = 10).

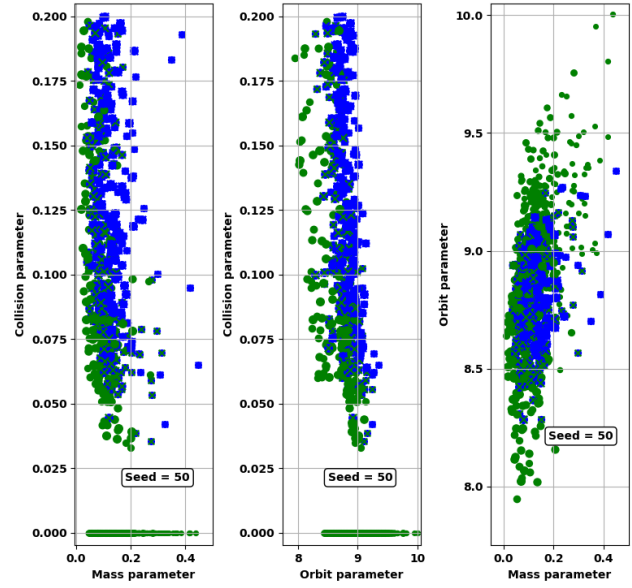


Figure 6.8: Objective space projected onto 2D (seed = 50).

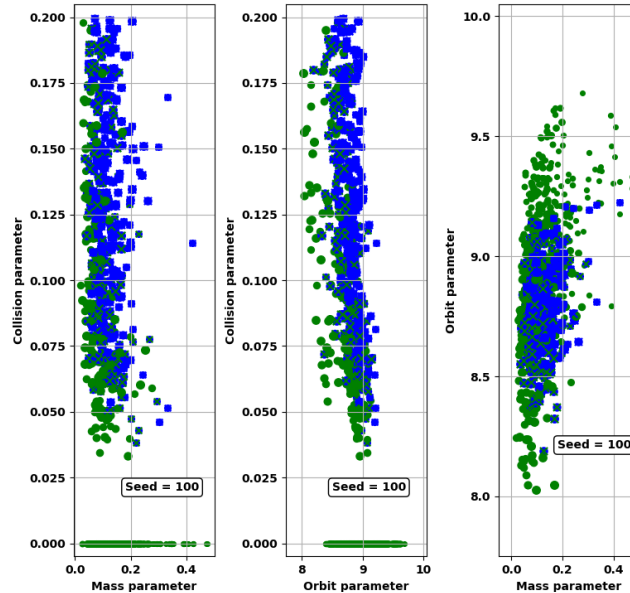


Figure 6.9: Objective space projected onto 2D (seed = 100).

First the focus is given to the Collision and Mass parameter graphs. They show that although zero Collision parameters can be reached with low values of the Mass parameter, still the lowest Mass parameter values do present higher values for the Collision parameter. There also seems to be a wide variety of Mass parameter values for zero Collision parameter, although this can also be seen for Collision parameter values around 0.06.



The same cannot be said for the Collision and Orbit parameter graphs: zero values of the Collision parameter cannot be reached with the lowest Orbit parameters. It seems clear that to lower the Orbit parameter increasing the Collision parameter is necessary. The contrary is also valid (and physically obvious): with high values of the Collision parameter, high Orbit parameter values are not reached.

Lastly, the Orbit and Mass parameter graphs are harder to interpret as the values seem to be more spread out. The previous two projections showed that green individuals (the Pareto individuals) tend to the left, while here they are more spread apart. It can however be identified that higher values of the Orbit parameter are accompanied by a higher Mass parameter. Physically this makes sense: a higher orbit disturbance requires bigger maneuvers. The opposite is also true, lower Orbit parameters show lower Mass parameters. These two areas are also where the green individuals are focused on, the upper and lower quadrant of the graphs. With the problem at hand it would be interesting to know what values of Collision parameter are linked to the lower quadrant of the graphs.

However, combining these findings is hard especially when the optimization has more individuals. The lower part of the third graphs is identified as an interesting region for the optimal solution, but they cannot easily be linked back to the other graphs making it impossible to distinguish the Collision parameter values that they have. Overall, it can be said that the projections can be interpreted individually but merging their conclusions is impossible, and so again the optimal results cannot be found.

As before interpretation is difficult. A gathering of optimal individuals can be identified on the bottom of the two first subgraphs in the Figures above, but pinpointing them in the third subplot remains hard. These points have low Collision parameter values but generally higher Mass and Orbit parameters. This gathering can be explained by investigating the evolution of the optimization algorithm.

The first generations provide very good Collision parameter results, but they do not improve the other two parameters. Along the generations the algorithm pushes for minimizing the other two parameters as well, thus increasing the Collision parameter. At this stage it starts running into the penalties for the Collision parameter. The balance between minimizing the other two parameters and not having Collision parameter penalties is tricky and so there is a tendency of having several points with an ideal Collision parameter but not in the other two parameters which is visualized by the straight lines.

In short, the issue with this projection is that the Pareto fronts are identified in the three-dimensional problem and so the projections shown in the Figures above do not display the Pareto fronts correctly. Alternatively, new Pareto fronts could be calculated comparing only two objectives at a time, but with that the third objective's contribution would be lost. Comparing the results of the three different seeds, similar behaviors are identified but as the optima cannot be identified no real conclusion on the stability of the results can be drawn.

## 6.2. Review of optimization methodology

As the current formulation of the optimization problem does not provide results that can be interpreted in a clear manner a review is necessary. Recommendations or conclusions on how the operators should react cannot be made at the moment. The optimization method is not wrong per se, but it does not lead to useful results so it was decided to review the process.

The proposal is to reformulate it as a two-dimensional problem, where Pareto fronts can be directly identified and so lead to a fruitful and clear trade-off between collision avoidance and cost. For this, two objectives are combined into one. As already hinted, the problem at hand from an operator's point of view is between collision avoidance and cost to the system. Two objectives deal with the cost at the moment, the Mass and the Orbit parameter, both to be minimized, so they are merged into a single parameter.

The computation remains the same until the final definition of the fitness function. The three objectives are computed individually as before, but then the Mass and Orbit parameter are merged to be input into the fitness function. To choose a new combined objective made up from the Mass parameter and the Orbit parameter, the results shown in this chapter are used. It should be noted that any combination can be used to generate this new objective, and it could be varied according to the needs of the operator.

First, it is important to set both objectives to the same starting point as otherwise the new objective would be biased. A value of 8 is used as the Orbit parameter intercept (noted  $p$ ). The range of the Orbit parameter is 2 while the range of the Mass parameter is 0.5 (cf. Table 4.8). The Mass parameter is multiplied by the ratio of

the two ranges (denoted by  $n_1$ ), while the Orbit parameter is multiplied by 1 (denoted by  $n_2$ ). This leads to the following equation for the Combined objective, also called the Cost parameter.

$$f_{\text{cost.}}(x) = \frac{n_1 \cdot f_{\text{mass}}(x) + n_2 \cdot (f_{\text{orbit}}(x) - p)}{n_1 + n_2} \quad (6.1)$$

This means that in the Cost parameter, the Mass parameter contributes to 80% of the value and the Orbit parameter to 20% of the value. Following the objective definition reasoning in Subsection 4.5.2 it makes sense that the orbit disturbance weighs less than the propellant mass consumption.

As this parameter is made up from two parameters that were being minimized, the objective continues to be an objective that is to be minimized. The new fitness function is then defined as follows, where the definition of the Collision parameter remains as in Equation 4.15 while the Cost parameter is defined as in Equation 6.1.

$$f(x) = \begin{bmatrix} f_{\text{cost.}}(x) \\ f_{\text{coll.}}(x) \end{bmatrix} \quad (6.2)$$

## 6.3. New approach results

Applying the combined method, new results are obtained and new comparisons can be done between the results provided in Delftblue and the local machine. Checking this comparison again determines whether the Combined method allows for a proper interpretation of the results and for identification of Pareto fronts, or if new adaptations are required. The results can be seen in Figures 6.10 to 6.12 for seeds 10, 50, and 100. These three runs are combined into final Pareto fronts in Figure 6.13. The same presentation as before is used: individuals marked green belong to a generation's Pareto front, and crosses are results from Delftblue while dots are results from the local machine<sup>a</sup>.

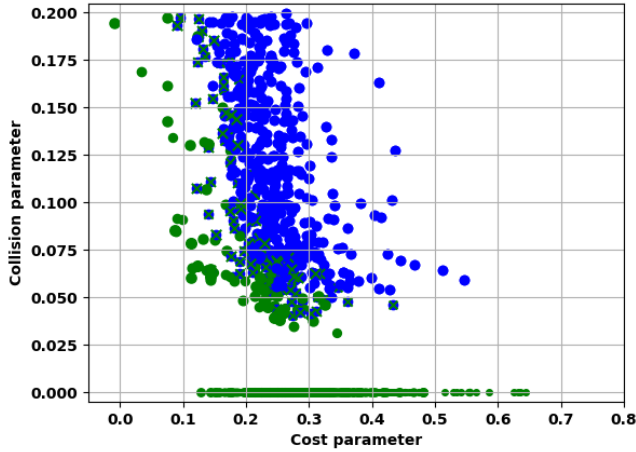


Figure 6.10: Objective space for combined method (seed = 10).

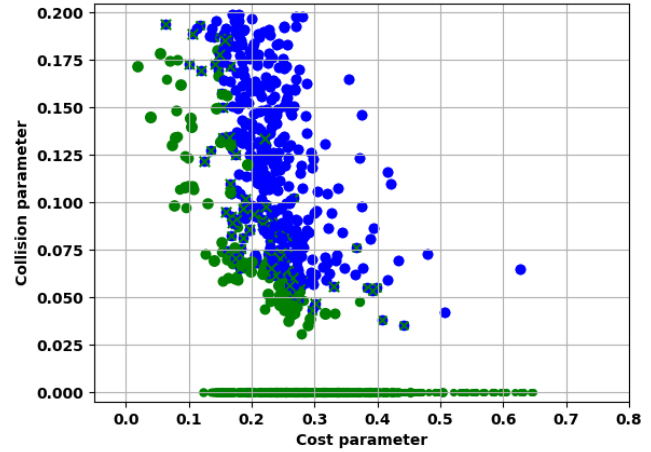


Figure 6.11: Objective space for combined method (seed = 50).

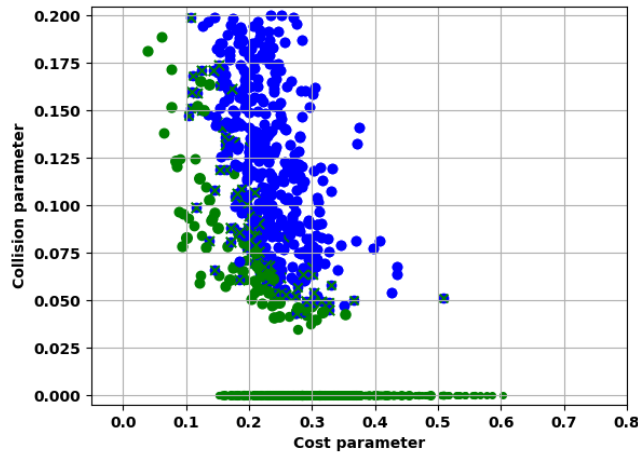


Figure 6.12: Objective space for combined method (seed = 100).

This representation supports a more clear definition of Pareto fronts. They still appear convoluted in the figures above because the results are shown for all generations, but a trend barrier on the left side of the graphs can be identified with the green individuals. The three different seeds show similar behaviors but different results: seed 10 identifies a lower Cost parameter than the other two seeds, while seed 100 tends to have higher minimum Cost parameter values. Moreover, seed 10 seems to present a better spread of individuals in the Pareto front compared to the other two (this can be seen better in Figure 6.13).

It should also be noted that seed 10 presents a Cost parameter value that is negative. Instinctively, this does not seem to be possible physically as the Cost parameter is made up from the propellant mass used and the orbit disturbance caused; both values cannot be negative. However, the Cost objective equation shown in Equation 6.1 includes the subtraction of an intercept value set at 8. If the Orbit parameter would go below 8, its contribution to the Cost parameter would be negative. Thus negative values should not be of concern and simply indicate low orbit disturbances.

<sup>a</sup>Due to the change in fitness formulation, the differences previously identified between the Delftblue and local machine are harder to identify. However, upon zooming in the results they can still be seen.)

The discrepancy between the results for different seeds indicates that the baseline optimization model chosen is not adequate and tuning of the optimization parameters should be conducted. The results of the tuning are presented in Section 6.4 following the methodology described in Subsection 4.5.3.

As before, straight horizontal lines are present in the graphs with Collision parameter values of zero. The same reasoning as before applies to their existence and they are valid optimal individuals part of the Pareto front. The optimizer has a tendency to solve for the Collision parameter using a high Cost parameter, while evolving it tries decrease the Cost parameter and subsequently increases the Collision parameter. This populates the higher values of Collision parameter. Simply it means that an operator could choose to minimize the collision probability to zero with a wide range of Cost parameter values, which physically makes sense. Here, it would be up to the operators discretion to choose how much to spend, but it would be logical to then opt for the most left individual present in the straight line.

There is also a gap between the cloud of individuals above the straight line. The straight line implicates a value of zero collision probability while the cloud of optimums presents Collision parameters as limiting at around 0.025 which means  $10^{-40}$  (in Figure 6.11 for example or 0.05 equivalent to  $10^{-20}$  in Figure 6.13) collision probability. Analyzing the raw fitness values from the optimization it seems like the limiting number is  $10^{-29}$  which is represented by a Collision parameter of 0.0345. At such low collision probability values operators do not consider the risk worth mitigating so their reaction will not change when seeing a collision probability of  $10^{-29}$  or  $10^{-40}$ . Hence, this gap is not considered as detrimental for the analysis.

Additionally, comparing the overlap between crosses and dots in this Combined method to the original method shown in Section 6.1, an improvement is noticed. Differences can still be identified but in general there are less outliers in between the two different machines. This can be attributed to the fact that the degree of complexity has been lowered with now only two objectives, both to be minimized.

To begin the tuning of the optimization model used in the Combined approach, a baseline for comparison should be set. The tuning is done based on the final Pareto fronts obtained over the different seeds, so in Figure 6.13 the final Pareto fronts for the Combined method baseline model can be found. As mentioned before, the Pareto front is scarce on the left side with several gaps and the different seeds find different minima. This underlines the need for tuning. The clock run time of this model (with 3 seeds) is around 47 minutes.

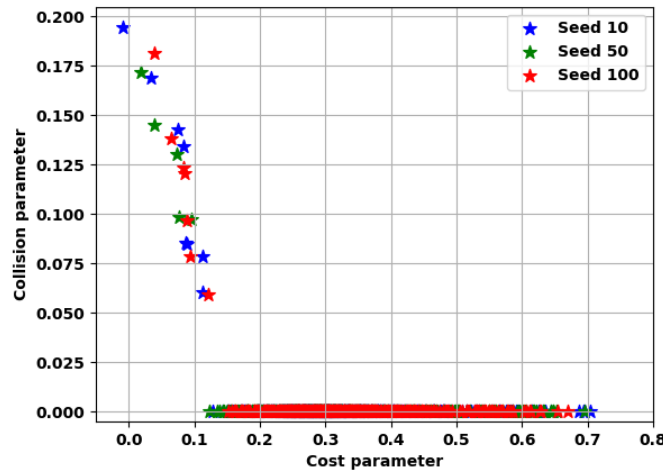


Figure 6.13: Combined method baseline Pareto front over different seeds.

## 6.4. Tuning the new optimization algorithm

The most efficient way to conduct the tuning is by comparing the results obtained from different optimization runs. For this the Pareto front of each tuning run is presented in this section, in the same style as Figure 6.13 which shows the baseline model against which the tuning runs are compared. To aid in understanding the changes between the runs, tables are presented that detail the models. The best optimization model for this problem is identified visually. No convergence criteria has been applied.

### Generation tuning

To conduct the tuning on the number of generations for the model, the number of generations is progressively increased from the baseline. This is portrayed in Table 6.1, while Figures 6.14 to 6.16 show the results for the three runs. Increasing the number of generations allows the optimization algorithm to change the individuals more and hopefully then reach better results and fully populate the Pareto front.

Table 6.1: Optimization model definition for the generation tuning ('x' indicates that the value has not changed).

	Population	Generation	C1	C2	Omega	Diversity mechanism
<b>Baseline model</b>	<b>50</b>	<b>25</b>	<b>2</b>	<b>2</b>	<b>0.5</b>	<b>Crowding mechanism</b>
<b>Run 1</b>	x	50	x	x	x	x
<b>Run 2</b>	x	100	x	x	x	x
<b>Run 3</b>	x	150	x	x	x	x

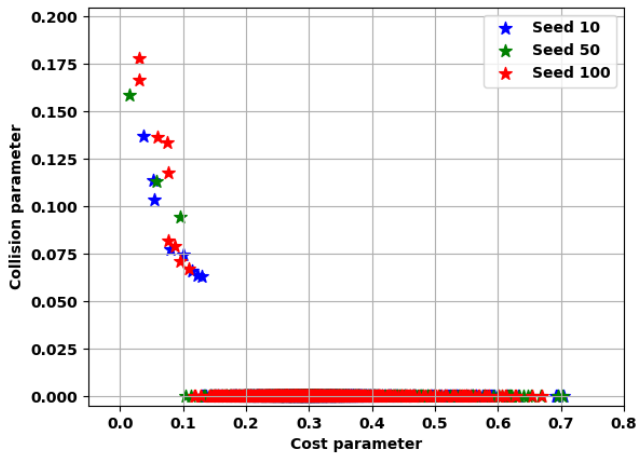


Figure 6.14: Generation tuning (50) - Run 1 Pareto front over different seeds.

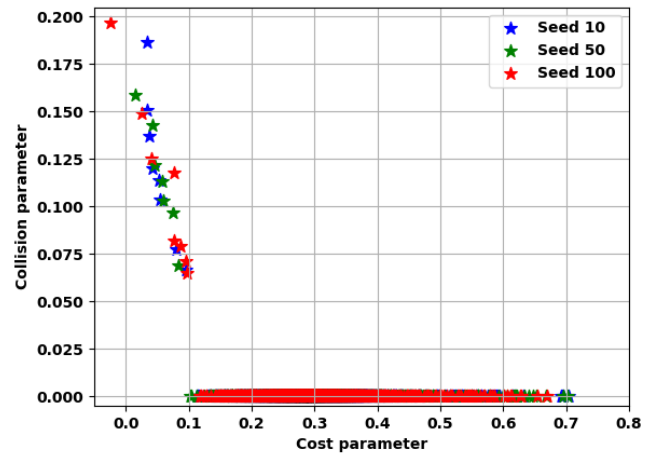


Figure 6.15: Generation tuning (100) - Run 2 Pareto front over different seeds.

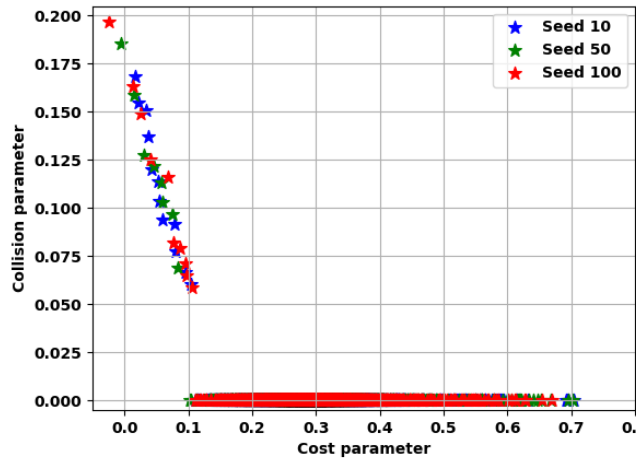


Figure 6.16: Generation tuning (150) - Run 3 Pareto front over different seeds.

Comparing these results to Figure 6.13, it can be concluded that increasing the number of generations leads to a more full Pareto front while also shifting it to the left, meaning the objective values are further minimized. Another interesting comparison is the computational effort necessary to conduct these tuning runs. This will not have a strong influence in the tuning choice so only rough averages are provided here. The baseline model runs took approximately 47 minutes, while Run 1 took approximately 1:18, Run 2 2:36 and Run 3 3:50. This means that increasing the number of generations by 25 leads to half an hour longer computation times while increasing it by 50 generations leads an hour and 15 minutes longer computation times<sup>b</sup>.

<sup>b</sup>Delftblue allows to choose the number of nodes utilized, for ease of comparison it was decided to keep this the same along the tuning.

At this stage it is decided that 25 generations is too low of a baseline number and so it was increased to 50 (as shown in Figure 6.14). The benefits of more converged results were worth the increase in computational effort. Figures 6.15 and 6.16 do show even better results, but those come at a price of about a factor three in CPU time.

### Population tuning

Next the population tuning is conducted by increasing the initial population size at each try. Having more individuals leads to a bigger spread within the objective space and hopefully then more full and converged Pareto fronts. The different models are introduced in Table 6.2, while the results are presented in Figures 6.17 to 6.19.

Table 6.2: Optimization model definition for the population tuning ('x' indicates that the value has not changed).

	Population	Generation	C1	C2	Omega	Diversity mechanism
Baseline model	50	50	2	2	0.5	Crowding mechanism
Run 1	75	x	x	x	x	x
Run 2	100	x	x	x	x	x
Run 3	150	x	x	x	x	x

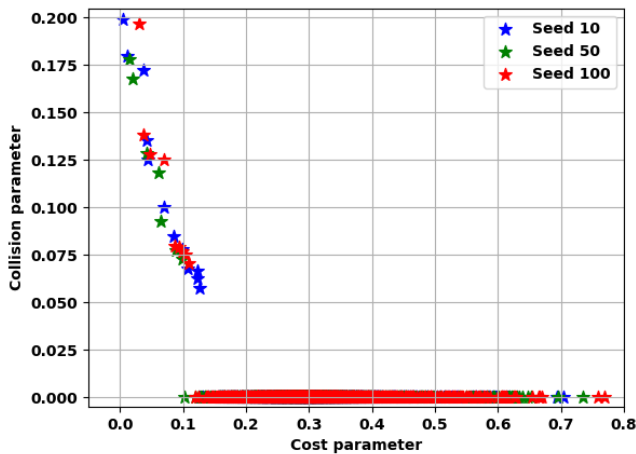


Figure 6.17: Population tuning (75) - Run 1 Pareto front over different seeds.

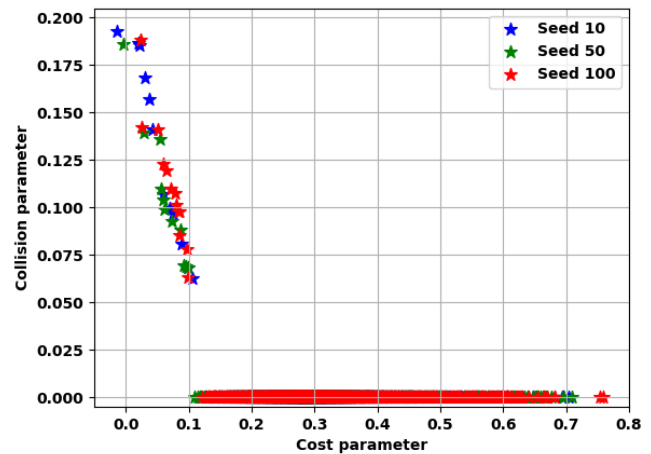


Figure 6.18: Population tuning (100) - Run 2 Pareto front over different seeds.

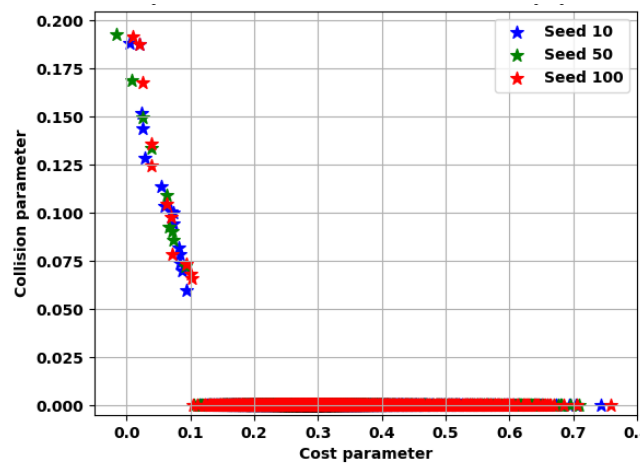


Figure 6.19: Population tuning (150) - Run 3 Pareto front over different seeds.

However, it was noticed that not all nodes were being used by each run meaning that the wait time was longer (waiting for the nodes to free up) with no benefit in the computational time. Hence, they were lowered with no impact on the run times.

Comparing the population tuning runs to the new baseline Figure 6.14, leads to the conclusion that increasing the population number does indeed lead to more individuals in the Pareto front. An initial population of 75 individuals allows for finding lower Cost parameters across all seeds. Increasing that number to 100 leads to even lower values, but the seeds show more diverse results indicating that the Pareto front has not yet converged. Finally, a population of 150 (Figure 6.19) shows many more individuals in the Pareto front especially for Collision parameter values between 0.05 and 0.1 (or  $P_c = 10^{-20}$  and  $10^{-10}$ ); an already important range of operators to make choices.

Interestingly, increasing the population size does not have such a big effect on the computational time as increasing the number of generations. This is because the parallel computing method implemented allows individuals to be run on different nodes. Run 1 increased the run time to 1:48 while Run 2 increased it to 1:50. The difference is negligible so if at the end of the tuning for the final model a choice needs to be made between 100 or 75 individuals, the former should be chosen. However, Run 3 showed an increase in run time to 2:18.

### C1 tuning

Next the C1 parameter tuning is presented. More runs are conducted with this parameter as shown in Table 6.3 because no difference was identified between the tuning runs. However, increasing the parameter even in the extreme case of C1 = 25 did not produce differences so Figures 6.20 to 6.22 show only the first three runs for illustration purposes.

Table 6.3: Optimization model definition for C1 tuning ('x' indicates that the value has not changed).

	Population	Generation	C1	C2	Omega	Diversity mechanism
Baseline model	50	50	2	2	0.5	Crowding mechanism
Run 1	x	x	1	x	x	x
Run 2	x	x	4	x	x	x
Run 3	x	x	6	x	x	x
Run 4	x	x	10	x	x	x
Run 5	x	x	25	x	x	x

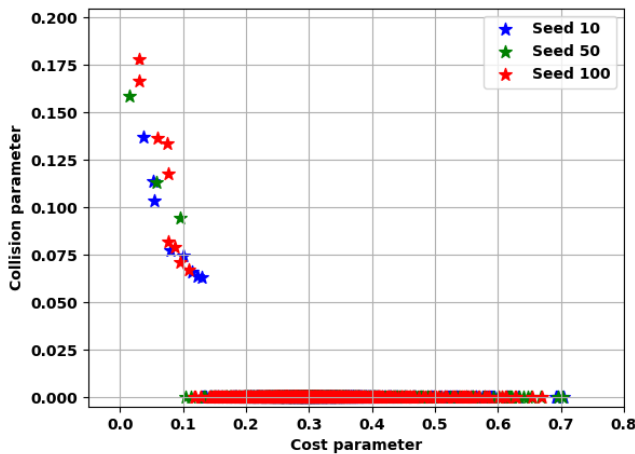


Figure 6.20: C1 tuning (1) - Run 1 Pareto front over different seeds.

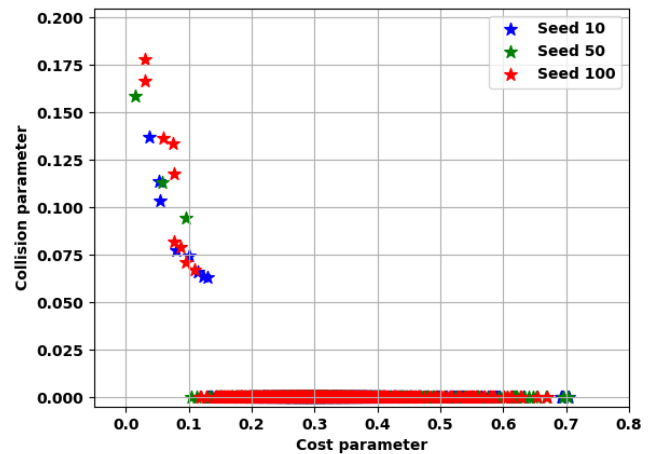


Figure 6.21: C1 tuning (4) - Run 2 Pareto front over different seeds.

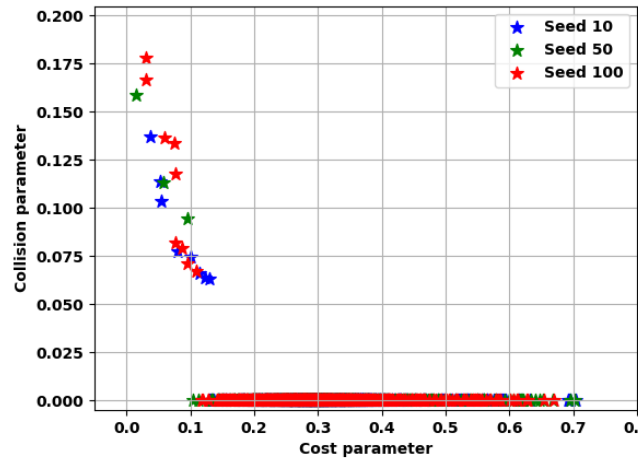


Figure 6.22: C1 tuning (6) - Run 3 Pareto front over different seeds.

The tuning runs for the C1 parameter show the same Pareto fronts as Figure 6.14. As altering this parameter did not affect the results, this parameter will not be further discussed.

### C2 tuning

Besides the C1 parameter, also the C2 parameter is tuned. As both parameters are similar they were tuned in the same fashion but the C2 parameter tuning did show differences in results. The tuning is conducted in three runs as displayed in Table 6.4. The results are shown in Figures 6.23 to 6.25.

Table 6.4: Optimization model definition for C2 tuning ('x' indicates that the value has not changed).

	Population	Generation	C1	C2	Omega	Diversity mechanism
<b>Baseline model</b>	<b>50</b>	<b>50</b>	<b>2</b>	<b>2</b>	<b>0.5</b>	<b>Crowding mechanism</b>
<b>Run 1</b>	x	x	x	1	x	x
<b>Run 2</b>	x	x	x	4	x	x
<b>Run 3</b>	x	x	x	6	x	x

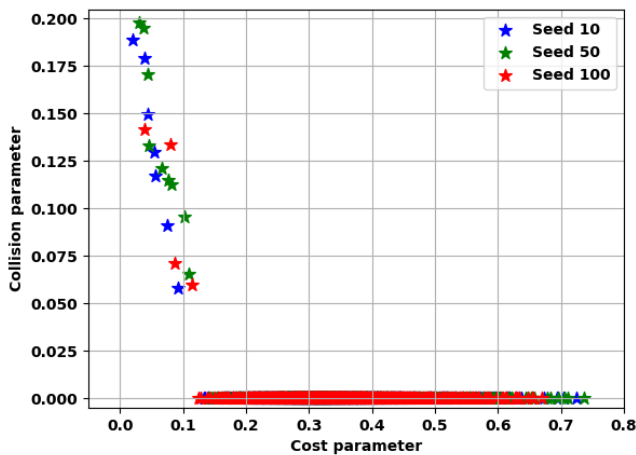


Figure 6.23: C2 tuning (1) - Run 1 Pareto front over different seeds.

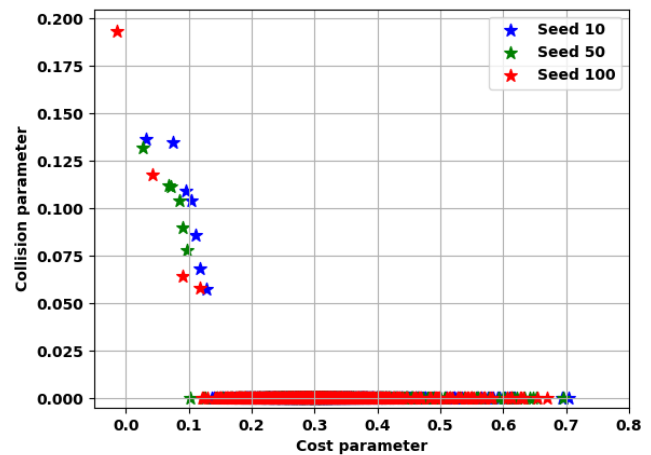


Figure 6.24: C2 tuning (4) - Run 2 Pareto front over different seeds.



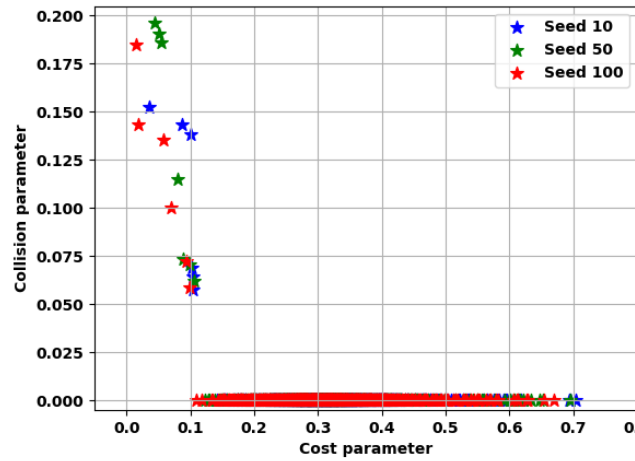


Figure 6.25: C2 tuning (6) - Run 3 Pareto front over different seeds.

The C2 parameter represents the magnitude of the force, applied to the particle's velocity, in the direction of its global best position. The baseline model has a C2 value of 2 so when comparing the results for increasing C2 values (Figures 6.14 and 6.23 to 6.25), an increase in sparsity of the results can be seen. The optimum values part of the Pareto front tend to diverge more. This is not a desired behavior, hence keeping the C2 parameter small is better for the quality of the solutions. In terms of computational time, no significant variation is noticed due to this parameter.

### Diversity mechanism tuning

The next optimization model parameter, the diversity mechanism, only has three possibilities: the crowding mechanism, the max-min and the niche count. Their differences have been explained in Subsection 4.5.3. The baseline model used the first option, meaning only two tuning runs need to be conducted. They are shown in Table 6.5. The results of both runs are shown in Figures 6.26 and 6.27 respectively.

Table 6.5: Optimization model definition for the diversity mechanism tuning ('x' indicates that the value has not changed).

	Population	Generation	C1	C2	Omega	Diversity mechanism
<b>Baseline model</b>	<b>50</b>	<b>50</b>	<b>2</b>	<b>2</b>	<b>0.5</b>	<b>Crowding mechanism</b>
<b>Run 1</b>	x	x	x	x	x	Max-min
<b>Run 2</b>	x	x	x	x	x	Niche count

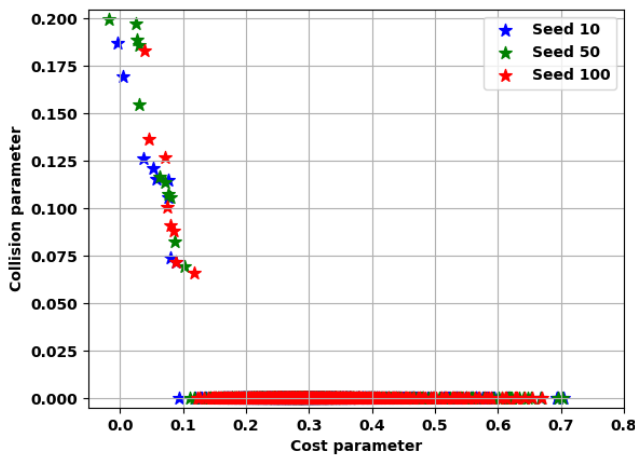


Figure 6.26: Diversity tuning (max-min) - Run 1 Pareto front over different seeds.

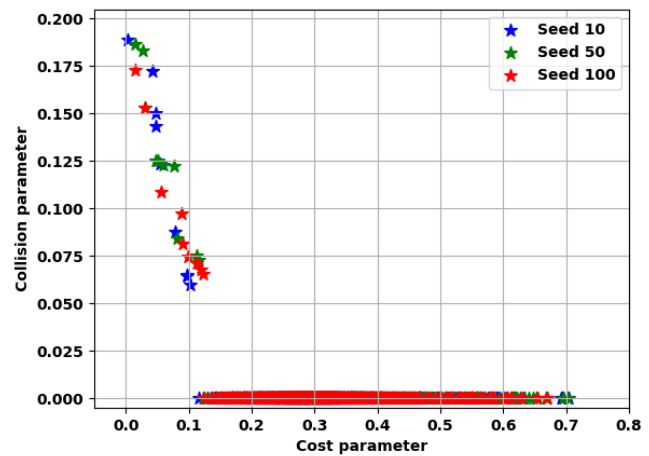


Figure 6.27: Diversity tuning (niche count) - Run 2 Pareto front over different seeds.

Different diversity mechanisms are tried to test the level of population diversity that can be achieved. The goal is to have a diverse Pareto front. Comparing these two diversity mechanisms with the baseline model shown in Figure 6.14, both show an improvement in range within the Pareto front in comparison to the baseline

diversity mechanism chosen. However, Figure 6.27 (Run 2; niche count) shows a high concentration of optima around 0.075 for the Collision parameter for seed 100. This higher concentration does not allow for a fully populated Pareto front and a diverse Pareto front is not achieved. While in Figure 6.26 (Run 1; max-min) more Collision parameter values are represented. This indicates a bigger gain from using the max-min diversity mechanism.

Even though having different diversity mechanism imply a different functioning of the algorithm, there are no significant differences in computation time between both tuning runs. Both took around 10 minutes more than the crowding mechanism but this is not considered significant.

### Omega tuning

The last tuning parameter is on omega which is known as the parameter to control the exploration in the search space. This parameter can be varied between 0 and 1. The baseline model utilized a value of 0.5, so values of 0.1, 0.7 and 0.9 are explored to allow for a range comparison, as reported in Table 6.6. This parameter tuning produced interesting results which are shown in Figures 6.28 to 6.30.

Table 6.6: Optimization model definition for omega tuning ('x' indicates that the value has not changed).

	Population	Generation	C1	C2	Omega	Diversity mechanism
<b>Baseline model</b>	<b>50</b>	<b>50</b>	<b>2</b>	<b>2</b>	<b>0.5</b>	<b>Crowding mechanism</b>
<b>Run 1</b>	x	x	x	x	0.1	x
<b>Run 2</b>	x	x	x	x	0.7	x
<b>Run 3</b>	x	x	x	x	0.9	x

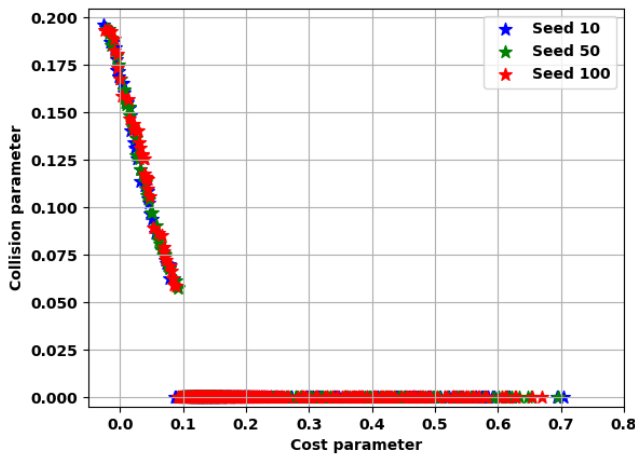


Figure 6.28: Omega tuning (0.1) - Run 1 Pareto front over different seeds.

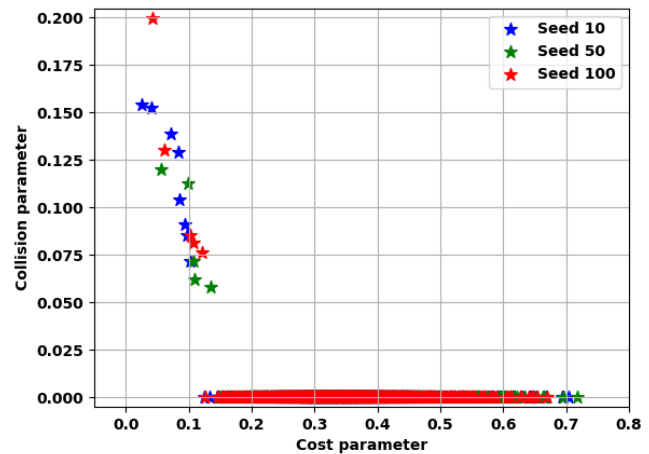


Figure 6.29: Omega tuning (0.7) - Run 2 Pareto front over different seeds.

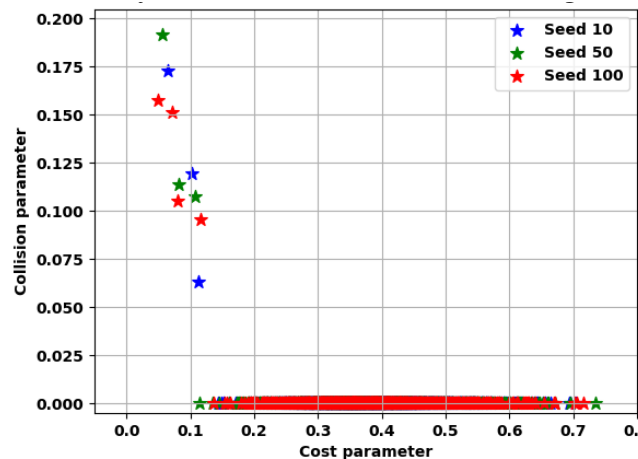


Figure 6.30: Omega tuning (0.9) - Run 3 Pareto front over different seeds.

It becomes quickly evident that the first tuning run using  $\omega = 0.1$  has amazing results, a complete Pareto front can be identified for each seed. On top of that, the three Pareto fronts are very close together indicating a converged and stable result. Several minimized values of the Cost parameter smaller than 0.1 are found, and there is less focus on the higher values of this Cost parameter. Contrarily, increasing the  $\omega$  value leads to Pareto fronts that can barely be identified.

As there is again no significant computation time increase from changing this tuning parameter, it becomes clear that using  $\omega = 0.1$  is the best option. As the results with  $\omega = 0.1$  are better than results with large population size and number of generations, some extra tuning is conducted. This extra tuning is shown below and it uses as baseline model  $\omega = 0.1$  as in Figure 6.28.

### Extra tuning

When analyzing the results of the previous tuning it is evident that the  $\omega$  value should be changed to 0.1. When doing so, good results could potentially be reached even with a lower population size and number of generations. This is tested in an extra round of tuning. Additionally, a tuning run is also conducted with a larger population size and number of generations to see if perhaps more optimal results could be found. The details of the extra tuning runs are shown in Table 6.7, while the results are shown in Figures 6.31 to 6.35 respectively.

Table 6.7: Optimization model definition for extra tuning runs ('x' indicates that the value has not changed).

	Population	Generation	C1	C2	Omega	Diversity mechanism
Baseline model	50	50	2	2	0.1	Crowding mechanism
Run 1	50	25	x	x	x	x
Run 2	25	25	x	x	x	x
Run 3	50	100	x	x	x	x
Run 4	25	50	x	x	x	x
Run 5	150	150	x	x	x	x

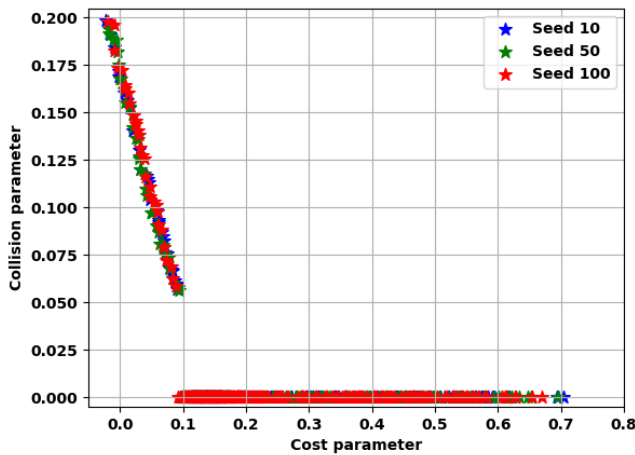


Figure 6.31: Extra tuning - Run 1 Pareto front over different seeds.

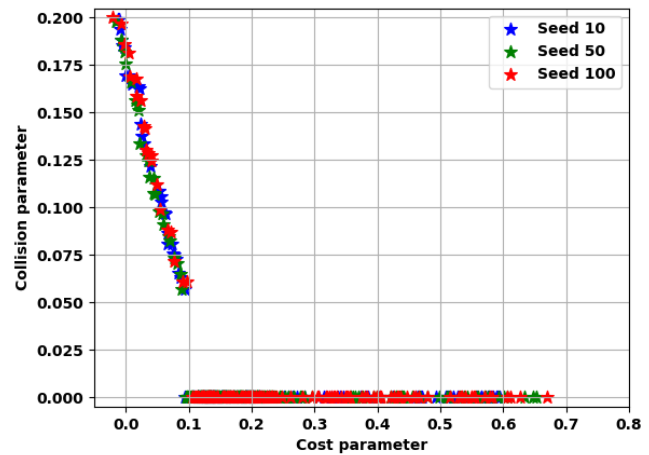


Figure 6.32: Extra tuning - Run 2 Pareto front over different seeds.

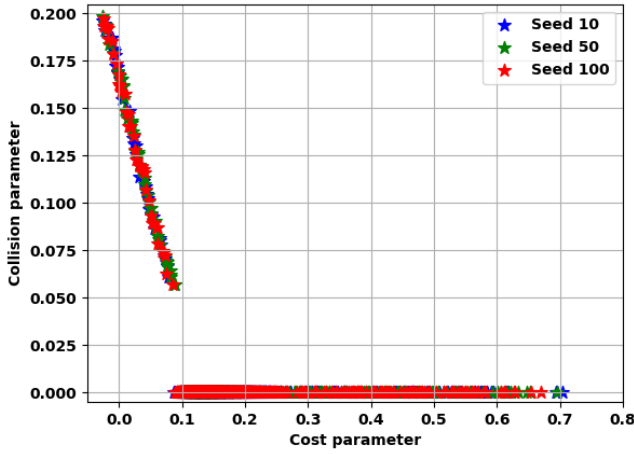


Figure 6.33: Extra tuning - Run 3 Pareto front over different seeds.

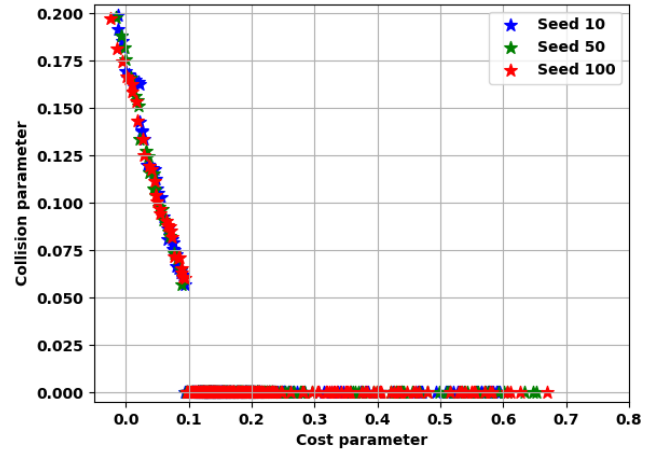


Figure 6.34: Extra tuning - Run 4 Pareto front over different seeds.

The graphs shown above should be compared to Figure 6.28 which is the new baseline model. Run 3 has more generations than the baseline but a big difference in final results is not noticed. There are less gaps in the Pareto front than in the baseline model. It would indicate that augmenting the number of generations could be beneficial but within certain bounds as it is not as necessary.

The effect of lowering the population size and number of generations is visible in Figure 6.32. The Pareto fronts become more spread out but a clear trend is still recognizable. The computational benefit would not be worth it.

From Run 1 to Run 2 twenty minutes can be saved by lowering the population size by 25. However, increasing the number of generations leads to an increase of around 50 minutes between Run 2 and Run 4. As already stated before, increasing the number of generations has a worse impact on the computation time than increasing the population size. Obviously, Run 3 had the worse run times at around 3:11.

The comparison between Figures 6.31 and 6.34 (Run 1 and Run 4) independently is also interesting as the effect of decreasing the number of generations can be directly compared to the effect of decreasing the population size. As Run 4 shows a less converged answer compared to Run 1, it can be said that the population size is of more importance in this problem.

Overall, it is still recommended to slightly increase the population size and number of generations based on these results. There is no need for it to go to the limits that were seen in these tuning tests. However, one final attempt at increasing both the population size and the number of generations to 150 is made to test whether better results could be reached. The result is shown in Figure 6.35.

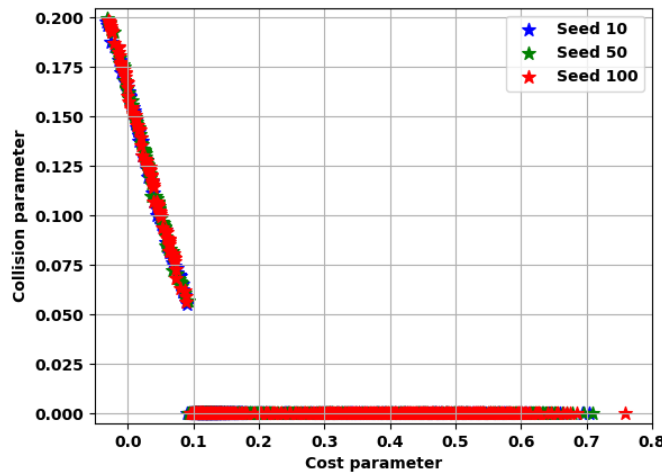


Figure 6.35: Extra tuning - Run 5 Pareto front over different seeds.

The graph shows a Pareto front with more individuals than the previous runs, yet the same minimum results are reached. The Pareto front is not further shifted to the left and it is not extended. The only new component is

an individual at around Cost parameter 0.75, which does not bring any benefit to the operator. The computation time is increased to around 9:24. Clearly, these results do not justify the increase in run time.

Finally, the results from the parameter tuning can be finalized and a final model can be chosen. The final optimization model chosen is described in Table 6.8.

- The omega parameter is set to 0.1.
- In accordance with Run 1 from the extra tuning, the population size is set to 50 while the number of generations is set to 25.
- The C1 parameter is proven to not have any impact on the outcome and because it does not affect the run time, it is decided to maintain it at its original value of 2.
- The C2 parameter did impact the results so it is set to 1 in accordance with Run 1 from the C2 tuning.
- For the diversity mechanism it is decided to proceed with the max-min method as it presented better results.

**Table 6.8: Final optimization model definition.**

	<b>Population</b>	<b>Generation</b>	<b>C1</b>	<b>C2</b>	<b>Omega</b>	<b>Diversity mechanism</b>
<b>Final model</b>	<b>50</b>	<b>25</b>	<b>2</b>	<b>1</b>	<b>0.1</b>	<b>Max-min</b>



# Simulation scenarios

Now that the optimization problem has been tuned, both in parameter settings and in objective size and formulation, it can be used for the study of representative conjunction problems; different study cases need to be defined. By testing how different scenarios will evolve, conclusions can be drawn on the applicability of the program designed and the potential actions by operators. The study cases are presented in Section 7.1, and in Section 7.2 the relevant inputs are defined.

## 7.1. Study cases

To decide if a combined action between operators would lead to an optimized collision avoidance process, the negotiation between operators should also be taken into account. Chapter 8 will note that in trying to set up an STM system some cases need special considerations. These involve big constellations, derelict spacecraft, CubeSats, and space debris in orbit around Earth. They will be expanded further in Chapter 8.

In setting up the study cases, it is important to make sure these special considerations are included such that the optimization problem can also help answer what an STM system should include. Additionally, it is valuable to check whether this dual-maneuver optimization algorithm also allows for solutions in a single-maneuver case. For this purpose, the four study cases presented below are proposed.

### Case 1: CubeSat versus normal spacecraft

CubeSats have become an important contributor in LEO. They are often used to test new technologies and conduct experiments. They are attractive due to their small sizes and cost but often do not contain thrusters (or powerful thrusters) for maneuvering and rely on differential drag methods. Case 1 will handle a CubeSat with a small thrusting capacity to see how it can contribute to the collision avoidance process. This will also help investigate how its small size impacts the collision avoidance process. This case was already the baseline selected for the dynamics model definition, the CAM set-up, and the optimization algorithm set-up and tuning presented in Chapters 4 and 6.

### Case 2: Constellation spacecraft versus spacecraft with orbit requirements

Recently, several plans for the design and usage of big constellations in LEO have been developed as shown in Section 2.2. This will trigger many more conjunction warnings between two operating spacecraft (i.e. the Starlink/AEOLUS case) which is why such a case needs to be looked at. The constellation spacecraft in this study case will be equivalent to a normal spacecraft and so the whole system will be maneuverable. This will help find the optimal maneuvers for combined action, accounting for out-of-orbit time. When considering the negotiation between operators, other aspects need to be taken into account for a big constellation such as the occupied orbits and general increase in conjunction warnings.

### Case 3: Constellation spacecraft versus spacecraft without orbit requirements

A variation of the previous case is a constellation spacecraft in conjunction with a maneuverable spacecraft that does not need a precise orbit. This could be for the case where the payload does not work anymore and yet the spacecraft still has maneuvering capabilities. It is also relevant for de-orbiting spacecraft, that need to pass through dense regions of LEO to re-enter the atmosphere. This case also allows to test the limitations of the optimization algorithm designed.

### Case 4: Normal spacecraft versus space debris

The final study case investigates the typical conjunction warning event with space debris. This is usually a tiny fragment of a spacecraft or a piece from a launch system. Here, a rocket body will be used as the second

object in the conjunction. This allows to determine the effect of a single-maneuver avoidance scenario and if the optimization algorithm can produce useful and valid results.

However, these cases can be further split up by the number of active spacecraft and if the mission performance loss needs to be included or not. This can be seen in Table 7.1. It becomes clear that Case 1 has four different configurations and Case 5 has two different configurations. This is because CubeSat could have maneuvering capabilities but it is not certain and slight alterations to the orbit generally do not affect a CubeSat's mission. For Case 4, the debris is non-maneuverable so the normal spacecraft must maneuver. Whether or not the mission performance loss is taken into account a different maneuver can be found.

Table 7.1: Division of the proposed cases.

	Number of active spacecraft	Mission performance loss
Case 1	1-2	Yes, No
Case 2	2	Yes
Case 3	2	Yes, No
Case 4	1	Yes, No

With this division, the total number of cases to be analyzed would be seven. Considering the time restriction of the thesis project it is decided to implement priorities to the cases. The most important ones are done first and the others are done if time allows it. Additionally, it is necessary to have a baseline to compare to. This is chosen to be Case 1 because it tackles all the aspects of the problem: two maneuverable spacecraft, restrictions in propellant usage, and mission performance loss.

Moreover, when a case has only one maneuverable spacecraft it is equivalent to imagining the other spacecraft is a piece of debris as it will not be able to maneuver. This leads to Case 1 with one maneuverable spacecraft being similar to Case 4. Thus, it is decided to not run such similar cases. This is applicable regardless if the mission performance loss is accounted for or not.

Case 2 is the second-priority case because it deals with constellation satellites that have become an important topic in the space community. Then, Case 3 with two active spacecraft and no mission performance loss has priority as it underlines how the mission performance loss changes the situation. Finally, Case 4 with and without mission performance loss is given the least priority as they represent current collision avoidance maneuvers. So, in summary, the following cases will be studied:

- Baseline: Case 1
- 1<sup>st</sup> priority: Case 2
- 2<sup>nd</sup> priority: Case 3 with two active spacecraft and mission performance loss
- 3<sup>rd</sup> priority: Case 4 with mission performance loss for one spacecraft

Still, for each case, different variants can be considered. Case 1 can have varying weights for the object's contributions to the fitness function. The purpose of varying is to test the importance of individual operator weights. It also helps in the discussion where the optimization results are merged with the cooperation process to be explained in Chapter 8.

Case 2 variants serve to understand how much the maneuvering capabilities of the individual spacecraft affect the optimization. This allows to determine how the cooperation process between the operators could look with different systems.

The final variations are considered for Case 4. As this one deals with the one-sided avoidance of a rocket body, the maneuvering capabilities can be changed to check how much  $\Delta V$  contribution is necessary to properly avoid it.

## 7.2. Input for selected cases

After selecting the cases that are interesting for analysis by order of importance, they need to be set up. This includes selecting the appropriate CDMs and their representation in the optimization algorithm. The parameters that vary by case are:

- CDM number
- Object masses, sizes,  $I_{sp}$ , maneuverability and definition



- Propellant usage limits
- Object's propellant mass contribution weights
- Object's orbit disturbance contribution weights

In terms of CDM number and objects used, the cases are defined in three batches as follows:

1. Cases 1, 1.1, 1.2, 1.3, and 1.4 use CDM number 86 as input. This conjunction scenario has as chaser Delfi-N3XT and as target SICH 2<sup>a</sup>. The chaser mass is 3 kg and the target mass is 175 kg. The cross sections used are 0.0995 and 1.7321 m<sup>2</sup>, respectively.
2. Cases 2, 2.1, and 3 use CDM number 86 as input as well. However, the first object is switched for a constellation spacecraft: Starlink-1689<sup>b</sup>. This spacecraft is in the list of conjunctions with the Delfi satellites. This means that the same geometry as the previous cases is assumed with the same state vector, only the masses and sizes change for the chaser: 260 kg and 23.657 m<sup>2</sup>.
3. Cases 4, 4.1, and 4.2 use a different CDM because a scenario with a rocket body is opted for. However, the chaser remains the Starlink satellite described for Cases 2, 2.1, and 3. The new target is 2019-017B with mass 2800 kg and cross section 39.133 m<sup>2</sup>.

The constraints and decision variable ranges defined in Section 4.5 are also used as input for the cases. They can be varied if need be. Their values are:

- $\lim_{m_{p,1}} = 0.05$ ,  $\lim_{m_{p,2}} = 0.05$ ,  $I_{sp1} = 300$  s,  $I_{sp2} = 300$  s
- $t_{\Delta V_{1,min}}$  and  $t_{\Delta V_{2,min}} = 0.25$ ,  $t_{\Delta V_{1,max}}$  and  $t_{\Delta V_{2,max}} = 0.667$
- $\Delta V_{1,R,min}$ ,  $\Delta V_{1,I,min}$ , and  $\Delta V_{1,C,min} = -0.01$  m/s and  $\Delta V_{1,R,max}$ ,  $\Delta V_{1,I,max}$ , and  $\Delta V_{1,C,max} = 0.01$  m/s
- $\Delta V_{2,R,min}$ ,  $\Delta V_{2,I,min}$ , and  $\Delta V_{2,C,min} = -0.01$  m/s and  $\Delta V_{2,R,max}$ ,  $\Delta V_{2,I,max}$ , and  $\Delta V_{2,C,max} = 0.01$  m/s

The first batch of cases focuses on changing the weights of the objectives of each object. This can be seen in Table 7.2. Besides the weights, there are no other changes between the cases.

**Table 7.2: First batch of cases definition.**

	$w_{p1}$	$w_{p2}$	$w_{O1}$	$w_{O2}$
<b>Case 1</b>	0.5	0.5	0.5	0.5
<b>Case 1.1</b>	0.2	0.8	0.5	0.5
<b>Case 1.2</b>	0.8	0.2	0.5	0.5
<b>Case 1.3</b>	0.5	0.5	0.2	0.8
<b>Case 1.4</b>	0.5	0.5	0.8	0.2

The second batch of cases tests using different  $I_{sp}$ 's and switching off one object's orbit disturbance contribution. This is done to test the case of a maneuverable and inactive object: the (new) orbit is not important. The details are given in Table 7.3.

**Table 7.3: Second batch of cases definition.**

	$w_{p1}$	$w_{p2}$	$w_{O1}$	$w_{O2}$	$I_{sp1}$	$I_{sp2}$	$\lim_{m_{p,1}}$	$\lim_{m_{p,2}}$
<b>Case 2</b>	0.3	0.7	0.7	0.3	300	300	0.1	0.05
<b>Case 2.1</b>	0.3	0.7	0.7	0.3	500	300	0.1	0.05
<b>Case 3</b>	0.5	0.5	1	0	300	300	0.05	0.05

For the third batch, the same propellant usage limits and the object's propellant mass and orbit disturbance contribution weights are used. These are defined as such since one object is non-maneuverable and inactive:  $\lim_{m_{p,1}} = 0.05$ ,  $\lim_{m_{p,2}} = 0.0$ ,  $w_{p1} = 1$ ,  $w_{p2} = 0$ ,  $w_{O1} = 1$ ,  $w_{O2} = 0$ . The changes between the cases belonging to the third batch are shown in Table 7.4. The focus is on the maneuverability of the first object, so the decision variables that pertain to that vehicle only are changed.

<sup>a</sup>SICH 2 is a dead spacecraft, however for the sake of the analysis it is assumed maneuverable.

<sup>b</sup>Starlink satellites, in reality, use low thrust, however, instantaneous maneuvers are assumed.

Table 7.4: Third batch of cases definition.

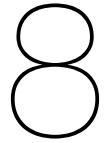
	$\Delta V_{1,R,min}$	$\Delta V_{1,I,min}$	$\Delta V_{1,C,min}$	$\Delta V_{1,R,max}$	$\Delta V_{1,I,max}$	$\Delta V_{1,C,max}$
<b>Case 4</b>	-0.01	-0.01	-0.01	0.01	0.01	0.01
<b>Case 4.1</b>	-0.02	-0.02	-0.02	0.02	0.02	0.02
<b>Case 4.2</b>	-0.05	-0.05	-0.05	0.05	0.05	0.05



## Cooperation process and implemented combined action

The last part of this work deals with the proposal of the cooperation process framework between operators. The reasoning and final proposal are presented in Chapter 8. Then, the optimization results are displayed in Chapter 9, along with a discussion to merge the results with the cooperation process. Finally, this work is achieved with the conclusions and recommendations in Chapters 10 and 11, respectively.





# Cooperation process

To answer the second part of the research question of this thesis on negotiation proposals between operators, STM is delved into. STM is a challenging question the aerospace community has to deal with. Frameworks need to be defined that would work internationally and preferably with a certain automation level to ensure an all-encompassing and efficient system. However, in this thesis, the focus will be on the cooperation process between operators in a collision avoidance scenario.

To explain the cooperation process, this chapter firstly defines how STM is interpreted in this thesis in Section 8.1. The current or proposed practices are explained in Section 8.2. As this will be an intricate system with many conditions, the special considerations are explored in Section 8.3. Ideas for an approach are discussed in Section 8.4, where an evaluation will determine which approach to follow for the final framework proposal. In Section 8.5, constraints are discussed that need to be accounted for when designing the framework to maximize the chance that it is applicable in real-life. Finally, in Section 8.6 a general framework is proposed which will be made specific when the outcome of the combined collision avoidance is analyzed.

## 8.1. STM definition

There are different definitions for STM. Some are specific in listing that it should include on-orbit synchronization (U.S. National STM Policy) [9], whereas others are more general that list the safety and sustainability of space (ITU and International Academy of Astronautics) [9]. The National Space Traffic Management Policy mentions the inclusion of planning and coordination in their definition [42]. Other space actors view STM as an augmentation of SSA or the Air Traffic Management [17]. Generally, the question is approached from technical and regulating perspectives and there is a concern about the governance and legal perspectives. STM should not interfere with self-governance of nations, but then how will it be enforced?

This thesis will not focus on answering such questions. Rather, it will propose a framework for cooperation between operators. For this purpose, STM will be defined as a system to promote safety and sustainability of space including planning, coordination, launch of missions as well as interference monitoring. Here, the aspect of planning and coordination of missions will be looked into, specifically on the topic of on-orbit synchronized maintenance. This leads to the need of defining a collision avoidance procedure between operators. The emphasis is on technology and communication.

Continuous and real-time data sharing is essential to reach coordination between operators [43]. Specifically for collision avoidance, data regarding the maneuverability of spacecraft, ephemerides, and uncertainties is crucial. As will be shown in Section 8.2, current approaches use email and telephone contact between operators. This method is outdated; for a well-functioning system, more timely communication is necessary, with the inclusion of automation. Besides that, the operators need to be transparent on their reaction thresholds and methods used [43].

A solution would be to have a Middle Man scenario<sup>a</sup>, an agent working between the SSA database and the operators. This service would need to receive information from the operators regarding the trajectory, maneuver, and control plans and the SSA data from for example CSpOC<sup>b</sup> [17]. The Middle Man could provide services related to alerts, assistance, and coordination with other operators. If this Middle Man is used by a significant number of operators, it would aid in having a combined approach to spacecraft collision avoidance.

The necessity of including (preferably) all operators in this system is clear. At the moment, 44% of operators report that their collision avoidance processes are conducted mostly manually, on a single-operator level, with

<sup>a</sup>Current Middle Man systems in place for CNES and NASA will be explained in Section 8.2.

<sup>b</sup>CSpOC is the successor of the JSpOC [44].

analysts operating their tools [37]. To have an effective system that can deal with any conjunction warning, it will need to be able to interact with all operators possible.

With STM being clearly defined now more definitions can be implemented regarding maneuver strategies. For this, the proposal of splitting space objects into four categories from Hobbs, Collins, and Feron [42] will be used, as well as the intent of maneuvering and efficiency of maneuver:

- (I) Inactive: this object cannot be communicated with and cannot be maneuvered. Examples are rocket bodies, space debris, and derelict spacecraft.
- (NM) Non-Maneuverable: this object can be communicated with but cannot be maneuvered. Reasons for this could be propellant resources, risk scenarios, or CubeSats with no propulsion system.
- (NC) Non-Communicating: this object cannot be communicated with yet there is a possibility to regain communication in the future. Commonly, such spacecraft also do not maneuver but with the advances in automatic spacecraft-based maneuvers, this category should be included.
- (M) Maneuverable: this object can be communicated with and maneuvered as ordered by the operator. This category includes most active spacecraft.

With the aid of this classification of space objects, the conjunction scenarios can be categorized as well. This is related to the state of the space object with regard to maneuvering and how efficient the collision avoidance process will be.

**Intent of maneuver:**

- Benign intent: the other object in the conjunction will not maneuver.
- Benevolent intent: the other object will maneuver according to the rules previously agreed upon (the negotiation framework that will be defined). The operators have agreed to their maneuvers mutually.
- Malevolent intent: the other object will maneuver negatively.

**Efficiency of collision avoidance:**

- Weak: Maneuvers are not dual-coordinated, nevertheless have benign intent.
- Semi-strong: Dual-coordinated maneuvers with benign intent.
- Strong: Dual-coordinated maneuvers with benevolent intent.
- Defensive: Malign intent maneuvers.

The goal of designing a cooperation process framework between operators is to have strong efficiencies of collision avoidance. If a conjunction is between two maneuverable spacecraft, the ideal scenario would be to have them cooperate to avoid the collision together by performing optimal maneuvers with benevolent intents.

## 8.2. Current practices

From analyzing current practices the advantages and pitfalls of different STM systems can be identified. This is useful when generating a new system. The advantages are taken on and solutions can be found for the pitfalls. All current practices analyzed have the common factor that they do not include any coordination with other operators; this is the knowledge gap that will be focused on for the new system proposal.

This section will explain the functioning of emerging systems such as the one used by DLR called iSpace or the proposal of MISS. Additionally, the system used by Starlink will be broadly explained as all detailed information is confidential or even unavailable. Finally, this section delves into better-known systems such as the one used by ESA or the Middle Man approach used by CNES and NASA. All this information will be summarized with a comparison matrix so that the highlights of each system can be directly identified.

### 8.2.1. DLR

Recent development in the aerospace community leads the German space agency (DLR) to announce it will be using the iSpace traffic management system by Lockheed Martin. This system is composed of three different elements that can work together or independently [45].

The bottom layer is called the "iSpace Sensor Mission Processor". It works with several sensors and takes available data to generate a catalog of space objects that is more complete than the one provided by the SNN. This data can then be fed into the other layers. The middle layer called "iSpace C2/BMC2" processes the measurements of the bottom layer or other entities and manages the catalog automatically. As such it can detect a conjunction with all its conditions and auto-generate "Courses-of-Actions" (COAs). The top layer, "iSpace Space Event Risk Assessment" (SERA) takes the COAs from the middle layer and uses artificial intelligence

to predict risks, to define if it is a good action to take or not.

The system proposed is fully automated, the detection is done in near-real time, catalog management has minimal manual interaction and there are continuous processes in making predictions. The data flow between layers simulates different entities working together, but there is no external communication with other operators, suggesting that this has to be done outside of the system by classic means available at DLR. Additionally, the COAs generated seem to be analyzed only in terms of risk and not in terms of mission performance impact.

### 8.2.2. Politecnico di Milano

The Maneuver Intelligence for Space Safety (MISS) is under development by researchers at Politecnico di Milano funded by the European Research Council. It is intended for onboard use and does not have autonomous operations included yet. With the use of analytical and semi-analytical methods, the algorithms are efficient and simple [46]. MISS can optimize impulsive maneuvers for maximum displacement and minimum collision probability. The optimization can be done for low-thrust maneuvers if information about the thrust acceleration, the time of the maneuver, and the length of the thrust arc is available.

The first aspect is the necessity of having conjunction information, which cannot be auto-generated by spacecraft if it is not continuously fed catalog information. This step requires data to be uploaded from ground stations. The proposal uses information in CDM format coming from external SSA sources, although these are not specified yet. The CDM input could be uploaded directly from the federated SSA services without the need to pass by the operator. For the collision maneuvering aspect that takes place onboard the spacecraft, three blocks are defined. The first one model's orbital modifications using Keplerian elements and uses analytical models for impulsive maneuvers, while semi-analytical ones are used for low-thrust maneuvers. The second block maps these onto changes of state at TCA. The last block analyzes the second block's output to get the effect of the maneuver in the B-frame. The blocks are independent and so can be altered if necessary without breaking the system.

In this system there is also no aspect of coordination or negotiation between operators included. It is not specified if the maneuvers that are auto-generated by the spacecraft include mission performance cost considerations.

### 8.2.3. SpaceX

The Starlink constellation by SpaceX is being built up in different phases; currently around 4327 spacecraft are already functioning in LEO [47]<sup>c</sup>. This generates a big number of spacecraft to monitor and plan maneuvers for. To aid in taking into account the high number of conjunction warnings Starlink has an automatic collision avoidance system which is spacecraft based. However, there is not much information available about how the system works. SpaceX uses the catalog of objects tracked by the United States Air Force (USAF) for their autonomous maneuvers, yet there are concerns that the CDMs generated by USAF are not a sufficiently wide database for maneuver decisions [42] (military spacecraft remain "hidden").

Due to the lack of information available, nothing can be said about the coordination with other operators or the assessment of cost on mission performance for the auto-generated maneuvers. However it should be mentioned that an agreement between NASA and SpaceX exists relating to Starlink spacecraft avoiding collisions with NASA assets [48]. It is possible that more such agreements exist and that the maneuvers decided upon take these into account.

### 8.2.4. ESA

ESA's Space Debris Office has its own collision avoidance service [49]. It is used for several of their missions and is also available to third-party customers. The Database Information System Characterizing Objects in Space (DISCOS) contains information about objects in orbit. The system also allows for external tracking data to be introduced to improve the knowledge of the chaser object and its uncertainty covariance in the Orbit Determination by Improved Normal Equations (ODIN) software. The object's information is used in the Meteoroid and Space Debris Terrestrial Environment reference model (MASTER) and the Debris Risk Assessment and Mitigation Analysis (DRAMA) tool suite to perform risk analysis.

In Figure 8.1 the process followed for collision avoidance at ESA is described. It is linked to several players (displayed in orange boxes) and includes many different software and tools working together. The gray central

<sup>c</sup>Value from July 2<sup>nd</sup> 2023.

box denotes the automated part of the process, meaning that these tools communicate with each other without human intervention, but can be included if required.

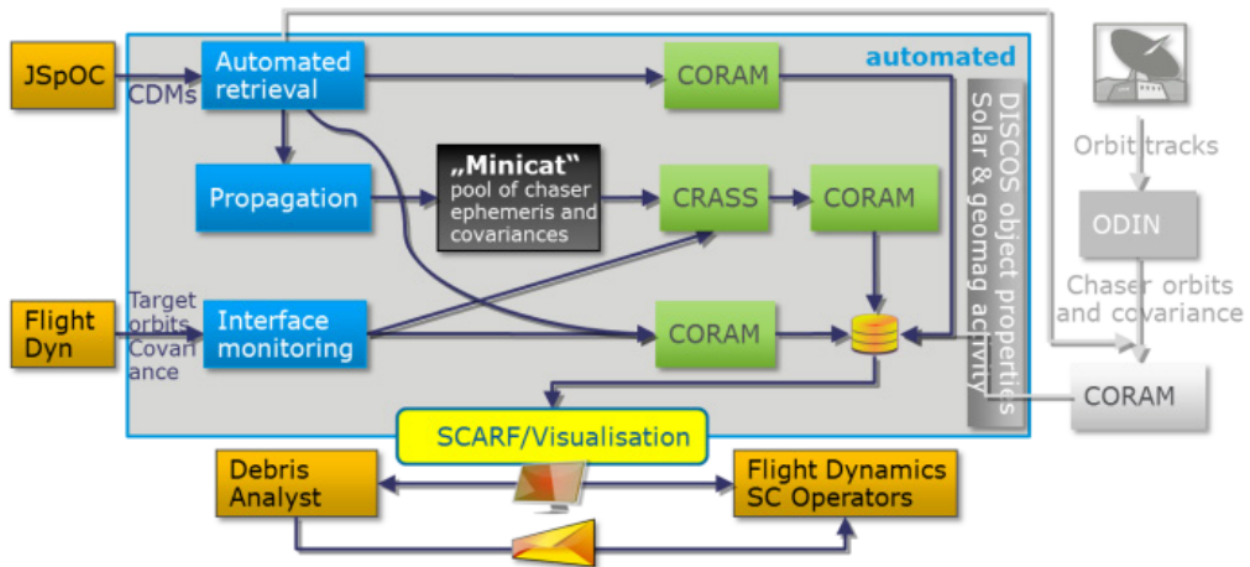


Figure 8.1: Collision avoidance process used at ESA/ESOC [49, p. 3].

The CDMs received at ESA are treated automatically and the risks are computed with the Collision Risk Assessment and Avoidance Maneuver (CORAM) software and the DISCOS database which provides them with the object's geometry. The results are also stored in a database. In the "Minicat", the propagated chaser state vectors of objects close to the target spacecraft are stored. This is done automatically with every CDM received. CORAM can be used with CDM information, along with information from "Minicat" or the operator's ephemeris data or TLE's. In CORAM two software's are present: Collision Risk Computation Software (CORCOS) and the Collision Avoidance Maneuver Optimization Software (CAMOS). Their function is evident from their names.

The maneuvers can be impulsive or low-thrust. Their directions can also be provided in different reference systems (Mean Earth equator of epoch J2000.0, true/mean equator and equinox of data, local orbital or local intrinsic). The maneuver parameters can be bounded and constraints can be implemented. Finally, the cost function can be the collision risk, the total  $\Delta V$ , or the distance of the closest approach. The pitfall is that CAMOS uses local optimization techniques meaning that local optima may be found; the results should be analyzed critically for the global optimum.

The operational ephemeris is plugged into the Collision Risk ASsessment (CRASS) software to find possible conjunctions that might not have CMD's due to the screening volume used by CSpOC. If any are found, these are plugged into CORCOS again. CRASS was originally developed to be used with TLE data. It is used whenever the "Minicat" is updated or whenever new ephemeris data is delivered. This new data is then again stored in the database. With this, the decided maneuver trajectories can be re-checked directly without having to pass through CSpOC, on the condition that the trajectory difference is smaller than CSpOC's screening volume.

Finally, all this information is plugged into the Spacecraft Conjunction Assessment and Risk Frontend (SCARF). This is a web-based tool for visualization and collaboration. The visualization part displays the target and chaser motion over time with their uncertainties. The main function of SCARF is to provide fast and efficient situational pictures for each conjunction event. It helps the different teams to communicate effectively and there are plans to continue expanding it. It is partly in the automated section of the diagram because it generates automatic email notifications.

### 8.2.5. CNES/NASA

CNES and NASA both use Middle Man services for their collision avoidance procedure: Conjunction Analysis and Evaluation Service: Alert and Recommendations (CAESAR) and Conjunction Assessment Risk Analysis (CARA) respectively. CAESAR was developed by the COO team from CNES in 2014 [17]. The Middle Man service allows for a collaborative work with the operators. The functions are to allow real-time connections (currently done through phone and email), to ensure the same interpretation of the conjunction situation and to enable different levels of information visualization [50]. There should be a two-way communication line with



acknowledgment of receipt on both sides as well information sharing regarding methods and databases used.

CARA and CAESAR work closely together by sharing information and capacities. CARA has direct access to the CSpOC data and CAESAR provides efficient tools such as JAC. This tool serves as a way to detect conjunctions with high risk levels. It monitors the first analysis of incoming data automatically to determine which require a manual, more in-depth analysis.

The procedure followed by CNES is described in Figure 8.2. It shows five different steps to manage conjunction warnings and propose maneuvers [51]. Stage 1 is taken care of by JAC.

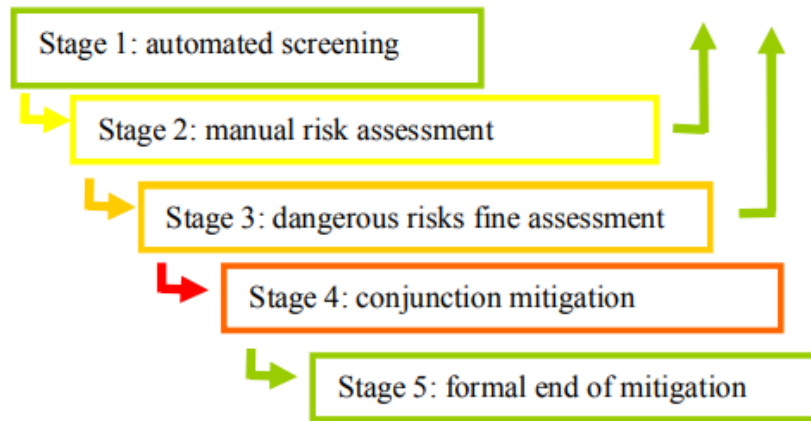


**Figure 8.2: Collision avoidance procedure used by CNES [51]. The green arrows leading from Stages 2 and 3 show that they can lead to the process starting over.**

In the automated screening step, JAC does collision risk prediction up to a week in advance. All the conjunctions are filtered once for target objects within a certain distance to the chaser. Then, the collision probabilities are calculated. For all results over  $10^{-4}$  reports are sent automatically to a team of engineers. In the second stage, the manual risk assessment, the team first updates all the data necessary. This allows them to screen the conjunctions with the latest information. The screening is done based on collision probability, orbit uncertainty, miss distance, conjunction geometry and object size. The evolution of the collision geometry and probability are also tracked, which is then compared to a statistical analysis of collision probability distribution through different geometries. The third stage starts again with an update of the data and if necessary completion through radar measurements or models. This stage will select which conjunctions should move along in the collision avoidance procedure. Any of the following criteria will lead to the conjunction being selected for the following stage:

1. Radar measurements available for the target object's orbit and collision probability exceeds  $10^{-3}$ .
2. Radar measurements not available for the target object's orbit and collision probability exceeds  $10^{-2}$ .
3. Collision probability risk is confirmed by NASA.

Then, the selected conjunction warnings go to Stage 4, the conjunction mitigation. A meeting is scheduled to decide on a maneuver taking into account the mission, platform, and operational constraints and the potential new conjunctions that could arise post-maneuver. During the process, new information is tracked and updated. If necessary, a second maneuver is designed to return to the nominal orbit.

The system used by NASA (CARA) is essentially the same. Additionally, tracking information can be asked on the chaser object if necessary [50]. CAESAR uses real-size values for their own assets and DISCOS information for chaser objects [52]. If that information is not available, CDM data can be used to broadly categorize the object as small, medium, or large.

The systems allow for communication about the conjunction, though not about the avoidance process to follow. This means that again there is no coordination between operators directly in this system.

### 8.2.6. Comparison

To compare the different methods shown in this section it is important to underline that none have a dual-maneuver or negotiation process with other operators integrated into it. Additionally, no information about the requirements of the avoidance maneuvers was found so it cannot be said if the different systems account for the cost of maneuver only in terms of propellant or also mission downtime. It is also interesting to delve into

the different information sources available. This is summarized per practice in Table 8.1. To understand it, the following information about the databases is useful. USSTRATCOM provides a publicly available catalog of space objects around Earth that is constructed with observations from CSpOC. The 18<sup>th</sup> Space Control Squadron (18 SPCS) performs the space surveillance mission for the U.S. Air Force (USAF) and provides the necessary information for SSA. DISCOS and Minicat are ESA self-generated databases, also available to other operators. Finally, iSpace generates its own database combining information from several different sensors.

Table 8.1: Databases used by each current system analyzed.

System	Database
DLR	Lockheed Martin sensors and commercial and international sensors <sup>a</sup>
Politecnico di Milano	Federated SSA services which provide CDM data (CSpOC)
SpaceX	18 SPCS
ESA	DISCOS, CSpOC, Minicat
CAESAR/CARA	DISCOS, CSpOC

<sup>a</sup>Lockheed Martin Sensors (FireOPAL, Space Fence), Commercial sensors (ExoAnalytic, Krotos, numerica), and international sensors (TIRA, GRAVES, BIRALES).

All information gathered in this section can be used to generate a comparison matrix of the current practices shown in Table 8.2. The information relating to the sources of information is enclosed under the criteria "Databases" in the comparison matrix. The other comparison criteria are "Automated", which denotes whether the system is automated or not, and "External communication" to determine if the system has implemented links outside itself.

Table 8.2: Comparison of current practices.

Options \ Criteria	Automated	External communication	Databases
DLR	Auto-generates actions and checks risks with machine learning. <span>green</span>	Not mentioned. <span>red</span>	Generates database from combined sources. <span>green</span>
Politecnico di Milano	Intended for autonomous on-board use, but does not have decision-making component to it yet. <span>yellow</span>	Not mentioned. <span>red</span>	Different links from federal databases and operator. <span>green</span>
SpaceX	Fully automated response, spacecraft based. <span>green</span>	Not mentioned. <span>red</span>	Only USAF is used. <span>yellow</span>
ESA	Many automated links in the inner part. <span>blue</span>	Back and forth regarding database, no established communication lines with other operators. <span>yellow</span>	Different information sources combined for final decision. <span>green</span>
CNES/NASA	Primary screening is automated to tackle large number of CDMs. <span>yellow</span>	Email and telephone alerts set-up. <span>yellow</span>	Combined sources of databases and own calculations performed. <span>green</span>

<span>green</span>	4	<span>blue</span>	3	<span>yellow</span>	2	<span>red</span>	1
--------------------	---	-------------------	---	---------------------	---	------------------	---

iSpace and Starlink are very positive regarding the "Automated" criteria, but they have no external communication lines set up. This is also the case for MISS, which on top of that is not fully automated either. The Starlink system has the additional downside of only using one source of information for its data. On the other hand, the systems at place at ESA and CNES/NASA have partial communication lines and use different

sources of information.

Ideally, the system that will be proposed here will be able to excel at all three criteria. However, the main focus is to establish a link between operators in this thesis. At a later stage, a complete automation of the system can be proposed.

## 8.3. Special considerations

The framework proposal will work on negotiation guidelines aimed at the optimum technical result of a dual-maneuver collision avoidance action. However, in many cases, the technical result will not propose a direct solution that can be used. These will reflect special considerations. Their consequences need to be thought of, for the interaction between operators to work out correctly. Systems that require special consideration are: derelict spacecraft and space debris, small spacecraft, mega-constellations, and manned spacecraft. Spacecraft operators often need to perform CAM's against such systems which negatively impact their own mission. A solution would be to hold other operators accountable, either in a technical way requiring a certain maneuver or in a financial way. Yet this is not always possible and will probably not be widely accepted by space actors.

### 8.3.1. Derelict spacecraft and space debris

These two types of objects are discussed together because they both fit into the category of Inactive spacecraft. They cannot be communicated with and cannot be maneuvered. This means that the intent of the maneuver is benign (see Section 8.1); at least the operator of the maneuverable spacecraft can be sure that the other object will stay on this course. This scenario aligns with the current collision avoidance procedures.

However, in a system that takes the fairness of procedures into account, the owners of such objects should still be held accountable. Derelict spacecraft and space debris have a launching state that is responsible for them even after the mission end and liable for any damage caused. As they cannot participate in any avoiding maneuver, they should compensate the operator that does maneuver in some way. Solutions for this scenario should be thought of. For space debris, the question goes one level deeper: should the owner still be held accountable even if they are not at fault for the formation of the space debris?

### 8.3.2. Small spacecraft

Small spacecraft, or more precisely CubeSats regularly do not have active maneuvering capabilities and so fall under the category of Non-Maneuverable spacecraft. When they do have orbit maneuvering capabilities it is often with drag influences, leading to larger response times and lower reliability [11]. Logically, the other spacecraft in the conjunction will need to perform the CAM. Again, this is a benign intent of maneuver and the response of the other object in the conjunction can be known more precisely in some cases. There should also be a compensation clause that describes this scenario in the proposal for negotiation guidelines.

The additional problem that comes with small spacecraft is that often their size increases the difficulty of detecting, tracking, and categorizing them. It can be difficult to catalog small spacecraft that were launched together [17]. This is mainly due to the decreased return of radar and/or optical signals [53]. If the communication is lost with the spacecraft, its mission lifetime will be lower than its orbital lifetime. This could even affect whether it meets the 25 years guideline for de-orbiting in LEO.

Furthermore, small spacecraft have allowed for easier access to space due to lower costs and rapid prototyping. Still, this could imply that the owners or operators of such small spacecraft do not have the experience and might not be aware of the risks, rules, regulations, and guidelines as opposed to the bigger operators [53]. This could endanger the space environment, in particular, if the concepts are pushed fast because of the low cost and ease of trying again.

Solutions to tackle this could be including better monitoring guidelines in an STM system. By making their small spacecraft more visible, operators would allow them to be tracked and identified. Besides this, there should be a system in place to allow for a direct link of information sharing related to the spacecraft's ephemerides (including uncertainties), the maneuver plans, the status of the spacecraft, and also the traceable objects within a certain area of that orbit. For efficiency, this should be done automatically. Including this factor of transparency will allow for the space environment to be more manageable with the increasing number of small spacecraft.

### 8.3.3. Mega-constellations

Mega-constellations are an emerging category of missions: they are often placed in LEO in already crowded regions. Spacecraft in such a constellation should not be seen as individuals. Instead, they should be seen as part of the whole system, as once a conjunction appears it is likely that others will follow [11]. For the other operators, this causes several problems: when maneuvering their spacecraft to avoid one collision they could trigger other conjunction warnings or have another series of spacecraft belonging to the constellation to be avoided.

Bi-lateral agreements are a good way to solve this, they can be drawn up between the constellation operator and operators that have important spacecraft in the same regions. An example of such an agreement is the 2021 NASA/SpaceX agreement where it is stated that Starlink spacecraft will perform evasive maneuvers to "mitigate close approaches and avoid collisions with all NASA assets" [48]. Such agreements reassure other operators that will not need to perform CAMs when passing by a constellation.

However, only one agreement is not the solution. They need to be drawn up between other operators as well and should be registered in a common database as well so that the rest of the space community is aware of them. The agreements can also be taken further: they could stipulate that once a conjunction event happens with a spacecraft from a constellation it would be required that the rest of the system conduct preventive maneuvers to avoid future conjunctions.

### 8.3.4. Manned spacecraft

When talking about manned spacecraft, the first object that comes to mind is the International Space Station (ISS). It carries astronauts since 2000 and is almost as big as a football field. Earlier in 2021, the Chinese space station was also launched; the Tiangong Space Station, carrying three astronauts. Furthermore, with the increase in space interest, sub-orbital flights are becoming a reality with the SpaceShipTwo and New Shepard as well as civilian orbital flights with SpaceX. Manned spacecraft are not numerous, but their numbers are growing and bigger concerns are raised with them: the consequences of a collision with a manned spacecraft are not only related to a drastic increase in space debris and loss of material but also, and foremost loss of human lives.

The ISS has a Trajectory Operations and Planning Group (TOPO) that is in charge of deciding if CAMs are necessary. CSpOC notifies TOPO if any object is predicted to pass within a certain volume<sup>d</sup> centered around the ISS within the next 72 hours [54]. From this information, TOPO can compute the probability of collision and notifies the flight control teams under certain conditions: TCA  $\leq 48$  hours,  $P_c \geq 10^{-6}$ , or the local vertical miss distance  $\leq 0.5$  km. Until TCA, TOPO continues computing the collision probability with updated information. An Emergency Debris Avoidance Maneuver (DAM) is performed according to the flight rules in place which depend on future ISS activities and thresholds<sup>e</sup>. TOPO also models different maneuver options and sends them to CSpOC for clearing. Here, an iterative process between TOPO and CSpOC starts until a safe maneuver is found. In case of a late-notice conjunction with high risk, the crew must shelter inside the Soyuz capsule. There is another system in place called the Pre-determined Debris Avoidance Maneuver (PDAM). It allows the ISS to maneuver with as little as a three hours notice, but the  $\Delta V$  applied is limited to discrete options [54].

The system used by the ISS is similar to the systems described in Section 8.2. The rules are more strict and there are contingency plans in place, such as the astronauts entering the escape pod. For other space stations, it is important to have similar practices at hand. It is also important to keep the volume of space around them protected to a certain degree. By doing so conjunction warnings with active spacecraft are averted completely and the ISS can focus its propulsion capabilities to avoid objects in the Inactive category.

## 8.4. Developing an approach: aspects and ideas

Now that STM has been defined, the current practices have been outlined, and the special consideration discussed, an approach can be developed to solve the negotiation aspect between operators. To do so, aspects and criteria for the comparison of different approaches need to be defined. The system developed should lead efficiently to correct solutions. Then, already proposed approaches will be described and finally evaluated based on the defined criteria.

<sup>d</sup> $\pm 2$  km (local vertical) x 25 km x 25 km (local horizontal)

<sup>e</sup>Black if  $P_c \geq 10^{-2}$ , red if  $P_c \geq 10^{-4}$ , yellow if  $P_c \geq 10^{-5}$ , and green if  $P_c < 10^{-5}$ .

### 8.4.1. Aspects/criteria

To generate a system that is efficient and does not set any operator at a disadvantage, aspects related to fairness, transparency, effectiveness, and objectivity should be considered [48]. The best technical decision will not always be the most fair decision, so these scenarios need to be thought out before they happen. Moreover, different constraints will be raised relating for example to security and politics. These will be expanded upon in Section 8.5, thereafter a proposal will be drafted.

Fairness implies that no operator suffers more on a resource base than the others. The cost of the operations should be shared fairly according to the decided approach and capabilities of each operator. Transparency is important because there are different collision avoidance procedures available with different thresholds for action. Sharing data related to the spacecraft, the conjunction messages received, and also the interpretation and outcome of the analysis is important to ensure that both operators come to the same conclusion and are in accordance regarding which approach to take. This should also be done related to the decided approach; the operators should share how they interpret the approach and what it means for that specific scenario. Effectiveness is important because it guarantees that the best solution will be found and on time. There should be no case where the outcome is no solution. Finally, objectivity is needed because different interpretations would not allow for an effective solution. It is also the basis for automation; an automated process acts purely on following the commands given and does not interpret them, thus avoiding subjectivity.

It can be argued that objectivity is already included in the other three criteria. For the system to be fair, transparent, and effective, it needs to be objective as well. For this reason, this criterion will not be included directly in the evaluation.

Besides these criteria, an automation criterion is necessary for two reasons. The first is that operators already need to deal with a large number of conjunction warnings and this is expected to increase in the coming years with the evolution of the space environment. A manual system will not be able to handle all these warnings. The second reason is that adding this negotiation approach to current collision avoidance processes will generate a more complex system. More checks will need to be made and more communication links established. So, not only would manual systems need to handle more conjunction warnings, they would also need to perform many new steps. A system that includes automation will facilitate the procedure significantly.

### 8.4.2. Approaches

The approaches to finding negotiation guidelines that will be discussed here are: the "rules-based-system", the "auction-based-system", the "resource-based-system", the "impact-based-system", and the "dual-maneuver implicit cost split system" [18, 48]. These have been already filtered from more possible approaches as the ones that are most promising.

In the "rules-based-system" both operators will need to agree on and perform compatible maneuvers. This needs to be accompanied by bi- or multi-lateral agreements and/or national/international laws to guarantee the cooperation of operators. These agreements are a step in the right direction for transparency of operations regarding collision avoidance. However, depending on the formulation of the rules there is a potential for a systematic exploitation of the rules [48]. The operator could figure out a loophole in the rules and avoid needing to perform maneuvers.

The "auction-based-system" works in an auction format as the name indicates. One of the operators of the conjunction would propose to move their spacecraft for financial compensation, then the other operator would counter the offer. This is a back-and-forth scenario until both agree on a maneuver and the financial compensation accompanying it. If the operators set their limits beforehand the system can work with a certain level of automation and so speed up the process. However, the evolution of the conjunction geometry with time will alter the interests and so also the prices and maneuvers to be performed. Not to mention, it could trigger operators to have a malevolent intent: cause conjunction to propose a maneuver and be financially compensated. If the financial compensation is greater than the cost of maneuvering, this is a potential risk.

For the "resource-based-system", the operator with the resources and the lower cost of collision avoidance is the one that performs the maneuver [18]. In this approach, the tricky part is defining the cost of collision avoidance. Every operator will have a different opinion on this if it also accounts for mission down-time. As the missions are different, the impact of the avoidance will be different in each case. Along this issue, the question of how the cost will be considered can be raised: will it be the total cost that matters, or how significant the cost

is for the operator.

The repercussions of the maneuver are accounted for in the "impact-based-system". This can include the cost of the maneuver and the effect on the mission [48]. That means that in the decision process of who maneuvers, the effect that the maneuver will have on the operator is accounted for. Again there is the difficulty of determining the cost definition and there is no compensation included in this approach. However, it can be automated with ease once the cost definitions are plugged in and the constant flow of information about spacecraft status is included.

Finally, in the "Dual-maneuver implicit cost split system" both spacecraft are supposed to maneuver in a way to divide the cost of propellant used and mission disruption or any other parameter decided upon beforehand [18]. The cost is then directly split up and does not require any financial compensation by any party. The same issue of cost definition is raised and the need for a direct communication link that is fully transparent is underlined as they are crucial to developing maneuver plans in accordance. The issue with this approach is that both spacecraft maneuvering is not necessarily the best technical solution (in terms of  $\Delta V$ ) and not all spacecraft are maneuverable.

### 8.4.3. Evaluation

The approaches described above are now categorized in an evaluation matrix based on the criteria decided upon: fairness, transparency, automation and effectiveness. This is shown in Table 8.3. An explanation is included of why a certain score was awarded.

Table 8.3: Evaluation of possible approaches.

Options \ Criteria	Fairness	Transparency	Automation	Effectiveness
<i>Rules-based</i>	Systematic exploitation of rules possible. <small>red</small>	Bi-lateral agreements between operators necessary. <small>blue</small>	Direct automation possible. <small>green</small>	Compatible maneuvers ensured. <small>green</small>
<i>Auction-based</i>	Favors bigger/richer operators. <small>red</small>	System requires constant communication. <small>yellow</small>	Can be implemented if operators set their limits directly, final decision needs to be man-made. <small>yellow</small>	Maneuvered spacecraft is financially compensated. <small>blue</small>
<i>Resource-based</i>	No compensation for spacecraft that conducts maneuver. <small>yellow</small>	Clear communication about spacecraft mission hard to achieve. <small>yellow</small>	Challenging to automate because of cost definition and different spacecraft categories. <small>blue</small>	Ensures minimum total cost of mitigation. <small>green</small>
<i>Impact-based</i>	Effects of decision taken into account when choosing maneuver. <small>green</small>	Stakeholders need to be included in decisions. <small>yellow</small>	Direct automation possible. <small>green</small>	Cost definition hard to establish. <small>yellow</small>
<i>Dual-maneuver implicit cost split</i>	Both spacecraft maneuver according to cost definition. <small>green</small>	Exchange of information can be achieved without security breaches. <small>blue</small>	Direct automation possible. <small>green</small>	Will not lead to the best technical solution. <small>yellow</small>

green 4
blue 3
yellow 2
red 1


From this evaluation, it can be said that different approaches stand out for certain criteria though none of them provide good solutions overall. For example, the dual-maneuver implicit cost split system has a good score in terms of fairness, transparency, and automation, but has a poor score for the effectiveness of the system. This approach does not guarantee that a solution is found for every conjunction scenario, as not all spacecraft are maneuverable. The rules-based system scores badly in fairness because it can be exploited, however, it scores well for the other criteria. The auction-based system cannot be automated with ease and also scores badly in fairness when different operator levels are considered. The resource-based system is good in terms of effectiveness, but since it has no compensation integrated in, it is not fair. In general, transparency is hard to achieve and will require a great international effort.

As a solution for the approach to be followed, a mix of the proposed approaches will be made. Based on their separate strong points the dual-maneuver implicit cost split, the resource-based, and the rules-based approaches are chosen. By combining the dual-maneuver implicit cost split and the resource-based approach

the minimum total cost of mitigation is ensured when having both operators cooperate, which is good in the long run for all of the space community. This does not necessarily mean that both spacecraft need to perform maneuvers; if there is no resource for it the other spacecraft must take it on, but if there is then both should take it on according to their capabilities. This is the closest to a technically optimal solution being implemented. Then, by adding on the rules-based approach, agreements that will ensure cooperation can be set up. The rules will be defined with the resource and dual-maneuver in mind and will account for different types of conjunctions. Setting the rules will also aid when implementing the automation process. This new approach will be called the "rule and resource following shared approach", its scoring according to the criteria is presented in Table 8.4.

Table 8.4: Evaluation of chosen approach.

Criteria \ Options	Fairness	Transparency	Automation	Effectiveness
<i>Rule and resource following shared approach</i>	Both spacecraft maneuver according to cost definition. <small>green</small>	Bi-lateral agreements between operators necessary. <small>blue</small>	Challenging automation due to cost definition but possible when bi-lateral agreements between operators are set up. <small>blue</small>	Ensures minimum total cost of mitigation. <small>green</small>



Although the scoring of this new approach is not perfect at the moment - it lacks in the transparency and automation department - further insight provided in Section 8.6 will allow strengthen its transparency criteria. In terms of automation, some ideas are proposed throughout the thesis. For example the automation of maneuver options for both spacecraft. However, it is recommended that more investigation be conducted in this domain.

## 8.5. Real-world constraints

For the defined approach to be relevant it must account for real-world constraints. Many concerns can be raised related to security and safety but also about who will be providing these tasks and how long will it take for these guidelines to be accepted on a global scale. The constraints could be identified as [17, 55]: cyber security of the system, real-time coordination and communication, task sharing between the private and public sector, ambiguity and collision avoidance objectivity, and sharing of methodologies and threshold levels. Another important constraint to implement is politics and interaction between different nations.

Regarding the sensitivity of the data that needs to be shared for the coordination between operators to work, public agencies are the best suited to deal with it as they should be neutral and secure [17]. Public agencies can guarantee that the approach will be followed regardless of the interests of private operators. This agent does need to interfere with other aspects of security and the use of space by the operators.

Real-time coordination and communication are key because even if operators do exchange data on their collision avoidance process, misinterpretation can lead to different conclusions [48]. Political and economic interests as well as cultural customs can influence decisions and cause an uncoordinated approach. This means that the operators need to come to the same evaluation by approaching the problem in the same way. However, it can be hard to achieve such communication links between different operators.

To solve for these real-world constraints a system such as the Middle Man used by CNES and NASA is proposed. This could be region-based to avoid having only one service proposing all the maneuvers, in which case the regional agents would communicate with each other. This would aid in the global acceptance of this proposal by different nations. It should also be ensured that the Middle Man agent created is from the public sector to guarantee data safety. The operators would need to relay information about their spacecraft and planned maneuvers for orbit maintenance. The Middle Man would receive conjunction information from CSpOC, or any other such database service. The information received from CSpOC and the operators would be combined by the Middle Man, who would then follow the procedure established for collision avoidance and then feed back



the maneuver to be conducted by each operator. Figure 8.3 visualizes how such a system would work.

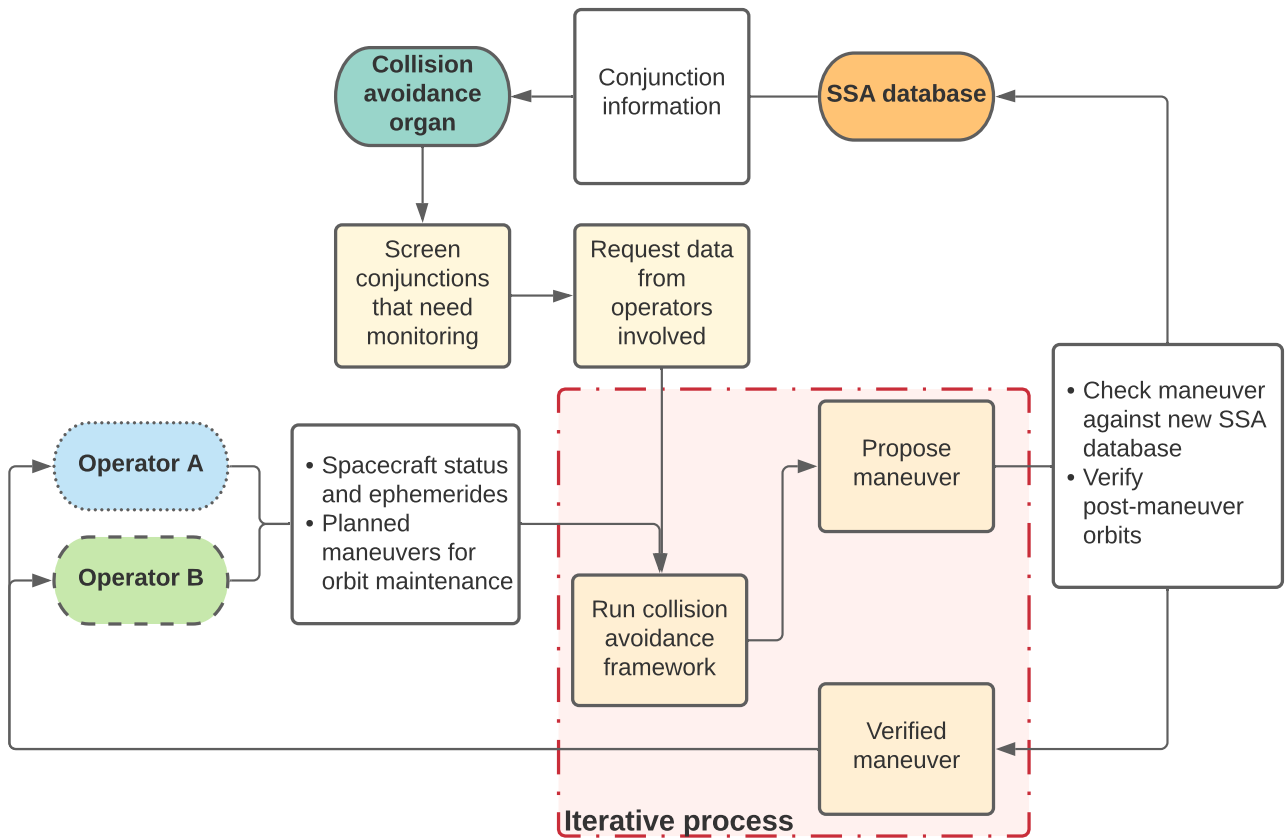


Figure 8.3: Flow of collision avoidance process if Middle Man service is included. The iterative process is conducted by the Middle Man.

## 8.6. Framework for decision making

With the Middle Man concept in mind and the chosen approach of a "rule and resource following shared approach" the framework shown in Figure 8.4 is defined. It shows several links between the operators, the Middle Man agent (acting the green and purple parts), and the SSA database.

The set-up assumes that operators are willing to share information about their planned maneuvers and their spacecraft ephemerides. Information about the spacecraft status, resources, and the cost definition for the maneuver based on mission impact are assumed to be initially kept private by the operators. It is unlikely that this information would be shared freely because of the competitive market of space services.

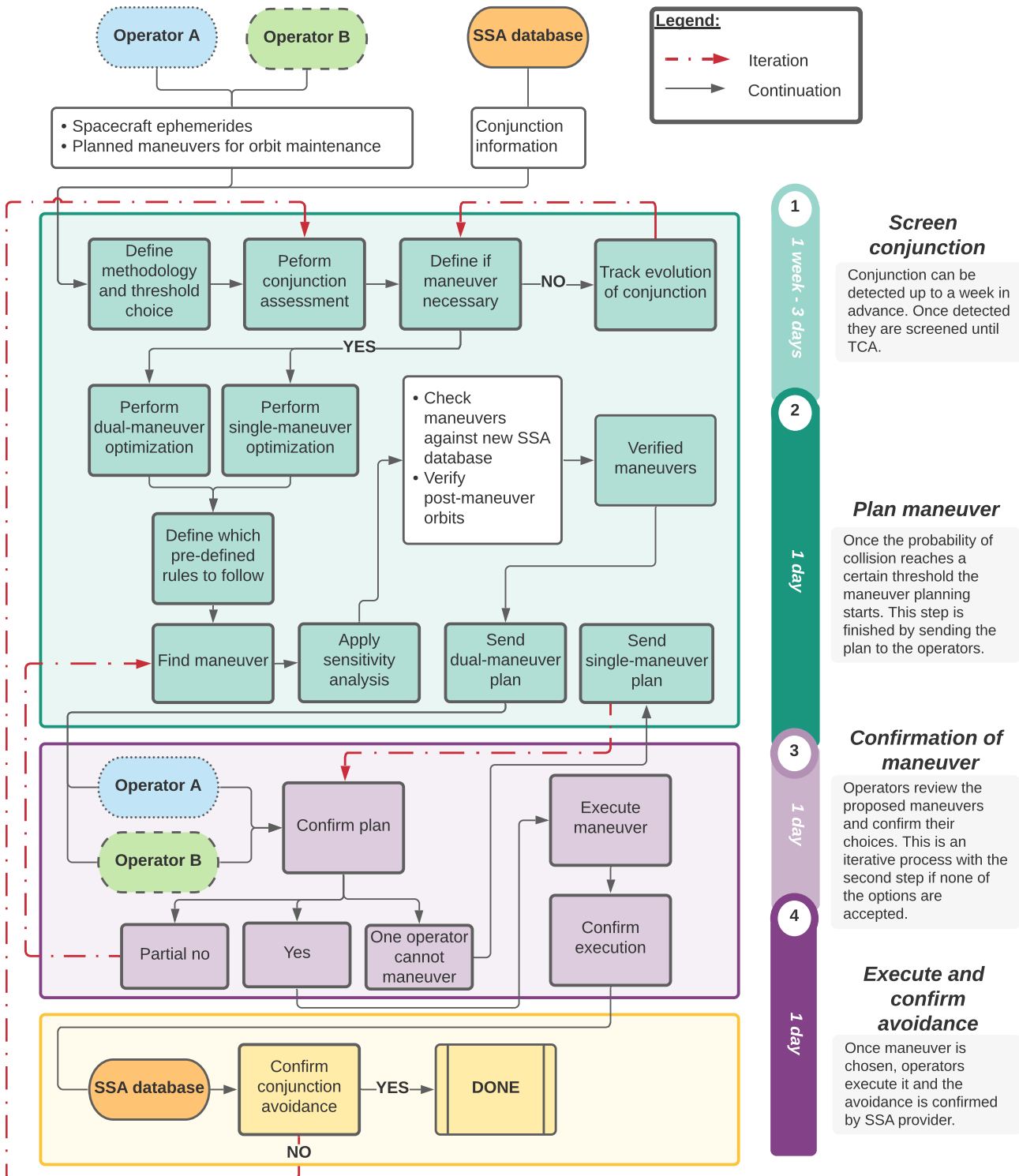


Figure 8.4: Negotiation flow with Middle Man agent proposal. The Middle Man interacts with the operators and the SSA database. It acts mainly in the green and purple parts.

The limitations in information hinder the effectiveness of the system. If spacecraft resources and cost definitions were known beforehand the Middle Man agent could propose maneuvers that meet the operators' requirements directly. Now a more iterative process is necessary, where the agent will propose a maneuver and the operator answers whether they want another solution. To make the process more time effective, the proposal for the agent will be made with a sensitivity analysis. This means that several maneuver combinations will be proposed at once to the operators; some will impact the mission more or less while some will require more or less propellant mass. These maneuvers will already have been screened as valid maneuvers. During this first proposal, it is assumed that both spacecraft can maneuver to a certain extent.

The operators can answer by accepting a combination of the maneuvers proposed, in which case they can proceed with the maneuver and avoid the conjunction. Another possible answer is that one operator cannot maneuver, in which case a single-maneuver plan is sent to the other operator (again with a range of maneuvers to choose from). This single-maneuver plan will have already been conducted alongside the dual-maneuver plan for improved efficiency in the process. If the operators decide that none of the proposed maneuvers are acceptable, they will indicate on which side of the sensitivity analysis the Middle Man agent needs to focus more on. Then, more maneuvers can be generated and proposed back until a combination is accepted by the operators.

These maneuver plans also pass through a block where pre-defined rules are chosen. This is related to the special considerations detailed in Section 8.3. When applied the rules will limit the possibilities of the maneuvers, or point towards certain actions. To make sure this is accepted by the operators, agreements have to be signed beforehand. Examples of the rules will be expanded upon at a later phase of the thesis after cases are analyzed for the technically optimum solutions.

This framework proposal is also in conformity with the criteria established beforehand for the proposal selection. By following the pre-defined rules and having a range of possible maneuvers it is fair in offering operators different options that will be compliant with their requirements and where both take action (if possible). It is transparent because the methodology and threshold are only carried out by the Middle Man agent and communicated to the operators. Moreover, the answers of the operators are communicated openly until the decision is made. This process also allows for automation as the range of maneuvers can be generated automatically, screened, and transmitted to the operators. The operators can have their own system which takes as input their requirements and the maneuvers proposed to screen which one is the best for them and so can automatically communicate back their answer. Finally, this proposal is also effective as many maneuvers are proposed at once and the back-and-forth interaction guarantees that a solution is found that in theory fits everyone in the scenario.



# Results

With the optimization algorithm finalized and the simulation scenarios defined, the concluding optimizations can be conducted. Their results are shown in this chapter. First, a short sensitivity analysis is presented in Section 9.1 for the baseline case used for the tuning. Afterwards, the different simulation cases results are shown in Section 9.2. This section includes the resulting Pareto fronts, but also a connection to the physical considerations. Finally, the results are used to complete the proposed framework for decision making in Section 9.3.

## 9.1. Sensitivity analysis

This section presents the sensitivity analysis conducted on the final model decided upon in Section 6.4. The same baseline scenario, Case 1, is used for the sensitivity analysis. This analysis is important to test the algorithm stability and to inform the operators on the level of certainty required from their maneuvers to reach the results predicted.

The first step is to combine the Pareto fronts generated for the seeds belonging to Case 1, into a final Pareto front. Then, seven<sup>a</sup> individuals are randomly selected to have their decision variables altered and new objective values calculated. As the individual with the smallest Cost parameter associated to a Collision parameter of 0 is of extra interest for operators, it is included in the selected individuals. An operator would normally not choose any of the other individuals on that straight line - this straight line can be seen for instance in Figure 9.1 - because it would cost them more in terms of propellant mass and orbit disturbance.

All the decision variables of these individuals are randomly altered, generating new individuals. These new individuals go through the propagation problem again where the objectives are recalculated. Finally, these are then compared to the original individuals. The individuals are marked with a number in the figures for ease of comparison between original fitness values and new fitness values.

The decision variables are not all altered by the same percentage as it would not represent a real situation. When a maneuver is executed, it will have cross-couplings into different axes which will differ. Hence, a random percentage is chosen in the sensitivity range to change the different  $\Delta V$  components. For consistency, the maneuver timing is also changed in the same manner, although it is, in reality, quite stable. The new individual decision variable function becomes, where  $S_{1,...,n}$  with  $n = 8$  is a randomly selected value in the sensitivity range:

$$x_{\text{new}} = \begin{bmatrix} t_{\Delta V_{1,\text{old}}} \cdot S_1, \\ t_{\Delta V_{2,\text{old}}} \cdot S_2, \\ \Delta V_{1,R,\text{old}} \cdot S_3, \\ \Delta V_{1,I,\text{old}} \cdot S_4, \\ \Delta V_{1,C,\text{old}} \cdot S_5, \\ \Delta V_{2,R,\text{old}} \cdot S_6, \\ \Delta V_{2,I,\text{old}} \cdot S_7, \\ \Delta V_{2,C,\text{old}} \cdot S_8 \end{bmatrix}^T \quad (9.1)$$

The sensitivity analysis produces individuals that receive a collision penalty, meaning that they have a collision probability,  $P_c$ , above  $10^{-5}$ . As defined by the optimization algorithm (Section 3.4), a large penalty is applied,

<sup>a</sup>This number proved to provide a good representation of the complete Pareto front.

making them strongly positive. The conversion from  $P_c$  to Collision parameter however makes them negative. Although the Collision parameter should be minimized, it should not be negative, as these are not better individuals.

Overall, varying the maneuver timing significantly leads to large changes in the individuals. In this scenario, a 5% change in maneuver time represents a change of around 18 minutes, while a 10% change in maneuver time represents a change of around 33 minutes. For orbits in LEO, that have periods around a couple hours, these changes are quite significant. In the cases used, the orbital periods are around 1 hour and 40 minutes. A change of 18 or 33 minutes is significant. This does not represent an uncertainty anymore but would represent for example the case of a maneuver abort that is re-tried some minutes later. It is recommended to upgrade the sensitivity analysis to include smaller variations in the maneuver timing decision variables.

The sensitivity analysis is presented in two steps. First the analysis is conducted for changes to all the decision variables up to  $\pm 5\%$  and then up to  $\pm 10\%$ . This is shown in Subsections 9.1.1 and 9.1.2, respectively.

### 9.1.1. Changes of $\pm 5\%$

The sensitivity analysis is first conducted with changes of  $\pm 5\%$ . The results are shown in Figures 9.1 to 9.3 for the three runs respectively<sup>b</sup>. The changes and the results are analyzed to identify what uncertainties the operator should be wary of.

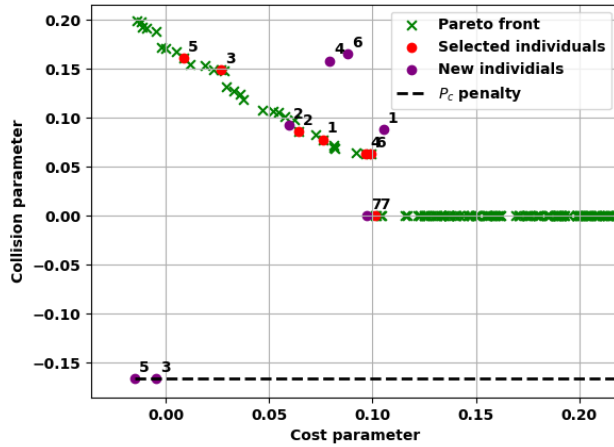


Figure 9.1: Sensitivity analysis variation of 5% on combined Pareto individuals (Run 1).

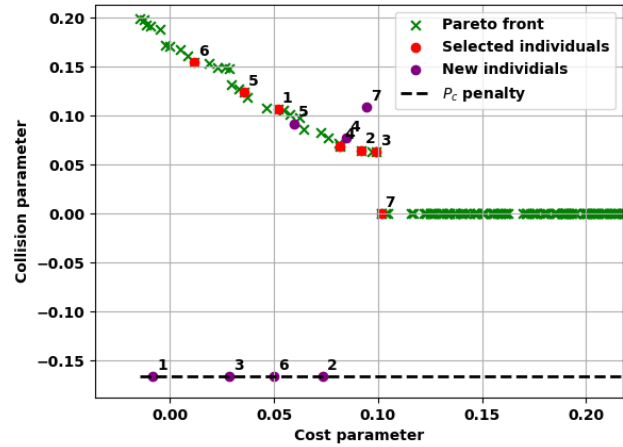


Figure 9.2: Sensitivity analysis variation of 5% on combined Pareto individuals (Run 2).

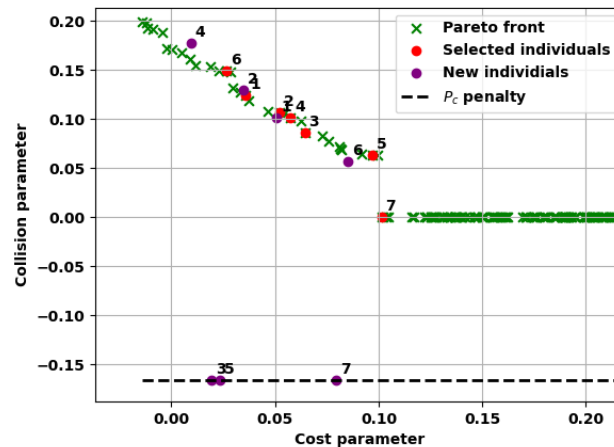


Figure 9.3: Sensitivity analysis variation of 5% on combined Pareto individuals (Run 3).

For the  $\pm 5\%$  sensitivity variation, the individuals tend to receive penalties though some stay within the Pareto front area. To investigate whether the results are due to poor combination of variations or whether a certain

<sup>b</sup>Three runs each with a different seed as the individuals are selected randomly.

decision variable is more relevant than another, Table 9.1 shows the variation attributed in maneuver timing to all individuals over the three runs. Further on, graphs focusing on the maneuver impacts are presented.

**Table 9.1: Change applied within  $\pm 5\%$  to each individuals decision variables over the three runs.**

Ind.	Run 1		Run 2		Run 3	
	$t_{\Delta V_1}$	$t_{\Delta V_2}$	$t_{\Delta V_1}$	$t_{\Delta V_2}$	$t_{\Delta V_1}$	$t_{\Delta V_2}$
1	1%	-4%	3%	3%	3%	0%
2	-1%	0%	0%	5%	-4%	2%
3	3%	-3%	-1%	5%	-2%	1%
4	-5%	-3%	-2%	0%	5%	-3%
5	-5%	-5%	-5%	-1%	-3%	3%
6	-1%	-5%	-3%	5%	-3%	5%
7	0%	0%	5%	0%	-2%	-4%

The individuals that show higher changes in maneuver timing correlate to some extent with the individuals that received penalties or that stray far from the Pareto front. The individuals that match this statement are:

- Run 1: individuals 3, 4, 5, 6
- Run 2: individuals 1, 2, 3, 6, 7
- Run 3: individuals 5, 7

Considering that these objects are in LEO, their maneuver timing is critical as differences can significantly change their position in the orbit. However, there are some individuals that do show high maneuver time changes and are not directly penalized. For example individual 4 of Run 3 (Figure 9.3), has changes of 5% and -3% to each maneuver time respectively and is still in the proximity of the Pareto front, although its Collision parameter value did increase. There are other examples where a matching behavior cannot be identified. The cause of this is difficult to determine as it could simply be that the sensitivity variation produced another response that is completely valid.

To investigate this further, the  $\Delta V$  components for each individual are plotted and compared for each run in Figures 9.4 to 9.6, respectively. The graphs show how the different components vary per  $\Delta V$  direction and between the two spacecraft. Furthermore, the graphs allow to compare  $\Delta V$  values per individual. This could help identify if changes in one direction are more important for the sensitivity if the individual presents higher  $\Delta V$  values to start with. The 'old' and 'new' labels represent the values before and after the sensitivity analysis.

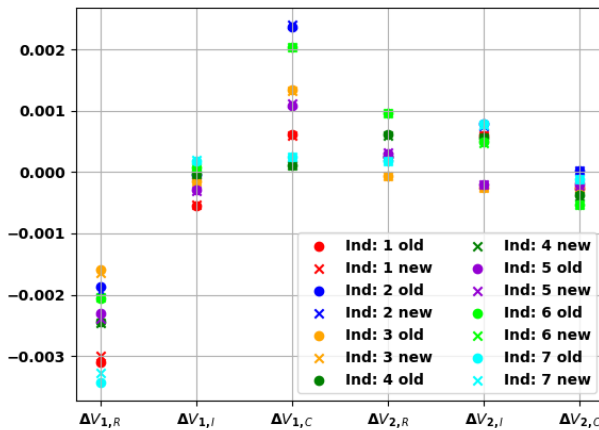


**Figure 9.4:  $\Delta V$  component values in [m/s] by individuals from sensitivity analysis of 5% (Run 1).**

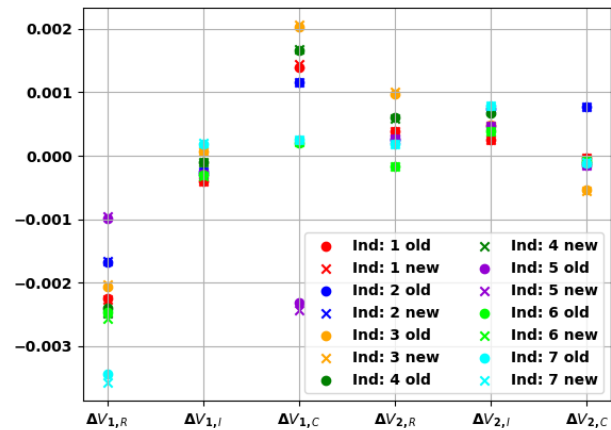


**Figure 9.5:  $\Delta V$  component values in [m/s] by individuals from sensitivity analysis of 5% (Run 2).**

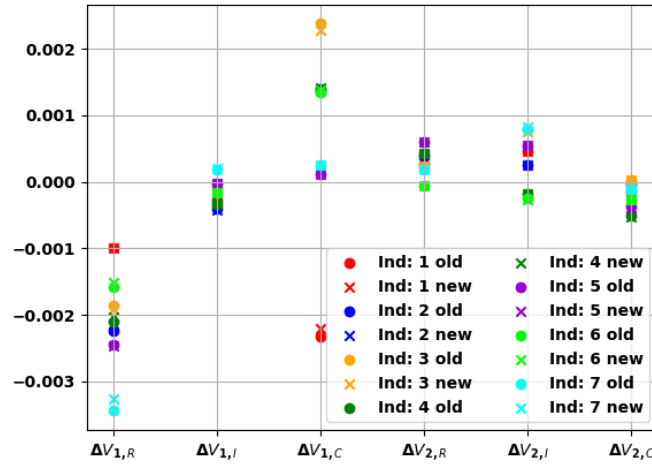


Figure 9.6:  $\Delta V$  component values in [m/s] by individuals from sensitivity analysis of 5% (Run 3).

In general, it can be identified that the chaser spacecraft (denoted by 1 in the graphs) has negative values of  $\Delta V$  in the radial direction, while the target spacecraft (denoted by 2) tends to have positive velocity changes in the radial direction. The cross-track contributions of the chaser are higher than those of the target and their in-track changes are similar although the target presents higher values in general.

Distinguishing whether the difference between the 'old' and the 'new' of a certain individual is higher than another individual is difficult as the orders of magnitudes are smaller. To aid Table 9.2 shows the norm of the  $\Delta V$  changes for each spacecraft (1 = chaser, 2 = target). Interestingly, individual 7 shows the largest changes for the chaser, but this is considered coincidental, as it is not the case for the sensitivity conducted with 10% which will be shown later.

Table 9.2: Norm of  $\Delta V$  changes in [m/s] for  $\pm 5\%$  sensitivity for each individual over the three runs.

Ind.	Run 1		Run 2		Run 3	
	$\ \Delta V_{diff,1}\ $	$\ \Delta V_{diff,2}\ $	$\ \Delta V_{diff,1}\ $	$\ \Delta V_{diff,2}\ $	$\ \Delta V_{diff,1}\ $	$\ \Delta V_{diff,2}\ $
1	0.000094	0.000003	0.000039	0.000002	0.000105	0.000003
2	0.000065	0.000034	0.000014	0.000003	0.000097	0.000016
3	0.000040	0.000003	0.000015	0.000043	0.000039	0.000041
4	0.000024	0.000006	0.000069	0.000012	0.000030	0.000015
5	0.000102	0.000001	0.000095	0.000004	0.000025	0.000008
6	0.000015	0.000006	0.000099	0.000001	0.000042	0.000005
7	0.000171	0.000015	0.000138	0.000014	0.000171	0.000023

Individual 4 of Run 3, that did not match the timing statements, shows small changes to the  $\Delta V$  norm and it has middle-range values for the  $\Delta V$  components as shown in Figure 9.6, although it has the lowest cross-track component for the target spacecraft. It can be said that the individual is not significantly affected by the high maneuver timing difference because it exhibits low changes to its  $\Delta V$  values. However, it should be noted, that its Collision parameter did increase significantly and so it can be assumed that if more changes had been made to the  $\Delta V$ , that it would have continued increasing and received a penalty.

The same analysis can be done for the other individuals. For example, individual 2 of Run 2, has a higher cross-track contribution for the target spacecraft than all the other individuals over the runs. It shows small changes in  $\Delta V$  magnitudes, and it has a high maneuver time change for the target spacecraft. After the changes, the individual has a similar Cost parameter, still it has a large enough Collision parameter for it to receive a penalty.

### 9.1.2. Changes of $\pm 10\%$

Next, the sensitivity analysis is also conducted with varying changes of  $\pm 10\%$  to the decision variables. As already established, changes of 5% are significant for the maneuver timing so here the focus is on individuals that have small changes in maneuver timing to see the effect of changing the maneuver impulse more.



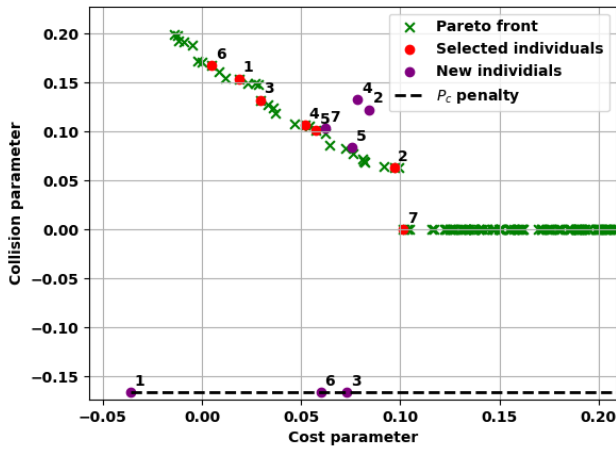


Figure 9.7: Sensitivity analysis variation of 10% on combined Pareto individuals (Run 1).

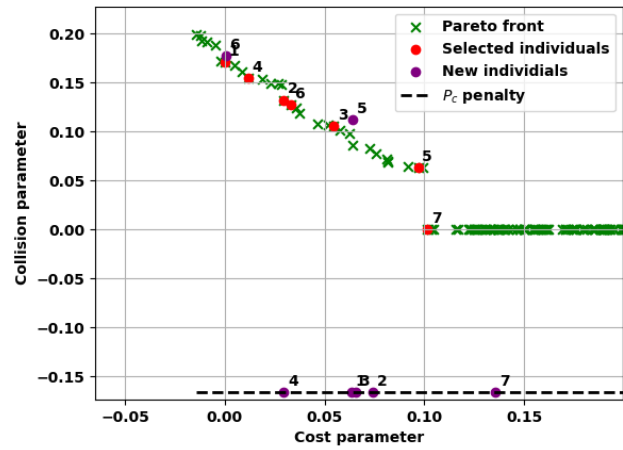


Figure 9.8: Sensitivity analysis variation of 10% on combined Pareto individuals (Run 2).

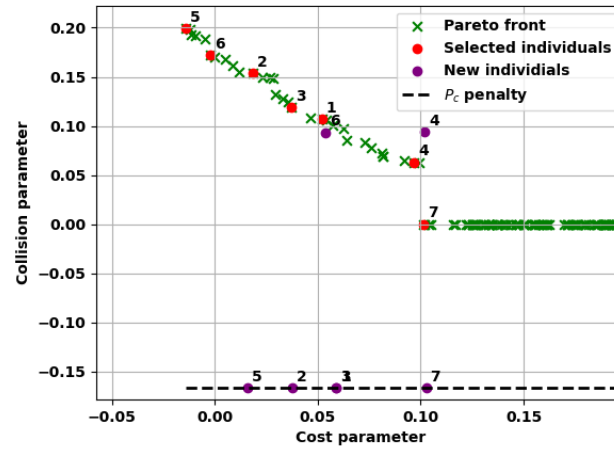


Figure 9.9: Sensitivity analysis variation of 10% on combined Pareto individuals (Run 3).

Overall, the changing of the fitness values is stronger. This is expected as the previous sensitivity analysis determined that up to  $\pm 5\%$  changes for the maneuver timing are significant. Hence, changes that are up to  $\pm 10\%$  maneuver timing logically should generate larger changes in results. Table 9.3 shows the percentage changes applied to the maneuver timing.

Table 9.3: Change applied within  $\pm 10\%$  to each individuals decision variables over the three runs.

Ind.	Run 1		Run 2		Run 3	
	$t_{\Delta V_1}$	$t_{\Delta V_2}$	$t_{\Delta V_1}$	$t_{\Delta V_2}$	$t_{\Delta V_1}$	$t_{\Delta V_2}$
1	9%	3%	6%	7%	0%	-7%
2	-7%	-1%	6%	-10%	0%	-4%
3	-7%	2%	0%	-5%	-8%	-8%
4	10%	-1%	1%	8%	0%	-3%
5	-6%	2%	0%	2%	7%	4%
6	3%	9%	-5%	-3%	-5%	-3%
7	1%	1%	7%	-6%	1%	-6%

In Run 1, the individuals with penalties, also have high percentage values (above 5%). This is also the case for Run 2. In Run 3, this matches for most individuals (1, 3, 5, and 7) except for individual 2. This last individual is then interesting for further analysis.

Figures 9.10 to 9.12 show the maneuver values by component for each spacecraft and for each individual. Again, it can be observed that the radial responses are opposite between each spacecraft in the conjunction.

In comparison to the previous graphs for the sensitivity analysis with  $\pm 5\%$ , here the different changes between the 'old' and 'new' individuals is more clear; for the higher percentages the crosses are further from the dots than before. For example, individuals 3 and 7 of Run 3 show larger changes than individuals 1 and 4.

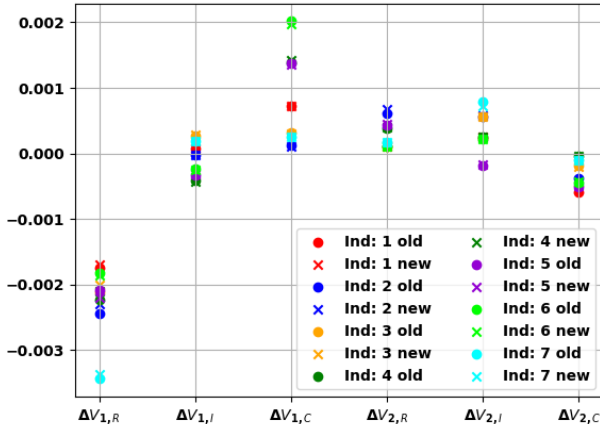


Figure 9.10:  $\Delta V$  component values in [m/s] by individuals from sensitivity analysis of 10% (Run 1).

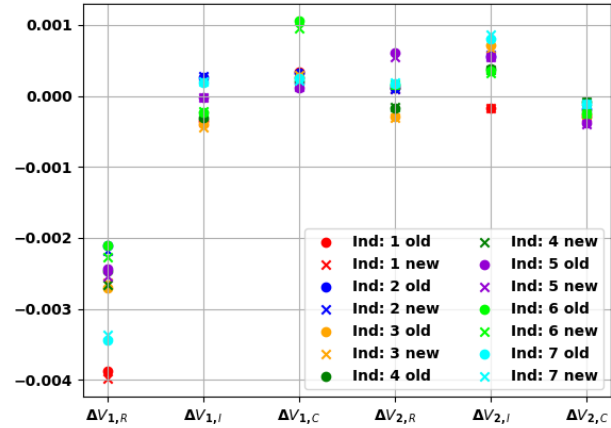


Figure 9.11:  $\Delta V$  component values in [m/s] by individuals from sensitivity analysis of 10% (Run 2).

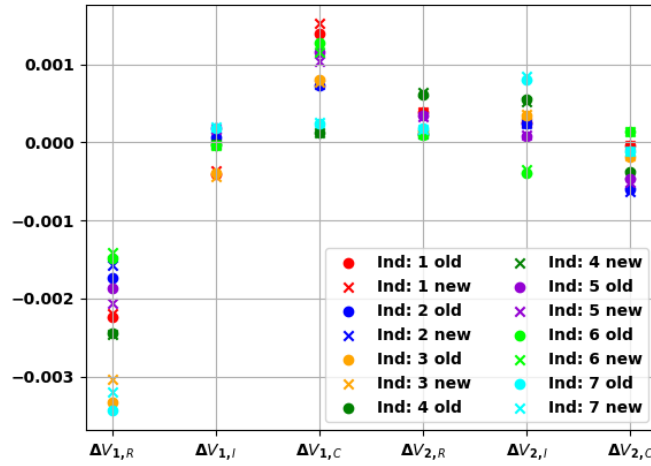


Figure 9.12:  $\Delta V$  component values in [m/s] by individuals from sensitivity analysis of 10% (Run 3).

Also here the magnitudes of  $\Delta V$  before and after are compared in Table 9.4. The example given before becomes clearer: individuals 3 and 7 have the largest  $\Delta V$  norm changes for the chaser in Run 3.

Table 9.4: Norm of  $\Delta V$  changes in [m/s] for  $\pm 10\%$  sensitivity for each individual over the three runs.

Ind.	Run 1		Run 2		Run 3	
	$\ \Delta V_{diff,1}\ $	$\ \Delta V_{diff,2}\ $	$\ \Delta V_{diff,1}\ $	$\ \Delta V_{diff,2}\ $	$\ \Delta V_{diff,1}\ $	$\ \Delta V_{diff,2}\ $
1	0.000054	0.000046	0.000113	0.000013	0.000025	0.000001
2	0.000147	0.000066	0.000060	0.000004	0.000153	0.000041
3	0.000103	0.000007	0.000072	0.000039	0.000294	0.000003
4	0.000092	0.000005	0.000193	0.000020	0.000025	0.000025
5	0.000078	0.000004	0.000098	0.000037	0.000106	0.000037
6	0.000004	0.000019	0.000111	0.000018	0.000130	0.000030
7	0.000068	0.000078	0.000069	0.000070	0.000238	0.000044

Previously, individual 2 of Run 3 was identified as an interesting point to study as it showed low maneuver time changes (0% for the chaser and -4% for the target) yet still received a penalty. Its  $\Delta V$  norm change is high for the chaser and, in comparison to the other individuals, relatively high for the target as well.

This individual shows standard values in its  $\Delta V$  components but has the lowest  $\Delta V$  component in the cross-

track direction for the target spacecraft. Combining these findings, it can be understood why it receives a penalty: the target changes its maneuver timing by 4% which is equivalent to around 14 minutes. On top of that, it has a relatively high cross-track  $\Delta V$  component and shows larger changes in  $\Delta V$  norm overall.

For the operator the sensitivity analysis conducted on the uncertainties indicates that the maneuver timing needs extra care to ensure that the collision is avoided as nominally predicted by the optimization algorithm. The 5% change present that represents an 18-minute change in maneuver timing, is not representative of a real-life scenario on maneuver timing uncertainty. The maneuver timing is strongly dependent on the on-board computer and close, a maximum of a few minutes could be attributed to maneuver timing uncertainty (less than 5 minutes). The maneuver timing sensitivity of the case where the maneuver is postponed and re-uploaded shortly after. The results presented in this section would indicate that if a maneuver is delayed by more than 5 minutes, the operator should find another CAM.

The importance of the  $\Delta V$  components is also to be kept; the larger the maneuver component, the more sensitive the collision avoidance is to changes within that component. When the cases are joined with the collaboration process proposed in Section 9.3, it will become clear that more information can be fed into the proposed system by the operators. With that in mind, the model can be enhanced to account for the operator uncertainties and produce better sensitivity results.

## 9.2. Cases

This section presents the results of the cases optimization runs. Since the case batches described in Section 7.2 deal with the same circumstances, they are presented together to ease the comparison between the options. As in the sensitivity analysis presented above, the three Pareto fronts found over different seeds are combined to generate a final Pareto front.

It is assumed that operators will focus their decision space on the varying values of Collision parameters and the lowest Cost parameter with Collision parameter 0.0. However, it could be that due to operator specific constraints other individuals are chosen. Nevertheless, this cannot be predicted.

The first batch of cases results are presented in Subsection 9.2.1, along with a physical analysis of interesting individuals. The second batch and its analysis are presented in Subsection 9.2.2. Finally, the third batch and its analysis are presented in Subsection 9.2.3. The orbital periods for the chaser and target are of 58695 seconds, or 1 hour and 37.8 minutes and 59095 seconds, or 1 hours and 38.5 minutes, respectively<sup>c</sup>

### 9.2.1. First cases batch

The first cases batch deals with the variation of the weights for each object applied in the objective function. Its goal is to show the effects of the varying weights. In Figure 9.13 the final Pareto fronts for Cases 1, 1.1, 1.2, 1.3, and 1.4 are shown. Presenting them together allows to compare to which extent the object's propellant mass usage and orbit disturbance contribute to the fitness values. It also allows to determine areas of interest where operators could have interesting choices to make. It should be noted that on the yellow line present at Collision parameter 0, also individuals from the other cases can be found. This is applicable to the next cases as well.

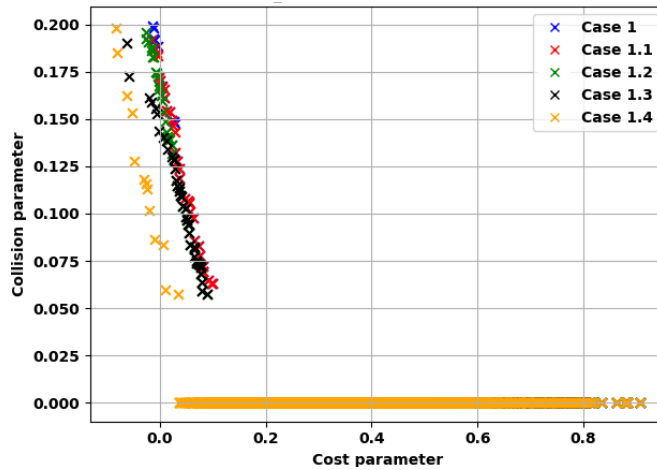


Figure 9.13: Final Pareto fronts for Cases 1, 1.1, 1.2, 1.3 and 1.4.

Cases 1, 1.1 and 1.2 result overall in similar results, indicating that giving more importance to the propellant mass contribution of the chaser or the target does not influence the results much. This can be explained because the same propellant usage limits are set for both objects and these limits are probably not reached during the optimization and so neither are favored in contributing to the maneuvering.

The  $\Delta V$  norm average over a number of individuals for both objects shown in Table 9.5 supports this claim. The  $\Delta V$  allowance in each direction was limited at  $\pm 0.01$  m/s, in the maximum scenario the norm is 0.0173 m/s. All of the presented  $||\Delta V||$  are an order of magnitude below the maximum allowed. For future research, it is recommended to restrain the decision variable range. The average  $||\Delta V||$  is computed twice, once for the domain where the Collision parameter  $\neq 0$  and once for the domain where it is equal to 0. This should allow for comparison in the approach taken for the collision avoidance.

<sup>c</sup>Chaser: With an perigee and apogee altitude of: 571 km and 712 km. Target: With an perigee and apogee altitude of: 675 km and 712 km.

**Table 9.5:**  $\|\Delta V\|$  average for both objects over the first cases batch. 30 individuals used per average calculation, values in m/s.

		Collision parameter $\neq 0$				
		Case 1	Case 1.1	Case 1.2	Case 1.3	Case 1.4 <sup>a</sup>
<b>Chaser</b>		0.002692	0.003182	0.00228	0.002417	0.0031
<b>Target</b>		0.000686	0.000603	0.000869	0.000652	0.00066
		Collision parameter $= 0$				
		Case 1	Case 1.1	Case 1.2	Case 1.3	Case 1.4
<b>Chaser</b>		0.00636	0.005366	0.006791	0.004536	0.007011
<b>Target</b>		0.006638	0.004279	0.006757	0.004224	0.005591

<sup>a</sup>Using 10 individuals.

This table allows the compare the  $\Delta V$  used for each object over the different cases. Over the two domains ( $\neq 0$  and  $= 0$ ) the chaser spacecraft has the same order of magnitude for its maneuvers over all the cases. The target spacecraft however presents maneuvers an order of magnitude higher for the Collision parameter  $= 0$  domain. This indicates that to avoid the collision with a low Cost parameter, the maneuver efforts should be for the chaser. When the target contributes accordingly, the Collision parameter is lowered as much as possible while the Cost parameter increases.

Next, the maneuver times for the individuals in the Pareto fronts can be investigated in pairs: Case 1.1 versus 1.2 in Figures 9.14 and 9.15 and Case 1.3 versus 1.4 in Figures 9.16 and 9.17. The maneuver times for Case 1 are similar to the results of the other first cases batch and is presented later in a comparison to Case 2 (cf. Figure 9.22. For these graphs the maneuver limits correspond to the allowable maneuver span defined in Subsection 4.5.1.

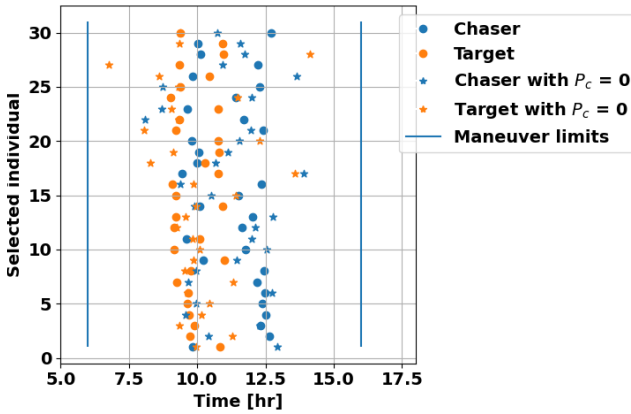


Figure 9.14: Maneuver times for individuals of Case 1.1.

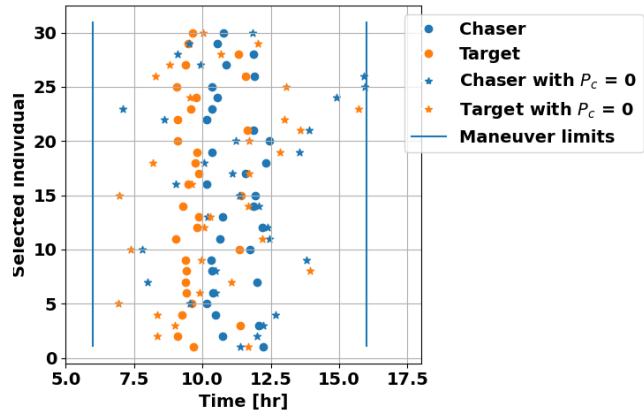


Figure 9.15: Maneuver times for individuals of Case 1.2.

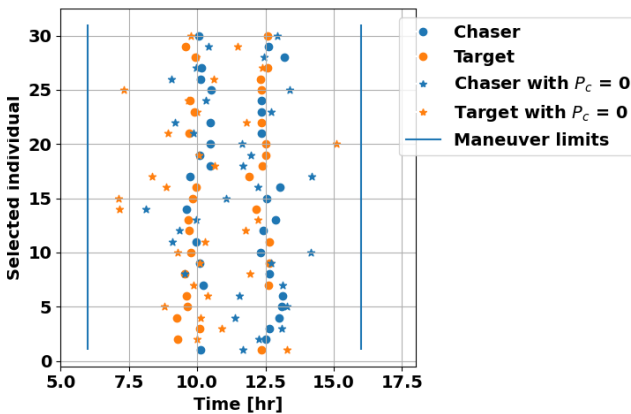


Figure 9.16: Maneuver times for individuals of Case 1.3.

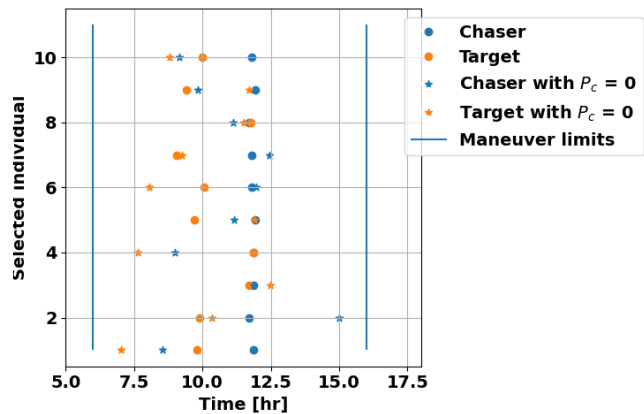


Figure 9.17: Maneuver times for individuals of Case 1.4.

Case 1.1 and 1.2 resulted in similar final Pareto fronts and varying but in the same order of magnitude  $||\Delta V||$  (cf. Figure 9.13 and Table 9.5). Additionally, their maneuver times from the randomly selected individuals differ. In Figure 9.14 a trend of maneuver times at 10 and 12.5 hours can be identified; the ideal chaser maneuver time is 2.5 hours after the target maneuver time. Interestingly a difference cannot be identified between the maneuver times for individuals with Collision parameter 0 and the other individuals. Although for Case 1.2 the outliers are individuals with Collision parameter 0 (Figure 9.15).

Case 1.1 and 1.2 differ in the propellant mass weights for the objects: 0.2 versus 0.8 for the chaser and 0.8 versus 0.2 for the target. Having a lower propellant mass weight for the target allows its maneuver time to have more freedom as can be seen in Figure 9.15.

Figures 9.16 and 9.17 show a more mixed behavior compared to Cases 1.1 and 1.2. The chaser's and target's maneuver times are blended at values of 10 and 12.5 hours. Case 1.4 has less individuals; as is shown in Figure 9.13, the Pareto front is scarce compared to the other cases. Once again, the maneuver times that stray from the 10- and 12.5-hour regions belong to individuals with a Collision parameter of 0.

Cases 1.3 and 1.4 do not differ in their propellant mass weights but do differ in the mission impact weights: 0.2 versus 0.8 for the chaser and 0.8 versus 0.2 for the target. Having a stronger mission impact weight makes the chaser stick to the 12.5 maneuver timing, while the target object has more freedom. Figure 9.17 indicates that maneuvering 12.5 hours into the collision avoiding window is beneficial for the mission impact.

Back to Figure 9.13, an interesting domain is identified for further comparisons between individuals: Collision parameter 0.125. For further analysis, an individual is chosen for each case that is the closest to this area. It shows a lower Cost parameter for Case 1.4, but similar results for the other cases. It indicates that only having a higher orbit disturbance contribution for the chaser leads to minimizing the Cost parameter for that  $P_c$  value.

In this area, Cases 1 and 1.1 have the same individual as do Cases 1.2 and 1.3. This led to the selection of 3 individuals: Ind. 1 stems from Case 1, Ind. 2 stems from Case 1.2 and Ind. 3 stems from Case 1.4. To investigate the difference further, the  $\Delta V$  contributions can be checked with the help of Figure 9.18.

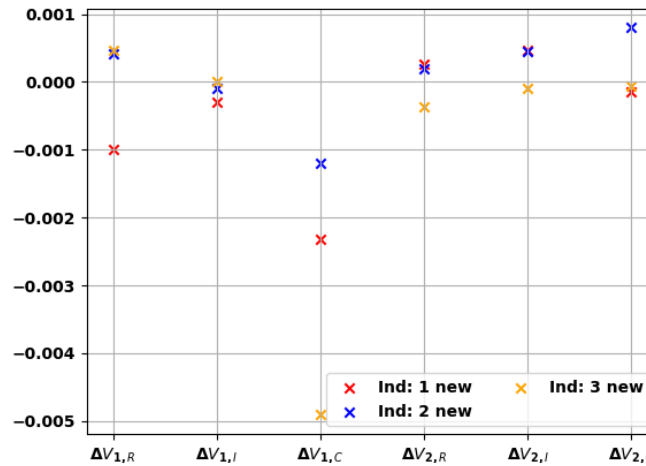


Figure 9.18:  $\Delta V$  component values in [m/s] for relevant individuals in the first cases batch.

A large difference is spotted in the  $\Delta V_{1,C}$  component. It is low for individual 2, medium for individual 1 and high for individual 3. For individuals 1 and 2 the  $\Delta V$  used does not vary significantly between the chaser and the target. The differences start appearing for Case 1.3 and then increase for Case 1.4. This indicates that in this scenario, varying the orbit disturbance contributions is more significant than varying the propellant mass, even with the Cost parameter being made up of 80% Mass parameter and 20% Orbit parameter (as defined in Section 6.2).

Individual 1 has equal propellant usage importance and individual 2 has a higher importance of the propellant mass of the chaser. This coincides with the results seen in the graph: the equal importance leads to a more stable distribution between  $||\Delta V_1||$  and  $||\Delta V_2||$ , while the larger importance on the chaser leads to smaller  $\Delta V$  values for the chaser in comparison to the other individuals.

Individual 3 has a higher orbit disturbance weight on the chaser, and it presents high  $\Delta V$  components in the radial and cross-track directions for the chaser and low component values overall on the target. To determine to which extent the orbit disturbance is altered, the position differences between the "no CAM" case and the individuals' orbits can be calculated. The results are shown in Figure 9.19.

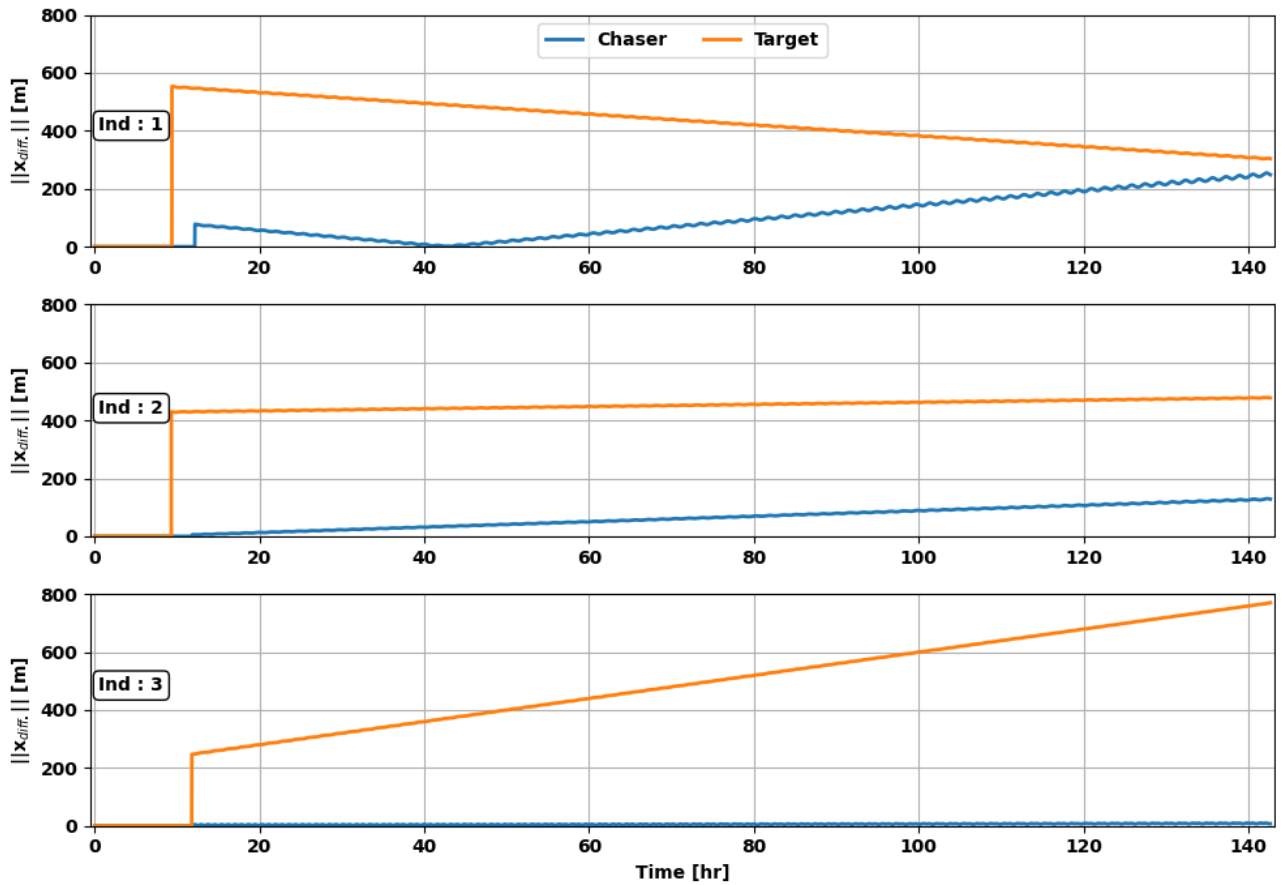


Figure 9.19: Norm of the position differences to the "no CAM" orbit for the relevant individuals in the first cases batch.

Looking at the position differences for individual 3 that has a high orbit disturbance weight for the chaser, the disturbance is much lower in comparison to the target and also in comparison to the other individuals. However, the target shows a higher final position difference that seems to continue growing in time.

### 9.2.2. Second cases batch

Cases 2 and 2.1 deal with constellation versus normal spacecraft scenario, where the only difference is in the  $I_{sp}$  used for the constellation spacecraft. From Figure 9.20, their final Pareto fronts are similar, as for the major part the individuals overlap. Case 3 is also shown in this graph as it belongs to the same batch. However, it has one spacecraft that does not take the orbit disturbance into account and can still maneuver; the orbit disturbance weight is set to 0 and the propellant mass weights are the same at 0.5.

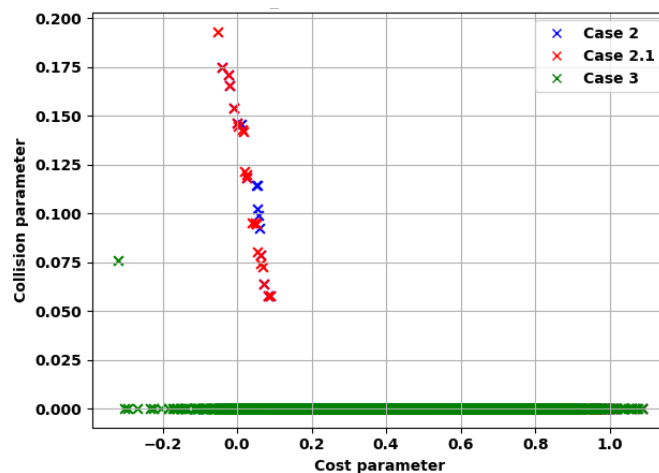


Figure 9.20: Final Pareto fronts for Cases 2, 2.1 and 3.

Case 3 presents the lowest values in the Cost parameter. This is according to the predictions as one orbit disturbance is not accounted for in the parameter. However, this does not mean that the target spacecraft does

not exhibit changes in its orbit. This will be shown later in Figure 9.24. Case 3 also has fewer Collision parameter values, indicating that without caring for one of the object's orbit disturbances, lower Collision parameters are reached with the same Cost parameter.

Although the comparison is clear and the results are as expected, the lack of optimal individuals indicates that the optimization algorithm should be re-tuned for this case. The goal would be to minimize the Cost parameter further and have more varying Collision parameters. It should be noted, that both objects' propellant mass is accounted for in the Cost parameter and that the target still has limits in its propellant usage. This means that its orbit cannot be changed drastically.

As the target object does not care about orbit disturbance it is interesting to see how it behaves in terms of  $\Delta V$ . Though it is not expected to produce shocking values as its propellant mass usage is still considered in the objective function and it has a propellant usage limit. Table 9.6 provides the average  $\Delta V$  norm over 15 individuals in two Pareto front domains (Collision parameter  $\neq 0$  and  $= 0$ ). Note that values for Case 3 are only given in the second domain as it has just a single individual with a different Collision parameter (cf. Figure 9.20).

**Table 9.6:  $\|\Delta V\|$  average for both objects over the second cases batch. 15 individuals used per average calculation, values in m/s.**

	Collision parameter $\neq 0$		
Chaser Target	Case 2	Case 2.1	
	0.000752	0.001009	
	0.000778	0.000879	
	Collision parameter = 0		
Chaser Target	Case 2	Case 2.1	Case 3
	0.004554	0.004932	0.002895
	0.004038	0.005774	0.003984

These results are different from the first cases batch; now the chaser and target spacecraft have maneuver magnitudes in the same order of magnitude. As the orbit disturbance is less relevant for the target, it presents a larger maneuver magnitude than in Table 9.5, while the chaser presents smaller maneuver magnitudes (0.0007 m/s compared to 0.003 m/s for Case 1.1). The  $\|\Delta V\|$  are larger for the Collision parameter  $= 0$  domain, indicating that once again to achieve smaller  $P_c$  a larger CAM is necessary from both spacecraft.

The difference between Case 2 and 2.1 is that the maneuvers are larger for Case 2.1. As the only change is the  $I_{sp}$ , this difference was expected to be seen in  $\|\Delta V\|$ .

In the same fashion as before, also the maneuver times for the individuals in the Pareto front can be analyzed. This is shown in Figure 9.21 for Case 2. The other cases belonging to the second cases batch are not shown here. They resemble the result of Case 2, where for Case 3 only individuals with Collision parameter 0 are displayed. For comparison, the maneuver times of Case 1 is provided here in Figure 9.22.

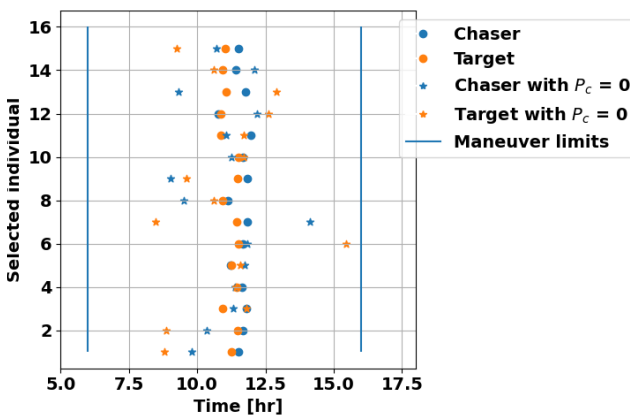


**Figure 9.21: Maneuver times for individuals of Case 2.**

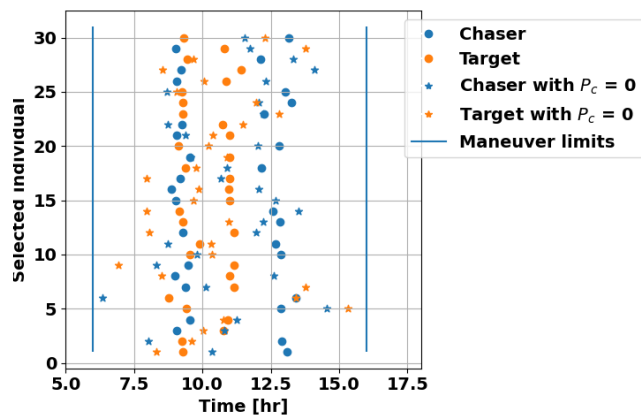


**Figure 9.22: Maneuver times for individuals of Case 1.**



The comparison is made between the maneuver times for Case 1 and Case 2. Looking at the graphs the difference is clear: Case 1 shows a behavior resembling to what was seen before while Case 2 has similar maneuver times for the chaser and target at around 11 hours. The common point is that the outliers remain individuals with Collision parameter equal to zero. As expected from the Pareto fronts in Figure 9.20, less individuals are present. For Case 1, the chaser prefers maneuvers at 10 and 12.5 hours while the target prefers maneuver times around 10 and 11 hours. For Case 2 the target has a tendency to maneuver right before the chaser but compared to Case 1 its preferred timing is pushed forward. This is interesting as the major difference between these two cases are the propellant mass weights - Case 2 has a higher propellant mass weight for the target than Case 1.

Compared to Cases 1.1, 1.2, 1.3, 1.4 (in Figures 9.14 to 9.17), Case 1 shows a more distributed trend in maneuver times. There are several target individuals with maneuver times in between the two regions identified beforehand (10 and 12.5 hours).

To understand how the maneuvers change between these cases, it is interesting to extract individuals for each case with a Collision parameter close to 0.075<sup>d</sup>. This leads to three individuals for further analysis: Ind. 1 stems from Case 2, Ind. 2 stems from Case 2.1 and Ind.3 stems from Case 3. Their individual  $\Delta V$  components can be analyzed as well as their position differences with respect to the "no CAM" orbit. The results are shown in Figures 9.23 and 9.24, respectively.

To analyze the results, the different contributions to the Cost parameter need to be kept in mind. As a refresher:

- Case 2 or Ind. 1:  $w_{p_1} = 0.3$ ,  $w_{p_2} = 0.7$ ,  $w_{O_1} = 0.7$ ,  $w_{O_2} = 0.3$
- Case 2.1 or Ind. 2: same as Case 2,  $I_{sp}$  value changes for chaser from 300 s to 500 s.
- Case 3 or Ind. 3:  $w_{p_1} = 0.5$ ,  $w_{p_2} = 0.5$ ,  $w_{O_1} = 1.0$ ,  $w_{O_2} = 0.0$

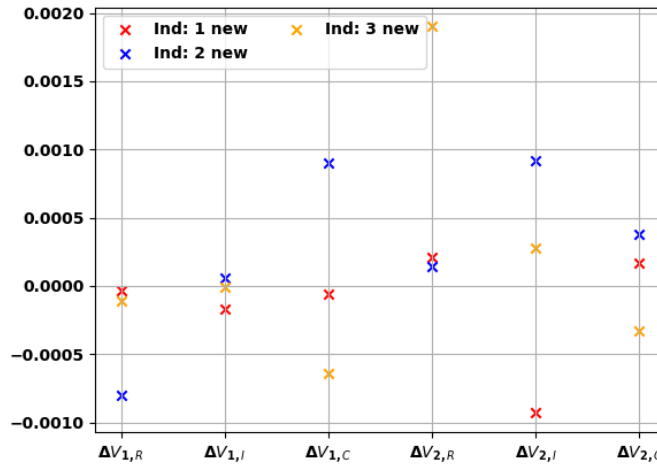


Figure 9.23:  $\Delta V$  component values in [m/s] for relevant individuals in the second cases batch.

In the figure, a clear pattern between the individuals cannot be identified. Individuals 1 and 2 have similar Cost parameters in the Pareto fronts, although they do not have similar  $\Delta V$  values per component and per spacecraft. The  $\Delta V$  magnitude of individual 1 per object is:  $||\Delta V_1|| = 1.83 \cdot 10^{-4}$  m/s and  $||\Delta V_2|| = 9.68 \cdot 10^{-4}$  m/s, while for individual 2 it is:  $||\Delta V_1|| = 12.06 \cdot 10^{-4}$  m/s and  $||\Delta V_2|| = 10.05 \cdot 10^{-4}$  m/s. The effect of having a higher  $I_{sp}$  for the chaser belonging to the second individual is clear: similar Cost parameters, but larger maneuver magnitudes for individual 2 in comparison to individual 1. The benefit is clear for the operator, however it does not change the cooperation process significantly, as similar Collision parameters are reached: 0.06224 ( $P_c = 8.57 \cdot 10^{-17}$ ), and 0.06271 ( $P_c = 1.13 \cdot 10^{-16}$ ) for individuals 1 and 2 respectively.

Comparing the target maneuvers between individual 3 and the others, a higher radial component is noticed. The  $\Delta V$  magnitudes for this individual are  $6.49 \cdot 10^{-4}$  m/s for the chaser and  $19.49 \cdot 10^{-4}$  m/s for the target. The chaser's maneuver is in the same maneuver range as the other individuals. The target's maneuver has a higher magnitude. This makes sense, as there is no limit to the orbit disturbance on the target. However, the increase is limited by the limits set to the propellant mass and the fact that both propellant masses are still accounted

<sup>d</sup>This value is chosen as it is the only Collision parameter for Case 3 besides 0.0.

for in the Cost parameter.

Finally, it would be also interesting to see the position differences between the individuals' orbits and the "no CAM" orbit. This is shown in Figure 9.24. This will allow to confirm that the lower Collision parameter for individual 3 is accompanied by orbit disturbances as mentioned before.

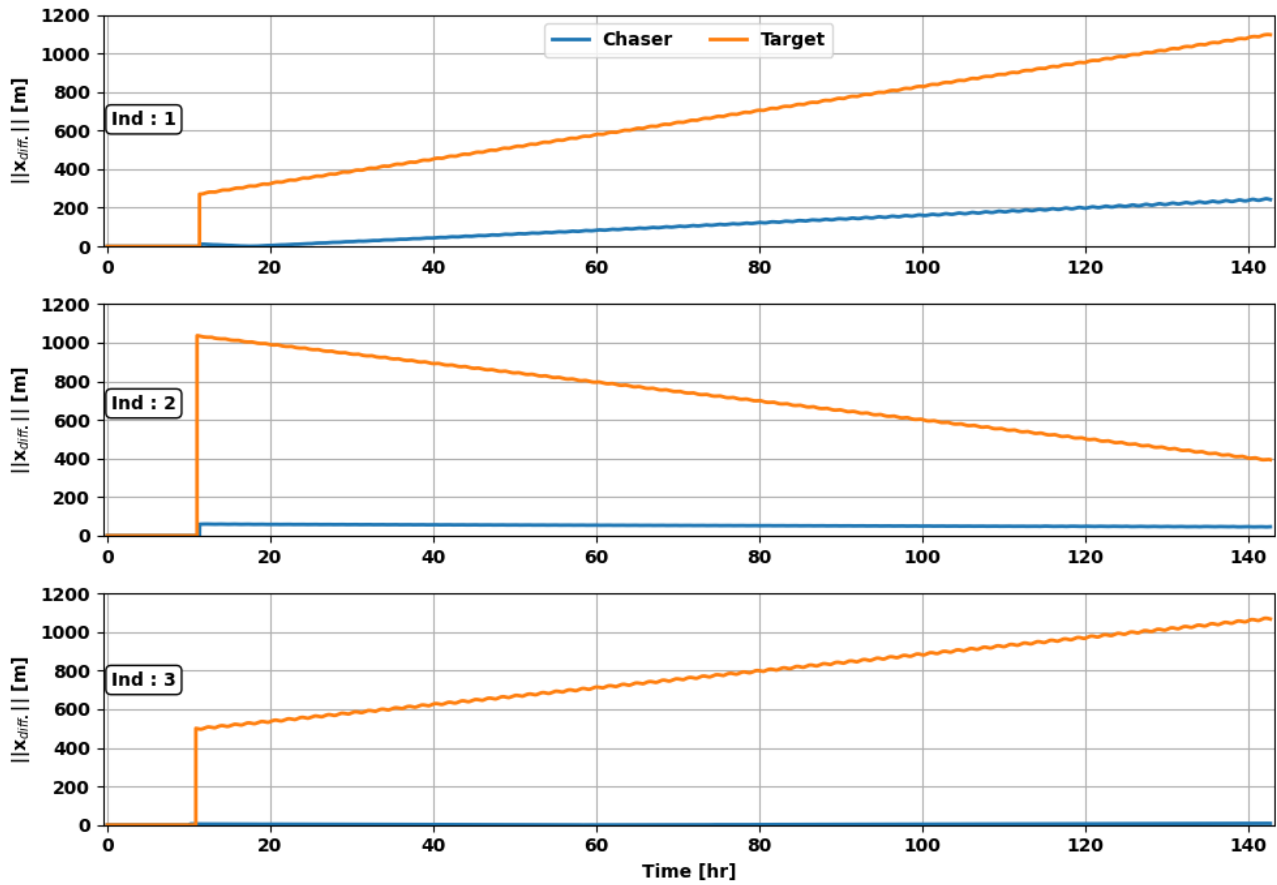


Figure 9.24: Norm of the position differences to the "no CAM" orbit for the relevant individuals in the second cases batch.

Individuals 1 and 2 only differ in terms of  $I_{sp}$  which translates to differences in maneuver magnitude for the target. They also show similar Cost parameters. Here, the position differences of the target in individuals 1 and 2 show inverted behaviors. For individual 1, there is a small step at the start and then the difference grows over time. Individual 2 has a large step at the start due to the larger maneuver conducted, and then has a decreasing position difference. As the orbit disturbance is quantified as the area under the yellow curves, it can be understood that the Cost parameter is similar in the end, even if the response on both individuals is different.

All individuals show a lower change in the chaser's orbit compared to the target's orbit. This is in line with the objectives of these Cases; the constellation spacecraft gives more importance to its orbit change. For individual 3, this is pushed further. The chaser seems to have very little change while the target has an increasing orbit change. This is in accordance with how the orbit disturbance weights are set up.

The scale can also be compared to the position differences calculated for Cases 1, 1.2 and 1.4 in Figure 9.19. The current cases have larger value of position differences overall. Case 3 shows a similar behavior to Case 1.4; low differences in chaser orbit and high differences in target orbit. Both deal with lower orbit disturbance values for the target, still the difference is more significant for Case 3.

### 9.2.3. Third cases batch

The final cases' batch deals with the single-maneuver conjunction scenario. The difference between the cases from this batch are only in the  $\Delta V$  limits for each component of the chaser spacecraft. The target spacecraft is assumed to do no maneuvering hence its contribution to the total propellant mass and orbit disturbance are set to zero. The final Pareto fronts for Cases 4, 4.1, and 4.2 are shown in Figure 9.25. There is an overlap

between the three Cases at the right side of the graph.

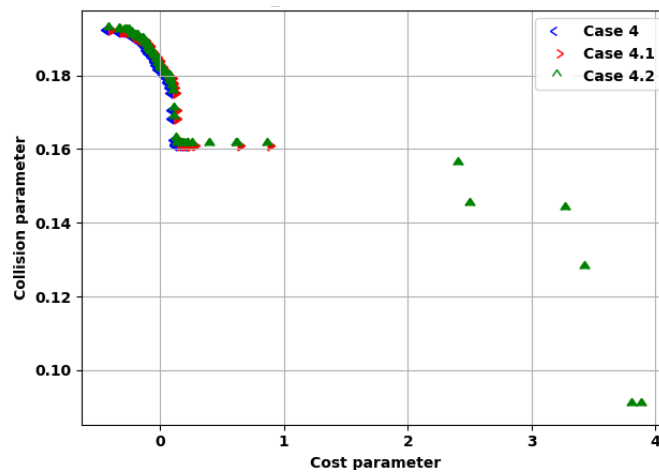


Figure 9.25: Final Pareto fronts for Cases 4, 4.1 and 4.2.

These Pareto fronts can be compared to the previous Pareto fronts shown in this chapter. The findings are:

- Low Collision parameter values are not reached, the minimum being around 0.09.
- There is no straight line at Collision parameter 0.0, although there seems to be one at 0.16 which afterward continues decreasing for Case 4.2.
- Higher values are reached for the Cost parameter, and the low values identified before are not present even though the orbit disturbance of one object is not accounted for.

These conclusions indicate that the single-maneuver avoidance does not allow to reach Collision parameters as low as the dual-maneuver approach. Additionally, it costs more to reach similar Collision parameters (compare to previous Pareto fronts at around Collision parameter 0.16). However, when results are reached the collision probability is lowered within the bounds recommended (0.16 is  $P_c = 5.6 \cdot 10^{-7}$ ). This means that the optimization algorithm also works for the single-maneuver case. The results illustrate why a dual-maneuver approach would be beneficial in a system that considers both objects in the conjunction together.

Table 9.7 shows the average  $\|\Delta V\|$  over 30 individuals belonging to the Pareto front. As a Collision parameter value of 0 is not reached for these cases, the table shows only the average for the non-zero domain.

Table 9.7:  $\|\Delta V\|$  average for both objects over the third cases batch. 30 individuals used per average calculation, values in m/s.

	Collision parameter $\neq 0$		
	Case 4	Case 4.1	Case 4.2
Chaser	0.000451	0.000866	0.006331

Each case has an increasing  $\Delta V$  magnitude limit:  $\pm 0.01$ ,  $\pm 0.02$  and  $\pm 0.05$  m/s, respectively. Here, an increase in average  $\Delta V$  norm is noticed: Case 4 < Case 4.1 < Case 4.2, matching the increasing  $\Delta V$  magnitude limits. However, the values presented are not higher than the values presented for the other cases batch in Tables 9.5 and 9.6. In comparison to the other cases, there is no significant increase or decrease when only the chaser spacecraft maneuvers.

This analysis is further supported by looking at specific individuals for each case. Here, an individual close to a Cost parameter of 0.5 is chosen for each case, which allows for comparison in reaching a Collision parameter of 0.16 with different maneuvering limits. The  $\Delta V$  component values are shown in Figure 9.26. This graph also verifies that the target spacecraft did not conduct any maneuvering as the  $\Delta V$  values are zero.

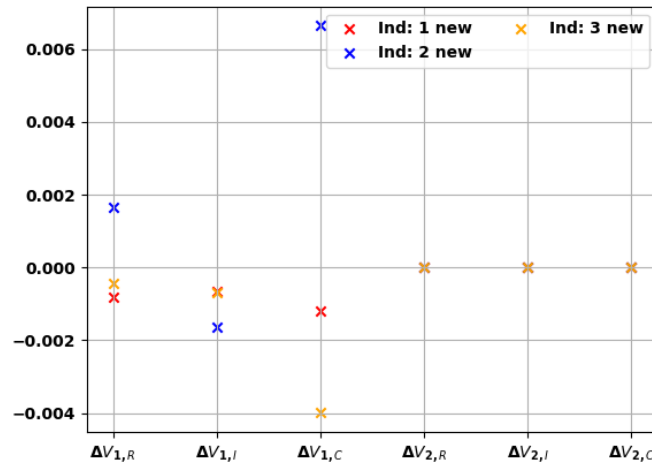


Figure 9.26:  $\Delta V$  component values in [m/s] for relevant individuals in the third cases batch.

Individual 1 comes from Case 4, while individual 2 comes from Case 4.1 and individual 3 from Case 4.2. Despite individual 3 having the larger  $\Delta V$  span, the higher values are observed for individual 2 with a high cross-track component leading to a  $\Delta V$  magnitude of  $70.31 \cdot 10^{-4}$  m/s, in comparison individual 3's magnitude is  $40.69 \cdot 10^{-4}$  m/s.

Furthermore, the component values tend to be larger than the previous  $\Delta V$  values seen in this section (Figures 9.18 and 9.23). They are also larger than the  $\Delta V$  values seen in the sensitivity analysis. Only individual 3 from Case 1.4 shows a cross-track component of -0.005 and a magnitude of  $0.0049.32 \cdot 10^{-4}$  m/s.

This shows that although the  $\Delta V$  range is expanded, the  $\Delta V$  values do not need increase to its limits to reach reasonable Collision parameters accompanied by reasonable Cost parameters. It should also be noted that the range is an order of magnitude higher than the values seen here. In the case of re-doing this analysis, limiting the range should be considered.

Next, the maneuver time can be looked into. Even if the chaser does not show larger maneuvers when acting alone, the ideal moment to conduct the maneuvers might have changed. This can be seen in Figures 9.27 and 9.28 for Case 4 and 4.1, respectively. The maneuver time results are not shown for Case 4.2 as they are akin to the two results displayed.

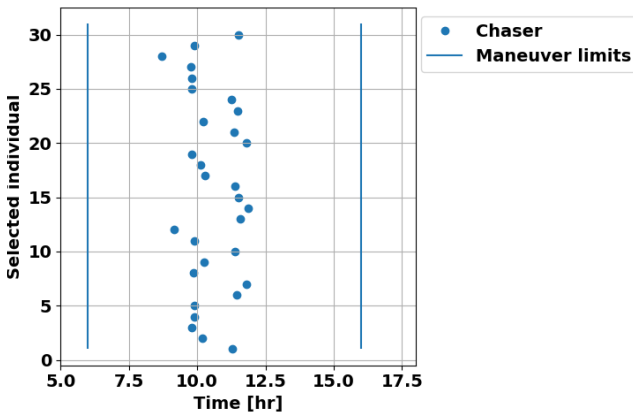


Figure 9.27: Maneuver times for individuals of Case 4.

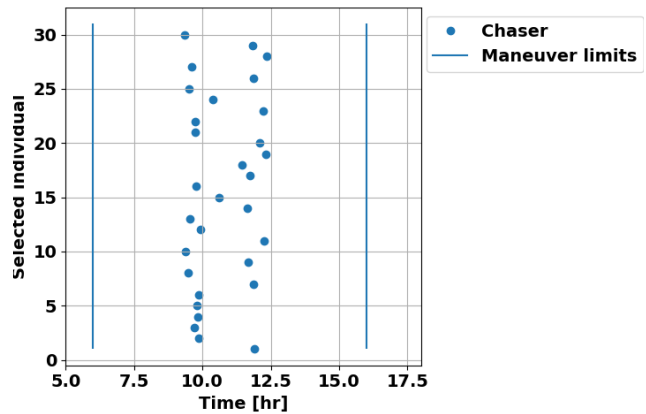


Figure 9.28: Maneuver times for individuals of Case 4.1.

These graphs are limited in information as this batch did not include maneuvering in the target and did not produce individuals with Collision parameter 0. Although less strong, the trend previously identified of maneuver timing around 10 and 12.5 hours is still clear. The ideal maneuvering areas remain around 10 and 12.5 hours. The chaser spacecraft has these two options of maneuver time for the CAM. The third cases batch have the chaser holding all the weight for the propellant mass and mission impact as it is the only maneuverable object in the collision avoidance problem. Although it carries the load, it sticks to similar maneuver times. These must be ideal in terms of minimizing mission impact and minimizing propellant mass usage while still minimizing  $P_c$ .

The last check that is conducted is the position differences to the original "no CAM" orbit. This is shown in Figure 9.29. The interesting individuals are used to investigate the position differences. For these cases, the

orbit disturbance of the target does not matter while the whole weight is given to the chaser's orbit disturbance, yet the target does not maneuver, and the chaser does so which explains the high Cost parameters seen in the Pareto fronts.

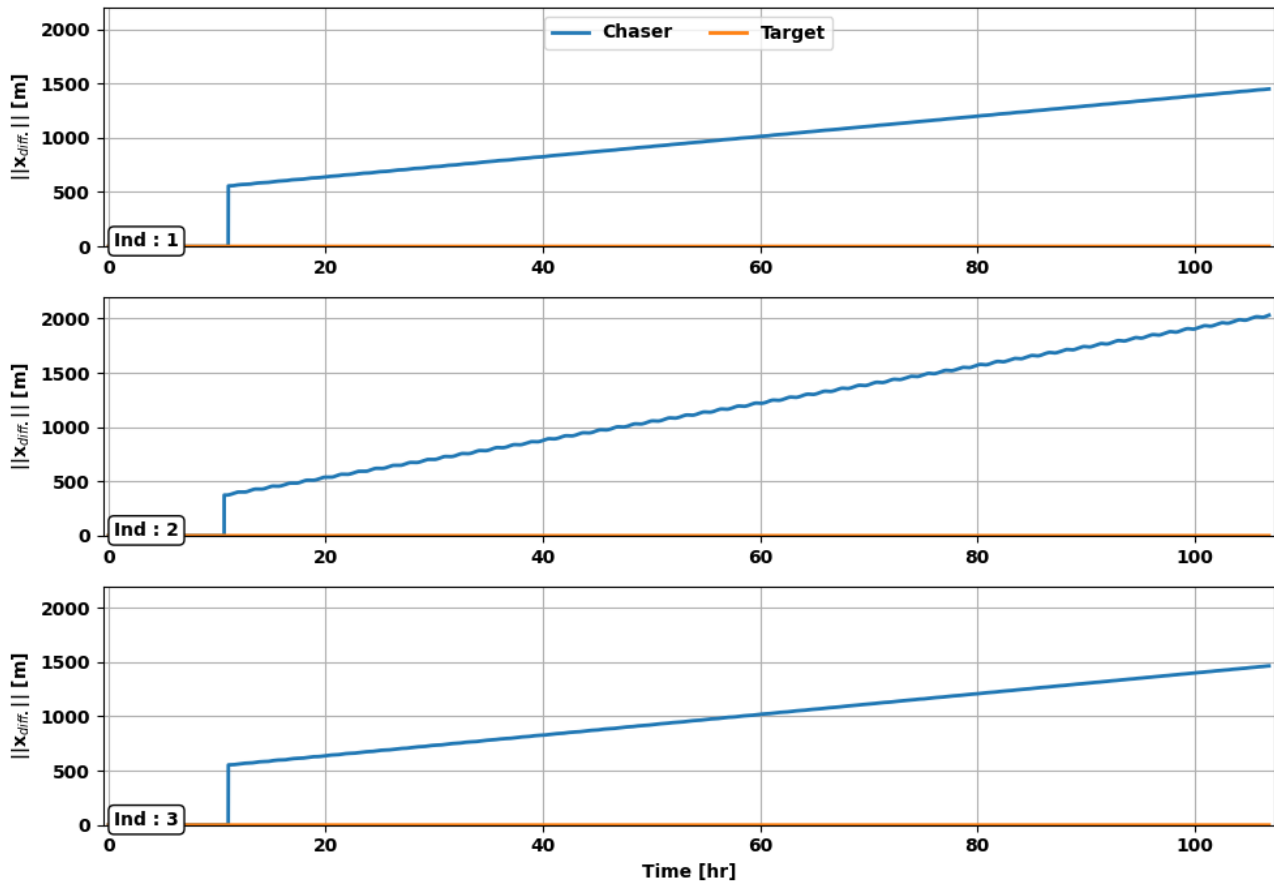


Figure 9.29: Norm of the position differences to the "no CAM" orbit for the relevant individuals in the third cases batch.

As expected, the target shows zero differences, and the chaser does all the job in avoiding the collision. This analysis shows high position differences in comparison to the previous cases. Even if the initial jump is not large, the orbits distances keep increasing and the chaser moves further and further away from its original orbit. In these situations, a second maneuver back to the original orbit after TCA would be considered by the operator if this new orbit is detrimental for the spacecraft's mission purpose.

## 9.3. Discussion

Following the sensitivity analysis and the cases results presentation some insights can be gathered. This section provides a summary of these insights and then combines them with an application of the Middle Man - operator interaction in Subsection 9.3.1.

Several results can be drawn from the sensitivity analysis:

- Both spacecraft in conjunction are seen to maneuver in opposite directions: the chaser spacecraft has negative values of  $\Delta V$  in the radial direction, while the target spacecraft has positive velocity changes in the radial direction. The cross-track contributions of the chaser are higher than those of the target and their in-track changes are similar although the target presents higher values in general.
- Although the maneuver timing variation is critical, when low changes are experienced in  $\Delta V$  values, the high maneuver timing difference does not always lead to penalties. However, the Collision parameter experiences an increase and so higher changes to  $\Delta V$  values would have induced a penalty.
- The opposite is also true: for medium changes to maneuver timing accompanied by high  $\Delta V$  components, penalties can be received.

In short, the operator should analyze to which extent uncertainties will be introduced into the CAM solution provided by the Middle Man. If significant, especially in the maneuver timing, it is best to ask the Middle Man

for a new solution corresponding to that timing. The Middle Man should also realize that the larger the  $\Delta V$  components are, the more sensitive they are. This could lead to prioritizing smaller maneuvers. The final finding from the sensitivity analysis is that if a maneuver time gets changed significantly (over 5 minutes), the Middle Man should be contacted to analyze the conjunction avoidance once again; a new maneuver might need to be selected.

From the cases results, the insights that can be drawn are the following:

- In general, the beneficial maneuver timing is found to be around 10 hours and 12.5 hours from the start of the propagation (TCA - 2 days). These values were consistent over most of the cases, with some preference in Case 2 for maneuvering at around 11 hours. While these ideal timings are accompanied by different maneuver magnitudes, they provide minimized mission impact values. This is true for the scenarios with two active spacecraft and only one active spacecraft.
- To avoid the collision with a low Cost parameter in a scenario similar to that of Case 1, the chaser should carry most of the maneuver efforts with a moderate contribution from the target.
- From the comparison between Cases 1.1 and 1.2, it is found that having a lower propellant mass weight for the target allows for a wider selection of maneuver timing.
- Still in the same scenario, findings from Cases 1.3 and 1.4 indicate that varying the orbit disturbance contributions is more significant than varying the propellant mass. This is interesting as the Cost parameter is made up of 80% Mass parameter and 20% Orbit parameter.
- The second cases batch show smaller changes in the chaser's orbit than in the target's orbit, which is in line with the way the objective weights are defined.
- The difference between Cases 2 and 2.1 is only the  $I_{sp}$  used. Their results did not show any conclusive differences, leading to the statement that  $I_{sp}$  does not drive the optimization results.
- The third cases batch shows that the optimization method allows for a single action to collision avoidance case as well. Low Collision parameters cannot be reached in this scenario, but they are minimized within the thresholds necessary. Adding on, the values for the Cost parameter are also higher in these cases.

### 9.3.1. Link to cooperation process

After analyzing and interpreting the results, the general framework proposed in Section 8.6 can be linked back to. As explained this framework works with a Middle Man proposing maneuvers that meet the operators' requirements and then communicating back to the Middle man whether they agree on a maneuver combination to avoid the conjunction or whether further insight is required and more proposals for maneuvers.

The format under which the optimization results are shown is perfect to allow for such cooperation. The Middle Man would get the input from the conjunction and the requirements from the operators and then run the optimization algorithm. The results would be similar to the Pareto fronts shown in Section 9.2. The Pareto fronts are exactly the range of different combinations that can be taken to avoid the conjunction that should be provided by the Middle Man.

The Pareto fronts could be previously filtered by the Middle Man to meet the operators' requirements, or these could be included as constraints in the optimization process. The Pareto fronts based on the Cost parameter, do not allow for one to backtrack the maneuver results or the orbital impact without knowing the inputs. Hence, the operators and their spacecraft's mission and capabilities would remain anonymous. The Middle Man could then choose a subset of solutions from the Pareto front to propose to the operators. To each operator more detailed information about their respective necessary maneuver and their orbit after the collision avoidance maneuver would be provided, to allow them to make the choice and take the necessary action. This information could be provided in terms of  $\Delta V$  values and orbit differences as shown in Section 9.2.

This system would also work for a single-maneuver plan and for the possibility of operators not agreeing on a combination. More proposals can be sent by the Middle Man either by re-running the optimization with a different decision variable range or by choosing another subset of solutions from the Pareto front. For example, the first subset proposal could have lower Collision parameter values and thus higher Cost parameters, while a second subset would have a compromise in the Collision parameter values.

This approach shows an implementation of the "rule and resource following shared approach". This means that also rules need to be defined beforehand on how operators are supposed to act in different cases. Of course, they need to be agreed upon previously. Here, the cases for which results were generated can be used to

propose some such rules, as they deal with some of the special considerations listed before in Section 8.3.

Case 1 and its variants (1.1, 1.2, 1.3, and 1.4) outline conjunctions with small spacecraft, although they are assumed to be maneuverable. They showed that solutions can be found in such scenarios where both operators are held accountable and cooperate to lower the collision probability. Similar cases could be run with lower or no maneuvering capabilities for the small spacecraft. However, one of the outcomes would be to enforce CubeSats to partake in the collision avoidance process if they have maneuvering capabilities.

Case 2 and Case 2.1 deal with a constellation spacecraft against a normal spacecraft. It assumes that the constellation spacecraft will have more propellant budget for collision avoidance and so it lowers its contribution to the Cost parameter. On the other hand, it also assumes that for constellations the orbits are more important to maintain so that contributed more to the Cost parameter. This is an assumption that could be agreed upon beforehand by the operators. The operator of a constellation would then have an agreement with the Middle Man that when conjunctions appear with their spacecraft, the Middle Man can apply these weights to their spacecraft.

Case 3 is between two maneuverable spacecraft where only one orbit disturbance is important. The example given for such a scenario was that one spacecraft could be de-orbiting and simply passing by that orbit to continue its re-entry procedure. In that case, the Middle Man could have rules in place that dictate that if one spacecraft comes in conjunction with another one during its de-orbiting phase, it should not care about its orbit after the CAM significantly. Nonetheless, the propellant mass is still important as it is important for the spacecraft to remain within budget for the de-orbiting.

The final example is Case 4, which is the equivalent of single-maneuver planning. No rules can be drawn directly from the cooperation for collision avoidance as only one spacecraft will bear the load. The results showed less decrease in collision probability and higher Cost parameter values, indicating that the solutions are less ideal than the dual-maneuver solutions. Per the 'rule and resource following shared approach', each spacecraft operator should contribute to collision avoidance according to their capabilities. For future research, it is recommended to find ways to entice operators of agreeing to this process.





## Conclusions

This thesis deals with the spacecraft collision avoidance processes and attempts a collaboration between operators. The research question first introduced in Chapter 1 and the sub-questions are:

*How should a combined action to optimal collision avoidance be implemented and what negotiation proposals can it lead to?*

1. Does the inclusion of three objectives relating to propellant consumption, collision probability, and orbital disturbance allow for an optimization algorithm to find the best dual maneuver solution?
2. What is the best dual maneuver solution, and what is the sensitivity of the objectives to changes in the control parameters?
3. Can different study cases help understand how systems should interact in space?
4. How do the best dual maneuver solutions translate into negotiation procedures between operators?
5. What are the limitations and challenges for an implementation of such negotiation procedures?

First, a refresher on how this problem is handled within the thesis. The collision avoidance scenario is modeled, and the dual maneuver approach indicates that both objects in the conjunction perform collision avoidance maneuvers. This is not possible in every conjunction scenario as many of them happen with space debris, but the relevant cases are introduced. The algorithm allows optimization of both maneuver magnitudes in three directions, as well as their timing.

The negotiation proposal was re-formulated as a cooperation process between the operators. This thesis does not propose rules or procedures which operators should abide by in the context of STM. What is presented is a proposal for communication flow and cooperation to avoid the conjunction together based on a Middle Man organ. The exact functioning of the Middle Man and its powers remains an open question for future research.

To answer the first sub-question, Chapter 6 is used. The chapter concluded that using three objectives does lead to new dual-maneuver solutions, but it determined that they cannot be directly introduced as a fitness function. When the objectives related to propellant consumption and orbital disturbance, are combined into a single cost objective, the optimization algorithm finds optimum solutions in a dual maneuver approach to collision avoidance. The solutions are based on several assumptions made during the span of the thesis and would require further operator insight to be finalized.

The second question cannot be answered by pinpointing a single solution. As shown by Section 9.1, there is no single best dual maneuver solution, whether there is a range of optimum solutions portrayed by Pareto fronts. The solutions present a wide range of maneuver combinations, any of which, could be used to successfully decrease the collision probability within the constraints defined in this thesis. Concerning the sensitivity of the control parameters, it was found that some were more sensitive than others, especially the maneuver times. Operators that would use this system, are urged to have precise maneuver timings or to select options that have lower  $\Delta V$  contributions as those were identified as being less sensitive.

When maneuver times differ by more than 5 minutes, the operators are urged to contact the Middle Man to access if the maneuver still contributes to the collision avoidance successfully. Though such a difference is not considered an uncertainty in maneuver timing but a maneuver change due to a potential abort or similar phenomena. The sensitivity is more stable for  $\Delta V$  components, but if all components experience high variations the maneuver might not contribute to the collision avoidance process as expected.

However, from the results it can be said the optimal solutions tend to have maneuver timing around 10 and 12.5 hours after the start of propagation which is two days pre-TCA. Additionally, there is a tendency over

the different scenarios for the chaser to contribute more to the collision avoidance than the target in terms of maneuver magnitudes although higher mission impact's are seen for the target. The maneuver magnitudes average vary between a maximum of 0.000451 m/s and 0.007011 m/s. The maximum position difference experienced at the end of propagation is: 2000 m for the chaser spacecraft in Case 4.1 and almost 1200 m for the target spacecraft in Cases 2, 2.1, and 3.

Sub-questions 3 and 4 can be answered together. Chapter 8 presents a study on current STM practices, pitfalls, and improvement points. It also presents interesting scenarios to be accounted for in hopes of understanding the interaction between different systems in space. Chapter 7 defines study cases or so-called simulation scenarios based on these findings. These scenarios were used to generate the optimization results. It was determined that operators can work together to avoid conjunctions, even if their maneuvering capabilities and orbital disturbance requirements are different.

The study cases allowed to determine that the chaser and target spacecraft can work together with the chaser spacecraft contributing in general more to the  $\Delta V$  magnitudes than the target spacecraft. Furthermore, the  $I_{sp}$  was found to not affect the collision avoidance process significantly. It is recommended to vary the  $I_{sp}$  more dramatically to further investigate this.

The more complicated aspect of it is related to real-world constraints, which relate to cyber security, collision avoidance objectivity, real-time coordination, task sharing between private and public sectors, and others. To deal with these, a system that is considered fair, transparent, effective, and automated to a certain degree was created. It is called "rule and resource following shared approach". The rules are not defined in this thesis besides idea gathering. The resource following the shared approach is presented as the collision avoidance optimization. An example of how the collaboration framework presented in Figure 8.4 can be given by using the results from Section 9.2.

- The Middle Man receives information from the operators and the SSA database. They determine whether collision avoidance maneuvers are necessary and if a dual-maneuver approach can be taken.
- If yes, the optimizations are carried out with the pre-defined constraints from the operators. The results are output in Pareto front format and the Middle Man filters them, approves them, and verifies the maneuvers.
- Afterwards, a combination of maneuvers is presented to the operators. The specific details in terms of  $\Delta V$  and orbital disturbance are hidden within the Cost parameter, they are presented to the operators independently.
- In case no maneuver combination is agreed upon by the operators, the process is repeated. The iteration occurs until an agreement is found. This is expected to be the most lengthy part of the cooperation.
- Finally, the agreed-upon maneuvers are conducted and confirmed. The conjunction is avoided!

The cases drawn up in this thesis allow for different scenarios such as the one above to play out. This illustrates how the dual maneuver solutions translate into the cooperation process between operators and successfully answers sub-question 4.

Sub-question 5 has been partly answered with sub-question 4. The challenges for drawing up a cooperation process lie in insuring that it is compatible with the real world-constraints listed above. Additional challenges are introduced when making sure that the system is transparent and automated. To maintain privacy, anonymity, and cyber-security the system cannot be fully transparent. That is why the concept of a Middle Man was introduced. The different operators and governments would be more willing to share private data with a public sector organ that does not present any competition, where even the idea of multiple regional Middle Man could be introduced. However, this would introduce even more interactions, further hindering the ease of automating the process. As shown in this thesis work, automating the CAM proposal is possible, nevertheless automating the communicating and data flow is proposed for future research. Another challenge comes with making sure that operators adhere to this Middle Man concept and go through the complete process of choosing a maneuver and implementing it.

Together the sub-questions answer the research question. This thesis proposes a method that successfully has a combined action to collision avoidance and simultaneously allows for cooperation between the operators. This method is the collision avoidance optimization carried out by the Middle Man with communication flows to the operators.

# Recommendations

In this chapter, recommendations for future work are presented in an itemized fashion. They are derived from the research findings and analysis in the report. These propose measures to address the identified challenges and improve the current state of combined approach to collision avoidance discussed in the thesis.

## 1. Optimization algorithm improvements:

- Within the optimization algorithm constraint setting, a check is included to ensure that no new warnings between the two objects in the conjunction occur within 3 days of the original TCA. This can be expanded further. The check should include all neighboring objects to ensure that no new conjunctions are created by avoiding the original conjunction. The pitfall of this constraint is that inaccessible information about all objects' orbits is necessary.
- Another suggestion within the constraints is to also include the 'Orbits within limits of nominal performance' constraint. At the moment, it is assumed to be partly accounted for in the orbital impact objective. To implement this constraint, the research needs to be linked to real spacecraft that have orbit requirements. This would help determine if a second maneuver to return to the limits of the original orbit is required.
- The backward maneuver was mentioned at different points in the research, yet it was not included. For future research, it is recommended to explore this second maneuver as well. The threshold for it could be orbital limits or large orbital impacts. When including this backward maneuver in the optimization, it is not expected that all individuals in the Pareto front would require such an action. If the backward maneuver is necessary, then its propellant mass usage should be included in the Cost parameter and thus the optimization results should be updated. The backward maneuver itself could also go through an optimization process to find its optimum  $\Delta V$  values and maneuver timing.
- In the combined objective optimization, the Cost parameter has two contributions: the Mass parameter and the Orbit parameter. Their respective weights are 80% and 20%. In future research, different combinations should be explored as they affect the results of the optimization and so the operator's options. A step further would be to implement a flexible combined objective that could be determined by the operator's needs.
- For future research, it is recommended to restrain the decision variable range. Bigger margins were set in accordance to literature but it proved to not be necessary in the scenarios examined. It is recommended that a study on the decision variable range be conducted before the optimization.
- Finally, the objects were propagated for only 2 days pre-TCA, with the constraints implemented on maneuver timing, the maneuvering time range was limited. It is recommended to increase the propagation time around TCA to allow for more maneuver options. Here a last minute scenario was demonstrated, for normal operations, longer maneuver planning ranges should be the standard.

## 2. Study cases amplifications:

- At the start of the thesis, it was decided to focus the efforts of this research to the LEO environment. For the Middle Man proposal to work in an all-encompassing way, it needs to be able to deal with other orbital regimes as well. Thus, it is recommended to extend this research towards GEO at a first stage<sup>a</sup>. GEO spacecraft move with respect to each other with low relative velocities and so correspond to long-term encounter predictions. The GEO orbit is important for communication purposes and should be protected from a longitudinal and frequency slot perspective. Therefore, conjunctions

<sup>a</sup>MEO environments are not a priority as they are scarcely populated.

in this orbit need to be monitored to avoid collisions. By investigating this case, interaction between GEO spacecraft and their respective operators can be looked into in more detail. This will allow for insight on how the GEO spacecraft should maneuver to avoid each other, but also stay within their station keeping box.

- Within the simulation cases chosen, the normal spacecraft versus space debris scenario was considered. The space debris was chosen to be a rocket body to check the extent of a one-sided  $\Delta V$  avoidance. Other space debris cases should also be considered, for example small fragments. This would allow to determine how small the maneuver needs to be, and if early tracking would be more beneficial for the system to avoid it early on, underlining the importance of current efforts to increase tracking capacity of space objects.
- Only high-thrust scenarios were considered in this work. With the advances in the space industry and the tendency to use high-thrust, also for CubeSats, it is recommended to re-do this analysis with electric thrust modeling for the CAMs.

### 3. Cooperation process further research:

- With respect to the cooperation process, it is recommended that future research investigate ways to entice operators to agree to taking part in the process. This could for instance, through widespread analysis of the state of their constellation if dual-maneuvering is not implemented - mostly useful for LEO. The Middle Man scenario only works if both operators in the conjunction are in agreement with the process. To ensure the efforts of building a Middle Man are worthwhile, this process should be widely accepted. To investigate the constraints around the Middle Man formulation, more research is necessary on the adoption of guidelines within the space industry.
- Another recommendation is to propose ideas that allow for a quick combined maneuver agreement, for example, an automatic answering process through an online interface. The decision to avoid conjunction is time-critical. In some cases, CDMs are received only three days in advance. The Middle Man needs to propose maneuvers and the operators need to agree within a certain period to allow the collision avoidance maneuvers to be conducted and verify the avoidance of the collision.
- The three criteria established for comparing current practices are "automated, external communication, and databases". The system proposed should excel in all three. However, the focus of this thesis is on the external communication and usage of databases. Although ideas for automation and quick analysis are provided, it is recommended that more research be done in that domain; proposing methods to automate the dual-maneuver optimization process conducted by the Middle Man and the review and selection of proposed maneuvers by the operators.
- The Middle Man concept is proposed as a public organ that ensures data privacy for the operators. To allow for better acceptability by the space industry an idea for its introduction would be to generate a system akin to the Space Data Association. Several operators willingly contribute ephemeris files to the association. It is recommended to investigate whether there is a possibility to extend the association to take in the Middle Man concept.

# Bibliography

- [1] ESA. *Predicted near miss between Aeolus and Starlink 44*. [https://www.esa.int/ESA\\_Multimedia/Images/2019/09/Predicted\\_near\\_miss\\_between\\_Aeolus\\_and\\_Starlink\\_44](https://www.esa.int/ESA_Multimedia/Images/2019/09/Predicted_near_miss_between_Aeolus_and_Starlink_44) [Accessed on: 19/06/2023]. Sept. 2019.
- [2] United Nations, Office for Outer Space Affairs. *Long-term sustainability of outer space activities*. <https://www.unoosa.org/oosa/en/ourwork/topics/long-term-sustainability-of-outer-space-activities.html> [Accessed on: 14/04/2021]. 2019.
- [3] Brian Weeden. *2009 Iridium-Cosmos collision fact sheet*. [https://swfound.org/media/6575/swf\\_iridium\\_cosmos\\_collision\\_fact\\_sheet\\_updated\\_2012.pdf](https://swfound.org/media/6575/swf_iridium_cosmos_collision_fact_sheet_updated_2012.pdf) [Accessed on: 02/09/2021]. Nov. 2010.
- [4] Jeff Foust. "ESA spacecraft dodges potential collision with Starlink satellite". In: *SpaceNews* (Sept. 2019). URL: <https://spacenews.com/esa-spacecraft-dodges-potential-collision-with-starlink-satellite/> (visited on 06/29/2023).
- [5] ESA Space Debris Office. *ESA's annual space environment report*. LOG Issue/Revision 7.0. Darmstadt, Germany: ESA ESOC, June 2023.
- [6] Statement from Chairwoman Jessica Rosenworcel and Commissioners Starks and Simington. *Space Innovation IB Docket No. 22-271 Mitigation of Orbital Debris in the New Space AGE IB Docket No. 18-313*. Tech. rep. FCC 22-74. Washington, D.C.: Federal Communications Commission, Sept. 2022. URL: <https://docs.fcc.gov/public/attachments/FCC-22-74A1.pdf>.
- [7] Jakub Drmola and Tomas Hubik. "Kessler Syndrome: System Dynamics Model". In: *Space Policy* 44-45 (2018), pp. 29–39. ISSN: 0265-9646. DOI: <https://doi.org/10.1016/j.spacepol.2018.03.003>. URL: <https://www.sciencedirect.com/science/article/pii/S0265964617300966>.
- [8] Mark A Sturza and G Saura Carretero. "Mega-Constellations—A Holistic Approach to Debris Aspects". In: *8<sup>th</sup> European Conference on Space Debris*. Ed. by T. Flohrer, F. Schmitz, and S. Lemmens. ESA. Darmstadt, Germany: ESA Space Debris Office, Apr. 2021, pp. 20–23.
- [9] Sebastien Morante, Tomas Hrozensky, and Marek Dvoracek. "ESPI Report 71-Towards a European Approach to Space Traffic Management-Full Report". In: (Jan. 2020). ISSN: 2076-6688 (online). URL: [www.espi.or.at](http://www.espi.or.at).
- [10] Carmen Pardini and Luciano Anselmo. "Evaluating the impact of space activities in low earth orbit". In: *Acta Astronautica* 184 (July 2021), pp. 11–22. ISSN: 00945765. DOI: 10.1016/j.actaastro.2021.03.030.
- [11] Theodore J. Muelhaupt et al. "Space traffic management in the new space era". In: *Journal of Space Safety Engineering* 6 (2 June 2019), pp. 80–87. ISSN: 24688967. DOI: 10.1016/j.jsse.2019.05.007.
- [12] European Union Agency for the Space Programme. *The new Iriss Constellation will be beneficial to EU citizens in several ways, find out 5 of them!* <https://www.euspa.europa.eu/newsroom/news/new-iriss-constellation-will-be-beneficial-eu-citizens-several-ways-find-out-5-them> [Accessed on: 11/04/2023]. Nov. 2022.
- [13] Inter-Agency Space Debris Coordination Committee and others. "IADC statement on large constellations of satellites in low earth orbit". In: *IADC-15-03* (Sept. 2017). Downloadable from IADC website: <https://www.iadc-home.org/>.
- [14] Juan Luis Gonzalo, Camilla Colombo, and Pierluigi Di Lizia. "Analytical Framework for Space Debris Collision Avoidance Maneuver Design". In: *Journal of Guidance, Control, and Dynamics* (2021). DOI: 10.2514/1.G005398. URL: <https://doi.org/10.2514/1.G005398>.
- [15] Michael Kan. "SpaceX: There was no near-collision between Starlink and OneWeb satellites". In: *PCMag* (Apr. 2021). URL: <https://spacenews.com/esa-spacecraft-dodges-potential-collision-with-starlink-satellite/> (visited on 07/13/2021).

- [16] Bhavya Lal et al. "Global trends in space situational awareness (SSA) and space traffic management (STM)". In: *IDA Science & Technology Policy Institute*, Available online at <https://www.ida.org/idamedia/Corporate/Files/Publications/STPIPubs/2018/D-9074.pdf> (2018).
- [17] Christophe Bonnal et al. "CNES technical considerations on space traffic management". In: *Acta Astronautica* 167 (2020), pp. 296–301. ISSN: 0094-5765. DOI: 10.1016/j.actaastro.2019.11.023. URL: <https://www.sciencedirect.com/science/article/pii/S0094576519314183>.
- [18] Sreeja Nag et al. "System Autonomy for Space Traffic Management". In: *2018 IEEE/AIAA 37<sup>th</sup> Digital Avionics Systems Conference (DASC)*. London, United Kingdom: Institute of Electrical and Electronics Engineers (IEEE), Sept. 2018, pp. 1–10. DOI: 10.1109/DASC.2018.8569343.
- [19] Karel F Wakker. *Fundamentals of Astrodynamics*. Delft, The Netherlands: Institutional Repository, Library Delft University of Technology, 2015. ISBN: 978-94-6168-419-2. URL: <http://resolver.tudelft.nl/uuid:3fc91471-8e47-4215-af43-718740e6694e>.
- [20] M. Navabi and R. Hamrah. "Close approach analysis of space objects and estimation of satellite-debris collision probability". In: *Aircraft Engineering and Aerospace Technology: An International Journal* 87.5 (Sept. 2015).
- [21] Gabriel Popescu. "Pixel geolocation algorithm for satellite scanner data". In: *International Conference of USAMVB "Agriculture for Life, Life for Agriculture"*. Bucharest, Romania: Scientific Papers Series E, Land Reclamation, Earth Observation & Surveying, Environmental Engineering, June 2014, pp. 127–136.
- [22] *Conjunction Data Message*. Recommended Practices for Space Data System Standards (Pink Book) Issue 1. Washington, D.C.: CCSDS: CCSDS 508.0-P-1.0.1, Dec. 2020.
- [23] Heiner Klinkrad. *Space debris: models and risk analysis*. Berlin, Germany: Springer Science & Business Media, 2006. ISBN: 978-3-540-25448-5. DOI: <https://doi.org/10.1007/3-540-37674-7>.
- [24] Lei Chen et al. "Calculation of Collision Probability". In: *Orbital Data Applications for Space Objects: Conjunction Assessment and Situation Analysis*. Singapore: Springer Singapore, 2017, pp. 135–183. ISBN: 978-981-10-2963-9. DOI: 10.1007/978-981-10-2963-9\_5.
- [25] Noelia Sánchez-Ortiz, Miguel Belló-Mora, and Heiner Klinkrad. "Collision avoidance manoeuvres during spacecraft mission lifetime: Risk reduction and required  $\delta v$ ". In: *Advances in Space Research* 38.9 (2006), pp. 2107–2116.
- [26] Jae-Dong Seong and Hae-Dong Kim. "Optimization of collision avoidance maneuver planning for cluster satellites in space debris explosion situation". In: *Proceedings of the Institution of Mechanical Engineers, Part G: Journal of Aerospace Engineering* 232.3 (2018), pp. 407–422. DOI: 10.1177/0954410016682270.
- [27] Mahesh Kumar, Perumal Nallagownden, and Irraivan Elamvazuthi. "Advanced Pareto Front Non-Dominated Sorting Multi-Objective Particle Swarm Optimization for Optimal Placement and Sizing of Distributed Generation". In: *Energies* 9 (Nov. 2016), p. 982. DOI: 10.3390/en9120982.
- [28] Jae-Dong Seong and Hae-Dong Kim. "Collision avoidance maneuvers for multiple threatening objects using heuristic algorithms". In: *Proceedings of the Institution of Mechanical Engineers, Part G: Journal of Aerospace Engineering* 229.2 (2014), pp. 256–268. DOI: 10.1177/0954410014530678.
- [29] Eun-Hyuek Kim, Hae-Dong Kim, and Hak-Jung Kim. "A Study on the Collision Avoidance Maneuver Optimization with Multiple Space Debris". In: *Journal of Astronomy and Space Sciences* 29.1 (Mar. 2012), pp. 11–21. DOI: 10.5140/JASS.2012.29.1.011.
- [30] Sang-Cherl Lee, Hae-Dong Kim, and Jinyoung Suk. "Collision avoidance maneuver planning using GA for LEO and GEO satellite maintained in keeping area". In: *International Journal of Aeronautical and Space Sciences* 13.4 (2012), pp. 474–483. DOI: 10.5139/IJASS.2012.13.4.474.
- [31] Jasper Wolfhagen. "Collision avoidance in the new space era". MA thesis. Delft, The Netherlands: Delft University of Technology, 2020.
- [32] Esmat Rashedi, Hossein Nezamabadi-pour, and Saeid Saryazdi. "GSA: A Gravitational Search Algorithm". In: *Information Sciences* 179.13 (2009). Special Section on High Order Fuzzy Sets, pp. 2232–2248. ISSN: 0020-0255. DOI: <https://doi.org/10.1016/j.ins.2009.03.004>. URL: <https://www.sciencedirect.com/science/article/pii/S0020025509001200>.

- [33] Xiaodong Li. "A Non-dominated Sorting Particle Swarm Optimizer for Multiobjective Optimization". In: *Genetic and Evolutionary Computation — GECCO 2003*. Ed. by Erick Cantú-Paz et al. Berlin, Heidelberg: Springer Berlin Heidelberg, 2003, pp. 37–48. ISBN: 978-3-540-45105-1.
- [34] Tudat Space. *Getting started with Tudat(Py)*. [https://tudat-space.readthedocs.io/en/latest/\\_src\\_first\\_steps/tudat\\_py.html](https://tudat-space.readthedocs.io/en/latest/_src_first_steps/tudat_py.html) [Accessed on: 16/06/2021].
- [35] Francesco Biscani and Dario Izzo. "A parallel global multiobjective framework for optimization: pagmo". In: *Journal of Open Source Software* 5.53 (2020), p. 2338. DOI: 10.21105/joss.02338. URL: <https://doi.org/10.21105/joss.02338>.
- [36] Stefano Speretta. *Delfi Program CDM files*. Private correspondance. Assistant Professor in the Department of Space Engineering at Delft University of Technology. Feb. 2022.
- [37] Emma Kerr and Noelia Sanchez. "State of the Art and Future Needs in Conjunction Analysis Methods, Processes and Software". In: *8<sup>th</sup> European Conference on Space Debris*. Ed. by T. Flohere, S. Lemmens, and F. Schmitz. ESA. Darmstadt, Germany: ESA Space Debris Office, Apr. 2021.
- [38] Gigi Laan. "Supporting Space Traffic Management". MA thesis. Delft, The Netherlands: Delft University of Technology, 2021.
- [39] Giacomo Acciarini. "Optimizing a Solar Sailing Polar Mission to the Sun". MA thesis. Delft, The Netherlands: Delft University of Technology, 2019.
- [40] Peter Pacheco. *An introduction to parallel programming*. Elsevier, 2011. ISBN: 978-0-12-374260-5. DOI: <https://doi.org/10.1016/C2009-0-18471-4>.
- [41] Delft High Performance Computing Centre (DHPC). *DelftBlue Supercomputer (Phase 1)*. <https://www.tudelft.nl/dhpc/ark:/44463/DelftBluePhase1>. 2022.
- [42] Kerianne Hobbs, Alexander R. Collins, and Eric Feron. "Towards a taxonomy for automatic and autonomous cooperative spacecraft maneuvering in a space traffic management framework". In: *ASCEND 2020*. 2020, p. 4240.
- [43] Stijn Lemmens and Francesca Letizia. "Space traffic management through environment capacity". In: *Schrogl KU. (eds) Handbook of Space Security* (2020), pp. 845–864. DOI: [https://doi.org/10.1007/978-3-030-22786-9\\_109-1](https://doi.org/10.1007/978-3-030-22786-9_109-1).
- [44] Joint Force Space Component Command Public Affairs. *Combined Space Operations Center established at Vandenberg AFB*. <https://www.afspc.af.mil/News/Article-Display/Article/1579285/combined-space-operations-center-established-at-vandenberg-afb/> [Accessed on: 18/10/2021]. July 2018.
- [45] Barry Schiff et al. "Attaining situational understanding in the space domain". In: *18<sup>th</sup> AMOS Advanced Maui Optical and Space Surveillance Technologies Conference*. Ed. by S. Ryan. Maui, Hawaii: Maui Economic Development Board, Sept. 2017, p. 47.
- [46] Juan Luis Gonzalo and Camilla Colombo. "On-Board Collision Avoidance Applications Based On Machine Learning And Analytical Methods". In: *8<sup>th</sup> European Conference on Space Debris*. Ed. by T. Flohere, S. Lemmens, and F. Schmitz. ESA. Darmstadt, Germany: ESA Space Debris Office, Apr. 2021, pp. 21–23.
- [47] Jonathan McDowell. *Starlink Launch Statistics*. <https://planet4589.org/space/con/star/stats.html> [Accessed on: 03/07/2023]. July 2023.
- [48] Martin Michel and Reinhold Bertrand. "Assessment of inter-operator rule-based collision avoidance operations". In: *8<sup>th</sup> European Conference on Space Debris*. Ed. by T. Flohere, S. Lemmens, and F. Schmitz. ESA. Darmstadt, Germany: ESA Space Debris Office, Apr. 2021.
- [49] K. Merz et al. "Current collision avoidance service by ESA's space debris office". In: *7<sup>th</sup> European Conference on Space Debris*. Ed. by T. Flohrer and F. Schmitz. ESA. Darmstadt, Germany: ESA Space Debris Office, Apr. 2017, pp. 18–21.
- [50] Monique Moury and Lauri Newman. "Middle man concept for in-orbit collision risk mitigation: CAESAR and CARA examples". In: *SpaceOps 2014 Conference*. AIAA. Pasadena, CA: ARC, May 2014, p. 1637.
- [51] François Laporte and Eloy Sasot. "Operational management of collision risks for LEO satellites at CNES". In: *SpaceOps 2008 Conference*. ESA and EUMETSAT in association with AIAA. Heidelberg, Germany: ARC, May 2008, p. 3409.

- [52] François LaPorte, Stéphane Christy, and Monique Moury. "Collaborative work environment for operational conjunction assessment". In: *Advanced Maui Optical and Space Surveillance Technologies Conference*. Maui Economic Development Boars, Inc. Maui, Hawaiï, Sept. 2015, p. 49.
- [53] Mark A. Skinner. "Small Satellites and Their Challenges to Space Situational Awareness (SSA) and Space Traffic Management (STM)". In: *Handbook of Small Satellites: Technology, Design, Manufacture, Applications, Economics and Regulation* (2020). Ed. by Joseph N. Pelton and Scott Madry, pp. 1–14. DOI: 10.1007/978-3-030-20707-6\_75-1.
- [54] James S. Cooney. *International Space Station (ISS) Orbital Debris Collision Avoidance Process*. Tech. rep. Greenbelt, MD: Stinger Ghaffarian Technologies, Oct. 2016.
- [55] Samuel Hilton et al. "Space traffic management: Towards safe and unsegregated space transport operations". In: *Progress in Aerospace Sciences* 105 (2019), pp. 98–125. ISSN: 0376-0421. DOI: 10.1016/j.paerosci.2018.10.006. URL: <https://www.sciencedirect.com/science/article/pii/S0376042118301660>.





## Appendix: CDM example

Below a CDM example from the files provided by the Delfi team is presented (file number 86). CDMs are use as inputs to the optimization problem tackled in this thesis. A total of 278 files were made available to the author, only one is presented here due to confidentiality reasons. The others cannot be made available even upon request.

CCSDS_CDM_VERS	=1.0
COMMENT	=CDM_ID:88854536
COMMENT MEETS EMERGENCY CRITERIA	
CREATION_DATE	=2021-04-26T22:11:37.000000
ORIGINATOR	=JSPOC
MESSAGE_FOR	=DELFI-N3XT
MESSAGE_ID	=000039428_conj_000037794_2021119205104_ 1162216301106
TCA	=2021-04-29T20:51:04.486000
MISS_DISTANCE	=773 [m]
RELATIVE_SPEED	=11527 [m/s]
RELATIVE_POSITION_R	=-17.9 [m]
RELATIVE_POSITION_T	=494.6 [m]
RELATIVE_POSITION_N	=-594.3 [m]
RELATIVE_VELOCITY_R	=-98.3 [m/s]
RELATIVE_VELOCITY_T	=-8859.6 [m/s]
RELATIVE_VELOCITY_N	=-7373.8 [m/s]
COLLISION_PROBABILITY	=0.0004240516
COLLISION_PROBABILITY_METHOD	=FOSTER-1992
COMMENT Screening Option = Covariance	
COMMENT Screened with = inertial state vector.	
OBJECT	=OBJECT1
OBJECT_DESIGNATOR	=39428
CATALOG_NAME	=SATCAT
OBJECT_NAME	=DELFI-N3XT
INTERNATIONAL_DESIGNATOR	=2013-066N
OBJECT_TYPE	=PAYLOAD
OPERATOR_CONTACT_POSITION	=https://www.space-track.org/expandedspacedata/ query/class/organization/object/ ~~39428/orderby/ORG_NAME,INFO_ID/format/ html/emptyresult/show/
OPERATOR_ORGANIZATION	=DelfiSpace
OPERATOR_PHONE	=https://www.space-track.org/expandedspacedata/ query/class/organization/object/ ~~39428/orderby/ORG_NAME,INFO_ID/format/ html/emptyresult/show/
OPERATOR_EMAIL	=https://www.space-track.org/expandedspacedata/ query/class/organization/object/ ~~39428/orderby/ORG_NAME,INFO_ID/format/



CTDOT_RDOT	=-0.000928574494127874	[m**2/s**2]
CTDOT_TDOT	=0.00005491361537859428	[m**2/s**2]
CNDOT_R	=0.006091461083163523	[m**2/s]
CNDOT_T	=-0.2598513998748706	[m**2/s]
CNDOT_N	=0.009275380959400312	[m**2/s]
CNDOT_RDOT	=0.0002809353898516049	[m**2/s**2]
CNDOT_TDOT	=-0.000009112507157911165	[m**2/s**2]
CNDOT_NDOT	=0.00002818949916217513	[m**2/s**2]
CDRG_R	=0	[m**3/kg]
CDRG_T	=0	[m**3/kg]
CDRG_N	=0	[m**3/kg]
CDRG_RDOT	=0	[m**3/(kg*s)]
CDRG_TDOT	=0	[m**3/(kg*s)]
CDRG_NDOT	=0	[m**3/(kg*s)]
CDRG_DRG	=0	[m**4/kg**2]
CSRP_R	=0	[m**3/kg]
CSRP_T	=0	[m**3/kg]
CSRP_N	=0	[m**3/kg]
CSRP_RDOT	=0	[m**3/(kg*s)]
CSRP_TDOT	=0	[m**3/(kg*s)]
CSRP_NDOT	=0	[m**3/(kg*s)]
CSRP_DRG	=0	[m**4/kg**2]
CSRP_SRP	=0	[m**4/kg**2]
COMMENT Screened with = inertial state vector.		
OBJECT	=OBJECT2	
OBJECT_DESIGNATOR	=37794	
CATALOG_NAME	=SATCAT	
OBJECT_NAME	=SICH 2	
INTERNATIONAL_DESIGNATOR	=2011-044G	
OBJECT_TYPE	=PAYLOAD	
OPERATOR_CONTACT_POSITION	=https://www.space-track.org/expandedspacedata/ query/class/organization/object/ ~~37794/orderby/ORG_NAME,INFO_ID/format/ html/emptyresult/show/	
OPERATOR_ORGANIZATION	=CIS, State Space Agency of Ukraine	
OPERATOR_PHONE	=https://www.space-track.org/expandedspacedata/ query/class/organization/object/ ~~37794/orderby/ORG_NAME,INFO_ID/format/ html/emptyresult/show/	
OPERATOR_EMAIL	=https://www.space-track.org/expandedspacedata/ query/class/organization/object/ ~~37794/orderby/ORG_NAME,INFO_ID/format/ html/emptyresult/show/	
EPHEMERIS_NAME	=NONE	
COVARIANCE_METHOD	=CALCULATED	
MANEUVERABLE	=N/A	
REF_FRAME	=ITRF	
GRAVITY_MODEL	=EGM-96: 36D 36O	
ATMOSPHERIC_MODEL	=JBH09	
N_BODY_PERTURBATIONS	=MOON,SUN	
SOLAR_RAD_PRESSURE	=YES	
EARTH_TIDES	=YES	
INTRACK_THRUST	=NO	
COMMENT Covariance Scale Factor = 1.000000		
COMMENT Exclusion Volume Radius = 5.000000 [m]		

TIME_LASTOB_START	=2021-04-25T22:11:37.283000	
TIME_LASTOB_END	=2021-04-26T22:11:37.283000	
RECOMMENDED_OD_SPAN	=6.48	[d]
ACTUAL_OD_SPAN	=6.48	[d]
OBS_AVAILABLE	=266	
OBS_USED	=264	
RESIDUALS_ACCEPTED	=98.9	[%]
WEIGHTED_RMS	=1.176	
COMMENT Apogee Altitude = 712	[km]	
COMMENT Perigee Altitude = 675	[km]	
COMMENT Inclination = 97.9	[deg]	
AREA_PC	=0.91	[m**2]
CD_AREA_OVER_MASS	=0.025852976797	[m**2/kg]
CR_AREA_OVER_MASS	=0.009198002442	[m**2/kg]
THRUST_ACCELERATION	=0	[m/s**2]
SEDR	=0.0000436155	[W/kg]
X	=1173.08363	[km]
Y	=949.195569	[km]
Z	=-6906.827792	[km]
X_DOT	=7.463536852	[km/s]
Y_DOT	=-0.314300234	[km/s]
Z_DOT	=1.233729158	[km/s]
COMMENT DCP Density Forecast Uncertainty = 2.450655520000000E-01		
COMMENT DCP Sensitivity Vector RTN Pos = -3.847933768272989E+00		
	6.023192873179089E+02	
	2.682900068864980E-02	[m]
COMMENT DCP Sensitivity Vector RTN Vel = -6.387343735001713E-01		
	2.064364626667960E-03	
	-3.813059942114456E-04	[m/sec]
CR_R	=26.56436883722938	[m**2]
CT_R	=-154.69699470357	[m**2]
CT_T	=24630.69140708176	[m**2]
CN_R	=7.140721176114232	[m**2]
CN_T	=20.92239899373807	[m**2]
CN_N	=12.81655962972045	[m**2]
CRDOT_R	=0.1439917707901812	[m**2/s]
CRDOT_T	=-26.02404517827065	[m**2/s]
CRDOT_N	=-0.02431968838611736	[m**2/s]
CRDOT_RDOT	=0.0275367473924755	[m**2/s**2]
CTDOT_R	=-0.02776716610050895	[m**2/s]
CTDOT_T	=0.08511788211342004	[m**2/s]
CTDOT_N	=-0.007626791577666917	[m**2/s]
CTDOT_RDOT	=-0.00006897513333835533	[m**2/s**2]
CTDOT_TDOT	=0.0000292769075201829	[m**2/s**2]
CNDOT_R	=0.003356570109109001	[m**2/s]
CNDOT_T	=0.006978324779539341	[m**2/s]
CNDOT_N	=0.008467298245050516	[m**2/s]
CNDOT_RDOT	=-0.000003029463235467328	[m**2/s**2]
CNDOT_TDOT	=-0.000003529871674213083	[m**2/s**2]
CNDOT_NDOT	=0.00001731295506179686	[m**2/s**2]
CDRG_R	=0	[m**3/kg]
CDRG_T	=0	[m**3/kg]
CDRG_N	=0	[m**3/kg]
CDRG_RDOT	=0	[m**3/(kg*s)]
CDRG_TDOT	=0	[m**3/(kg*s)]

---

CDRG_NDOT	=0	$[m^{**3}/(kg*s)]$
CDRG_DRG	=0	$[m^{**4}/kg^{**2}]$
CSRP_R	=0	$[m^{**3}/kg]$
CSRP_T	=0	$[m^{**3}/kg]$
CSRP_N	=0	$[m^{**3}/kg]$
CSRP_RDOT	=0	$[m^{**3}/(kg*s)]$
CSRP_TDOT	=0	$[m^{**3}/(kg*s)]$
CSRP_NDOT	=0	$[m^{**3}/(kg*s)]$
CSRP_DRG	=0	$[m^{**4}/kg^{**2}]$
CSRP_SRP	=0	$[m^{**4}/kg^{**2}]$



## Methodology extra information

This appendix presents additional information to the methodology given in the main body (Chapter 4). First, all the verification and validation values from the probability of collision calculation are given in Section B.1. Section B.2

### B.1. Collision probability verification and validation

In this section the complete collision probability verification and validation is presented. First the comparisons in miss distance and relative speed is checked and presented in Table B.1. Then, the comparisons in the collision probability values are presented in Table B.2. These values verify and validate the method used to calculate the collision probability.

**Table B.1: Miss distance (values in [m]) and relative speed (values in [m/s]) comparison between CDM data and calculations.**

CDM	$D_{miss,CDM}$	$D_{miss,code}$	Diff:	$\epsilon_{rel}$	$V_{rel,CDM}$	$V_{rel,code}$	Diff:	$\epsilon_{rel}$
2	370.00	370.19	0.19	0.05%	5748.00	5748.56	0.56	0.01%
4	287.00	287.42	0.42	0.15%	14296.00	14296.24	0.24	0.00%
5	211.00	211.55	0.55	0.26%	14296.00	14296.24	0.24	0.00%
25	657.00	657.17	0.17	0.03%	14497.00	14497.36	0.36	0.00%
26	863.00	863.56	0.56	0.06%	14150.00	14150.18	0.18	0.00%
27	657.00	657.17	0.172	0.03%	14497.00	14497.36	0.36	0.00%
48	89.00	89.79	0.79	0.89%	12380.00	12380.77	0.77	0.01%
50	54.00	54.75	0.75	1.39%	12380.00	12380.77	0.77	0.01%
51	485.00	485.93	0.93	0.19%	12380.00	12380.69	0.69	0.01%
53	453.00	453.98	0.984	0.22%	14959.00	14959.13	0.13	0.00%
54	832.00	832.72	0.72	0.09%	9649.00	9649.49	0.49	0.01%
55	852.00	852.41	0.41	0.05%	9649.00	9649.50	0.50	0.01%
56	814.00	814.11	0.11	0.01%	9649.00	9649.48	0.48	0.00%
63	165.00	165.63	0.63	0.38%	11583.00	11583.34	0.34	0.00%
64	698.00	698.11	0.11	0.02%	13107.00	13107.85	0.85	0.01%
66	364.00	364.07	0.07	0.02%	7662.00	7662.10	0.10	0.00%
69	879.00	879.28	0.28	0.03%	11632.00	11632.71	0.71	0.01%
86	773.00	773.40	0.40	0.05%	11527.00	11527.12	0.12	0.00%
98	449.00	449.23	0.23	0.05%	10149.00	10149.27	0.27	0.00%
100	211.00	211.59	0.59	0.28%	10149.00	10149.27	0.27	0.00%
108	678.00	678.90	0.90	0.13%	14420.00	14420.37	0.37	0.00%
120	204.00	204.64	0.64	0.32%	14304.00	14304.63	0.63	0.00%
121	487.00	487.66	0.66	0.14%	6632.00	6632.02	0.02	0.00%

Table B.1: continued from previous page

CDM	$D_{miss,CDM}$	$D_{miss,code}$	Diff:	$\epsilon_{rel}$	$V_{rel,CDM}$	$V_{rel,code}$	Diff:	$\epsilon_{rel}$
122	183.00	183.29	0.29	0.16%	6632.00	6632.00	0.00	0.00%
124	195.00	195.69	0.69	0.36%	6631.00	6632.00	1.00	0.02%
127	80.00	80.12	0.125	0.16%	6378.00	6378.01	0.01	0.00%
142	969.00	969.08	0.08	0.01%	14349.00	14349.23	0.23	0.00%
144	134.00	134.42	0.42	0.32%	15032.00	15032.27	0.27	0.00%
146	134.00	134.22	0.22	0.17%	14349.00	14349.22	0.22	0.00%
150	33.00	33.63	0.63	1.91%	14349.00	14349.22	0.22	0.00%
157	640.00	640.65	0.652	0.10%	12703.00	12703.58	0.58	0.00%
158	358.00	358.41	0.41	0.11%	13255.00	13255.27	0.27	0.00%
160	801.00	801.00	0.00	0.00%	11111.00	11111.60	0.60	0.01%
169	755.00	755.75	0.75	0.10%	3819.00	3819.95	0.95	0.02%
171	997.00	997.36	0.36	0.04%	6050.00	6050.36	0.36	0.01%
173	182.00	182.71	0.71	0.39%	3819.00	3819.95	0.95	0.02%
177	851.00	851.20	0.204	0.02%	14571.00	14571.48	0.48	0.00%
179	894.00	894.46	0.46	0.05%	14571.00	14571.49	0.49	0.00%
181	137.00	137.92	0.92	0.67%	14571.00	14571.52	0.52	0.00%
183	291.00	291.20	0.20	0.07%	14571.00	14571.52	0.52	0.00%
188	248.00	248.21	0.21	0.09%	5770.00	5770.73	0.73	0.01%
203	310.00	310.36	0.36	0.12%	13400.00	13400.22	0.22	0.00%
204	47.00	47.30	0.30	0.63%	9482.00	9482.85	0.85	0.01%
206	460.00	460.37	0.37	0.08%	7535.00	7535.01	0.01	0.00%
209	392.00	392.34	0.34	0.09%	7535.00	7535.02	0.02	0.00%
215	933.00	933.82	0.82	0.09%	14631.00	14631.19	0.19	0.00%
218	916.00	916.09	0.09	0.01%	14631.00	14631.23	0.23	0.00%
227	508.00	508.93	0.93	0.18%	14648.00	14648.53	0.53	0.00%
229	729.00	729.99	0.99	0.14%	14648.00	14648.53	0.53	0.00%
248	621.00	621.24	0.24	0.04%	14718.00	14718.19	0.19	0.00%

Table B.2: Probability of collision [-] comparison between CDM data and calculations.

CDM	$P_{c,CDM}$	$P_{c,code}$	$O_{diff}$	Diff:	$\epsilon_{rel}$
2	1.77E-06	1.77E-06	0.000	-8.12E-11	0.00%
4	5.87E-06	5.82E-06	0.003	-4.54E-08	-0.77%
5	5.85E-06	5.73E-06	0.009	-1.19E-07	-2.04%
25	1.63E-06	1.60E-06	0.008	-3.15E-08	-1.93%
26	8.40E-06	8.33E-06	0.003	-6.58E-08	-0.78%
27	1.63E-06	1.60E-06	0.008	-3.15E-08	-1.93%
48	3.06E-03	3.20E-03	0.020	1.45E-04	4.76%
50	1.12E-03	1.06E-03	0.025	-6.29E-05	-5.61%
51	1.29E-03	1.29E-03	0.000	5.72E-07	0.04%
53	6.34E-06	6.30E-06	0.003	-4.24E-08	-0.67%
54	2.29E-04	2.30E-04	0.002	8.10E-07	0.35%



Table B.2: continued from previous page

CDM	$P_{c,CDM}$	$P_{c,code}$	$O_{diff}$	Diff:	$\epsilon_{rel}$
55	3.61E-05	3.57E-05	0.005	-3.94E-07	-1.09%
56	5.89E-05	5.80E-05	0.006	-8.61E-07	-1.46%
63	2.23E-04	2.23E-04	0.000	-1.41E-07	-0.06%
64	2.82E-04	2.82E-04	0.000	-1.89E-07	-0.07%
66	1.97E-03	1.97E-03	0.000	-1.48E-07	-0.01%
69	1.42E-04	1.42E-04	0.001	2.81E-07	0.20%
86	4.24E-04	4.23E-04	0.001	-6.88E-07	-0.16%
98	3.11E-06	3.18E-06	0.010	7.38E-08	2.37%
100	7.18E-06	6.76E-06	0.026	-4.23E-07	-5.89%
108	8.59E-05	8.60E-05	0.001	1.07E-07	0.12%
120	2.91E-03	2.90E-03	0.001	-7.97E-06	-0.27%
121	2.29E-03	2.29E-03	0.000	-2.07E-07	-0.01%
122	1.82E-03	1.82E-03	0.001	-3.05E-06	-0.17%
124	8.46E-03	8.45E-03	0.000	-2.62E-06	-0.03%
127	3.12E-04	3.00E-04	0.017	-1.21E-05	-3.87%
142	2.91E-04	2.89E-04	0.003	-1.98E-06	-0.68%
144	3.13E-06	3.17E-06	0.006	4.19E-08	1.34%
146	6.13E-03	5.93E-03	0.014	-1.94E-04	-3.16%
150	8.28E-03	7.87E-03	0.022	-4.08E-04	-4.93%
157	8.75E-04	8.76E-04	0.001	1.21E-06	0.14%
158	5.77E-05	5.61E-05	0.012	-1.60E-06	-2.77%
160	6.26E-05	6.27E-05	0.000	6.81E-08	0.11%
169	7.14E-06	7.15E-06	0.001	8.61E-09	0.12%
171	4.45E-06	4.45E-06	0.000	2.94E-09	0.07%
173	2.63E-05	2.64E-05	0.001	5.21E-08	0.20%
177	1.36E-03	1.37E-03	0.002	4.85E-06	0.36%
179	4.67E-04	4.71E-04	0.003	3.66E-06	0.78%
181	5.31E-03	5.30E-03	0.000	-1.20E-06	-0.02%
183	5.79E-03	5.86E-03	0.005	6.94E-05	1.20%
188	1.73E-03	1.73E-03	0.000	4.41E-08	0.00%
203	1.70E-03	1.70E-03	0.001	4.05E-06	0.24%
204	4.46E-03	4.41E-03	0.005	-4.86E-05	-1.09%
206	1.40E-03	1.40E-03	0.000	1.81E-07	0.01%
209	1.41E-03	1.41E-03	0.000	8.92E-07	0.06%
215	1.10E-04	1.12E-04	0.008	2.05E-06	1.86%
218	2.66E-04	2.67E-04	0.001	4.19E-07	0.16%
227	3.64E-04	3.48E-04	0.019	-1.59E-05	-4.38%
229	1.82E-05	1.86E-05	0.008	3.23E-07	1.77%
248	3.32E-04	3.38E-04	0.008	6.10E-06	1.84%

## B.2. Maneuver implementation

To support the maneuver implementation described in Section 4.4, the evolution of the Keplerian orbit elements can be looked into. Here, the change in each element is shown over the course of the propagation. This is calculated by subtracting the current orbital element value from the first initial step one. An initial propagation of around 2.5 hours is done, after which a maneuver is implemented and propagated further for another 2.5 hours. This is line with maneuver implementation described in Subsection 4.4.2.

Here, three different figures are shown, each representing the implementation of a maneuver in another direction; maneuver in the radial direction is shown in Figure B.1, maneuver in the in-track direction is shown in Figure B.2 and the cross-track maneuver is shown in Figure B.3. Physically a cross-track maneuver should not affect the semi-major axis and the eccentricity, it should however affect the inclination and the right ascension of ascending node (RAAN). The argument of periaapsis should be affected by all maneuvers implemented. Additionally, it is expected that the in-track maneuver generates bigger changes than the radial maneuver. The true anomaly is shown to determine the value during the maneuver but it is not expected to change with any maneuver. As the maneuver moment is the same for the three cases and selected arbitrarily, the effects are not expected to be consistent with the maximum effect possible at the same magnitude but optimized timing.

The propagation is done for a purely Keplerian orbit characterized by the following orbital elements:  $a = 7500$  km,  $e = 0.3$ ,  $i = 45^\circ$ ,  $\omega = 235.7^\circ$ ,  $\Omega = 100.4^\circ$ . The changes in orbital element where no maneuver effect is expected should be in an order of magnitude similar to numerical errors.

The maneuvers implemented have a magnitude of 10 m/s. This is much higher than expected maneuver magnitudes for pure collision avoidance purposes. Within, the optimization of this thesis' problem it is expected that the effect on the orbit will be much lower.

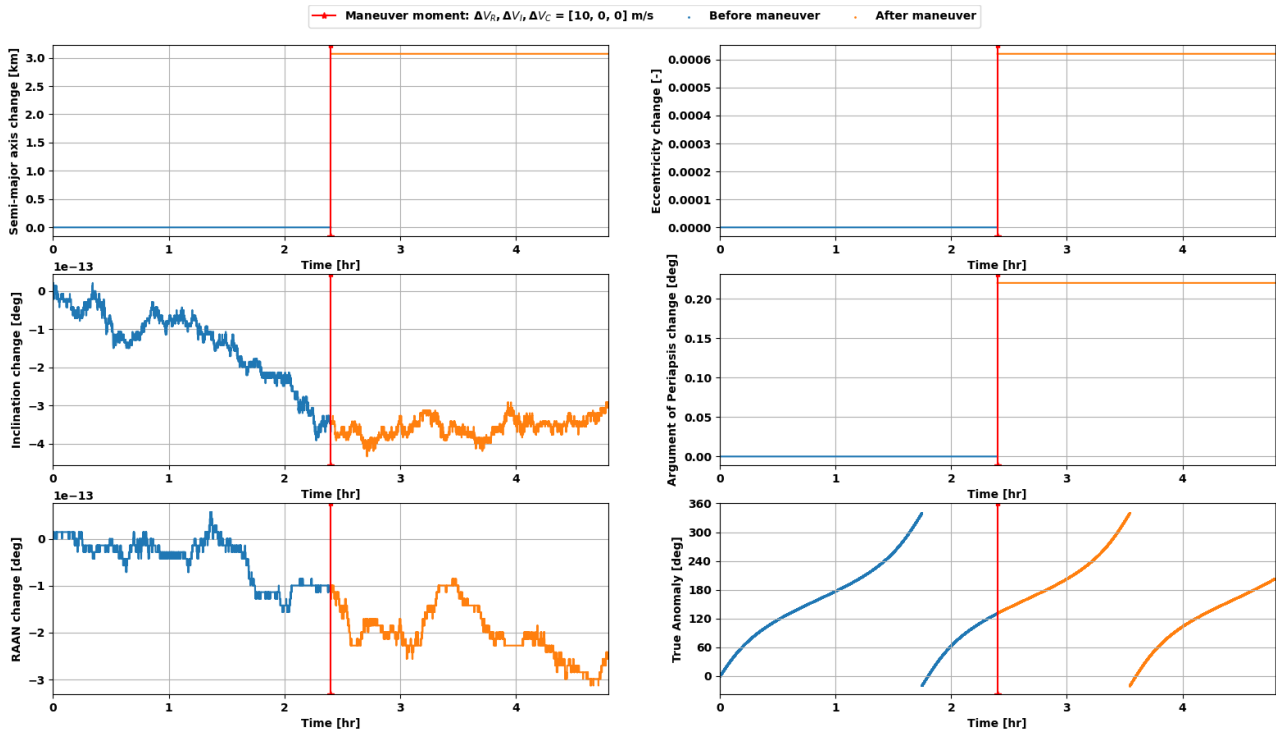


Figure B.1: Orbital elements change propagation before and after maneuver in radial direction.

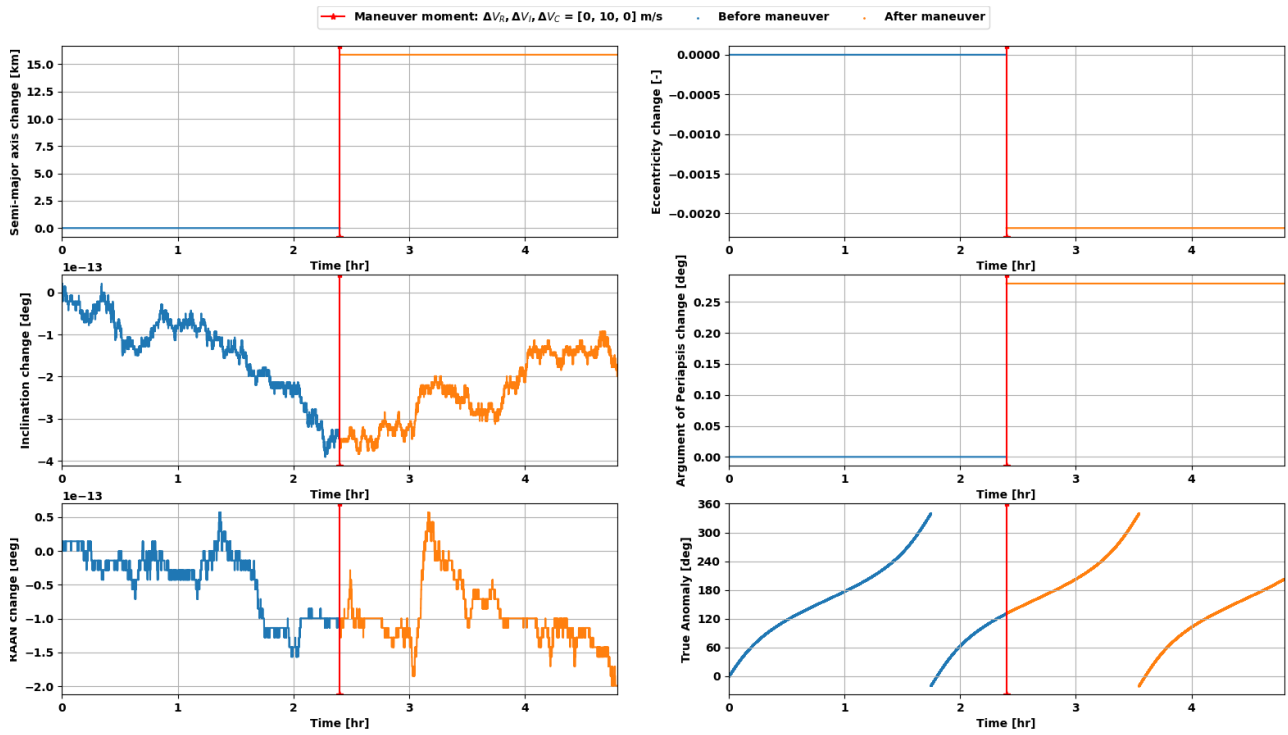


Figure B.2: Orbital elements change propagation before and after maneuver in in-track direction.

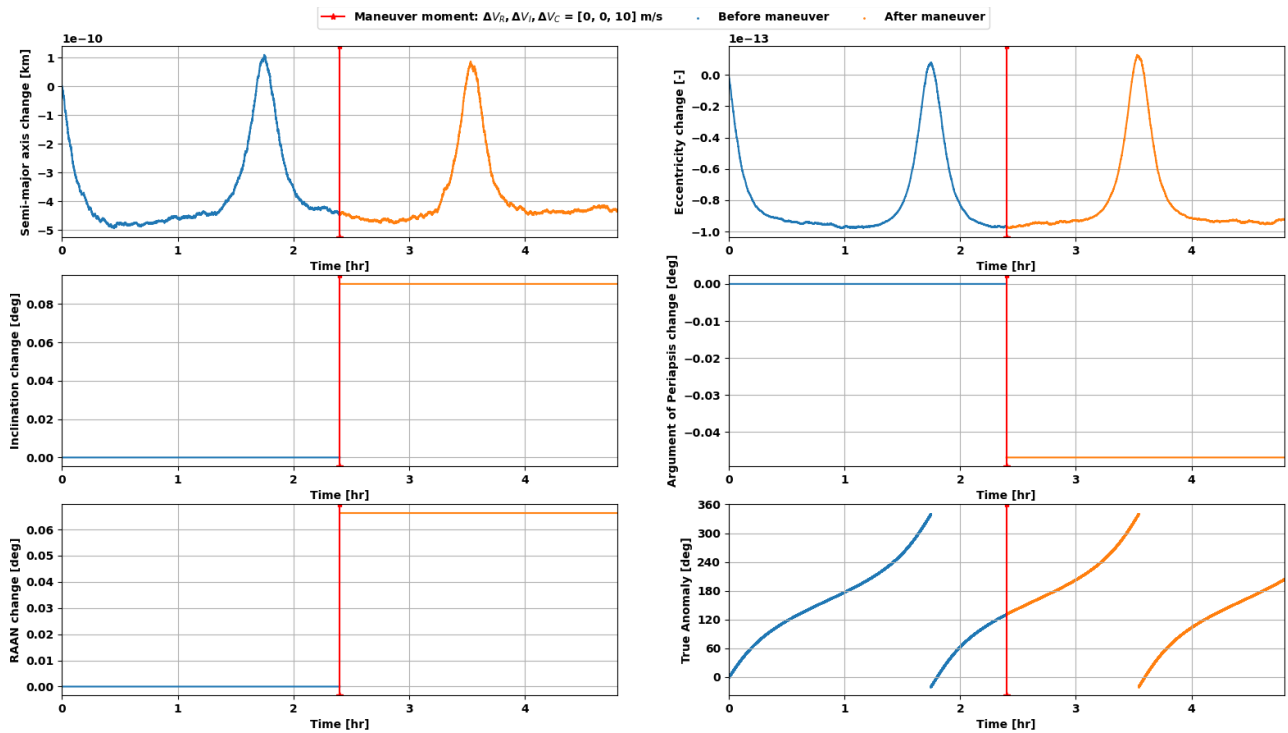


Figure B.3: Orbital elements change propagation before and after maneuver in cross-track direction.

The figures above show the expected and desired effects. This supports the correct implementation of the maneuver model.